# Sex Differences in Type I Interferon production by Plasmacytoid Dendritic Cells




Oliver L. Sampson

St Edmund Hall

University of Oxford

A thesis submitted for the degree of

*Doctor of Philosophy*

Hilary Term 2023

# Acknowledgements

I must begin by acknowledging my supervisor Prof. Philip Goulder. I would also like to acknowledge my co-supervisor Prof. Manu Vatish, IITM advisor Prof. William James, and rotation supervisors Prof. Quentin Sattentau and Prof. Helen McShane.

I would like to thank members of the Peter Medawar Building for their academic and, more importantly, moral support over several turbulent years: Philipp Hackstein, Vinicius Vieira, Ane Ogbe, Matt Jones, Lucia Parolini, David Malone, Cecilia Jay, Nick Lim, and, of course, Penny Zacharapoulou – without whom this thesis would have been completed far sooner, though with far fewer tea breaks.

For their contributions to my sanity throughout the most informative years of my life; it would have been a very different experience without my friends. To Dan, Sean, Jamie, George, Rachael, and co-inhabitants of the Michael Bubblé Andy and Pip; thank you.

I cannot also understate the importance of my family throughout. Your unwavering belief and continual grounding has meant more than I can ever say. Thank you to my grandparents Lynne and Ken, aunt Sonia, cousin Sophie, parents Mark and Judith, and my brother Elliot – "It's Ox-bridge not Cam-ford".

I lastly owe most to my partner Dana: for simply being yourself, I could not have asked for more. Thank you, for everything.

# Abstract

The importance of immune sex differences is widely gaining recognition as critically important in determining differential outcome in health and disease between males and females. The female immune response is generally more pro-inflammatory and shows a greater $T_H2$-skew than the male response which is generally more tolerant and $T_H1$-skewed. Central to this difference the production of type I interferon (IFN-I) by the principal responsible cell type, plasmacytoid dendritic cells (pDCs), is greater in females as the upstream receptor, TLR7, is encoded by the X-chromosome and is biallelically expressed in ∼30% of female immune cells. However, study of pDCs is historically difficult as they constitute only 0.1-0.5% of peripheral blood mononuclear cells and their activity declines rapidly *ex-vivo*.

The aim of this thesis was therefore to investigate further the sex-differential behaviour of pDCs; for which a new assay to stimulate their IFN-I production within whole blood was developed and revealed that adult male pDCs respond to stimulation with greater upregulation of activation markers despite lower IFN-I production than adult female cells. The pDC response between sexes was also compared within a cohort of adolescents co-vaccinated with Pfizer BioNTech BNT162b2 and live-attenuated influenza vaccine where increased activation in male pDCs corresponded to a delay in reaching the same level of IFN-I production as female pDCs. Additionally, male androgens were found to suppress pDC IFN-I which paradoxically increased antibody titres to BNT162b2 and suggests high immune activation is not beneficial to new mRNA vaccines as it is for traditional protein-subunit vaccines.

Despite these differences, transcriptional profiling of the largest pDC single-cell RNA sequencing dataset generated to-date revealed remarkable similarities between male and female pDCs with no difference for transcription of IFN-I or markers of activation. Differentially-expressed genes revealed subtle differences with a focus on cytokine signalling in female pDCs and antigen presentation in male pDCs; further supporting their delayed activation compared to female pDCs.

Lastly, sex-differential IFN-I has been linked to selection for increased IFN-I -resistance and decreased viral replicative capacity (VRC) during *in-utero* transmission of HIV-1 to females. Here no such selection for VRC is seen for heterosexual

adult-to-adult HIV-1 transmission which suggests the adult-to-adult transmission bottleneck differs from the *in-utero* mother-to-child bottleneck.

Overall, data in this thesis supports a model wherein monoallelic TLR7 expression increases the activation threshold for male pDCs which delays IFN-I production relative to female pDCs with biallelic TLR7 expression.

# Statement on the Impact of the COVID19 Pandemic

My initial DPhil proposal concerned the role of macrophages in the sex discordant transmission of HIV-1 *in-utero*. For this I had established collaborations with Prof. Manu Vatish to study *in-vitro* wild-type HIV-1 infection in primary placental tissue, and Prof. William James to investigate the influence of sex hormones on HIV pseudotype infection via a human induced pluripotent stem cell model. Additionally, I was to continue work I had begun during a rotation in Prof. Philip Goulder's lab to investigate the role of interferon (IFN) -resistance and viral replicative capacity (VRC) in defining the HIV-1 selection bottleneck for heterosexual transmission between adults.

I began my DPhil work in September 2019 but had to cease in March 2020 in line with University of Oxford COVID19 policy. During the subsequent nationwide lockdowns I received no information regarding extensions from my funding body, the Wellcome Trust. I therefore shifted my focus to the COVID19 work being undertaken at the Peter Medawar Building. This continued until Autumn 2020 when restrictions were lifted on non-COVID19 work. During this time, Prof. Goulder had established a cohort in which to study the response to natural SARS-COV2 infection in families. This led me to develop a whole blood assay to measure the IFN response in plasmacytoid dendritic cells (pDCs). A subsequent cohort was then established to investigate the response to primary Pfizer BNT162b2 vaccination in adolescents in Autumn 2021, and it was decided that the whole blood assay would be included. With only 12 months remaining until my original submission deadline of October 2022 I decided to subsequently develop this project rather than return to the original proposal.

Only in December 2021 did the Wellcome Trust communicate they would provide a 3-month extension of funding. I subsequently applied for and received 3 months further extension funding via the University of Oxford Coronavirus Student Extension Fund, increasing my submission deadline to April 2023. In wanting to develop a coherent thesis I did not return to the original proposal and instead used this additional time to investigate an observed sex-differential phenotype via single-cell RNA sequencing.

The only original project I continued was the adult-to-adult HIV-1 transmission study with the aim of relating it to the pDC work via IFN-resistance measurements. I could not replicate the IFN-resistance assay during the maternity leave of the post-doc who developed the assay so only VRC data could be presented in this thesis.

# Statement on Data Contribution

The work and analyses presented in this thesis are entirely my own. Nonetheless, the collaborative nature of certain projects means contributions have been made by fellow researchers towards data acquisition and analysis tools.

The experimental design of Chapter 2 was my own, but Nicholas Lim, University of Oxford, assisted in the collection of some experimental data and provided code for the linear modelling. Blood from healthcare workers was sampled by PITCH cohort staff, courtesy of Prof. Susie Dunachie, University of Oxford, and for families sampled by Prof. Philip Goulder, University of Oxford.

Blood samples for Chapter 3 were taken by Prof. Philip Goulder. SARS-CoV2 MSD measurements were performed with the assistance of Dr. Stephanie Longet, University of Oxford, and Influenza HA ELISA measurements were provided by Cecilia Jay, University of Oxford. Serum androgen concentrations were measured courtesy of Prof. Wiebke Arlt, Imperial College London. LASSO modelling was undertaken based on code provided by Stella Mebb and Prof. Andreas Groll, both TD Dortmund University, Germany.

The scRNA-seq data of Chapter 4 was jointly acquired by myself and Nicholas Lim; I stimulated, isolated, and sorted cells from healthy donors and he performed scRNA-seq via SeqWell (Gierahn et al. 2017) with minor contributions from myself. The presented analysis was performed entirely by myself and the pipeline employed was based on code provided by Evelyn Yuhzou Tong, Massachusetts Institute of Technology. WGCNA was undertaken based on code from Nicholas Lim and Panagiota Zacharopoulou, University of Oxford.

Donor plasma for Chapter 5 was provided by Prof. Eric Hunter, Emory University. The chimeric virus production and viral replicative capacity (VRC) assay were undertaken by myself using protocols provided by Dr. Emily Adland, University of Oxford, who also provided VRC data from a pilot study.

# Let's Talk about Sex

The subject of sex is recurrent throughout this thesis so I would like to clarify that all references to 'male' and 'female' are independent of gender and refer exclusively to biological sex; that is, the genetic presence of XY or XX sex chromosomes, respectively.

Where gendered terms are used in discussions of an individual's hormonal environment – whether naturally occurring or medically influenced – references to the masculine refer to a testosterone-dominated environment, and the feminine to oestrogen and progesterone -dominated environments.

# Word Counts

- Abstract: 396
- Pre-amble: 758
- Introduction: 9,045
- Chapter 2: 6,261
- Chapter 3: 7,254
- Chapter 4: 8,450
- Chapter 5: 5,350
- Conclusion: 568
- Total: 38,082

# Contents

**List of Figures** **xxiii**

**1 Introduction** **1**

1.1 RNA Virus Life-cycles . . . . . 2

1.1.1 HIV-1 Life-cycle and Infection . . . . . 2

1.1.2 SARS-CoV2 Life-cycle and Infection . . . . . 4

1.1.3 Influenza Life-cycle and infection . . . . . 6

1.2 Type I Interferons . . . . . 9

1.2.1 IFN-I Subtypes . . . . . 9

1.2.2 Pattern Recognition Receptors . . . . . 10

1.2.3 IFN-I Signalling . . . . . 12

1.2.4 Interferon-Stimulated Genes . . . . . 14

1.2.5 IFN antagonism by RNA viruses . . . . . 16

1.3 Plasmacytoid Dendritic Cells . . . . . 20

1.4 Sex differences in pDCs: the IFN-I/TLR7 axis . . . . . 24

1.5 Wider Immune Sex Differences . . . . . 26

1.5.1 Immune Sex Differences in RNA Virus Infection . . . . . 28

1.5.2 Immune Sex Differences in Responses to Vaccination . . . . 30

1.6 The Role of Sex Hormones in Immune Sex Differences . . . . . 32

1.6.1 Male sex hormones: Androgens . . . . . 33

1.6.2 The immune-suppressive role of androgens . . . . . 34

1.6.3 Duality within Female Sex Hormones: Oestrogen and Progesterone . . . . . 36

1.6.4 Female Sex Hormones and Immunity . . . . . 37
1.6.5 Clinical Implications of Immune- Sex Hormone Interactions . 39
1.7 Introduction Summary . . . . . 42

**2 Development of a Whole Blood Assay for the study of pDC IFN-I 43**
2.1 Abstract . . . . . 45
2.2 Introduction . . . . . 47
2.3 Materials and Methods . . . . . 51
2.3.1 Ethics Statement . . . . . 51
2.3.2 Stimulation of Whole Blood . . . . . 51
2.3.3 PBMC Isolation and Cryopreservation . . . . . 52
2.3.4 Stimulation of PBMC . . . . . 52
2.3.5 Cell Staining for Flow Cytometry . . . . . 52
2.3.6 Flow cytometry & Sample Analysis . . . . . 54
2.3.7 Linear Modelling . . . . . 55
2.3.8 IFN-α ELISA . . . . . 55
2.4 Results . . . . . 57
2.4.1 pDC Stimulation in PBMC is not feasible . . . . . 57
2.4.2 pDC IFN-I production can be captured by direct stimulation of whole blood . . . . . 62
2.4.3 Sex differential IFN-I production by pDCs is lost after overnight incubation . . . . . 62
2.4.4 Kinetics of the pDC response to CL097 in Whole Blood . . . 65
2.4.5 6hrs incubation best captures sex differential pDC activation and IFN-α production . . . . . 68
2.4.6 pDC activation and IFN-α production is highest in immediately in-tube stimulated whole blood . . . . . 69
2.4.7 pDC cytokine production is best maintained at 37°C . . . . 71
2.4.8 Low temporal variability between biological repeats confirms longitudinal robustness . . . . . 74

2.4.9 Whole blood assay demonstrates a sex difference in pDC IFN-α response in a clinical research setting . . . . . 78

2.5 Discussion . . . . . 81

**3 Sex-related characteristics of pDCs and effect of differential IFN-I production following primary Pfizer BioNtech BNT162b2 + LAIV co-/vaccination in adolescents in the United Kingdom 85**

3.1 Abstract . . . . . 87

3.2 Introduction . . . . . 89

3.3 Materials and Methods . . . . . 93

3.3.1 Ethics Statement . . . . . 93

3.3.2 Whole blood measurement of pDC IFN-I . . . . . 93

3.3.3 Plasma and serum isolation from whole blood . . . . . 94

3.3.4 Measurement of androgen levels . . . . . 94

3.3.5 Determination of anti-CoV2-IgG responses and prior infection 95

3.3.6 Determination of anti-HA-IgG influenza responses . . . . . 95

3.3.7 Data Analysis & LASSO modelling . . . . . 96

3.4 Results . . . . . 97

3.4.1 Cohort Demographics . . . . . 97

3.4.2 High pDC activation and cytokine secretion following co-vaccination . . . . . 99

3.4.3 Delayed activation kinetics and IFN-I production in male pDCs 101

3.4.4 Total testosterone and free testosterone correlate with sex and age in adolescents . . . . . 104

3.4.5 Sex and age-specific factors influence pDC IFN-I . . . . . 106

3.4.6 Larger cohort validates pDC IFN-α influences . . . . . 109

3.4.7 Sex differential outcome of BNT162b2 is masked by prior SARS-CoV2 infection . . . . . 109

3.4.8 LAIV outcome is not affected by sex . . . . . 110

3.4.9 LAIV co-vaccination increases BNT162b2 response . . . . . 113

3.4.10 LAIV increases activation of CD4+ T-cells via IFN-α . . . . 113

3.4.11 LAIV co-vaccination and free testosterone significantly affect BNT162b2 IgG responses . . . . . 116

3.5 Discussion . . . . . 119

**4 scRNA-seq finds similar expression for IFN-I genes and classic pDC markers between males and females but differential cytokine response and antigen presentation following TLR7 stimulation 127**

4.1 Abstract . . . . . 129

4.2 Introduction . . . . . 131

4.3 Materials and Methods . . . . . 137

4.3.1 Ethics Statement . . . . . 137

4.3.2 Confirmation of BDCA2 Expression by pDCs following TLR7 Stimulation . . . . . 137

4.3.3 pDC Enrichment from Whole Blood before and after TLR7 Stimulation . . . . . 138

4.3.4 pDC isolation via Fluorescence-Activated Cell Sorting . . . . 139

4.3.5 Single-Cell Gene Expression Measurement via SeqWell . . . 139

4.3.6 Single-Cell Data Processing . . . . . 140

4.3.7 Data Analysis . . . . . 140

4.4 Results . . . . . 143

4.4.1 BDCA2 allows high purity pDC isolation from multiple donors simultaneously . . . . . 143

4.4.2 Data Cleanup post- scRNA-seq . . . . . 146

4.4.3 Identification of a small population of "AS-DCs" . . . . . 150

4.4.4 Functional Dichotomy within Unstimulated and CL097-stimulated pDCs . . . . . 155

4.4.5 Convergence of Male and Female pDCs following CL097-stimulation . . . . . 158

4.4.6 Sex differential pDC IFN production is not mirrored at the transcriptional level . . . . . 161

4.4.7 Expression of canonical pDC markers does not differ between males and females . . . 163

4.4.8 Sex Hormone Module Scores Correlate with pDC Phenotypes 168

4.4.9 Differentially-expressed Genes reveal differences in the biology of male and female pDCs . . . 172

4.5 Discussion . . . 177

**5 The HIV-1 Clade C transmission bottleneck is different for heterosexual adult-to-adult transmission than *in-utero* mother-to-child transmission 185**

5.1 Abstract . . . 187

5.2 Introduction . . . 189

5.3 Materials and Methods . . . 193

5.3.1 Study Participants . . . 193

5.3.2 Generation of chimeric NL4-3::*gag-pro* viruses . . . 193

5.3.3 Confirmation of transmission pairs . . . 194

5.3.4 Determination of stock viral concentrations . . . 194

5.3.5 Determination of viral replicative capacity of chimeric NL4-3::*gag-pro* virus . . . 195

5.3.6 Data Analysis and phenotype prediction via Random Forest 195

5.4 Results . . . 197

5.4.1 Cohort Demographics . . . 197

5.4.2 Transmission pairs cluster phylogenetically . . . 199

5.4.3 VRC does not vary according to donor or recipient sex in adults 201

5.4.4 Recipient VRC is determined by donor VRC in adults . . . 202

5.4.5 TF VRC is not affected by sampling delay . . . 203

5.4.6 Gag-Pro amino acid sequence is conserved between donor and recipient in adults . . . 204

5.4.7 Random Forest prediction identifies C-terminal mutations that influence VRC . . . 206

5.5 Discussion . . . 211

**6 Conclusion: a model for sex differential pDC IFN-I via delayed activation kinetics in males 217**

**Appendices**

**A Appendix 223**

A.1 Unstimulated Adolescent pDCs Day 0 to Day 1 . . . . . 224

A.2 Stimulated Unvaccinated Control Donor pDCs Day 0 to Day 1 . . . 226

A.3 Sex-stratified Unstimulated Adolescent pDCs Day 0 to Day 1 . . . . 228

A.4 Adolescent pDC IFN-α LASSO Correlation Matrix . . . . . 230

A.5 Adolescent Day 35 anti-CoV2 IgG correlated with plasma free Testosterone . . . . . 231

A.6 scRNA-seq Confirmation of TLR7 Stimulation via IFN-α ELISA . . 232

A.7 Summary Table of Cell Numbers pre- and post- data Cleanup . . . 233

A.8 pDC scRNA-Seq Top 25 Genes per cluster pre-exclusion . . . . . 235

A.9 scRNA-Seq Top 50 Genes by Cluster post-exclusion; as used for GSEA 237

A.10 scRNA-seq GSEA Index Genes for GSEA Pathways Identified within Clusters . . . . . 239

A.11 scRNA-seq Heatmap of Top 10 DE Genes per Cluster . . . . . 241

A.12 WGCNA Gene Modules; as used for GSEA . . . . . 242

A.13 scRNA-seq GSEA Pathway Enrichment within WGCNA Gene Modules 244

A.14 scRNA-Seq Top 50 DE Genes by Sex and Stimulation; as used for GSEA . . . . . 246

A.15 scRNA-seq GSEA Pathway Enrichment within Top50 Differentially-expressed Genes between Males and Females . . . . . 248

A.15.1 Unstimulated pDCs . . . . . 249

A.15.2 CL097-stimulated pDCs . . . . . 250

A.16 Confirmation that VRC for overlapping chimeric NL4-3::*gag-pro* viruses correlate for two investigators . . . . . 251

A.17 Determination of optimal tree number for Random Forest . . . . . 252

A.18 VRC of NL4-3::*gag-pro* chimeric viruses by amino acid for positions identified by Random Forest . . . . . 253

A.19 Protease alignment . . . . . 257

A.20 N-terminal Gag-polyprotein alignments . . . . . 258

A.20.1 Gag p17 N-terminus . . . . . 258

A.20.2 Gag p2/p7 cleavage site . . . . . 259

A.20.3 Gag p6 N-terminus . . . . . 260

**References** **261**

# List of Figures


1.1 **HIV-1 Life-cycle** . . . 3

1.2 **SARS-COV2 Life-cycle** . . . 5

1.3 **Influenza Life-cycle** . . . 7

1.4 **PRR Signalling Pathways** . . . 11

1.5 **IFNAR Signalling Pathways** . . . 13

1.6 **Infographic of Female Hormone Cycles** . . . 36

2.1 **pDC Gating Strategy** . . . 54

2.2 **Comparison of in-tube stimulated whole blood incubated for 6hrs or overnight** . . . 65

2.3 **Kinetics of pDC response to CL097 in Whole Blood** . . . 66

2.4 **pDC activation and IFN-α production in whole blood compared to PBMC and cryopreserved PBMC** . . . 70

2.5 **Effect of simulated transport temperature on pDC activation and cytokine response** . . . 73

2.6 **Longitudinal robustness of pDC activation and cytokine production for individual donors** . . . 75

2.7 **Longitudinal robustness of pDC activation and cytokine production grouped by sex** . . . 77

2.8 **Application of immediate whole blood stimulation in a large clinical research cohort** . . . 80

3.1 **pDC Activation following Co-vaccination** . . . 100

3.2 **Sex Divergent pDC Activation following Co-vaccination** . . . 103

3.3 **Adolescent androgen measurements** . . . 105

3.4 **Day 35 IgG responses to SARS-CoV2 antigens** . . . . . 110

3.5 **Sex-stratified IgG responses to Influenza HA pre- and post-vaccination** . . . . . 112

3.6 **Effect of LAIV co-vaccination on Day 35 IgG responses to SARS-CoV2** . . . . . 114

3.7 **Effect of LAIV Co-vaccination on Early Immune Activation** 115

3.8 **A model for boosting of mRNA vaccine responses by androgens** . . . . . 124

4.1 **Example of simultaneous 4-donor pDC purification via BDCA2** 145

4.2 **BDCA2 Expression in Unstimulated and CL097-stimulated pDCs** . . . . . 146

4.3 **Quality Control Metrics for Unclean scRNA-seq Data** . . . 148

4.4 **Quality Control Metrics for Cleaned scRNA-seq Data** . . . 149

4.5 **UMAP clusters of pDC scRNA-seq data pre- AS-DC exclusion** . . . . . 151

4.6 **Top 2000 Most Variable Genes pre-AS-DC exclusion** . . . . 152

4.7 **Top 2000 Most Variable Genes post-AS-DC exclusion** . . . 152

4.8 **UMAP clusters of pDC scRNA-seq data post- AS-DC exclusion** . . . . . 154

4.9 **GSEA Pathway Identification for Individual Clusters** . . . . 157

4.10 **Distribution of Arrays by Cluster** . . . . . 159

4.11 **GSEA Pathway Identification for WGCNA co-expressed Genes** . . . . . 160

4.12 **Percentage Expression of *IFNA* and *TNF* transcripts between sexes** . . . . . 161

4.13 **pDC Expression of IFN-I and *TLR7*** . . . . . 164

4.14 **pDC Expression of canonical markers and markers of activation** . . . . . 166

4.15 **Seurat Module Scores for pDC activity** . . . . . 167

4.16 **Seurat Module Scores for GSEA Sex Hormone Modules** . . 169

4.17 **Correlation matrix for Seurat Module Scores** . . . . . 171

4.18 **Volcano Plot of Differentially-Expressed Genes by Sex for Unstimulated pDCs** . . . . . 172

4.19 **Volcano Plot of Differentially-Expressed Genes by Sex for CL097-stimulated pDCs** . . . . . 173

4.20 **GSEA Pathway Identification for top 50 sex-DE genes in unstimulated and CL097-stimulated pDCs** . . . . . 174

5.1 **Phylogenetic tree for p17/p24 of HIV-1 heterosexual transmission pairs** . . . . . 200

5.2 **VRC of Donor and Recipient Viruses by Sex** . . . . . 202

5.3 **Relationship between Donor and Recipient Virus VRC** . . . 203

5.4 **Relationship between recipient VRC and time post-EDI** . . 204

5.5 **Conservation of Amino Acid sequence between recipient and donor virus** . . . . . 205

5.6 **Gag-Pro amino acids predicted to influence VRC via Random Forest** . . . . . 207

5.7 **Positions of VRC-related amino acids within Gag polyprotein** 210

# 1

# Introduction

Infectious diseases represent a major burden to global health with over 25% of deaths in 2019 attributable to communicable diseases (WHO 2022b). Viruses are amongst the leading causes of morbidity and mortality within communicable diseases; many of which have genomes which consist of ribonucleic acid (RNA).

Human Immunodeficiency Virus 1 (HIV-1) has infected an estimated 80 million people since its emergence in the 1980s, including 38 million current infections, and still kills over 1 million people annually (UNAIDS 2022).

More recently, Severe Acute Respiratory Syndrome Coronavirus 2 (SARS-CoV2) exemplified the capacity for emerging infectious diseases to cause global pandemics with significant morbidity and mortality; with over 600 million reported infections and more than 6.5 million deaths since 2020 (correct to September 2022) (John Hopkins COVID-19 Resource Centre; see Dong et al. 2020).

Likewise, seasonal influenza is responsible for 290,000 to 650,000 deaths annually and between 3 and 5 million severe respiratory infections (WHO 2022a) which carries a serious impact on the global economy in both the cost of hospitalisation and lost productivity (Putri et al. 2018).

## 1.1 RNA Virus Life-cycles

The Baltimore virus classification scheme includes four categories of RNA virus; defined by their genomic organisation. The first two are the double-stranded RNA and negative-sense, single-stranded RNA (ssRNA) viruses, from which positive-sense messenger RNA (mRNA) is directly synthesised by a viral RNA-dependent RNA polymerase (rdrp). The other two are positive-sense ssRNA groups; the first of which is converted into negative-sense RNA for mRNA synthesis via a viral rdrp, whilst the second is reverse-transcribed into copy DNA (cDNA) from which a viral or host DNA-dependent RNA polymerase can synthesise new mRNAs (Koonin et al. 2021).

Crucially, each RNA virus life-cycle involves at least one RNA intermediate that is not conventionally seen within the cytoplasm of a cell; offering a molecular signature with which cell infection can be identified (McNab et al. 2015).

### 1.1.1 HIV-1 Life-cycle and Infection

HIV-1 is an enveloped virus with a 9kb positive-sense ssRNA genome which undergoes reverse transcription into cDNA before integration into the host genome.

A HIV-1 viral particle consists of two genome copies packaged with nucleocapsid p7 and protein p6 into a viral capsid of the p24 protein and surrounded by a matrix of protein p17. This is then enveloped within a host-cell derived plasma membrane containing trimers of the envelope protein gp120 anchored to the fusion protein gp41 (Freed 2015).

HIV-1 cell entry is mediated by gp120 binding of CD4, which exposes a secondary binding site on gp120 for the co-receptors CCR5 and CXCR4. Co-receptor engagement leads to the insertion of gp41 into the host cell membrane and fusion with the viral envelope to deposit the capsid into the host cell cytoplasm. The genome is reverse transcribed by viral reverse transcriptase and p24 is degraded whilst the

capsid traffics to the nucleus where the cDNA enters via a nucleopore. There it is integrated into the host genome by viral integrase, whereupon it is transcribed into mRNA by host RNA polymerases (Frankel and Young 1998). Translation yields Gag polyproteins which anchor in the host cell membrane and bind full-length genomic RNAs before new particles are released by budding and mature extracellularly through the cleavage of the polyproteins (Freed 2015) (see Figure 1.1).

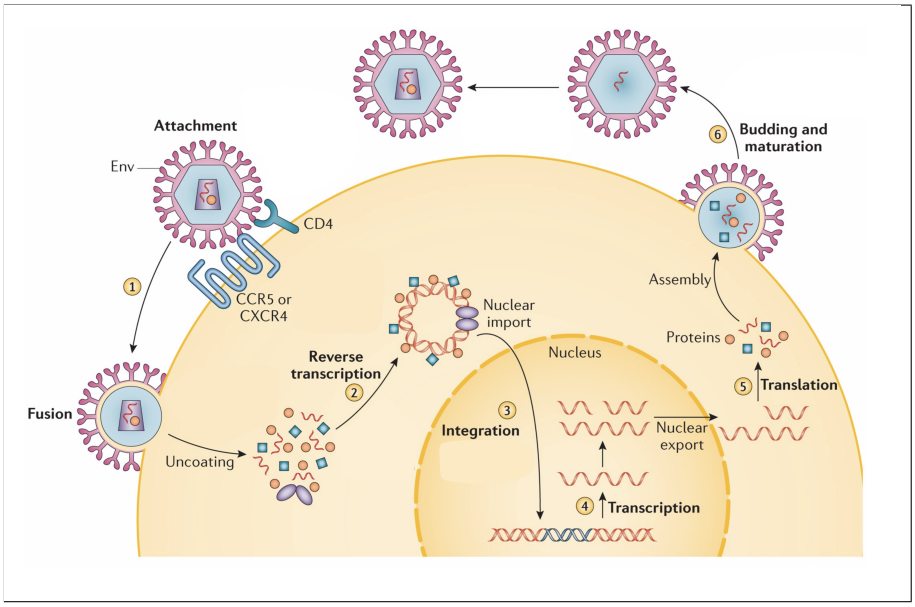



**Figure 1.1: HIV-1 Life-cycle.** Viral binding of CD4 and CCR5 or CXCR4 leads to membrane fusion (1) before the genome is uncoated and reverse transcribed into cDNA (2) for nuclear import and integration into the host genome (3). mRNA is then transcribed from the proviral DNA (4) and translated into viral polyproteins (5) before assembly, budding, and extracellular maturation (6). Adapted from: Deeks *et al.* (2015) *Nat. Rev. Dis. Primers*, doi: 10.1038/nrdp.2015.35.

HIV-1 infection is sexually transmitted and is incurable. Transmission is inefficient with only ∼1% of sexual encounters leading to infection (Patel et al. 2014). The viruses, or typically single virus, responsible for establishing infection in the recipient is termed the 'transmitter-founder' (TF) virus. TF viruses are restricted in tropism by their exclusive use of CCR5 as the co-receptor which limits initial infection to activated CD4+ T-cells and a subset of macrophages found sparsely in mucosal

tissue (Joseph et al. 2015). HIV-1 antigen is detectable in lymphoid tissues within 2 days of infection and in the blood within 10 days (Deeks et al. 2015). During this stage, the innate immune response peaks and is characterised by high levels of interferon type 1 (IFN-I) (Stacey et al. 2009). Peak viraemia is seen at 30 days and coincides with seroconversion, whereupon the viral load decreases ∼100-fold to a stable 'setpoint', thought mostly to be controlled by cytotoxic CD8+ T-cells rather than antibodies as the former targets the more conserved Gag protein whilst the latter targets the rapidly mutating envelope. Without treatment, CD4 counts decline slowly and infected individuals develop acquired immune deficiency syndrome (AIDS) within a period of 10 years and succumb to opportunistic infections (Deeks et al. 2015).

### 1.1.2 SARS-CoV2 Life-cycle and Infection

SARS-CoV2 is also an enveloped, positive-sense ssRNA virus but undergoes extra-nuclear replication within the cytoplasm, protected inside microvesicles.

As a betacoronavirus the SARS-CoV2 genome is considerably larger than HIV-1. Its' 30kb genome is packaged similarly by a nucleoprotein (N), but sits directly within the lipid envelope. Membrane (M) proteins are embedded within the lipid envelope and trimers of the virus receptor-binding spike protein (S) protrude through the external surface (V'kovski et al. 2021).

SARS-CoV2 S binds the human ACE2 protein and the genome enters the host cell cytoplasm after either endocytosis or direct membrane fusion via the additional non-essential engagement of TMPRSS2. Two large open reading frames, ORF1a and ORF1b, are immediately transcribed by viral rdrp to produce non-structural proteins that form viral replication organelles made of host endoplasmic reticulum. Inside, the genome is replicated to form double-stranded RNA replicative intermediates, from which nested transcription yields sub-genomic mRNAs for structural proteins. The mRNA is translated into structural proteins in the replication organelles which

bind full-length genomes to form viral particles that are released by exocytosis via the Golgi apparatus (Malone et al. 2021; V'kovski et al. 2021) (see Figure 1.2).

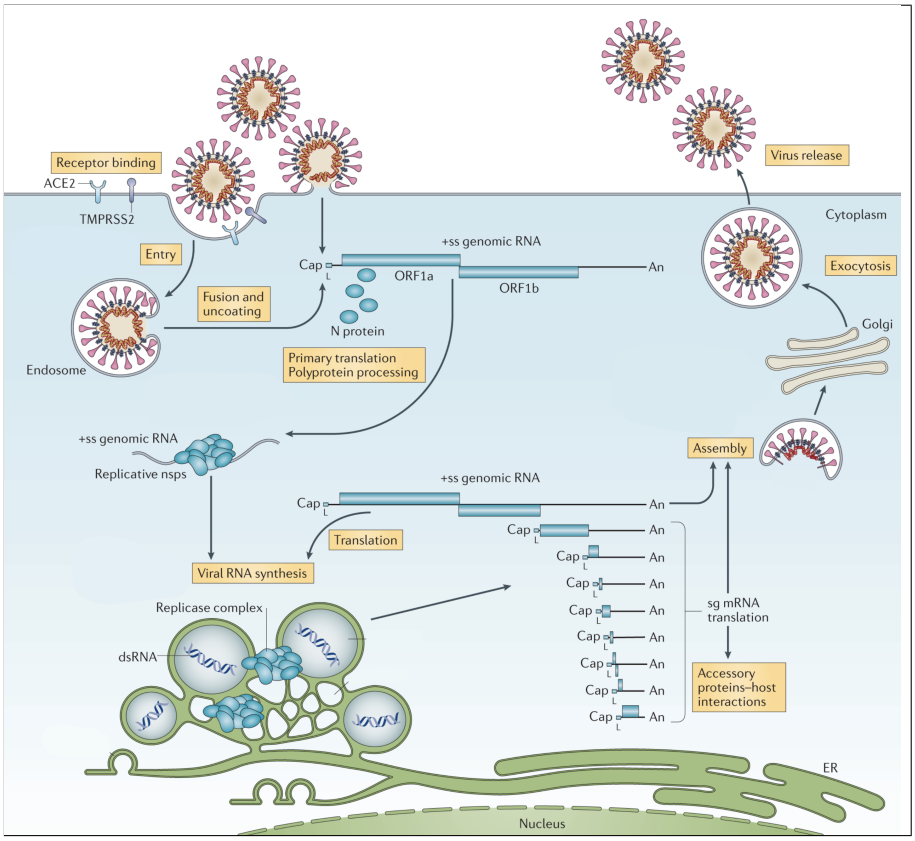



**Figure 1.2: SARS-COV2 Life-cycle.** Viral binding of ACE2 and TMPRSS2 leads to membrane fusion and the open reading frames ORF1a and ORF1b are translated directly from the genome in the cytoplasm. Resulting non-structural proteins (nsps) form double-stranded RNA replicative intermediates via replicase complexes inside replication organelles formed by nsps within the endoplasmic reticulum. Structural proteins are then produced with nested transcription and new viral particles are assembled in the endoplasmic reticulum for export via exocytosis through the golgi. Adapted from: V'kovski *et al.* (2021) *Nat. Rev. Microbiol.*, doi: 10.1038/s41579-020-00468-6.

SARS-CoV2 is highly transmissible and primarily infects the upper respiratory tract; causing a spectrum of disease ranging from asymptomatic to fatal, with age the largest risk factor (Scully et al. 2020). Peak viraemia is seen 5-7 days post-infection and coincides with the start of symptoms (Wölfel et al. 2020; Cevik et al. 2021). SARS-CoV2 is a strong inducer of IFN-I, and nasal IFN-I gene signatures correlate

with viral load; peaking at the time of symptom onset (Lopez et al. 2021). A systematic review found 80% of people clear the virus within two weeks after experiencing mild or asymptomatic illness (Cevik et al. 2021). 20% however develop severe pneumonia and require intensive care and ventilation, with a quarter of these progressing to acute respiratory distress syndrome and multi-organ failure, proving fatal in many cases (Cevik et al. 2021).

Immunity to SARS-CoV2 is short-lived and natural infection poorly protects from re-infection. Anti-S antibodies peak several weeks post-infection but have an estimated plasma half-life of only 36-156 days and were estimated to provide no protection from reinfection by 21 months (Townsend et al. 2022). Virus-specific CD4+ and CD8+ T-cells peak around 14 days post-infection and likewise have an estimated half-life of only 200 days (Moss 2022).

### 1.1.3 Influenza Life-cycle and infection

The main human influenza viruses are influenza A and influenza B. They consist of negative sense ssRNA genomes segmented into 8 parts and replicate in the nucleus via a positive-sense ssRNA intermediate. Within the virus particle the genome segments are packaged with the NP nucleoprotein inside a shell of the M1 matrix protein and enveloped in a lipid membrane displaying both neuraminidase (NA) and haemagglutinin (HA) (Taubenberger and Morens 2008).

Influenza infects the respiratory tract and binds epithelial cell sialic acid via HA to initiate endocytosis into the host cell. The viral particle is broken down by endosome acidification and the genome segments released as viral nucleoproteins into the cytoplasm by M1-mediated fusion of the viral envelope and endosome. From the cytoplasm, genomic segments enter the nucleus and are replicated via a positive-sense ssRNA intermediate which is directly transcribed for enzymatic and structural proteins. New viral particles are assembled on the inside of the plasma

membrane and released by budding (Dou et al. 2018; Krammer et al. 2018) (see Figure 1.3).

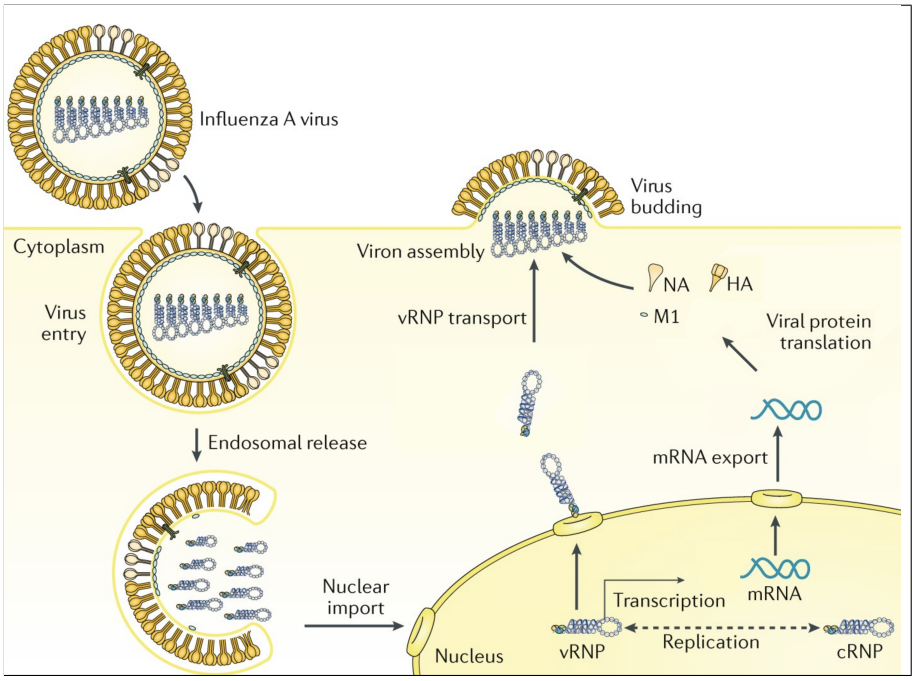



**Figure 1.3: Influenza Life-cycle.** Viral binding of sialic acid initiates viral entry via endocytosis and genomic segments are released by envelope fusion and translocate to the nucleus. Here they are replicated via a positive-sense ssRNA intermediate (cRNP) which is also transcribed for viral proteins. New viral particles are assembled at the cell membrane and released by budding. Adapted from: Krammer *et al.* (2018) *Nat. Rev. Dis. Primers*, doi: 10.1038/s41572-018-0002-y.

Unlike the pandemic viruses HIV-1 and SARS-CoV2, influenza is now described as endemic and follows an annual seasonal pattern of infections, peaking in winter months (Taubenberger and Morens 2008). Influenza infects the upper respiratory tract and causes an acute respiratory disease with peak viraemia 48 hrs post-infection. Symptoms are generally not life-threatening and last for 7-10 days, but people with chronic pulmonary diseases, children, and the elderly, can develop severe pneumonia which can prove fatal in as short a time as 48 hrs (Taubenberger and Morens 2008).

Antibody responses to influenza can be seen after 7 days and, like SARS-CoV2, peak at around day 28 post-infection (Rajendran et al. 2021). Both CD4+ and

CD8+ influenza-specific T-cells are detectable in the lungs after 10 days, and their presence is closely associated with viral clearance (Wang et al. 2015). The early innate immune response to influenza is also characterised by a strong IFN-I signature (Dunning et al. 2018) on account of widespread pattern-recognition receptor triggering by the cytoplasmic ssRNA genome (Iwasaki and Pillai 2014).

Like against SARS-CoV2, adaptive immunity against influenza does not offer long-term protection. This however results from a distinct mechanism; through mutations induced by the highly error-prone viral rdrp 'antigenic drift' causes rapid changes in HA, thereby constantly mutating one of the major targets for the adaptive immune response, and specifically neutralising antibodies (Krammer et al. 2018).

## 1.2 Type I Interferons

The adaptive immune response offers a highly targeted defence mechanism against an invading pathogen with minimal off-target damage to host cells, and allows the generation of an immunological memory to protect against future exposure to the same pathogen. It is however slow to develop and vertebrate organisms still therefore rely on an evolutionarily conserved innate immune system to immediately and indiscriminately identify and respond to non-self entities as potential threats.

This 'innate' immune system is built around the recognition of conserved pathogen-associated molecular patterns (PAMPs) with a series of germ-line encoded pattern-recognition receptors (PRRs). These are the membrane-associated toll-like receptors (TLRs) which identify extracellular and endosomal PAMPs, and the cytoplasmic non-TLR PRRs which identify PAMPs intracellularly (Kawai and Akira 2010).

Of importance to RNA viruses is the ability of PRRs to induce interferon type I (IFN-I). Every nucleated cell in the human body expresses the IFN-I receptor (IFNAR) and can produce IFN-I when exposed to pathogenic stimuli (McNab et al. 2015). So-called because the undefined historical preparation from *in-vitro* influenza-infected cells 'interfered' with influenza infection of further naïve cells (Isaacs and Lindenmann 1957), IFN-I's are pleiotropic cytokines that act in both autocrine and paracrine fashion to induce a powerful antiviral state within cells to limit virus spread through tissues (McNab et al. 2015).

### 1.2.1 IFN-I Subtypes

Within the IFN-I cytokines are 14 canonical members, 13 subtypes of IFN-α plus IFN-β, then several newer, less well-defined cytokines; IFN-ε, IFN-τ, IFN-κ, IFN-ω, IFN-δ, and IFN-ζ (Gibbert et al. 2013; Moll et al. 2011). As understanding of the non-canonical IFN-I's is limited, references to IFN-I henceforth refer only to the canonical IFN-I's.

IFN-β has the highest affinity for IFNAR (De Weerd et al. 2013), but is less highly produced and less well-studied than the IFN-α subtypes which are: IFN-α1, 2, 4, 5, 6, 7, 8, 10, 13, 14, 16, 17, and 21 (Lazear et al. 2019). These have different IFNAR binding affinities and can be grouped depending on their biological activity *in-vitro*: low-potency (IFN-α1), mid-potency (IFN-α2, IFN-α4, IFN-α5, IFN-α16, and IFN-α21) and high-potency (IFN-α6, IFN-α7, IFN-α8, IFN-α10, and IFN-α14) (Moll et al. 2011). Importantly, this distinction is only seen at sub-saturating concentrations of IFN-α and it is therefore unknown whether this represents a physiological difference between subtypes within the saturating IFN-I concentrations surrounding an infection *in-vivo* (Moll et al. 2011).

### 1.2.2 Pattern Recognition Receptors

Several PRRs are important for the production of IFN-I in response to RNA viruses, and each drives the production of IFN-I. The cognate ligands of PRRs for RNA viruses are detailed in Table 1.1.

**Table 1.1:** Pattern regognition receptors for RNA Viruses

| PRR | Full name | Cellular Location | PAMP |
|---|---|---|---|
| TLR3 | Toll-like receptor 3 | Endosomal | double-stranded RNA |
| TLR7 | Toll-like receptor 7 | Endosomal | single-stranded RNA |
| TLR8 | Toll-like receptor 8 | Endosomal | single-stranded RNA |
| RIG-I | Retinoic acid -inducible gene I | Cytoplasmic | double-stranded RNA |
| MDA5 | Melanoma differentiation-associated gene 5 | Cytoplasmic | double-stranded RNA |
| cGAS | cytosolic GAMP synthase | Cytoplasmic | DNA |

Most PRRs share the same signalling intermediates; converging on the activation of I-ϰB kinase-ε (IKKε) and TANK-binding kinase 1 (TBK1) which phosphorylate interferon regulatory factors (IRFs) IRF3 and IRF7. These translocate to the

nucleus and recruit additional factors including NFκB and activator protein 1 (AP-1) to initiate transcription of so-called 'interferon-stimulated genes' (ISGs) via binding of IFN-stimulated response elements (ISREs) within ISG promoters (McNab et al. 2015) (see Figure 1.4).

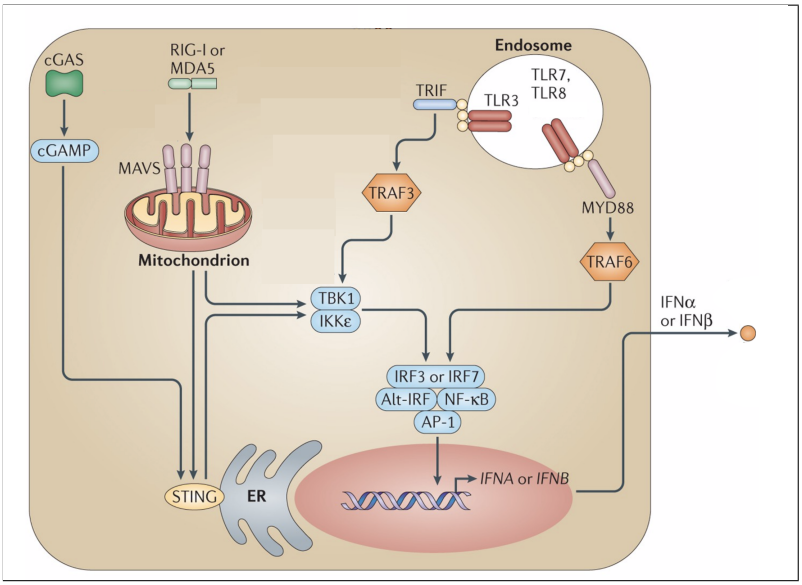



**Figure 1.4: PRR Signalling Pathways.** Cytoplasmic PRRs include cyclic GAMP synthase (cGAS) which acts via the stimulator of IFN genes (STING); and retinoic acid -inducible gene I (RIG-I) and melanoma differentiation-associated gene 5 (MDA5) which act via the mitochondrial antiviral signalling protein (MAVS). Endosomal PRRs include TLR3 which acts via TIR domain-containing adaptor protein inducing IFN-β (TRIF) and tumour necrosis factor -associated factor (TRAF) 3. Signals converge on the I-κB kinase-ε (IKKε) and TANK-binding kinase 1 (TBK1) pathways for phosphorylation of IRF3 and IRF7 leading to recruitment of nuclear factor kappa-light-chain-enhancer of activated B cells (NFκB) and activator protein 1 (AP-1) for expression of interferon stimulated genes (ISGs) via binding of interferon response elements in gene promoters. TLR7 and TLR8 signal via myeloid differentiation primary response protein 88 (MyD88) and TRAF6 for direct IRF3 and IRF7 phosphorylation. Adapted from: McNab *et al.* (2015) *Nat. Rev. Immunol.*, doi: 10.1038/nri3787.

Cytoplasmic PRRs include cyclic GAMP synthase (cGAS) which in the case of RNA viruses recognises cytoplasmic DNA intermediates and activates IKKε and TBK1 via the stimulator of IFN genes (STING) (Hertzog and Rehwinkel 2020). Additionally, retinoic acid -inducible gene I (RIG-I) and melanoma differentiation-associated

gene 5 (MDA5) both directly recognise cytoplasmic dsRNA and activate IKKε and TBK1 via the mitochondrial antiviral signalling protein (MAVS) (Rehwinkel and Gack 2020).

The endosomal TLRs all signal via an adapter molecule containing a Toll/IL-1R (TIR) domain; TLR3 signals via TIR domain-containing adaptor protein inducing IFN-β (TRIF), and TLR7 and TLR8 signal via myeloid differentiation primary response protein 88 (MyD88). These adapters in-turn recruit a further tumour necrosis factor -associated factor (TRAF) adapter. TRIF recruits TRAF3 which activates IKKε and TBK1 for phosphorylation of IRF3 and IFRF7 whereas MyD88 recruits TRAF6 for direct phosphorylation of IRF3 and IRF7 (Akira and Takeda 2004) (see Figure 1.4).

### 1.2.3 IFN-I Signalling

IFN-I is produced by cells either in direct response to infection, or in response to paracrine IFN-I produced by surrounding cells. Production proceeds in two rounds; the first only involves IRF3 and produces IFN-α4 and IFN-β which subsequently act in a paracrine fashion to induce *de-novo* IRF7 production in a second round of IFN-I consisting of the remaining IFN-α subtypes (Honda et al. 2006).

Interestingly, the main cell type responsible for IFN-I production, plasmacytoid Dendritic Cells (pDCs) (see Section 1.3) dispense with the first round of signalling, thereby minimising the time between pathogen exposure and production of all IFN-I subtypes. pDCs instead constitutively express IRF7 and it is retained pre-complexed with MyD88 inside endosomes, removing any delay between stimulation and IFN-I production (Honda et al. 2005).

The receptor for IFN-I, IFNAR, is a heterodimer consisting of the subunits IFNAR1 and IFNAR2. Binding of IFNAR by IFN-I initiates a signalling cascade that converges on the phosphorylation of signal transducer and activator of transcription 1 (STAT1) and STAT2 leading to their dimerisation and recruitment of interferon

regulatory factor 9 (IRF9) and together this complex translocates to the nucleus to bind ISREs (Pestka et al. 2004) (see Figure 1.5). Binding of IFNAR by IFN-α leads to the phosphorylation of the proximal kinases tyrosine kinase 2 (TYK2) or Janus kinase 1 (JAK1) which in turn phosphorylate STAT1 and STAT2, whereas binding of IFNAR by IFN-β leads to direct STAT1 and STAT2 phosphorylation independent of TYK2 or JAK1 (Pestka et al. 2004). Arguably this difference has evolved to minimise the time before ISG expression as IFN-β is the principal IFN-I produced in the first wave of IFN-I signalling (see Section 1.2.3).

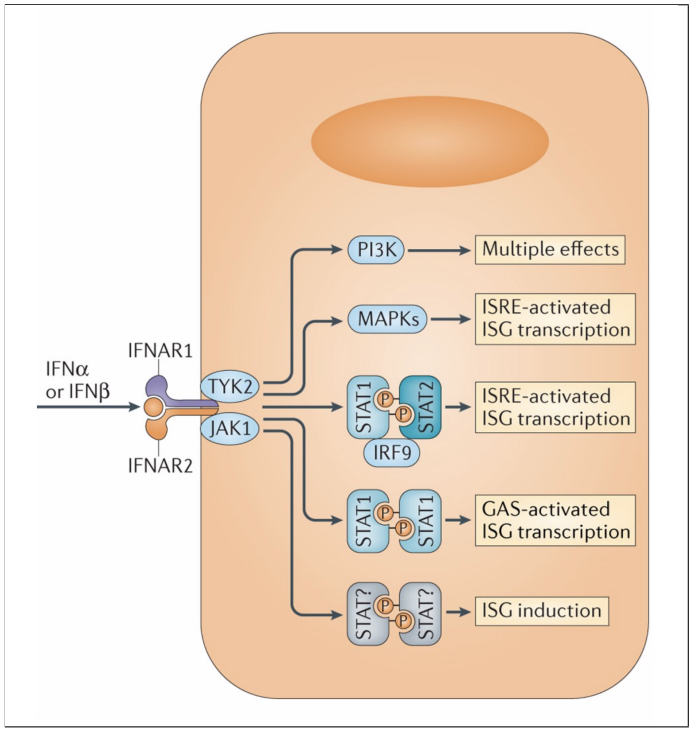



**Figure 1.5: IFNAR Signalling Pathways.** IFNAR binding by IFN-I activates tyrosine kinase 2 (TYK2) or Janus kinase 1 (JAK1) for phosphorylation of signal transducer and activator of transcription (STAT) 1 and STAT2, which dimerise and recruit interferon regulatory factor 9 (IRF9) to bind genomic interferon response elements (ISREs) for expression of interferon stimulated genes (ISGs). Homodimerisation of phosphorylated STAT1 also leads to ISG expression, as does activation of mitogen-induced protein kinases (MAPKs). Additional activated pathways include phosphoinositide 3-kinase (PI3K). Redundancy of STAT1 and STAT2 in ISG induction implies the existence additional STAT-like signal transducers yet to be elucidated (STAT?). Adapted from: McNab *et al.* (2015) *Nat. Rev. Immunol.*, doi: 10.1038/nri3787.

There also appears to be some redundancy in IFNAR signalling, underscoring the evolutionary necessity of IFN-I; for example STAT1 can homodimerise and activate ISG transcription via the cGAS pathway, thereby removing the need for STAT2 (McNab et al. 2015) (see Figure 1.5).

Similarly, whilst the downstream effects of the non-canonical IFN-I's is largely unstudied, there are reports that binding of IFNAR by IFN-ω can initiate ISG production via mitogen-induced protein kinases (MAPKS) and IFNAR binding by IFN-ε can initiate housekeeping-like activities like proliferation, differentiation, and motility via phosphoinositide 3-kinase (PI3K) (Pestka et al. 2004).

### 1.2.4 Interferon-Stimulated Genes

ISG induction primes the cell into a non-discriminate state of hostility towards viral replication, necessarily ceasing all normal homeostatic function since the virus relies on host machinery for replication; causing the death of the infected cell but ultimately limiting viral spread.

There are two canonical examples of ISG pathways, the first driven by 2',5'-oligoadenylate synthetase (OAS) and the second by protein kinase R (PKR). Both proteins are constitutively expressed at low levels by all IFNAR-expressing cells but are massively upregulated following IFN-I stimulation (Sadler and Williams 2008).

Upon activation by cytoplasmic dsRNA OAS converts ATP to a unique messenger intermediate, 2',5'-oligoadenylate. This is a co-factor required to activate the catalytic activity of RNaseL, which is constitutively produced in an inactive isoform. Activated RNaseL non-specifically degrades all cytoplasmic ssRNA, thereby preventing nascent viral assembly by preventing translation of viral mRNAs (Clemens and Williams 1978).

Protein synthesis is also the stage of viral replication targeted by the PKR pathway; once activated, PKR phosphorylates eukaryotic initiation factor 2 to inactivate its

guanidine exchange activity necessary for translation initiation, thereby halting all mRNA translation and preventing nascent synthesis of viral proteins (Roberts et al. 1976).

The number of other reported ISGs now runs in to the hundreds and whilst many of these doubtless interfere with viral replication, only a handful have experimentally-validated roles in truly antagonising viral replication and are therefore accepted as *bona-fide* ISGs (Schoggins 2019).

Amongst these are the tripartite motif (TRIM) family of ubiquitin ligases that target viral proteins for proteasomal degradation via ubiquitination (Schneider et al. 2014). Related, TRIM25 is responsible for the process of so-called 'ISG-ylation'; extending the cytoplasmic half-life of host antiviral proteins via the addition of the widely-recognised ISG, ISG15. A ubiquitin homologue, ISG15 acts akin to K63-ubiquination to increase levels of IFN-I signalling intermediates like JAK1 and STAT1, the ISGs RNaseL and PKR, and the transcription factor IFR3; increasing cellular sensitivity to subsequent IFN-β production in the initial waves of IFN-I signalling in surrounding cells (Sadler and Williams 2008) (see Section 1.2.3).

The remaining *bona-fide* ISGs show specificity to one or a limited range of viruses. This is best exemplified by the myxovirus resistance (MX) family of nuclear import -blocking GTPases; MX1 prevents replication of influenza but not HIV-1, whilst the inverse is true for MX2 (Goujon et al. 2013).

Necessarily to limit host damage, the IFN-I response cannot perpetuate unchecked and several ISGs have also been identified as effectors in the downregulation of the IFN-I response. The main mechanism of IFN-I desensitisation in activated cells is through upregulated endocytosis and turnover of IFNAR, which is augmented by ISGs named suppressors of cytokine signalling (SOCS) that occlude phosphorylated sites of activated JAK and STAT molecules to cease IFNAR signal transduction (Schneider et al. 2014).

Additionally, the ISG ubiquitin-specific peptidase 18 (USP18) has a bi-functional role in IFN-I modulation; firstly by binding the intracellular domain of the IFNAR2 subunit to competitively inhibit JAK binding, and secondly through an as-yet undefined mechanism that leads to the downregulation of ISG-ylation, allowing the timely proteasomal degradation of ISGs and IFNAR signalling intermediates (Ritchie et al. 2004).

### 1.2.5 IFN antagonism by RNA viruses

Testament to the inescapability of IFN-I triggering by RNA viruses, each takes considerable evolutionary effort to antagonise the IFN-I response, often dedicating large proportions of their evolutionarily-streamlined genome to antagonising antiviral ISGs (García-Sastre 2017).

The most interesting interplay is seen during HIV-1 infection; the virus must replicate in the face of the initial IFN-I spike during the acute phase of infection, whilst the host needs to limit self-damage from sustained, low-level IFN-I induction by the virus during the chronic phase of infection (Hardy et al. 2013). Indeed, humanised mice depleted of the primary IFN-I -producing cell type, pDCs (see Section 1.3), have higher viral loads during the acute phase but have slower CD4 decline during the chronic phase (Li et al. 2014). Likewise, the natural host for simian immunodeficiency virus (SIV) are proposed to maintain a non-pathogenic chronic infection because the IFN-I response is resolved following the acute phase (Chahroudi et al. 2012).

The main mechanism through which HIV-1 induces IFN-I is via TLR7; inescapable due to the ssRNA structure of the genome exposed in the cytoplasm during infection and more importantly assembly (Doyle et al. 2015). Contributions of DNA-sensing pathways are significantly less despite reverse transcription yielding cytoplasmic DNA since host-intrinsic 3'-repair exonuclease 1 (TREX1) non-specifically degrades

cytoplasmic DNA with high efficiency so few reverse transcription intermediates remain for RIG-I mediated PAMP detection.

Intense study of the IFN-I response to HIV-1 has revealed several so-called 'restriction factors'; host ISGs that are both cell intrinsic and upregulated by IFN-I during infection which antagonise the virus at several stages of the viral lifecycle and to which HIV-1 has therefore evolved specific antagonistic strategies; see Table 1.2 (Doyle et al. 2015).

**Table 1.2:** HIV-1 Restriction Factor Antagonism

| **Restriction Factor** | **Function** | **Antagonism by HIV** |
|---|---|---|
| Apolipoprotein B mRNA-editing enzyme, catalytic polypeptide-like 3 (APOBEC3) family | Genome hypermutation during RT via cytidine deamination | Viral infectivity factor (Vif) mediates APOBEC ubiquitination for proteasomal degradation |
| Sterile α-motif domain and histidine aspartic acid domain 1 (SAMHD1) | Degradation of cytoplasmic dNTPs to limit RT | Especially high affinity of HIV-1 RT for dNTPs (vs. SIV Viral protein x (Vpx) mediating SAMHD1 ubiquitination for degradation) |
| Tripartite motif-containing protein 5α (TRIM5α) | Capsid ubiquitination for proteasomal degradation | Error-prone RT induces capsid TRIM5-α-escape capsid mutations |
| Myxovirus resistance 2 (MX2) | Binds capsid to prevent nuclear import of cDNA | Error-prone RT induces capsid MX2-escape capsid mutations |
| Tetherin | Binds viral and host membranes to prevent new virions budding | Viral protein unique (Vpu) mediates tetherin ubiquitination for proteasomal degradation |

Conversely, SARS-CoV2 limits TLR7 activation to the less influential (relative to endocytosis) process of autophagy by containing replication within host ER -derived organelles and is therefore predominantly detected by cytoplasmic PRRs leading to IFN-I induction via the MAVS pathway (see Section 1.2.2). Despite its relatively recent emergence, global study of SARS-CoV2 has identified many viral proteins that interact with intermediates across the PRR and IFNAR signalling pathways; most commonly through preventing IRF3 phosphorylation and nuclear translocation.

The S protein, ORF6 and ORF9b all directly inhibit phosphorylation of IRF3 (Freitas et al. 2022; Lei et al. 2020; Han et al. 2021) whilst the protease NSP5 degrades phosphorylated IRF3 before it can translocate to the nucleus (Fung et al. 2021). NSP13 acts further upstream and prevents the MAVS signalling cascade by inhibiting activation of TBK1 (Vazquez et al. 2021). By preventing TBK1 activity, NSP13 also antagonises subsequent IFNAR signalling, as does the nucleocapsid which downregulates activation of both Tyk2 and STAT2 (Vazquez et al. 2021).

Paradoxically, NSP1 acts similarly to a canonical ISG; by preventing cytoplasmic mRNA translation, NSP1 limits host synthesis of both IFN-I and ISGs, whilst viral mRNAs are protected from NSP1 inside the SARS-CoV2 replication organelles (Vazquez et al. 2021).

The notion of dedicating genomic space to antagonising the inescapable IFN-I response is shared by HIV-1 and SARS-CoV2 but an alternative strategy is exemplified by the spatial separation between genome replication and PRRs achieved by influenza through its nuclear replication. Protected inside the nucleus, influenza avoids direct genome recognition by cytoplasmic PRRs and autophagic recognition by endosomal TLRs (García-Sastre 2017).

Nonetheless, there are still cytoplasmic stages to the influenza lifecycle (see Section 1.1.3) and the main detection of cellular infection is via RIG-I (Varga et al. 2011). Influenza NS1 however acts at both ends of the virus lifecycle by preventing RIG-I

signalling and IRF3 phosphorylation during initial cell infection (Talon et al. 2000), then by binding nascent dsRNA genome segments to occlude PRR recognition during assembly (Wang et al. 1999). PB2 additionally binds nascent dsRNA and, along with PB1, can also inhibit MAVS signal transduction to further prevent RIG-I -mediated IFN-I induction (Weber-Gerlach and Weber 2016; Varga et al. 2011).

The commonality of IFN-I antagonism between RNA viruses despite their differing replication strategies demonstrates the inescapability of the IFN-I response and its powerful antiviral capability; the implied necessity of evolving such antagonistic mechanisms therefore highlights the essential role played by IFN-I in the innate immune response to RNA viruses.

## 1.3 Plasmacytoid Dendritic Cells

The main source of IFN-I in the body are plasmacytoid dendritic cells (pDCs); so-called because their membranous cytoplasm renders them morphologically similar to plasma cells (Siegal et al. 1999). pDCs represent only 0.1-0.5% of circulating PBMCs and their primary role is the production of IFN-I in response to infection. Accordingly they express high levels of TLR7 for detection of ssRNA during viral infections and are able to produce IFN-I within 1-3hrs of infection (Reizis 2019).

pDCs produce ∼1000 times more IFN-α than any other cell (Siegal et al. 1999) and this implicates aberrant pDC responses in several autoimmune responses, most notably systemic lupus erythematosus (SLE) which presents with a significant female bias (Souyris et al. 2018a) (see Section 1.6.5). Accordingly, pDCs have a high turnover rate to reduce the potential for runaway responses; they have a short half-life of only several days and are continually replenished from precursors in the bone marrow rather than via peripheral proliferation (Zhan et al. 2016).

The developmental origin of pDCs is unclear and they can reportedly differentiate from both the common myeloid progenitor (CMP) and common lymphoid progenitor (CLP). A CLP-derived phenotype of so-called “pre-pDCs” was recently described as the primary source of pDCs in murine bone marrow (Rodrigues et al. 2018) but is opposed by arguments of their relative rarity and similar transcriptional pattern betwee pDCs and the CMP-derived common dendritic cell progenitor (Reizis 2019). Labelling experiments however suggest that the kinetics of pDC production do not align with the development of either the CMP or CLP (Lin et al. 2018). Instead pDC fate may be determined at the level of the pluripotent haematopoietic stem cell as their development is absolutely dependent on fms -like tyrosine kinase 3 (FLT3; CD135) and the transcription factor TCF4, both of which are expressed in all haematopoietic precursors and they thus develop into pDCs without additional input (Reizis 2019). The pDC phenotype is therefore evolutionarily hardwired into immune cell development and that their development occurs seemingly via pDC-by-default highlights their essential role in immunity. Indeed, cells with a

matching phenotpe are conserved in other primates (Chung et al. 2005) and lower mammals like mice and rats (Crozat et al. 2010; Aiello et al. 2018).

The role of IFN-I production by pDCs is well established for several important RNA viruses; most notably HIV-1 (Meier et al. 2009) and SARS-COV2 (Laurent et al. 2022). Given the rapidity with which pDCs can produce IFN-I, it is unsurprising that they are subject to heavy immune regulation to mitigate their autoimmune potential and only a limited percentage of pDCs will produce IFN-I when stimulated by TLR7 (Berghöfer et al. 2006; Meier et al. 2009; Seillet et al. 2012; Laffont et al. 2014; Ziegler et al. 2017; Webb et al. 2019; Hagen et al. 2020; Sampson et al. 2022; Abbas et al. 2022). Drastically, further regulation is achieved through the induction of massive apoptosis within these IFN-I producing pDCs following stimulation to limit IFN-I maxima (Swiecki et al. 2011).

Despite their developmental dissimilarity, pDCs show functional convergence with the antigen-presenting role of 'conventional' myeloid dendritic cells (cDCs) and they express low levels of major histocompatibility complex II (MHC-II) and the T-cell co-stimulatory molecules CD80 and CD86 at baseline (Asselin-Paturel et al. 2001). These undergo massive upregulation upon pDC activation, and drive a differentiation of the pDCs into antigen-presenting cells (APCs), supported by *de-novo* expression of the additional T-cell co-stimulatory molecule CD40 and the lymph node -homing receptor CCR7 (Psarras et al. 2021; Young et al. 2008).

The primary role of pDCs however remains IFN-I production, and the transition to APC occurs only after the cessation of IFN-I release. The molecular switch for this change appears to come from the antagonistic relationship between IFN-I and tumour necrosis factor α (TNF-α), a secondary cytokine produced by pDCs upon stimulation and shown to antagonise pDC cytokine release and promote their APC phenotype (Psarras et al. 2021).

Further, flow cytometry reveals 3 pDC populations following 24 hour stimulation with both influenza and SARS-CoV2; P1 (Programmed Death Ligand 1 (PD-L1)+/CD80-) characterised by high IFN-I production, P2 (PD-L1+/CD80+)

representing a non- IFN-I -producing, low antigen-presenting intermediate, and P3 (PD-L1-/CD80+) characterised by high antigen-presenting capability (Alculumbre et al. 2017; Onodi et al. 2021). Interestingly these populations were mutually exclusive yet displayed a unidirectional inter-population conversion from P1 to P2 and thence P3; resulting in sequential accumulation of the respective populations over the 24 hour time course. Consistent with the need for tight regulation of pDC IFN-I, P1 peaked at 12 hours and declined up to 24 hours whilst P2 and P3 increased, with the role of autocrine TNF-α signalling in inter-population conversion supported by increasing numbers of TNF-α stimulated genes in P2 and then P3 (Alculumbre et al. 2017).

Mechanistically, TNF-α -mediated IFN-I antagonism is driven by the downregulation of TLR7 signalling intermediates like MyD88 and IRF7, and interruption of the autocrine IFN-I loop through IFNAR1 and IFNAR2 downregulation. Additional autocrine TNF-α -driven pro-inflammatory signals are also downregulated through the induction of the NFκB inhibitor (Psarras et al. 2021) and accompanied by upregulation of antigen-presenting genes like MHC-II and T-cell co-stimulatory molecules (Young et al. 2008).

From their production in the bone marrow pDCs are continually disseminated to peripheral tissues via the blood, but are only sparsely detectable in tissue due to their reactogenic potential and accumulate only in instances of infection (Villadangos and Young 2008). Rather than the non-specific sampling of extracellular fluid by macropinocytosis, as undertaken by cDCs, pDCs sample antigen by selective uptake via clathrin-mediated endocytosis. Uptake is mediated by the binding of antigen carbohydrate moieties to c-type lectins including the dendritic cell immunoreceptor (DCIR) expressed by all dendritic cells, and blood dendritic cell antigen 2 (BDCA2) which is exclusive to pDCs (Meyer-Wentrup et al. 2008).

Up-taken antigen is then digested inside the resultant endosome and the exposed PAMPs are recognised by the endosomal TLRs leading to the initiation of the signalling pathway responsible for IFN-I production (see Section 1.2.2).

Through their strong IFN-I production and autocrine IFNAR stimulation pDCs are considered mostly refractory to infection (Reizis 2019) but low-level productive infection can still be detected for some RNA viruses, where IFN-I production is maintained through direct recognition of cytoplasmic RNA by RIG-I (Bruni et al. 2015) or delivery of antigen to endosomes via autophagy (Lee et al. 2007).

## 1.4 Sex differences in pDCs: the IFN-I/TLR7 axis

Given the evolutionary essentiality of IFN-I in terms of population survival via protection from viral infections (Hedrick 2004), pDCs present a surprising genetic and functional divergence between the biological sexes in their most widely-recognised and well-studied behaviour; IFN-I production in response to TLR7 stimulation (Reizis 2019).

It is widely reported that pDCs from female donors produce more IFN-I in response to TLR7 stimulation than pDCs from male donors; for both synthetic TLR7 ligands (Berghöfer et al. 2006; Seillet et al. 2012; Laffont et al. 2014; Ziegler et al. 2017; Webb et al. 2019; Hagen et al. 2020; Sampson et al. 2022) and more importantly to viral RNA (Meier et al. 2009; Abbas et al. 2022).

This phenotype is deeply rooted in genetics and relates to the sex chromosomes. Male sex is determined by the Y-chromosome and males have an XY genotype whereas females have two copies of the X chromosome with an XX genotype. Unlike the Y-chromosome, the X-chromosome is therefore present in both sexes and is thus free to carry additional genes unrelated to sexual characteristics (Schurz et al. 2019). To control for the resulting difference in X-chromosome gene dosage, either the maternal or paternal X-chromosome is randomly silenced by each cell in females through the process of X-chromosome inactivation (XCI) (Sahakyan et al. 2017). However, around 20% of genes on the X-chromosome demonstrably escape XCI, including several immune genes, most notably TLR7 and TLR8 (Schurz et al. 2019).

The majority of pDC activation occurs through endosomal TLR signalling (see Section 1.3) and importantly a study of XCI within immune cells showed that ∼30% of pDCs from female donors consistently had detectable biallelic TLR7 expression (Souyris et al. 2018b). Moreover, pDCs do not express TLR8 (Kioon et al. 2018) so biallelic TLR7 expression introduces sexual dimorphism into the main pathway for

IFN-I production in the body and can therefore be directly linked to increased IFN-I production by female pDCs in response to TLR7 stimulation (Hagen et al. 2020).

## 1.5 Wider Immune Sex Differences

Sexual dimorphism within immunity is not limited to the IFN-I/TLR7 axis and is widespread amongst both the innate and adaptive immune responses with stark consequences for the natural progression of infections. Evolutionarily, this can be thought to represent the different 'parental investment' of each sex in reproduction (Zuk 2009). The female immune response is generally stronger and more short-lived since prolonged illness conceivably risks malnourishment of a developing foetus or breastfeeding neonate, in which they have 'invested' long-term. The male 'investment' in reproduction is comparatively limited with the absolute requirement to provide only genetic material. This favours the development of sexual characteristics over immune function at the cost of longer or more frequent illness (Zuk 2009); exemplified by the immune-suppressive role of testosterone (see Section 1.6). Importantly, immune sex dimorphism is not limited to humans and is seen in higher primates, other mammals, lower vertebrates, and invertebrates (Klein and Flanagan 2016).

The most widely cited innate immune sex difference is greater production of IFN-I by females (see Section 1.4) but there are many other sex differences in the innate immune response that support the inflammatory skew of the female immune response. The phagocytic activity of neutrophils and macrophages is higher in females, and female immune cells express greater numbers of TLR signalling pathway intermediates; both allowing females to more efficiently present antigen and activate T-cells (Jaillon et al. 2017). Further, activated female macrophages produce more IL-10 and this is characteristic of the sexual divergence in innate priming of the adaptive response; skewing female adaptive immunity towards a $T_H2$ response (Klein and Flanagan 2016). This favours the humoral adaptive immune response and correspondingly, females have higher numbers of B-cells and CD4+ T-cells, which more readily activate and proliferate upon stimulation, leading to greater antibody titres than in males in response to infection and vaccination (Klein et al. 2010).

Conversely the male adaptive immune response is skewed towards $T_H1$ cells which produce pro-inflammatory cytokines like TNF-α and the macrophage-activating IFN-γ to drive a predominantly cell-mediated response (Klein and Flanagan 2016). This is conceivably underpinned by the weaker innate immune response than females; with reduced TLR signalling decreasing IFN-I and antigen presentation, the male adaptive response may have to adopt a different strategy than females to viral infections given the opportunity for wider virus spread afforded by the lag of initial inflammation and delayed antigen presentation for the adaptive response. The male adaptive immune response is therefore likely skewed for the clearance of already infected cells via cytotoxic effector cells whilst the female response is likely skewed for preventing spread of virus between uninfected cells via antibodies. Similar to that seen for a strong innate response, the male adaptive response is subject to heavier regulation than the female adaptive immune response with greater numbers of regulatory T-cells ($T_{reg}$s) such that, despite higher numbers of cytotoxic CD8+ T-cells and natural killer cells (NKs) in males, their cytotoxicity is still lower than those from females (Klein and Flanagan 2016).

Such dimorphism has stark clinical implications not only for infectious diseases, but also other conditions where inflammation is important. Due to the strength of the female inflammatory response, reports of adverse reactions to vaccination are consistently more frequent in females (see Section 1.5.2). Additionally, over 80% of autoimmunity is seen in females; importantly the two with the greatest female bias, SLE and Sjögren's syndrome, are strongly associated with dysregulation of TLR7 signalling and IFN-I production (Wang et al. 2021) (see Section 1.6.5). Further, this propensity for inflammation leads to an increased prevalence and severity for several inflammatory-mediated diseases such as irritable bowel and Crohn's disease, asthma, and eczema, amongst females whilst conversely protecting them from cancers such that males have a 1.6-fold increased risk of malignancies (Klein 2012).

### 1.5.1 Immune Sex Differences in RNA Virus Infection

No more so is immune sexual dimorphism evidenced than in HIV-1 infection. Female viral setpoints are on average 0.5 $\log_{10}$ lower than males with matched CD4 counts and time-post-infection (Gandhi et al. 2002). Females are also five-fold more likely to achieve so-called 'elite control' of virus replication but both situations are characterised by higher levels of immune activation (IA) (Goulder and Deeks 2018). Whilst higher IA in females is beneficial for viral control during the acute phase of infection (Sandler et al. 2014), IA sustained at higher levels in females into the chronic phase of infection means they are more likely to lose elite control if achieved (Yang et al. 2017), and progress to AIDS faster than males with matched viral loads given the increased availability of activated CD4+ T-cells for the virus to infect (Sterling et al. 2001). Importantly, HIV-1 IA correlates with IFN-I (Hardy et al. 2013); implicating pDCs in the sex differential outcome of infection. Indeed, when stimulated with a HIV-1 -derived RNA, pDCs from female donors produce more IFN-I than those from male donors (Meier et al. 2009).

Additionally, the global surveillance effort for COVID-19 offered insights into sex differential outcome from infection with an RNA virus on an unprecedented scale. From these studies male sex is consistently associated with increased severity of disease and mortality from COVID-19; an observation that transcends geographical location and socio-economic status to suggest a more deeply rooted biologic underpinning (Scully et al. 2020). A more robust T-cell response in females is associated with better prognosis from COVID-19 (Takahashi et al. 2020) and antibodies peak sooner and reach higher titres in females (Zeng et al. 2020; Huang et al. 2021). These are commonly related to better priming of the adaptive immune response in females due to their ability to produce increased quantities of IFN-I during infections than males (Arnold et al. 2022; Takahashi and Iwasaki 2021). The importance of IFN-I in reducing COVID-19 severity is highlighted by the isolation of anti- IFN-I autoantibodies from patients with severe COVID-19, with a significant male bias linked to carriage of a single X-chromosome (Bastard et al. 2021a, 2021b),

and by the mortality of male patients carrying loss-of-function TLR7 polymorphisms (van der Made et al. 2020; Asano et al. 2021). TLR7 is indeed essential to IFN-I production in response to SARS-CoV2 and this highlights a role for pDCs in determining the sex differential outcome of COVID-19 since their presence is non-dispensable for IFN-I production during SARS-CoV2 infection in mice (Laurent et al. 2022).

Conversely, the role of pDC-driven IFN-I in influenza virus infection, and any sex difference therein, is more nuanced since pDCs are not the sole source of IFN-I in response to influenza (Laurent et al. 2022). Nonetheless, one of the hallmarks of influenza infection is still a large TLR7-driven IFN-I response (Karaba et al. 2021; Diebold et al. 2004) and, converse to the apparently protective role this plays in SARS-CoV2, high IFN-I levels are associated with more damaging lung pathology characteristic of severe influenza-driven pneumonia (Karaba et al. 2021; Davidson et al. 2014). Interestingly, it appears that the lung epithelial cells are themselves responsible for the remaining IFN-I during influenza infection via RIG-I signalling (Jewell et al. 2007), clouding a sex-dependent role for pDCs within influenza outcome.

That said, there are notable clinical differences between the sexes for influenza infection and converse to the protection offered by IFN-I to females with SARS-CoV2 infection, influenza infection presents with greater severity and mortality in females (Klein et al. 2012; Klein and Flanagan 2016). Importantly, viral loads do not differ between males and females and instead the increased severity of female influenza infection can be related to the increased strength of their innate immune response; with greater overall inflammation leading to more incidences of loss-of-control in a cytokine 'storm' leading to acute respiratory distress syndrome (Klein et al. 2012). This is supported by observations of influenza infection in mice where increased NFκB-driven cytokine production in the lungs of females leads to significantly higher levels of pro-inflammatory cytokines like TNF-α, IL-6, and the APC chemoattractant CCL2 which drive up inflammation-associated pathology (Karaba et al. 2021; Davidson et al. 2014; Larcombe et al. 2011).

### 1.5.2 Immune Sex Differences in Responses to Vaccination

One of the most commonly cited consequences of immune sex dimorphism is the differential response to vaccination between males and females, with females generally producing stronger responses than males (Klein et al. 2010; Klein and Flanagan 2016; Flanagan et al. 2017). The most overt demonstration of this is the seasonal influenza vaccine to which, despite a new formulation annually to represent the most common circulating strains, females consistently produce higher antibody titres with greater neutralisation capacities (Engler et al. 2008; Furman et al. 2014). This is by no means limited to influenza however, and there is a growing body of literature that supports the greater capacity for the female immune response to produce higher antibody titres in response to vaccination. In one meta-analysis, concerning virally-vectored vaccines, 65% of studies found a female bias in the humoral response, whilst a male bias was seen in only 20% (Klein et al. 2010). A second, considering all vaccines, found 82% of studies reported greater responses in females and only 12% reported greater responses in males (Flanagan et al. 2017).

Mechanistically this can be attributed to the composition of the female immune response (see Section 1.5); the $T_H2$ skew with greater numbers of CD4+ T-helper cells and B-cells is underpinned by greater antigen presentation by APCs and increased immune activation via cytokine production from enhanced TLR signalling (Klein et al. 2010) (see Table 1.3).

A sex difference in the response to vaccines designed to raise a cell-mediated response is less clear-cut, with equal reporting of female and male biases (Klein et al. 2010). The male adaptive immune response is $T_H1$-skewed with higher numbers of cytotoxic CD8+ T-cells, but this is countered by immune-suppression by testosterone (see Section 1.6), a greater frequency of $T_{reg}$ cells, and a generally lower level of immune activation (see Section 1.5). Thus, a balance is struck for cell-mediated vaccines between a greater propensity for cell-mediated immunity in males but lower immune activation, and vice versa for females.

**Table 1.3:** Consequences of immune sex differences for vaccine responses

| Feature | Sex difference | Consequence |
|---|---|---|
| TLR signalling | Greater in females | Increased innate activation |
| Cytokines (IFN-I) | Greater in females | Increased adaptive activation |
| Antigen presentation | Greater in females | Better adaptive activation |
| CD4+ T-cells | Greater in females | Increased B-cell help |
| T-cell skew | $T_H2$ in females | Increased B-cell help |
| B-cells | Greater in females | Increased antibodies |
| NK cells | Greater in males | Increased CMI |
| CD8+ T-cells | Greater in males | Increased CMI |
| $T_{reg}$ cells | Greater in males | Overall downregulation |

Accordingly, lower levels of immune activation in males are considered to underpin the increased incidence of adverse reactions to vaccines amongst females (Klein et al. 2010; Flanagan et al. 2017). In the meta-analyses above, a female bias in adverse reactions was reported in 100% of the studies considered by one (Flanagan et al. 2017) and 80% in the other, with only a single study, in infants, reporting a male bias (Klein et al. 2010).

Such reports may however be subject to the female reporting bias recognised within health research. General healthcare seeking behaviour is reportedly higher in females (Thompson et al. 2016), and this includes attitudes to vaccine uptake (Lindholt et al. 2021). As such, the threshold for reporting a health concern is generally lower for female participants in healthcare studies than for male participants (Oksuzyan et al. 2010).

## 1.6 The Role of Sex Hormones in Immune Sex Differences

Alongside the genetic influence of TLR7 XCI (see Section 1.4) another major contributor to sex differences within the immune response is modulation by sex hormones. So-called androgen response elements (AREs) and oestrogen response elements (EREs) are present in the promoters and enhancer elements of many immune genes (Flanagan et al. 2017; Hannah et al. 2008). Whilst the effect of this is not easily delineated, a clear shift occurs in the immune response between the sexes during puberty and after the female menopause which suggests a role for sex hormones in regulating the immune response (Flanagan et al. 2017).

Receptors for both male and female sex hormones are detectable on immune cells throughout the immune system (), which supports their role in differentially shaping the immune response between males and females (Gubbels Bupp and Jorgensen 2018; Ben-Batalla et al. 2020). The androgen receptor (AR), for example, is expressed by all myeloid progenitor cells and CD3+ T-cell subtypes (Gubbels Bupp and Jorgensen 2018); androgens are generally considered anti-inflammatory and the immune systems of males with androgen deficiencies resemble those from females (see Section 1.6.5). Likewise, the oestrogen receptor is similarly expressed by the haematapoetic stem cell and is strongly expressed by cells from both myeloid and lymphoid lineages ("Estrogen receptors regulate innate immune cells and signaling pathways" 2015). Moreover, the oestrogen receptor (ER) is demonstrable expressed by pDCs and ER signalling has been linked specifically with increased IFN-I production by female pDCs (Seillet et al. 2012; Laffont et al. 2014; Scott et al. 2015).

Related, expression of autosomal immune genes can also be influenced by epigenetic modifications of the genome and differs between males and females due to the influence of sex hormones (Shepherd et al. 2021). Opposing patterns were reported for CpG methylation patterns in individuals undergoing gender affirming hormone therapy; with an increase in the number of sites following androgen therapy after 12

months and a decrease following oestrogen therapy (Shepherd et al. 2022). Further, a study of epigenetic changes during puberty found alterations in methylation patterns occurred predominantly near EREs and the affected genes were enriched for immune and inflammatory pathways (Thompson et al. 2018) which further supports the role of sex hormones in shaping the immune responses of males and females.

### 1.6.1 Male sex hormones: Androgens

Androgens are the male sex hormones and the central androgen is testosterone; a steroid hormone synthesised from cholesterol in the testes, adrenal glands, and adipose tissue, and distributed via the circulation bound predominantly to sex hormone binding globulin (SHBG) or albumin (Davey and Grossmann 2016; Anderson 1974).

Locally, dissociation from the binding protein allows diffusion of testosterone across the cell membrane to bind the AR in the cytoplasm; a so-called 'nuclear transcription factor' that subsequently translocates to the nucleus to control gene expression through ARE binding (Davey and Grossmann 2016).

Additionally, testosterone can be locally metabolised by 5-α-reductase found in more androgen-influenced tissues like the liver, skin and most notably the prostate (Thigpen et al. 1993). The resultant compound, dihydrotestosterone (DHT) is a more powerful androgen than testosterone with a 2-fold higher affinity for the AR and a 5-fold lower dissociation rate leading to stronger AR signalling (Grino et al. 1990).

Testosterone is predominantly a male hormone and females typically have 10-fold lower serum testosterone levels than men (Kulle et al. 2010). Female testosterone is synthesised in the ovaries and adrenal cortex and, although typically low, varies according to the menstrual cycle (see Section 1.6.3). Another large influence on testosterone levels is age. From birth testosterone levels increase for both sexes with

little difference between them except for a spike in males between 3 and 6 months during a so-called 'mini-puberty'. The large difference in testosterone levels observed between the sexes coincides with the onset of puberty where male levels increase 10-fold and female levels remain at pre-pubertal levels (Kulle et al. 2010). Levels are stable throughout early reproductive years but serum testosterone reduces from early adulthood and is especially marked in males over 60 (Morley et al. 1997). However, a post-menopausal increase in testosterone level is seen in females due to a decrease in SHGB production leading to increased levels of bioavailable unbound, or 'free', testosterone (Burger 2002; Abraham 1974).

### 1.6.2 The immune-suppressive role of androgens

Androgens are viewed as widely immune-suppressive and measurements like serum testosterone levels correlate negatively with classic pro-inflammatory markers such as TNF-α and macrophage inflammatory protein 1β (Bobjer et al. 2013).

Indeed, immune modulation by testosterone is most readily studied in macrophages and *in-vitro* treatment of macrophages with testosterone decreases their production of the pro-inflammatory proteins TNF-α and IL-1β and simultaneously increases their production of the classic anti-inflammatory proteins IL-10 and TGF-β (Corcoran et al. 2010; D'agostino et al. 1999). Further, there is evidence for direct antagonism of innate PRR signalling by androgens as TLR4 is downregulated in testosterone-treated macrophages meaning that in response to its cognate ligand, bacterial lipopolysaccharide, they adopt a markedly less inflammatory phenotype, with decreased production of TNF-α and reactive oxygen species, associated with a reduced role in sepsis than for female macrophages (Rettew et al. 2008). Similarly, cDCs exposed to testosterone *ex-vivo* show marked reduction in TNF-α, IL-1β and IL-6 production in response to stimulation (Corrales et al. 2009).

Evidence for androgen-mediated innate immune suppression also extends further to non-APC cell types; both neutrophils and NK cells show reduced cytotoxic activity

following testosterone exposure (Deitch et al. 2006; Hou and Wu 1988). Likewise, this suppression affects the adaptive immune response; for example testosterone-treated myeloid cells are unable to fully activate naïve T-cells for a robust response (Der et al. 2014).

Additionally, direct treatment of naïve T-cells with testosterone reduces their ability to activate when stimulated and increases their production of the anti-inflammatory cytokine IL-10 in a dose-dependent manner, thereby confirming the immune-suppressive role of androgens within the adaptive response (Liva and Voskuhl 2001; Torcia et al. 2012). Similarly, the $T_H2$ response is already antagonised by the $T_H1$-bias of the male immune response, but is further antagonised by upregulation of the $T_H2$-suppressing cytokine IL-18 by androgens (Hepworth et al. 2010). Related, whilst B-cells do not directly express the AR, their numbers are increased in male mice after castration, providing another mechanism for $T_H2$-suppression by androgens (Trigunaite et al. 2015).

Further, the central male $T_H1$-biased response is also antagonised by desensitisation of naïve T-cells to the $T_H1$-differentiation cytokine IL-12 and antagonsim of T-cell IFN-$\gamma$ production (Kissick et al. 2014). Mechanistically, this is linked to AR signalling driving upregulation of the phosphatase Ptpn1, leading to the dephosphorylation of the signalling intermediates Tyk2 and Jak2, thereby preventing signal transduction from the IFN-$\gamma$ receptor (Myers et al. 2001).

Much of the current research concerning androgen modulation of interferons is limited to IFN-$\gamma$ and the response to IFN-$\gamma$ signalling, as discussed, and there is little literature on whether this extends to IFN-I. Nonetheless, putative AREs can be detected within the promoters of both TLR7 and the adapter MyD88, suggesting some degree of modulation by androgens (Flanagan et al. 2017; Jaillon et al. 2017). Likewise, pDCs from male infants during their mini-puberty produce less IFN-I in response to TLR7 stimulation than those from age-matched female infants (Wang et al. 2012). Importantly, this is the only time before puberty where a difference in IFN-I production by pDCs exists between males and females as the escape from XCI

by TLR7 in females is only seen following puberty (Webb et al. 2019), supporting the role of androgens in downregulating pDC IFN-I in Wang et al. 2012.

### 1.6.3 Duality within Female Sex Hormones: Oestrogen and Progesterone

The female sex hormone environment is more complicated than the male environment. Testosterone is still produced at a low level (Kulle et al. 2010) but the predominant female sex hormones are oestrogen (E2) and progesterone (P4); and all three vary accodring to the stage of the menstrual cycle (Brundin et al. 2021; Bui et al. 2013) (see Figure 1.6).

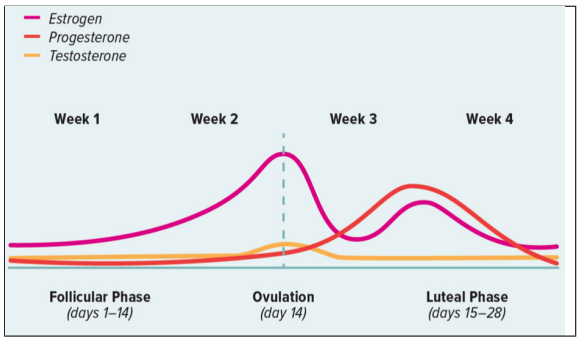



**Figure 1.6: Infographic of Female Hormone Cycling.** Infographic to display the relative fluctuations of Oestrogen, Testosterone, and Progesterone during the menstrual cycle. Not to scale. Adapted from: https://www.healthline.com/health/make-your-period-work-for-you (Accessed 22nd Nov 2022).

The menstrual cycle can be divided into four stages, each lasting around 7 days. The first is the early follicular phase wherein menstruation occurs, then hormone levels rise throughout the late follicular phase which ends with ovulation on day 14. This is followed by an early luteal phase during which the endometrium thickens before it begins to break down in the late luteal phase unless fertilisation has taken place (Owen 1975).

Testosterone levels remain relatively low for the majority of the menstrual cycle with only a slight rise around ovulation (Bui et al. 2013). Oestrogen rises over the follicular phases then decreases over the luteal phases whilst progesterone rises following ovulation and peaks between early and late luteal phases (Owen 1975) (see Figure 1.6). The menstrual cycle therefore introduces a cyclic hormonal environment alternating between two weeks dominated by oestrogen then two weeks by progesterone (Oertelt-Prigione 2012).

Oestrogen is synthesised in the ovaries and similarly to testosterone is transported by the blood bound predominantly to SHBG and albumin, and dissociates locally to act in target tissues like the liver, uterus, and mammary glands (Amenyogbe et al. 2020; Anderson 1974). As a steroid hormone, oestrogen enters cells via free diffusion and binds the ER in the cytoplasm. The ER also belongs to the nuclear receptor family and translocates to the nucleus to bind so-called oestrogen response elements (EREs) in the promoters of specific genes to influence transcription (Amenyogbe et al. 2020).

Progesterone is likewise synthesised in the ovaries and circulates in the blood bound to either albumin or corticosteroid binding protein. Similarly, it dissociates locally and freely diffuses into cells to bind the cytoplasmic progesterone receptor, another nuclear receptor that translocates to the nucleus and binds progesterone response elements in gene promoters (Mendel 1989; Azeez et al. 2021).

### 1.6.4 Female Sex Hormones and Immunity

The changing nature of female hormone levels makes it hard to determine their exact influence on immunity. Nonetheless, the general view is that oestrogen is pro-inflammatory and promotes the $T_H2$ response, and progesterone is anti-inflammatory and promotes the $T_H1$ response (Oertelt-Prigione 2012; Klein and Flanagan 2016).

ER expression can be seen for a variety of immune cells and oestrogen can be linked to increases in activity for both adaptive and innate immune cells (Brundin

et al. 2021; Klein and Flanagan 2016). In accordance with the $T_H2$ skew of the female immune response (see Section 1.5) oestrogen is linked to promotion of the $T_H2$ phenotype within CD4+ T-cells as well as increased IgM and IgG release from B-cells such that antibody titres in females is highest immediately pre-ovulation when oestrogen levels are highest (Souyris et al. 2018a; Lü et al. 2002).

Similarly, oestrogen acts to promote the differentiation of monocytes and myeloid precursors into dendritic cells, thereby increasing antigen presentation within females, which is further enhanced by an oestrogen-driven upregulation of TLR7 to increase their responsiveness to antigen stimulation (Jaillon et al. 2017).

Such modulation of TLR7 appears to extend to pDCs as exogenous provision of oestrogen to TLR7-stimulated pDCs from humanised mice enhances their IFN-α secretion, but this effect is not seen of ER-knockout mice (Seillet et al. 2012; Laffont et al. 2014; Scott et al. 2015). Similarly, pDCs from post-menopausal women (ie. oestrogen-naïve pDCs) showed greater IFN-I production following oestrogen treatment than at baseline (Seillet et al. 2012).

The progesterone receptor is likewise expressed by a range of immune cells (Teilmann et al. 2006) but conversely to oestrogen displays an anti-inflammatory profile. This may be rooted in its increasing production during pregnancy where maternal immune-tolerance is needed to prevent rejection of the developing foetus (Shah et al. 2019). This is best exemplified by the clear reprogramming of NK cells for tolerance by the high-progesterone environment specifically surrounding the uterus (Jaillon et al. 2017).

Indeed, the activities of progesterone are more comparable to those of testosterone than oestrogen; increasing the percentage of $T_{Reg}$ cells and decreasing the activity of CD8+ cytotoxic T-cells. Antigen presentation is also reduced by progesterone and CD80 and CD86 levels are decreased on cDCs leading to reduced overall B-cell activation and a reduction in antibody titres (Klein and Flanagan 2016).

This immune-suppressive role of progesterone looks to extend directly to the IFN-I/TLR7 axis as progesterone treatment of human pDCs *ex-vivo* reduces their ability to produce IFN-I in response to TLR7 stimulation (Hughes et al. 2008). Indeed, pDC IFN-α following stimulation with a HIV-derived ssRNA ligand negatively correlated with donor serum progesterone in one study (Meier et al. 2009). This can be linked to an inhibition of the interaction of MyD88 with IRF7 by progesterone which exhibits specificity to the IFN-I/TLR7 axis since polyI:C-driven IFN-I mediated by TLR9 was unaffected by progesterone (Hughes et al. 2008).

Nonetheless it appears that the female hormonal environment may still predominantly be pro-inflammatory as human bone marrow -derived pDCs from both sexes showed increased IFN-I production when implanted into female mice compared to implantation into male mice (Laffont et al. 2014).

### 1.6.5 Clinical Implications of Immune- Sex Hormone Interactions

The effect of sex hormones on immune cell behaviour can be studied *in-vitro* but the clinical relevance of the interactions is often confounded by natural human heterogeneity. Nonetheless, several patterns occur which support the importance of sex hormones in influencing clinical phenotypes.

One of the most commonly-cited TLR7-related pathologies is SLE; an autoimmune disease characterised by chronic IFN-I production caused by aberrant ssRNA-containing immune complexes triggering TLR7 (Kaul et al. 2016). Importantly, SLE presents with a 9:1 to 15:1 female-to-male bias and primarily affects females between puberty and the menopause, thus implicating a hormonal component (Kaul et al. 2016; Pons-Estel et al. 2010). Likewise, the frequency of an SLE flare-up in women receiving oestrogen/progesterone hormone-replacement therapy was a third greater than a placebo group (Buyon et al. 2005).

Similarly, pregnancy offers a window in to the hormonal influence of the immune system as both oestrogen and progesterone rise throughout gestation, exaggerating their likely effects. For example, a concurrent increase in the $T_H2$ bias of the female immune system (see Section 1.5) is seen with increasing gestation (Klein et al. 2010). Moreover, the risk of influenza infection is highest for females in the third trimester of pregnancy and indeed pregnant mice had higher mortality when infected with pandemic H1N1 influenza than non-pregnant female mice (Robinson and Klein 2012). This is related to an increase in the excess recruitment of neutrophil and CD8+ cytotoxic T-cells to the lung by high oestrogen levels, as this recruitment is beneficial for survival in non-pregnant females where oestrogen is less high (Robinson et al. 2005).

Related to this, the female immune advantage over males appears to decrease following the menopause when sex hormone levels subside in females (Brundin et al. 2021). Females with Turner Syndrome, who have only one functional X-chromosome and have significantly lower oestrogen levels compared to similarly-aged XX females (Wilson et al. 2003), are immunologically most similar to males rather than females (Klein and Flanagan 2016).

Likewise, males with Kleinfelter's Syndrome, who carry an extra X chromosome (XXY) are more immunologically similar to XX females than XY males and this phenotype can be reversed by treatment with testosterone (Kocar et al. 2000). The immune systems of men with androgen deficiencies also better resembles the pro-inflammatory female immune environment as they have higher levels of pro-inflammatory cytokines like TNF-$\alpha$ and IL-1$\beta$, a higher CD4/CD8 ratio, and higher antibody titres than males without androgen deficiencies, highlighting the immune-suppressive role ordinarily played by testosterone (Musabak et al. 2003; Klein and Flanagan 2016).

Lastly, the volume of data collected over the COVID-19 pandemic has offered some insight into the direct impact of sex hormone levels and infectious disease outcome. As might be expected by it's immune-suppressive capacity, levels of serum

testosterone correlate negatively with the severity of mortality and morbidity from COVID-19 (Lanser et al. 2021). This may well explain why elderly males are the highest risk group for COVID-19; with decreasing testosterone levels allowing a stronger immune response with greater symptom severity (Peckham et al. 2020). Concordantly, serum oestrogen levels correlate positively with COVID-19 severity, suggesting a link between a pro-inflammatory response and COVID-19 morbidity (Arnold et al. 2022). Taken together, these support the contribution of sex hormones to the sex discordance in the immune response to viral infection.

## 1.7 Introduction Summary

In summary, there is clear evidence that biological sex plays a role in determining the shape of the immune response, and that there is a clear discordance in both the innate and adaptive responses between males and females. IFN-I plays an integral role in the innate immune response to RNA viruses and antagonism of the IFN-I response is deeply ingrained in RNA viral genomes. There is evidence for sex discordance within the primary pathway for sensing viral infection via TLR7 and in the subsequent production of IFN-I. The IFN-I/TLR7 axis therefore sits at the centre of innate immune sex discordance and thus highlights a role therein for pDCs as the predominant cell type responsible for IFN-I production. Alongside the genetic component, there is also amounting evidence for the influence of sex hormones on the immune system which, if this extends to pDCs, adds an additional layer to innate immune sex discordance in response to viral infection.

To this end, my thesis is divided into four results chapters:

- The first concerns the development of a whole blood assay for studying IFN-I production by pDCs in clinical samples.
- The second utilises this assay to investigate the response of pDCs following BNT162b2 and live-attenuated influenza co-vaccination in adolescents, and investigates the role of androgens in defining pDC IFN-I production.
- The third is a single-cell RNA-seq investigation into potential transcriptional differences between male and female pDCs following TLR7 stimulation.
- The final chapter concerns the role of biological sex in relation to selection of transmitted virus at the HIV-1 transmission bottleneck of heterosexual adult-to-adult transmission pairs.

# 2

# Development of a Whole Blood Assay for the study of pDC IFN-I

This chapter outlines the requirement of a whole blood assay for the study of pDC IFN-I and the steps taken in the development and testing the reliability thereof; as published in the *Journal of Immunological Methods* (Sampson et al. 2022).

## 2.1 Abstract

Central to the sex differences observed in the outcome of infection and vaccination is the innate immune response; specifically the production of type I interferons (IFN-I) by plasmacytoid dendritic cells (pDCs). pDCs are the main source of IFN-I in the body and evaluation of their IFN-I production is therefore critical for studies of innate immune function.

However, reliable measurement of pDC IFN-I is hampered by reduced cell yields and cytokine production after cryopreservation or even after short delays in stimulating freshly isolated PBMCs.

This chapter describes the development of a simple yet robust method for measuring IFN-I production by pDCs that preserves cell activation and cytokine production through immediate stimulation of whole blood and subsequent maintenance at 37°C during laboratory transport and incubation.

## 2.2 Introduction

Differential production of IFN-I by male and female pDCs is a critical sex difference in the innate immune system (see Section 1.4). This leads to differential outcome to infectious disease; especially for RNA viruses where a stronger IFN-I response appears to benefit females in short-term viral control, but becomes detrimental if such inflammation is not resolved into longer-term infection (see Section 1.5.1).

The primary role of the innate immune system during an infection is to curtail immediate pathogen replication, but it has an equally important secondary role in priming and shaping the adaptive immune response (Jaillon et al. 2017). Importantly, there are notable differences between the adaptive immune responses mounted by males and females; with higher inflammation and a $T_H2$ skew in females and lower inflammation and a $T_H1$ skew in males (see Section 1.5).

The role of inflammation-driving cells is therefore central to immune sex differences. The study of immune cell populations is however undermined by the scale of biological heterogeneity between individuals introduced by factors like genetic polymorphisms, epigenetic changes, metabolic differences, and hormonal influences; resulting in low signal-to-noise ratios in human samples.

pDCs however offer a unique window through which to study sex differences in an inflammation-driving cell type since they are the primary, almost exclusive, source of IFN-I in the body (Siegal et al. 1999). Additionally, there is a measurable sex-differential phenotype in pDC IFN-I production and this is underpinned by a clear-cut genetic difference through TLR7 XCI in females (see Section 1.3) giving a stronger signal-to-noise ratio. A reliable assay for the large-scale study of IFN-I production by pDCs is therefore essential to further elucidating and understanding the importance of sex differential IFN-I production and the role of inflammation in sex differences in the wider immune response.

However, the potency of pDCs to incite inflammation is such that their presence in non-lymphoid tissues is negligible and their maintenance outside of infection

is limited to the blood where they still only comprise 0.1-0.5% of total PBMC (Reizis 2019). This presents challenges to blood sample collection where volumes are limited, for example the study of paediatric samples.

Likewise, the auto-immune risk associated with any runaway IFN-I response means pDCs are necessarily primed for apoptosis and therefore the maintenance of their biological activities is severely affected *ex-vivo*. Indeed, after only 4hrs *in-vitro* Grouard et al. 1997 reported levels of spontaneous apoptosis in pDC cultures of at least 40%. Similarly, massive apoptosis is observed for pDCs from mice infected with live Herpes Simplex Virus 1 for 8hrs and mechanistically is attributable to a negative IFN-I feedback loop thought to exist to inhibit self-perpetuation of the IFN-I response (Swiecki et al. 2011).

Thus, whilst conventional immunological assays measuring, for example, T-cell activities are unaffected by prolonged sample transport at ambient temperatures, Meier et al. 2008 observe a marked reduction in the responsiveness of pDCs to synthetic TLR ligands after even a minor delay between blood collection and processing for PBMC isolation. Indeed, when compared to samples processed and stimulated immediately after venepuncture (0hrs) they saw a 50% reduction in the recoverable percentage of IFN-α+ pDCs after only a 6hr delay in processing, increasing to 75% at 12hrs and nearly 90% by 24hrs.

Interestingly, individual pDC production of IFN-α, as measured through mean fluorescence intensity (MFI), dropped 35% from 0hrs to 6hrs but remained stable thereafter for 12hrs and 24hrs, thus reaffirming a role for apoptosis since the percentage of IFN-α+ cells continued to decrease despite no further reduction in their individual IFN-I production (Meier et al. 2008).

The alternative pDC cytokine, TNF-α, appears less sensitive to such delays and displays only a 10% reduction after 6hrs delay, 25% after 12hrs, and 40% by 24hrs (Meier et al. 2008). Therefore, any delays in pDC stimulation following venepunctiure may skew phenotypic observations towards TNF-α and overshadow any IFN-I

phenotype which would be further compounded by the antagonistic relationship between TNF-α and IFN-α in pDCs (see Section 1.3) (Psarras et al. 2021).

Concurrently, Ida et al. 2006 reported maximal IFN-α recovery from pDCs after only 2-3hrs incubation with a synthetic TLR7 agonist. Accordingly, they also reported an almost complete loss of recoverable IFN-α production by pDCs that have been cryopreserved, whilst TNF-α appears mostly preserved.

To this end we set out to establish an assay to measure pDC IFN-I in blood sampled away from the laboratory; hypothesising initially that stimulating pDCs via a TLR7 agonist within fresh PBMCs immediately after isolation would best preserve their *ex-vivo* activity. This was however severely affected by transport times of blood samples to the laboratory and directed the optimisation of a final assay combining immediate TLR7 stimulation of pDCs within the whole blood milieu and maintenance at 37°C during laboratory transport, followed by IFN-I measurement via flow cytometry.

## 2.3 Materials and Methods

### 2.3.1 Ethics Statement

For assay development whole blood was taken in sodium heparin vacutainers (BD), or where specified EDTA vacutainers (BD), from healthy donors (median age 23yrs; range 19-24yrs) in accordance with Human Study Protocols approved by the Research Ethics Committee (REC) at Yorkshire & The Humber – Sheffield (GI Biobank Study 16/YH/0247). Donors were recruited anonymously from a pool of healthy adults and were excluded if they reported illness or vaccination in the last 7 days to prevent obfuscation of the true IFN-I response.

Samples forming a second, larger dataset (median age 36.5yrs; range 6-69yrs) were obtained from healthcare workers and families who responded to an invitation to participate in a study of the immunological response to natural SARS-CoV2 infection in the summer of 2020 before SARS-CoV2 vaccination was available in the United Kingdom. Participants were excluded if they reported illness or vaccination in the last 7 days to prevent obfuscation of the true IFN-I response. Samples were collected in accordance with approval from the University of Oxford Medical Sciences Interdivisional Research Ethics Committee (reference R71346/RE001).

Written, informed consent was obtained for each participant or, in the case of those under 18yrs, assent with parental consent.

### 2.3.2 Stimulation of Whole Blood

Sodium heparin vacutainers (BD) were prepared in advance to contain 1ml R10 [RPMI (Gibco) + 10% FBS (Sigma) + 1% Pen/Strep (Sigma) + 1% L-Glutamine (Gibco)] + 2µg/ml CL097 (Invivogen) + 10µg/ml Brefeldin A (BFA) (BioLegend) and stored at 4°C for up to 18hrs. To achieve a 1:1 ratio, and 2-fold reagent dilution (final concentrations 1µg/ml CL097 + 5µg/ml BFA), 1ml whole blood was then collected directly into the vacutainer. Except for temperature experiments,

vacutainers were then placed in a dry block heater (Fisher) to maintain their temperature at 37°C. Blood was then transferred to sterile 5ml FACS tubes and placed in a 37°C cell culture incubator for requisite incubation durations.

### 2.3.3 PBMC Isolation and Cryopreservation

PBMCs were isolated from concurrently collected whole blood by Ficoll (Lymphoprep) separation in Leukosep tubes (Greiner) (1000g; 15mins; low deceleration), the mononuclear layer aspirated, and washed twice in 50mls RPMI (Gibco) (700g; 5mins, then 200g 7mins) before resuspension in the starting blood volume of R10.

Cells to be cryopreserved were then centrifuged (500g; 3mins) and resuspended in 200µl per-ml-starting-volume FBS + 10% DMSO to freeze at -80C with a Mr Frosty H container (Fisher). Cells remained at -80°C for no more than 14 days before being thawed to stimulate.

To thaw, vials were transferred to a 37°C water bath for 3mins, then cells transferred to Falcon tubes and washed three times in 15mls R10; the final resuspension being of original blood volume.

### 2.3.4 Stimulation of PBMC

5ml FACS tubes were prepared to contain 1ml 2X (R10 + Brefeldin + CL097), as for whole blood (see Section 2.3.2), then 1ml PBMC added. Tubes were then placed in a tissue culture incubator for requisite incubation.

### 2.3.5 Cell Staining for Flow Cytometry

Following incubation, whole blood samples were centrifuged (500g; 3mins) and plasma removed for addition of red blood cell lysis solution (BioLegend) for 20 minutes at room temperature. Tubes were then centrifuged, and resultant white

**Table 2.1:** Antibodies used for pDC Flow Cytometry

| Marker | Fluorophore | Stain | Dilution | Supplier | Catalogue |
|---|---|---|---|---|---|
| Live/Dead | Near-IR | Surface | 1/1250 | Fisher | L10119 |
| CD56 | BV605 | Surface | 1/50 | BioLegend | 318334 |
| CD19 | APC | Surface | 1/50 | BioLegend | 302212 |
| CD3 | AF700 | Surface | 1/50 | BioLegend | 317340 |
| CD14 | BV421 | Surface | 1/50 | BD | 563743 |
| CD11c | BV650 | Surface | 1/50 | BD | 563404 |
| HLA-DR | PE | Surface | 1/25 | BioLegend | 307606 |
| CD123 | PE-Dazzle594 | Surface | 1/25 | BioLegend | 306034 |
| IFN-α | FITC | Intracellular | 1/50 | Miltenyi | 130-116-872 |
| TNF-α | BV711 | Intracellular | 1/50 | BioLegend | 503940 |

cells washed twice more in PBS + 1% FBS + 20mM EDTA before transferring to 96-well plates for staining.

For PBMC experiments, tubes were centrifuged after incubation, the media aspirated, and cells transferred to 96-well plates for staining.

To stain, plates were centrifuged (500g; 2mins) and cells resuspended in 50µl live-dead + surface stain (antibodies detailed in Table 2.1) for 30mins at 4°C. Cells were then washed twice in 200µl PBS + 1% FBS + 20mM EDTA before incubation in 200µl Fixation/Permeabilization solution (Fisher) for 30mins 4°C. Cells were washed twice in Permeabilization Buffer (PB; Fisher) and resuspended in 50µl intracellular stain (antibodies detailed in Table 2.1) for 30mins at 4°C before two final PB washes and final resuspension in 130µl PBS. Stained cells were stored at 4°C for 12-48hrs prior to flow cytometry.

### 2.3.6 Flow cytometry & Sample Analysis

Flow cytometry was performed using an LSR II (BD), and *.fcs* files analysed with FlowJo v10.7.1 (BD). After PBMC, singlet, and live/dead gating, pDCs were defined as: CD56-/CD19-/CD3-/CD11c-/CD14-/CD123+/HLA-DR+ (see gating strategy in Figure 2.1).

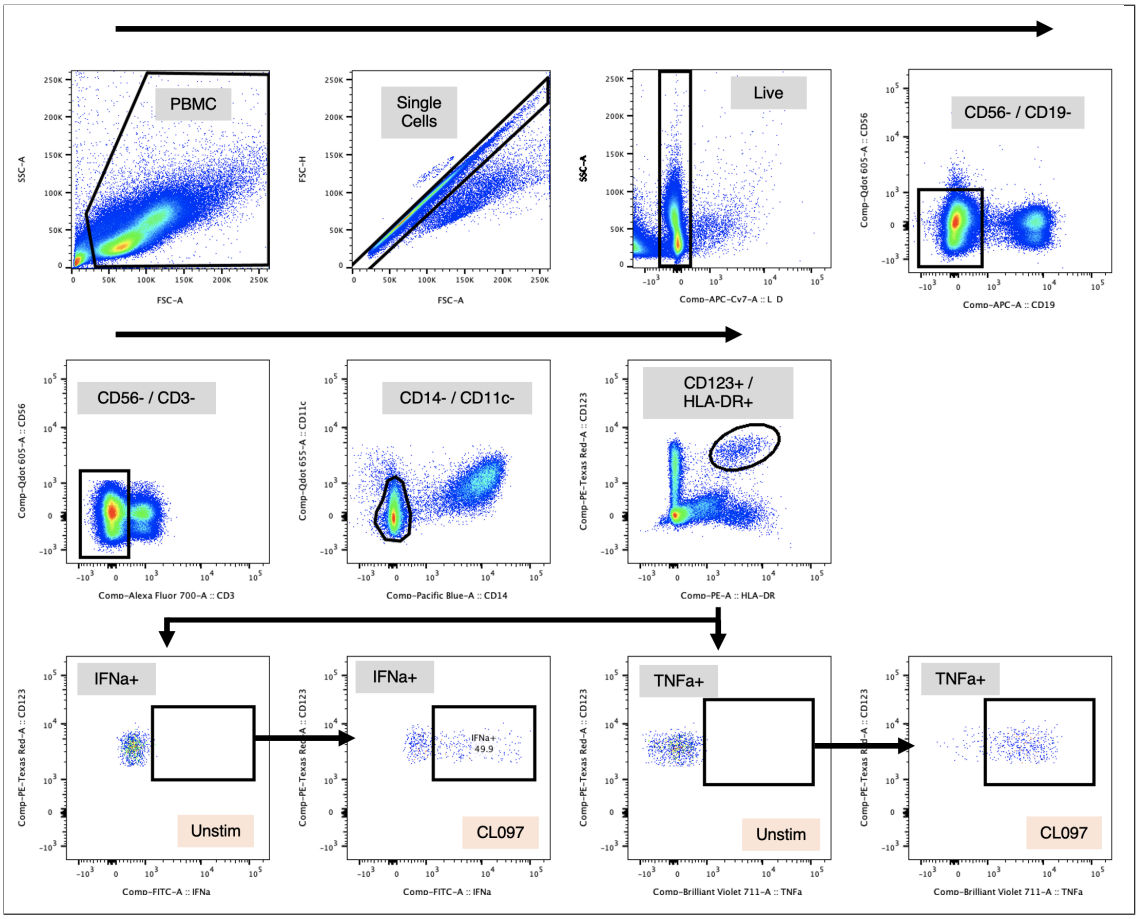



**Figure 2.1: pDC Gating Strategy.** After PBMC, singlet, and live/dead gating, pDCs are defined as: CD56-/CD19-/CD3-/CD11c-/CD14-/CD123+/HLA-DR+. Bottom row has example IFN-α and TNF-α gates (IFNa and TNFa, respectively) set using unstimulated controls and applied to CL097 stimulated samples.

The effect of variability in cytometer performance on MFI was controlled for by using the same 6 reference individuals during assay optimisation.

Graphs were plotted and analysed using R Studio running R v4.2.0 via base R and the package *ggpubr*; two-group continuous variables were analysed with a two-tailed Student's T-test for parametric data or unpaired Wilcoxon test (also known as Mann Witney U) for non-parametric data. Where appropriate, Bonferroni correction was performed for multiple comparisons.

### 2.3.7 Linear Modelling

Linear models to reflect each measured pDC parameter were constructed using R Studio running R v4.2.0 based on log transformed data of interest with sex, age and timepoint as variables. Variables were then separately regressed out of the model and the goodness of fit to the original model evaluated using the Wald Test to ascertain whether fit was significantly altered by removal of the variable for each parameter; p-values were corrected for multiple comparisons using the Bonferroni method.

### 2.3.8 IFN-α ELISA

IFN-α was measured in supernatant collected after stimulation from Whole Blood and PBMC samples for measurement with Human IFN Alpha multi-subtype ELISA (PBL Bioscience) as per manufacturers instruction, using a matrix of 50:50 Human AB Serum to R10 for standards dilution. Final concentration was then normalised to pDC number by dividing by cell count.

## 2.4 Results

### 2.4.1 pDC Stimulation in PBMC is not feasible

When aiming to develop an assay for reliably capturing sex differences in pDC IFN-I production a major consideration was the sample size required to detect the difference seen by other groups (see Section 1.4) where, despite the genetic underpinning, the confounding factors of biological heterogeneity mean there is still considerable overlap in the percentage IFN-α+ pDCs of males and females and the difference in their medians is typically in the region of 10-20%.

I therefore began with a literature search of the various methods employed to measure IFN-I in PBMCs and other mixed cell preparations; detailed in Table 2.2.

The reason for beginning with PBMC was because I was attempting to establish this assay during the COVID-19 pandemic and to maximise the number of samples available I wanted to integrate it with the regular receipt of blood samples our group had for our COVID-19 work. These were collected in EDTA vacutainers and I was concerned that it's $Ca^{2+}$-chelating properties would affect cell activation. However, of the 9 studies in Table 2.2 using PBMCs and specifying the anticoagulant, five used EDTA and four used heparin. I therefore reasoned that there would be no issue in using the EDTA-collected PBMCs processed by our lab.

All but two studies in Table 2.2 targeted TLR7/8 and, omitting $Gag_{RNA1166}$ and $Gp160_{RNA2093}$ due to the chemical instability of RNA-based ligands, 9 of the remaining 15 studies used R848, a TLR7/8-specific agonist. Since pDCs do not express functional TLR8 (see Section 1.3) this can be considered to specifically target TLR7 in pDCs.

R848 was used at varied of concentrations between 1-3µg/ml (Table 2.2) but in light of TLR7 XCI in female pDCs (see Section 1.4), the decision was taken to begin our optimisation with a higher concentration to maximise any observable difference between male and female pDCs by ensuring TLR7 saturation.

**Table 2.2:** Summary of published IFN-I Measurement Conditions

| Reference | Material | Collection | Agonist | Conc. | Incubation | Brefeldin | Measurement | Cells |
|---|---|---|---|---|---|---|---|---|
| Kirchner et al. 1982 | Whole blood | Heparin | PHA, SEA, ConA & OKT-3 | 2.5-20µg/ml | 24hrs | N/A | Inhibition of CPE by supernatant | Non-specific |
| McNerlan et al. 2002 | Whole blood | Heparin | PMA | 25ng/ml | 4hrs | All 4hrs | Flow Cytometry | CD3+ lymphocytes |
| Berghöfer et al. 2006 | PBMC | Heparin | R837 & R848 | Both 1µg/ml | 4hrs | N/A | ELISA | Non-specific |
| Ida et al. 2006 | Whole blood | Heparin | R848 | 10mM | 3hrs | Last 2hrs | Flow Cytometry | pDCs |
| Ida et al. 2006 | PBMC | Heparin | R848 | 10mM | 3hrs | Last 2hrs | Flow Cytometry | pDCs |
| Ida et al. 2006 | Cryopreserved PBMC | Heparin | R848 | 10mM | 3hrs | Last 2hrs | Flow Cytometry | pDCs |
| Meier et al. 2009 | PBMC | Not specified | CL097 | 1µg/ml | 6hrs | All 6hrs | Flow Cytometry | pDCs |
| Meier et al. 2009 | PBMC | Not specified | $Gag_{RNA1166}$ & $Gp160_{RNA2093}$ | 15µg/ml | 20hrs | All 20hrs | Flow Cytometry | pDCs |
| Seeds and Miller 2011 | Splenocytes | Tissue | CpG ODN2216 | 1µM | 9hrs | Last 4hrs | Flow Cytometry | pDCs |
| Seeds and Miller 2011 | Splenocytes | Tissue | CpG ODN2216 | 1µM | 9hrs | N/A | ELISA | Non-specific |
| Seillet et al. 2012 | PBMC | Not specified | R848 | 1-3/ml | 5hrs | Last 3hrs | Flow Cytometry | pDCs |
| Seillet et al. 2012 | PBMC | Not specified | R848 | 1-3µg/ml | 24hrs | N/A | ELISA | Non-specific |
| Coch et al. 2013 | Whole blood | EDTA & Heparin | R848 | 0.01-10µM | 48hrs | N/A | ELISA | Non-specific |

| | | | | | | | | |
|---|---|---|---|---|---|---|---|---|
| Laffont et al. 2014 | Humanised mice BM | Tissue | R848 | 1µg/ml | 5hrs | Last 3hrs | Flow Cytometry | pDCs |
| Laffont et al. 2014 | Humanised mice BM | Tissue | $Gag_{RNA1166}$ & $Gp160_{RNA2093}$ | Not specified | 5hrs | Last 3hrs | Flow Cytometry | pDCs |
| Ziegler et al. 2017 | PBMC | EDTA | CL097 | 1µg/ml | 16hrs | All 16hrs | Flow Cytometry | pDCs |
| Tran et al. 2019 | Whole Blood | Heparin | LPS | 2ng/ml | 4, 8, & 24hrs | During staining | Flow Cytometry | pDCs |
| Webb et al. 2019 | PBMC | Heparin | R848 | 1µg/ml | 20hrs | All 20hrs | Flow Cytometry | pDCs |
| Webb et al. 2019 | PBMC | Heparin | R848 | 1µg/ml | 16hrs | N/A | ELISA | Non-specific |
| Rodrigues et al. 2020 | Whole blood | TruCulture Tube | IFN-β | 25ng/ml | 22hrs | N/A | SIMOA | Non-specific |
| Hagen et al. 2020 | PBMC | EDTA | CL097 | 1µg/ml | 6hrs | All 6hrs | Flow Cytometry | pDCs |
| Hagen et al. 2020 | PBMC | EDTA | CL097 | 1µg/ml | 2hrs | N/A | ELISA | Non-specific |
| Hagen et al. 2020 | Purified frozen pDCs | EDTA | CL097 | 1µg/ml | 2hrs | N/A | qPCR | pDCs |
| Abbas et al. 2022 | PBMC | Not specified | R848 | 1.5µg/ml | 5hrs | Last 3hrs | Flow Cytometry | pDCs |
| Abbas et al. 2022 | PBMC | Not specified | $Gag_{RNA1166}$ | 130µg/ml | 5hrs | Last 3hrs | Flow Cytometry | pDCs |

**Agonists:** PHA = phytohaemagglutanin (non-specific); SEA = Staphylococcal Endotoxin A (non-specific); ConA = concanavalin A (non-specific); OKT-3 = orthoclone (non-specific); PMA = Phorobol Myristate Acetate (non-specific); R837 = imiquimod (TLR7-specific); R848 = resiquimod (TLR7/8-specific); CL097 = imidazoquinoline (TLR7/8-specific); $Gag_{RNA1166}$ & $Gp160_{RNA2093}$ = HIV-derived ssRNA (TLR7/8-specific); CpG ODN2216 = ODN Class A (TLR9-specific); LPS = lipopolysaccharide (TLR4-specific). **Measurement:** CPE = cytopathic effect; ELISA = Enzyme-linked Immunosorbent assay; SIMOA = propriety biomarker bead-based fluorescence detection.

Measurement of the IFN-I produced by ELISA, whilst offering higher throughput than flow cytometry, would not allow for specific attribution of any sex differences in IFN-I to pDC. A flow cytometry -based method was therefore chosen to allow IFN-α to be measured specifically within gated pDCs.

Thus, incubation required the addition of brefeldin A for the retention of secretory cytokines within cells for detection, but there was little consensus for incubation length or point of brefeldin addition in the literature search (Table 2.2). Therefore, since blood would arrive in our lab between mid-morning and mid-afternoon, an overnight incubation with brefeldin from T=0 was chosen to limit the need to undertake lab work outside working hours.

Summarised in Table 2.3 are the conditions trialled during the optimisation period that followed, during which measurable IFN-α levels in stimulated samples were no higher than for unstimulated gating controls despite varying: ligand concentrations, incubation time, and point of brefeldin addition. R837 was used as a TLR7-specific control.

**Table 2.3:** Unsuccessful PBMC stimulation optimisation conditions

| Experiment | Material | Collection | Agonist | Concentration | Incubation | Brefeldin |
|---|---|---|---|---|---|---|
| Stim. 1.1 | PBMC | EDTA | R837 | 5µg/ml | 24hrs | Last 6hrs |
| Stim. 1.2 | PBMC | EDTA | R848 | 5µg/ml | 24hrs | Last 6hrs |
| Stim. 2.1 | PBMC | EDTA | R837 | 5µg/ml | 18hrs | All 18hrs |
| Stim. 2.2 | PBMC | EDTA | R848 | 5µg/ml | 18hrs | All 18hrs |
| Tit. 1 | PBMC | EDTA | R837 | Titration 10, 5, 2.5, 1.25 µg/ml | 18hrs | All 18hrs |
| Tit. 2 | PBMC | EDTA | R848 | Titration 10, 5, 2.5, 1.25 µg/ml | 18hrs | All 18hrs |
| Low Stim. 1.1 | PBMC | EDTA | R837 | 1µg/ml | 18hrs | All 18hrs |
| Low Stim. 1.2 | PBMC | EDTA | R848 | 1µg/ml | 18hrs | All 18hrs |
| Low Stim 1.3 | PBMC | EDTA | CL097 | 1µg/ml | 18hrs | All 18hrs |

### 2.4.2 pDC IFN-I production can be captured by direct stimulation of whole blood

With growing concerns for the loss of pDC activity with the prolonged time *ex-vivo* incurred by sample transport and PBMC isolation (Meier et al. 2008), I turned alternatively to IFN-I measurement following stimulation of whole blood (Table 2.2) to remove the PBMC processing time from the delay between blood sampling and stimulation. Additionally, in discussions with collaborators, CL097 was recommended as an alternative TLR7/8 agonist (Hagen et al. 2020). CL097 is a water soluble derivative of R848 which removed the need to use the diluent Dimethyl sulfoxide (DMSO), which has been shown to reduce cytokine production in primary cell culture at a concentration of 0.1% (v/v) (De Abreu Costa et al. 2017), as used here. Table 2.4 summarises the conditions trialled with whole blood stimulations.

### 2.4.3 Sex differential IFN-I production by pDCs is lost after overnight incubation

The final two experiments in Table 2.4, WB4 and WB5, both yielded percentages of IFN-α+ pDCs in line with that seen across the literature; roughly 30-50% for males and 40-60% for females (data not shown). Serendipitously only heparin vacutainers were available for WB4 and WB5, and improved recovery of pDC IFN-α such that the decision was taken to use heparin as the anticoagulant going forwards.

As discussed above (see Section 2.4.1), sample arrival timings meant 6hrs incubation was inconvenient for a recurrent basis and I therefore wanted to determine if the sex difference in the percentage of IFN-α+ pDCs (see Section 1.4) is captured at 18hrs when compared to 6hrs, and whether either capture the significant sex difference reported in the literature.

Whole blood samples were taken from 168 healthy donors, immediately stimulated in-tube and transported to the laboratory for further incubation up to 6hrs (n=99;

**Table 2.4:** pDC Stimulation Optimisation Conditions

| **Experiment** | **Material** | **Collection** | **Agonist** | **Concentration** | **Incubation** | **Brefeldin** |
|---|---|---|---|---|---|---|
| WB 1 | Whole blood | EDTA | CL097 | 1µg/ml | 20hrs | All 20hrs |
| WB 2 | Whole blood | EDTA | CL097 | 1µg/ml | 20hrs | Last 19hrs |
| WB 3 | Whole blood | EDTA | CL097 | 1µg/ml | 20hrs | Last 18hrs |
| WB 4 | Whole blood | Heparin | CL097 | 1µg/ml | 18hrs | All 18hrs |
| WB 5 | Whole blood | Heparin | CL097 | 1µg/ml | 6hrs | All 6hrs |

male n=44 & female n=55) or overnight to 18hrs (n=69; male n=33 & female n=36), see Figure 2.2.

As expected, pDC recovery at 18hrs was significantly lower than at 6hrs for both raw count and percentage of live cells (Figure 2.2a. & b.). Accordingly, there was also a significant decrease in the percentage of IFN-α+ pDCs between 6hrs and 18hrs (p=0.0036) (Figure 2.2c.).

Interestingly, when stratified by sex, there was a significant decrease for pDC recovery only for females between 6hrs and 18hrs for both raw count (p=0.0045) and percentage of live cells (p=0.032) (Figure 2.2d. & e.), and this was reflected by a concurrent significant decrease in the percentage of IFN-α+ pDCs (p=0.038) (Figure 2.2f.). This is not seen for males and their IFN-α production is therefore comparable at 18hrs to 6hrs.

A sex difference is seen between the median percentage of IFN-α+ pDCs in males (41.5%) and females (53.7%) at 6hrs (p=0.13 after correction for multiple comparison) but there is no difference after 18hrs between males (40.0%) and females (44.5%) (p>0.99 after correction for multiple comparison) in line with a significant decrease for females (p=0.038) (Figure 2.2f.).

Thus it appears that whilst female cells produce more IFN-α than males in the short-term, this difference is lost with overnight incubation and a shorter incubation is essential for capturing sex differential IFN-α production by pDCs in whole blood.

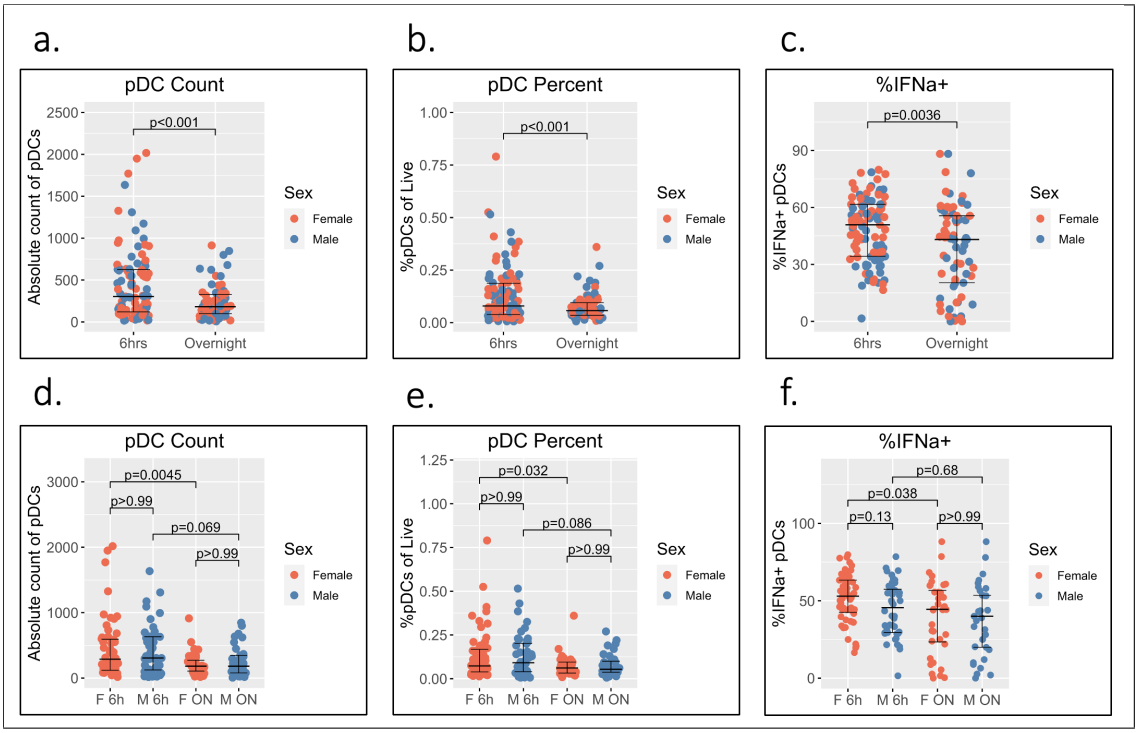



**Figure 2.2: Comparison of in-tube stimulated whole blood incubated for 6hrs or overnight** Blood was drawn for immediate in-tube stimulation as Section 2.3.2 for 168 healthy donors (male n=77 [blue] & female n=91 [red]) and, after transport to the laboratory, was incubated for a further 6hrs total (n=99; male n=44 & female n=55) or overnight (n=69; male n=33 & female n=36). Samples done in duplicate per donor. a), b), c) total cohort data for: raw count of gated pDCs, gated pDCs as a percentage of total Live cells, and percentage of gated pDCs expressing IFN-α (IFNa), respectively. d), e), f) sex-stratified data for: raw count of gated pDCs, gated pDCs as a percentage of total Live cells, and percentage of gated pDCs expressing IFN-α (IFNa), respectively. Pairwise comparisons were performed using Student's unpaired T-test for equal variance with Bonferroni correction for multiple comparisons. Bars show median with interquartile range.

### 2.4.4 Kinetics of the pDC response to CL097 in Whole Blood

Having established that whole blood stimulation can capture the widely-published sex differential production of IFN-I by pDCs, but that this sex difference is lost after prolonged incubation (see Section 2.4.3), it was then pertinent to investigate the kinetics of the pDC response to immediate stimulation in whole blood to understand this phenotype. I therefore began with a time course of incubation times spanning

2-24hrs, see Figure 2.3.

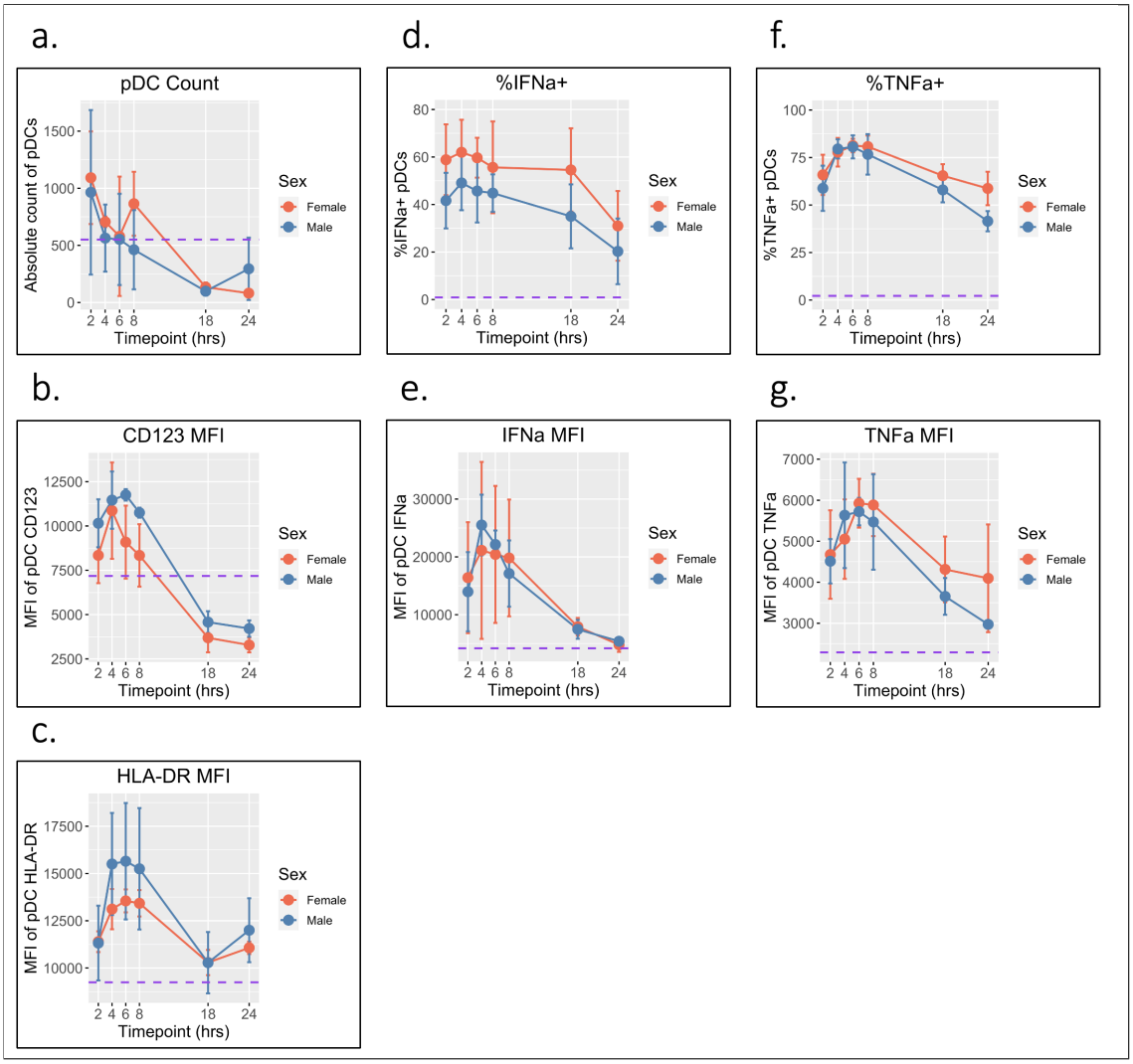



**Figure 2.3: Kinetics of pDC response to CL097 in Whole Blood.** Timecourse of pDC activation and cytokine production in whole blood stimulated immediately with CL097 in-tube (as Section 2.3.2) for 6 healthy donors (male n=3 [blue] & female n=3 [red]). Timepoints done in duplicate per donor. Dashed purple line represents the average of unstimulated controls processed at 4hrs. a) raw count of gated pDCs. b), c), e), g) mean fluorescence intensity (MFI) for gated pDCs of: CD123, HLA-DR, IFN-α (IFNa), and TNF-α (TNFa) respectively. d), f) percentage of gated pDCs expressing IFN-α(IFNa) and TNF-α (TNFa) respectively.

As in previous studies, there is a marked decrease in pDC numbers with time; with numbers especially low after overnight incubation (Figure 2.3a.). Activation within

pDCs through HLA-DR upregulation shows an increase in MFI to a plateau between 2hrs and 8hrs, which falls to baseline levels following overnight incubation (Figure 2.3c.). pDC activation through CD123 upregulation also follows a similar time course and interestingly falls below baseline levels following overnight incubation (Figure 2.3b.).

The percentage of pDCs expressing IFN-α does not differ significantly after 2-8hrs and decreases slowly out to 18hrs, before falling approximately 50% after 24hrs incubation (Figure 2.3d.). The MFI of the IFN-α+gate shows a similar time course (Figure 2.3e.).

TNF-α production and TNF-α MFI both show similar time courses to IFN-α production, with peak levels after 4-8hrs incubation (Figure 2.3f. & g.).

A regression analysis was also performed to identify differences in age, sex, and timepoint on the parameters evaluated in Figure 2.3 and showed that timepoint significantly impacted all. HLA-DR was the least influenced by timepoint but only became not significant after correcting for multiple comparisons (p=0.0230 before correction). Age was sufficiently controlled for and was not a significant factor in any parameter, but sex was determinant of the percentage of IFN-α pDCs and CD123 MFI (see Table 2.5).

**Table 2.5:** Regression coefficient p-values for whole blood time course

| **Parameter** | **Timepoint** | **Sex** | **Age** |
|---|---|---|---|
| pDC Count | 1.7e-14 | >0.99 | >0.99 |
| CD123 MFI | 6.6e-16 | 0.003 | 0.365 |
| HLA-DR MFI | 0.069 | >0.99 | 0.176 |
| %IFN-α+ | 1.7e-7 | 0.017 | 0.279 |
| IFN-α MFI | 9,9e-10 | >0.99 | >0.99 |
| %TNF-α+ | 4.8e-5 | 0.101 | >0.99 |
| TNF-α MFI | 6.2e-7 | >0.99 | >0.99 |

In summary, peak pDC activation and cytokine responses were observed after 4-8hrs incubation.

### 2.4.5 6hrs incubation best captures sex differential pDC activation and IFN-α production

Many studies in the literature repot that female pDCs produce more IFN-α than males when stimulated *in-vitro* (see Section 1.4), and indeed in the regression model for the time course sex was identified as a significant influence of the percentage of IFN-α+ pDCs (Table 2.5). I therefore considered the time course to determine whether other immune sex differences are apparent even among this small number of study participants.

The percentage of pDCs producing IFN-α was approximately 20% higher among females (Figure 2.3d.) which is consistent with the magnitudes seen in previous studies (Meier et al. 2009; Webb et al. 2019; Hagen et al. 2020). The MFI of IFN-α remained comparable between males and females (Figure 2.3e.) which suggests sex differential IFN-I production is not determined by the amount of IFN-I produced per cell, but rather the percentage of cells that produce IFN-I.

HLA-DR expression was markedly higher for male pDCs than female pDCs between 4-8hrs incubation (Figure 2.3c.). A similar pattern was also seen for CD123 (Figure 2.3b.); the sex-differential expression of which was also identification in a regression model (Table 2.5).

By contrast with IFN-α production, TNF-α production by pDCs was broadly similar for males and females studied at 2-8hrs incubation, with increased TNF-α production in females seen after overnight incubation (Figure 2.3).

Based on these data, the time points after pDC stimulation with CL097 that best capture the sex differential activation of pDCs and IFN-α production are 4-8hrs incubation. On this basis, and the fact that 6hrs represented the peak of CD123,

IFN-α MFI, and TNF-α production by pDCs, the single incubation time chosen for the whole blood assay going forwards was 6hrs incubation.

### 2.4.6 pDC activation and IFN-α production is highest in immediately in-tube stimulated whole blood

Since even a short delay in processing of PBMCs has reportedly resulted in significant reductions in pDC activity (see Section 2.2), the next step was to determine whether immediate stimulation of pDCs within whole blood does indeed best capture both cell activation and cytokine production.

Blood was therefore drawn from four healthy donors, matched for sex and age, and subjected to three conditions:

- Immediate in-tube stimulation and incubation using a dry block-heater (Thermo) for 2hrs, followed by transfer to a tissue culture incubator for a further 4hrs (denoted "WB")
- Kept at room temperature for 2hrs — to simulate transport from clinic to the laboratory — then PBMCs isolated and stimulated for 6hrs in a tissue culture incubator (denoted "PBMC")
- Remaining PBMCs from "PBMC" prior to stimulation were cryopreserved and thawed <14 days later for the same 6hrs stimulation (denoted "Frozen PBMC")

pDC yields in WB were similar to, or somewhat higher than, for PBMC (Figure 2.4a.), but pDC activation through CD123 and HLA-DR upregulation was consistently higher in WB than both other groups (2.4b. & c.).

Predictably, the percentage of IFN-α+ pDCs was substantially lower in Frozen PBMC (Figure2.4d.), except in one case — Donor 4207 — where pDC counts were

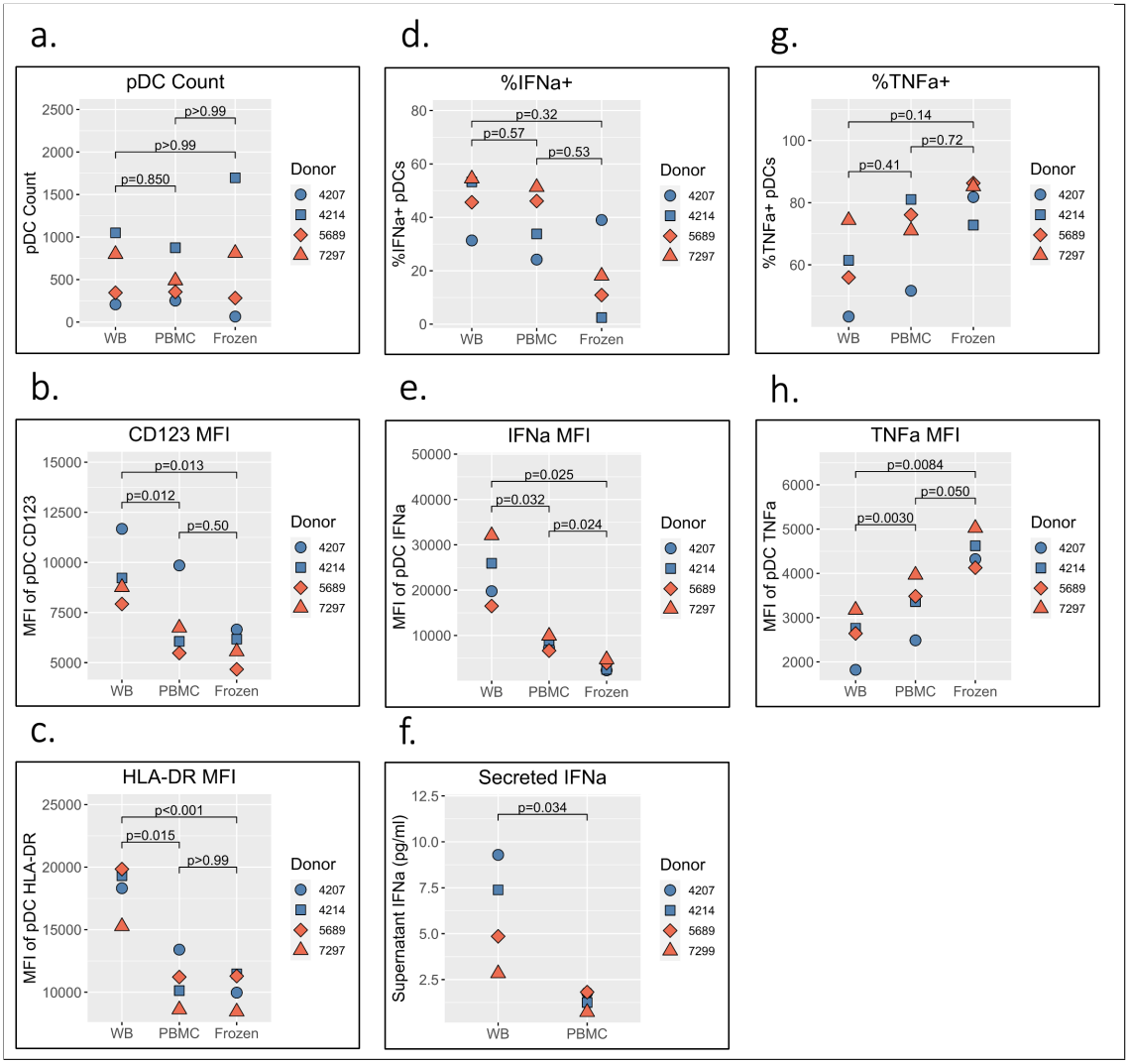



**Figure 2.4: pDC activation and IFN-α production in whole blood compared to PBMC and cryopreserved PBMC.** Blood was taken from 4 healthy donors (male n=2 [blue] & female n=2 [red]) and subjected to three conditions: i) immediate stimulation as for Section 2.3.2; maintained at 37°C by dry block heater for 2hrs, then incubated for a further 4hrs [WB], ii) PBMC isolated after 2hrs incubating blood at room temperature then stimulated for 6hrs [PBMC], iii) remaining PBMC's from ii) cryopreserved and thawed before 6hrs stimulation [Frozen PBMC]. Experiments were performed in duplicate per donor. a) raw count of gated pDCs. b), c), e), h) mean fluorescence intensity (MFI) for gated pDCs of: CD123, HLA-DR, IFN-α (IFNa), and TNF-α (TNFa) respectively. d), g) percentage of gated pDCs expressing IFN-α (IFNa) and TNF-α (TNFa) respectively. f) ELISA measurement of secreted IFN-α (IFNa) from a repeat experiment in the absence of brefeldin for just WB and PBMC. Pairwise comparisons performed via Student's paired T-test for equal variance with Bonferroni correction for multiple comparisons.

extremely low (Figure 2.4a.). In all cases however IFN-α MFI was lowest in Frozen PBMC (Figure 2.4e.).

Since the IFN-α MFI was significantly lower for PBMC than WB despite similar percentages of IFN-α+ pDCs, it was requested by a reviewer that IFN-α secretion was investigated. ELISA measurement of supernatant collected following stimulation confirmed significantly higher secretion of IFN-α for WB when compared to PBMC ($p=0.034$) (Figure 2.4f.).

By contrast, TNF-α production followed the converse pattern to IFN-α, with the percentage of TNF-α+ pDCs and TNF-α MFI being consistently lowest in WB (Figure 2.4g. & h.).

This tallies with that seen by Ida et al. 2006 and Psarras et al. 2021 insomuch as the cryopreserved pDCs produce less IFN-α whilst retaining full TNF-α production; antagonising and further reducing IFN-α production.

Therefore, the delay of processing blood to obtain PBMCs before stimulation is detrimental to the faithful recovery of pDC activation and cytokine production, and performing the assay with whole blood offers a way to immediately stimulate pDCs such that their behaviour still represents their true *in-vivo* activity.

### 2.4.7 pDC cytokine production is best maintained at 37°C

Since the use of the dry block-heater requires an electricity supply, the next step was to determine the necessity of this in the context of clinical research for sample transport between the clinic and laboratory. The effect of maintaining samples at 37°C during 2hrs simulated transport, opposed to ambient temperatures or refrigeration at 4°C was therefore compared.

Blood was again drawn from four healthy donors, matched for sex and age, for immediate stimulation in-tube as Section 2.3.2 and subjected to the three conditions:

- 2hrs incubation at 37°C in the dry block-heater before incubation in a tissue culture incubator up to 6hrs (denoted "37C")
- 2hrs incubation at room temperature (20-25°C) before incubation in a tissue culture incubator up to 6hrs (denoted "RT")
- 2hrs incubation in a transport box maintained at 4°C with ice packs before incubation in a tissue culture incubator up to 6hrs (denoted "4C")

Unexpectedly, pDC counts were highest in samples incubated at RT in all four donors (Figure 2.5a.), as was CD123 MFI though to a lesser extent (Figure 2.5b.). However, HLA-DR expression was highest following incubation at 37°C (Figure 2.5 c.). Similarly, the percentage of IFN-α+ and TNF-α+ pDCs as well as the MFI of both cytokines was also highest after incubation at 37°C (Figure 2.5d., e., f., & g.).

Therefore, in order to maximise the window for capturing sex difference in pDC IFN-I by preserving pDC activation and cytokine production, maintenance at 37°C is essential.

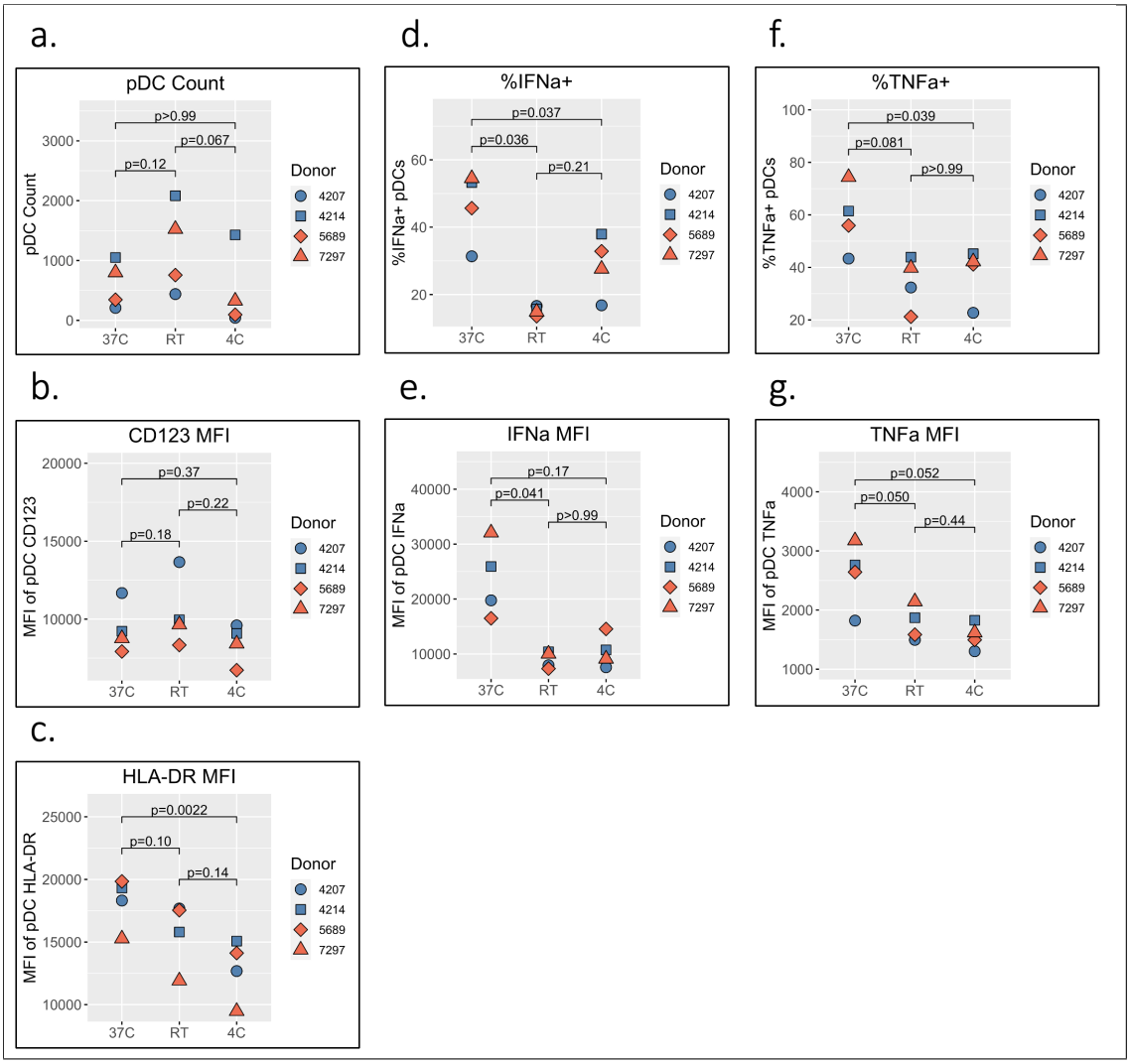



**Figure 2.5: Effect of simulated transport temperature on pDC activation and cytokine response.** Blood was taken from 4 healthy donors (male n=2 [blue] & female n=2 [red]) and incubated at either i) 37°C [37C], ii) room temperature (20-25°C) [RT], or iii) 4°C for 2hrs [4C] before 4hrs further incubation in a tissue culture incubator up to 6hrs post-stimulation. Conditions were done in duplicate per donor. a) raw count of gated pDCs. b), c), e), g) mean fluorescence intensity (MFI) for gated pDCs of: CD1123, HLA-DR, IFN-α (IFNa), and TNF-α (TNFa) respectively. d), f) percentage of gated pDCs expressing IFN-α (IFNa) and TNF-α (TNFa) respectively. Pairwise comparisons performed via Student's paired T-test for equal variance with Bonferroni correction for multiple comparisons.

### 2.4.8 Low temporal variability between biological repeats confirms longitudinal robustness

When studying human populations there is implicit temporal intra-donor heterogeneity and I therefore sought to determine the reproducibility of the assay through longitudinal sampling of the same 6 donors, matched for sex and age (Figure 2.6).

As expected when dealing with such a small population, there was variability in pDC numbers in the blood of the same individuals sampled at different time points (Figure 2.6a.). However, the other parameters measured were largely consistent for the 6 donors.

With the exception of one donor, 7296, CD123 varies only slightly with day, appearing to shift in the same pattern for all donors (Figure 2.6b.). Likewise, although HLA-DR varies more, it does so with the same pattern for each donor (Figure 2.6c.). This may represent small shifts in laser alignment and thus daily CST settings of the flow cytometer, especially when considering the heavy demolition occurring next-door to the Peter Medawar Building at the time. Indeed, although more consistent than CD123 and HLA-DR, the MFIs for IFN-α and TNF-α are both higher for Day 0 but then mostly consistent for Days 7, 13, and 20 (Figure 2.6e. & g.).

Nonetheless, the main difference cited between male and female pDCs is the percentage of IFN-α+ pDCs and this displays remarkable consistency across all four time points for each donor (Figure 2.6d.), as does the percentage of TNF-α+ as the secondary pDC cytokine (Figure 2.6f.).

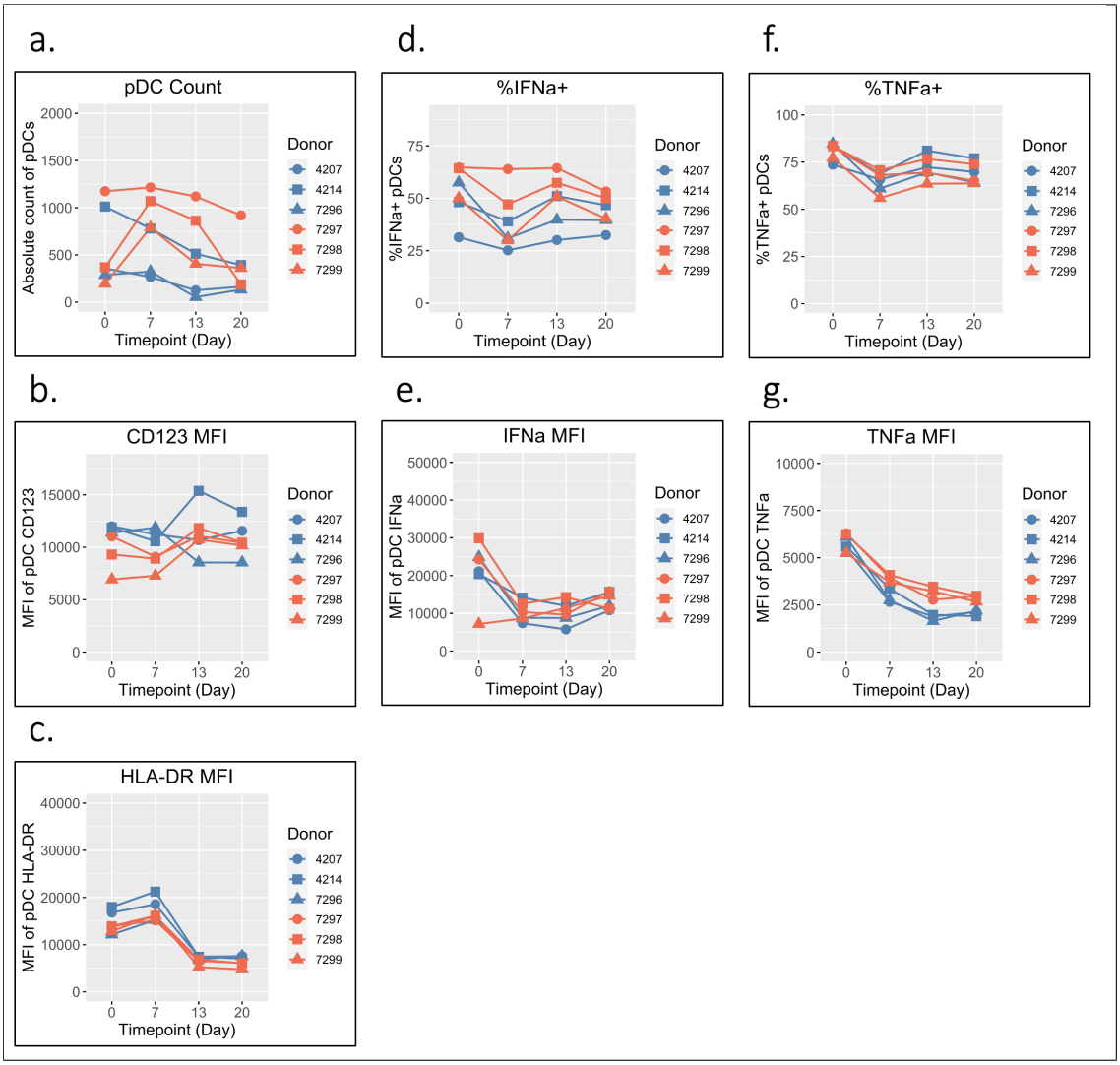



**Figure 2.6: Longitudinal robustness of pDC activation and cytokine production for individual donors.** Assay reproducibility over 4 weeks for 6 healthy donors (male n=3 [blue] & female n=3 [red]) for immediately in-tube stimulated blood maintained at 37°C and incubated for 6hrs as described in Section 2.3.2. a) raw count of gated pDCs. b), c), e), g) mean fluorescence intensity (MFI) for gated pDCs of: CD123, HLA-DR, IFN-α (IFNa) , and TNF-α (TNFa) respectively. d), f) percentage of gated pDCs expressing IFN-α (IFNa) and TNF-α (TNFa) respectively.

With these variabilities in mind, I wanted to confirm whether the assay is sufficiently robust to consistently detect sex differences in pDC behaviour and grouped the four time points by sex (Figure 2.7).

Interestingly, this revealed a potential sex difference for raw pDC numbers as they appear to have greater variability in females with time (Figure 2.7a.). Similarly, sex-stratifying the data in this way reveals a further inverse relationship between pDC count and CD123 since CD123 MFI dips in females at Day 7 which coincides with a spike in pDC number; whereas both are more consistent in males (Figure 2.7a. & b.).

Additionally, as seen in the time course (Figure 2.3b.), male CD123 expression is consistently higher than for females (Figure 2.7b.), as is HLA-DR (Figure 2.7c.).

Most importantly, the percentage of IFN-α+ pDCs remains consistently higher in females throughout, and the difference between males and females remains approximately 15% (Figure 2.7d.). There is consistently no difference for the percentage of TNF-α pDCs (Figure 2.7f.), nor is there a noteworthy difference between males and females for the MFI of both IFN-α and TNF-α (Figure 2.7e. & g.).

I therefore concluded that the whole blood assay was sufficiently robust to temporal changes and was suitable to detect sex differences in pDC behaviour in a research setting.

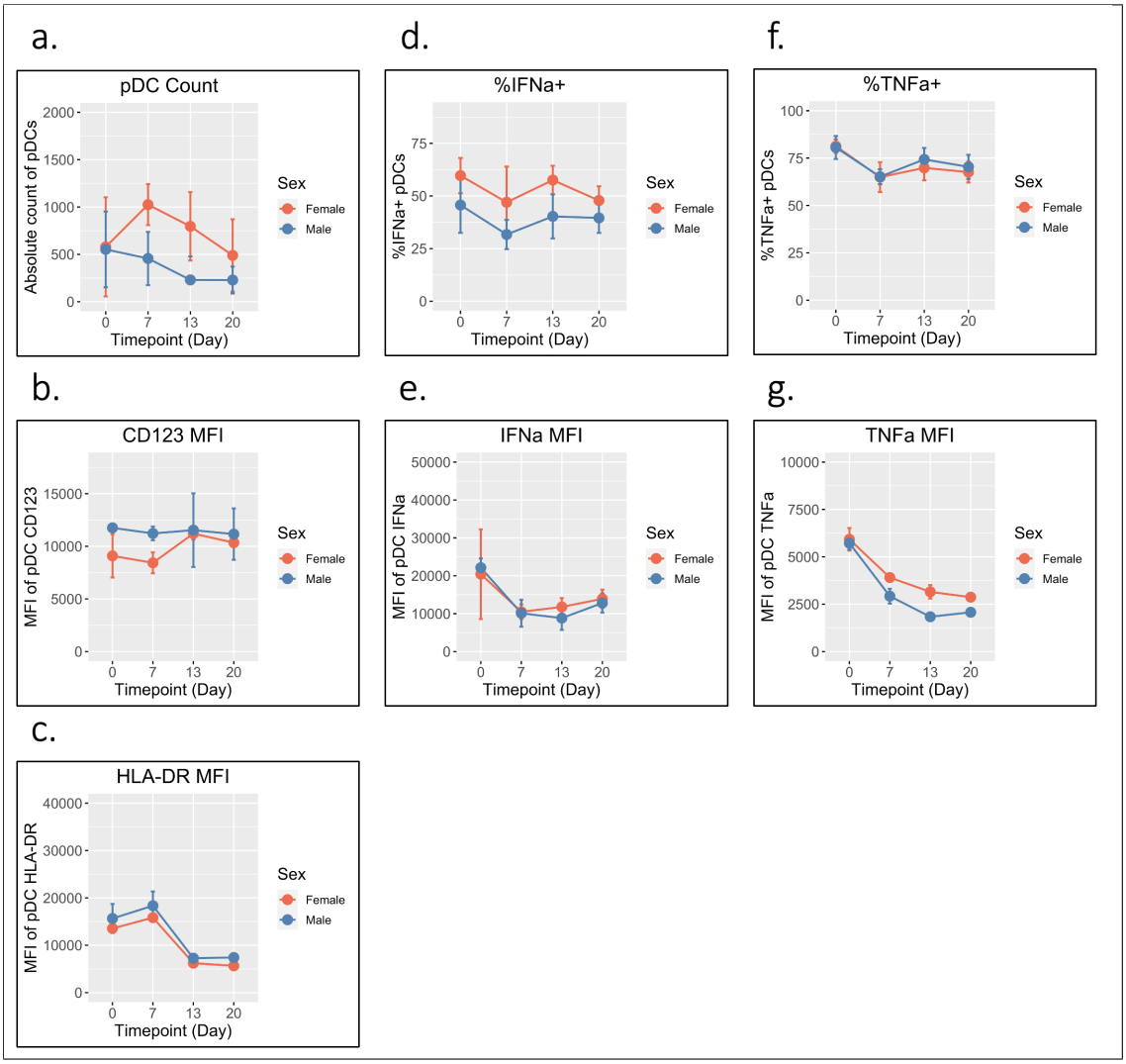



**Figure 2.7: Longitudinal robustness of pDC activation and cytokine production grouped by sex.** Assay reproducibility over 4 weeks for male and female donors (male n=3 [blue] & female n=3 [red]) for immediately in-tube stimulated blood maintained at 37°C and incubated for 6hrs as described in Section 2.3.2. a) raw count of gated pDCs. b), c), e), g) mean fluorescence intensity (MFI) for gated pDCs of: CD123, HLA-DR, IFN-α (IFNa), and TNF-α (TNFa) respectively. d), f) percentage of gated pDCs expressing IFN-α (IFNa) and TNF-α (TNFa) respectively.

### 2.4.9 Whole blood assay demonstrates a sex difference in pDC IFN-α response in a clinical research setting

Since the initial time course and regression model successfully identifies sex as a factor in the expression of IFN-α by pDCs (see Section 2.4.4), and the whole blood assay appears capable of reliably detecting this difference (see Section 2.4.8, I finally sought to confirm the suitability of the assay to a clinical setting and that it is sufficiently sensitive to detect the widely-reported increased production of IFN-α by female pDCs (Figure 2.8).

Blood was taken from 109 individuals (male n=44 & female n=65) spanning a range of ages (median age 36.5yrs; range 6-69yrs) enrolled on a study of healthcare workers and their families. Blood was immediately stimulated in-tube as Section 2.3.2 and the dry block-heater used to maintain samples at 37° immediately after sampling and during transport to the laboratory (median 2hrs). Data was stratified by age group to reflect broad hormonal stages; pre-pubertal (<8yrs), pubertal (9-15yrs), post-pubertal adult (16-54yrs), post-menopausal adults (>55yrs) (Figure 2.8) and there was no difference in the age distribution between males and females (Figure 2.8a.).

In line with the observations above, and whilst not stastically significant, CD123 expression appears higher in pubertal and post-pubertal males, interestingly decreasing below females in the older age group (Figure 2.8b.), supporting a hormonal role in pDC activation via CD123 expression. HLA-DR expression is broadly similar between male and female pDCs across all age groups (Figure 2.8c.).

The percentage of IFN-α+ pDCs is significantly lower for males than females in the post-pubertal adult group and does not differ for any other group (Figure 2.8d.). Consistent with previous observations, the MFI of pDC IFN-α does not differ between males and females for any age group (Figure 2.8e.), nor is there any difference in the percentage of TNF-α+ pDCs or MFI of pDC TNF-α (Figure 2.8f. & g.).

The whole blood assay is therefore suitable for use in a research setting to detect differences in IFN-I production by male and female pDCs when age is sufficiently controlled for.

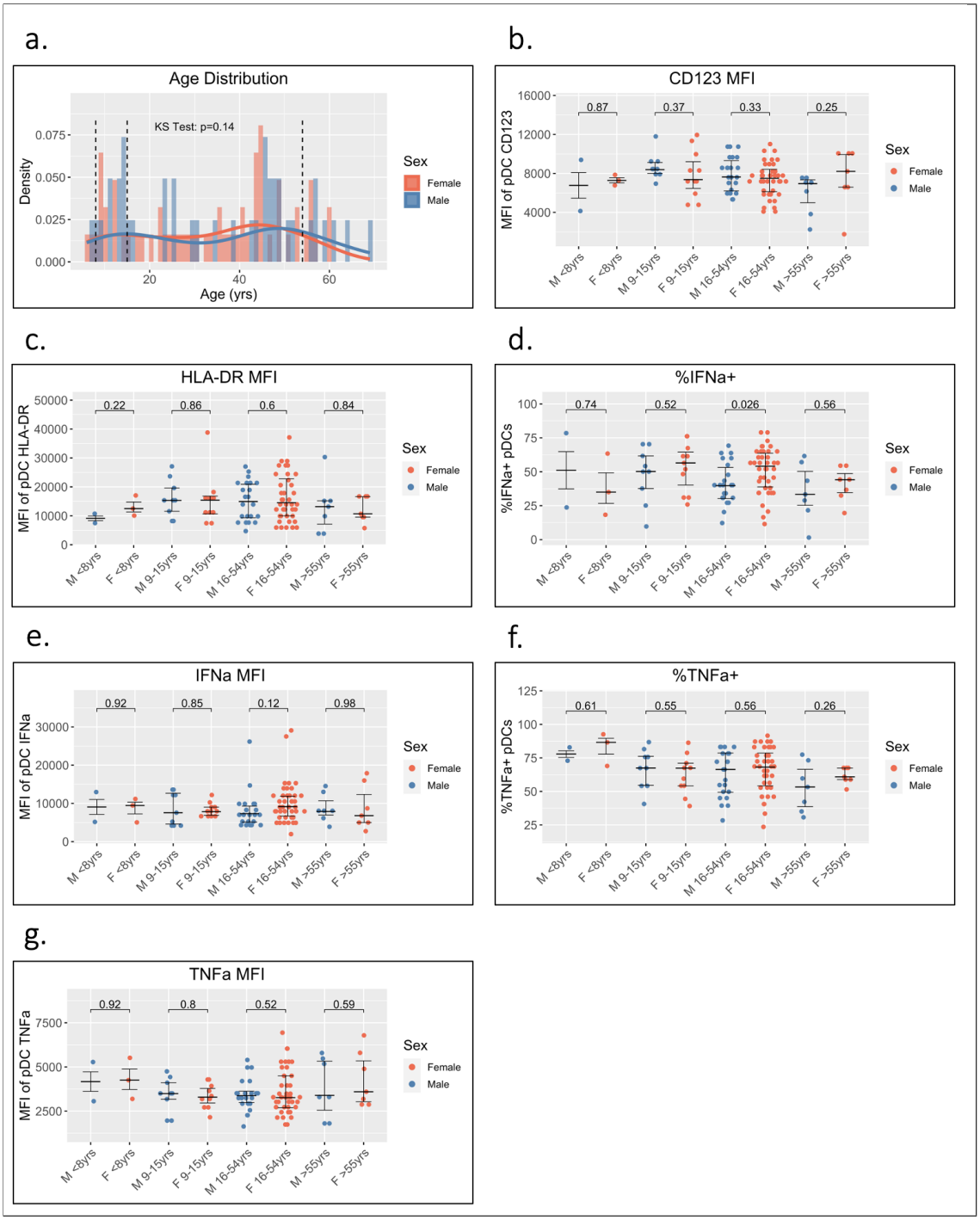



**Figure 2.8: Application of immediate whole blood stimulation in a large clinical research cohort.** Application of the whole blood assay in a large cohort (n=109; males n=44 [blue] & females n=65 [red]). a) histogram of cohort age distribution; dashed vertical lines indicate stratification groups. b), c), e), g) mean fluorescence intensity (MFI) for gated pDCs of: CD123, HLA-DR, IFN-α (IFNa), and TNF-α (TNFa) respectively. c), e) percentage of gated pDCs expressing IFN-α (IFNa) and TNF-α (TNFa) respectively. Pairwise comparisons performed via unpaired Wilcoxon test for equal variance. Bars show median with interquartile range.

## 2.5 Discussion

Since IFN-α production by pDCs plays a central part of the innate immune response it is therefore critical to be able to measure it accurately and reliably. The assay developed here addresses a major drawback to working with pDCs; their decreased recovery and reduction in activity with increasing time *ex-vivo* (Meier et al. 2008).

By drawing blood directly into collection tubes containing media and the TLR7/8 agonist CL097, then maintaining tubes at 37°C during transport to the laboratory, pDC activity is preserved and maximal cytokine production captured.

Indeed, the results here show that the delay in transporting blood to the laboratory to then isolate PBMCs incurs a marked reduction in IFN-α production at both the population percentage level and individual cell MFI level, which is further reduced with cryopreservation. Mechanistically, this appears to be underpinned by a lower relative capacity for pDCs to activate since both HLA-DR and CD123 are concurrently reduced.

Furthermore, the assay demonstrated suitability to a large cohort in a clinical research setting, wherein the sensitivity was sufficient to detect the widely-reported increased percentage of IFN-α production by female pDCs achieved through other methods (see Section 1.4).

Cells maintained at 37°C during transport displayed better activation through HLA-DR expression, and higher production of IFN-α and TNF-α in both percentage and MFI when compared to those kept at ambient temperatures or chilled to 4°C.

Moreover, 37°C was the only one of the three temperature conditions to detect the increased female percentage of IFN-α+ pDCs previously described in the literature (see Section 1.4). To this end we used this documented increased production of IFN-α by female pDCs as a proxy for the ability of the assay to detect differential IFN-α between groups generally. Indeed, we were able to detect higher female %IFN-α+ pDCs at each time point during the initial time course, yet the same is not true for IFN-α MFI. This suggests that female pDCs do not produce more IFN-α

individually, but that their biallelic TLR7 expression instead lowers the threshold required for their activation compared to male pDCs such that a greater percentage express IFN-α upon stimulation.

In support of this is higher expression of HLA-DR and CD123 for males at time points where there is the greatest difference between male and female %IFN-α+ pDCs, suggesting the need for greater activation by male cells to produce IFN-α. Indeed, the sex difference in HLA-DR expression, and to a lesser extent CD123, is mitigated with overnight incubation when the sex difference in %IFN-α+ pDCs is reduced. This is again seen when comparing whole blood to PBMC as CD123 MFI was increased in males despite lower %IFN-α+ pDCs than females and comparable IFN-α MFI.

Similarly, whilst no significant differences in pDC TNF-α production were seen in assay development, further support for the accelerated maturation of female pDCs is seen in the TNF-α data in the initial time course. TNF-α is thought to antagonise IFN-α production by pDCs and drive them towards a more antigen-presenting phenotype through upregulation of the co-stimulatory molecules CD80/86 and lymph node -homing receptor CCR7 (Psarras et al. 2021). The decrease in expression of TNF-α at both population percentage and individual cell MFI levels seen with overnight time points is lesser for females and, when combined with the higher percentages of IFN-α pDCs, supports my proposal that biallelic TLR7 expression allows female pDCs to produce an infection-stunting amount of IFN-I faster than males and so progress to presenting antigen sooner. Indeed, Webb et al. 2019 report higher expression of the T-cell co-stimulatory molecule CD86 on female pDCs than male pDCs after 20hrs stimulation with a TLR7 ligand.

Likewise loss of the significant sex difference when initially comparing samples incubated for 18hrs compared to 6hrs here, where the percentage of IFN-α+ pDCs significantly reduces for females and not males, supports the idea that female cells can end IFN-α production earlier than male cells.

Nonetheless, the application of the assay to the larger dataset failed to detect the other sex differences seen in the time course, which may be attributable to the larger numbers of donors across and greater variation in age; which is known to affect pDC function (Jing et al. 2009), and may therefore reduce signal-to-noise for other pDC sex differences through increased biological heterogeneity across ages; as supported by the correlations of CD123 and HLA-DR with age.

The assay was developed to detect the widely reported increased production of IFN-α by female pDCs compared to male pDCs. The field of pDC biology is small and assays to measure pDC IFN-I vary greatly; as such there is no "gold-standard" against which to compare the development of a newly developed assay. Thus, it was not possible to define success in a binary outcome which precludes the determination of assay success by the conventional metrics of sensitivity and specificity via, for example, a receiver-operating characteristic, or ROC, curve (**fawcett2006**).

The use of whole blood draws on the conclusions of Kirchner et al. 1982 who as early as the 1980s note the importance of maintaining the *ex-vivo* milieu of whole blood for successfully measuring IFN-I, albeit indirectly. Subsequent assays to detect IFN-I directly after specific TLR7 stimulation often involve a transfer step from the blood tube before incubation (Coch et al. 2013; Tran et al. 2019) which is impractical when sampling blood away from laboratory sites. Others measure secreted IFN-I into supernatant via ELISA (Coch et al. 2013; Tran et al. 2019) or SIMOA (Rodrigues et al. 2020), which does not allow for the measurement of IFN-I production by any specific cell type. Therefore a combination method involving in-tube stimulation of whole blood (Rodrigues et al. 2020) with immediate incubation at 37°C (McNerlan et al. 2002) followed by detection of IFN-I intracellularly via flow cytometry (Tran et al. 2019; McNerlan et al. 2002; Hagen et al. 2020) offers the optimal opportunity to capture maximum cytokine production by pDCs, particularly in e.g. paediatric samples where small blood volumes often limit cell recovery.

In conclusion, the assay developed here consistently detects sex differential pDC activation and cytokine production, which is temporally robust to the fluctuations

implicit in work involving human participants. As interest in the role of IFN-I in immunity grows, I believe this assay will be suited to investigating pDC IFN-I in large cohorts due to its simplicity and reliability, and will be particularly useful in resource-poor settings where times between clinics and laboratory processing are increased.

# 3

# Sex-related characteristics of pDCs and effect of differential IFN-I production following primary Pfizer BioNtech BNT162b2 + LAIV co-/vaccination in adolescents in the United Kingdom

This chapter outlines the behaviour of pDCs in response to BNT162b2 + LAIV co-/vaccination in adolescents, as measured through the whole blood assay developed in Chapter 2. After a consideration of the sex differences in the pDC response, an investigation into the relationship between IFN-I and the humoral response to both vaccines, including the role of sex hormones there in, follows.

## 3.1 Abstract

The role of the innate immune system is critical during the initial vaccine response to prime a robust adaptive immune response. New vaccine technologies introduced in response to the SARS-CoV2 pandemic have highlighted the limited understanding surrounding the mechanism by which vaccine adjuvants, specifically those eliciting type I interferon (IFN-I), determine vaccine outcome. Differential vaccine outcome is regularly observed between males and females and a key immunological sex difference is the greater production of IFN-I by the primary responsible cell type, plasmacytoid dendritic cells (pDCs), from females compared to males.

Here we study the behaviour of pDCs in response to primary Pfizer BNT162b2 + live-attenuated influenza vaccine (LAIV) co-vaccination in adolescents in the United Kingdom in October 2021 and develop a model to investigate the role played by sex in the pDC IFN-I response; identifying female sex and free testosterone as significant factors. Converse to literature surrounding other influenza vaccines, no sex difference is seen in the antibody response to LAIV, and a male bias is seen in the antibody response to BNT162b2 which is correlated with levels of free testosterone. Lastly, LAIV co-vaccination is identified as beneficial to the BNT162b2 response and correlates with IFN-I -driven immune activation of CD4+ T-cells. Overall, these data support the role of systemic IFN-I in driving a robust immune response to new RNA-based vaccine technologies but suggest that local modulation of IFN-I by androgens may reduce vaccine clearance to allow higher antibody titres to BNT162b2 in males.

## 3.2 Introduction

The emergence of RNA vaccine technologies in response to the SARS-CoV2 pandemic has exposed the gap in understanding the complex interplay between vaccine adjuvants and the innate immune response in shaping the adaptive response and subsequent outcome to vaccination.

Much of our understanding of vaccine immunology is based on protein-subunit vaccines. It is broadly accepted that the exogenous antigen introduced by vaccination is recognised as non-self by the innate immune system, leading to activation of myeloid cells such as macrophages, monocytes, and conventional dendritic cells (cDCs) (see Section 1.2.2). These uptake the peripheral antigen and home to draining lymph nodes to present it to CD4+ T-helper cells which drive development of cell mediated adaptive immunity via cytotoxic CD8+ T-cells and humoral adaptive immunity via B-cells and T follicular helper cells ($T_{FH}$) (Pulendran et al. 2021; Pollard and Bijker 2021).

However, the specific events surrounding how vaccine antigen recognition leads to innate immune activation remain poorly understood as vaccine formulations typically include an 'adjuvant' that has been shown empirically to improve the adaptive immune response to the vaccine and increase immunological memory. Inclusion of aluminium salts, for example, began serendipitously via salt purification methods and is speculated to prolong antigen retention at the injection site as it generally causes a $T_H2$-biased adaptive response but does not induce PRR signalling to activate innate cells (Gavin et al. 2006). MF59 is an oil-in-water emulsion used in seasonal influenza vaccines and likewise has an PRR-independent mechanism yet drives a characteristic cytokine profile dominated by CCL2 which drives recruitment of antigen-presenting myeloid cells to the vaccination site (Pulendran et al. 2021). When PRR signalling is triggered however, the response invariably includes a strong IFN-I signature; CpG1018, whilst acting via TLR9, still initiates IFN-I production by pDCs via the MyD88 signalling cascade (see Section 1.2.3), driving a strong $T_H1$-biased adaptive response (Guiducci et al. 2006). Similarly, AS03 induces a

strong early IFN-I gene signature when used in influenza vaccines for H1N1 (Sobolev et al. 2016) and H5N1 (Howard et al. 2017); the magnitude of which is predictive of antibody titres on day 56 post-vaccination (Howard et al. 2017).

The early IFN-I response can be expected to influence vaccine outcome since IFN-I plays a role in priming the adaptive immune response. IFN-I promotes the differentiation of CD4+ and CD8+ T-cells into effector and memory phenotypes, and enhances the development of $T_{FH}$ cells to aid survival and differentiation of cognate B-cells (Teijaro and Farber 2021). This is exemplified by the annual seasonal influenza vaccine where IFN-I levels at the outset of the immune response correlate with antibody titres for the trivalent influenza vaccine and live-attenuated influenza vaccine (LAIV) in adults (Bucasas et al. 2011; Nakaya et al. 2011) and more importantly also in children (Cao et al. 2014; Nakaya et al. 2016).

Concurrent with the differential production of IFN-I in males and females (see Section 1.3), a sex difference in the outcome is seen for influenza vaccination as females consistently produce higher antibody titres to the seasonal trivalent influenza vaccine (Klein et al. 2012). This almost certainly relates to the inherent $T_H2$-bias of the female immune system, but can be related specifically to the increased production of IFN-I by female pDCs as the main route of IFN-I induction by the seasonal trivalent influenza vaccine is via TLR7 (Koyama et al. 2007). This directly results in activation of CD4+ T-cells and B-cells through a strictly MyD88-dependent manner; supporting the role of IFN-I in the sex differential outcome of seasonal influenza vaccination.

Concurrent with biological sex, there also appears to be a role for the immune-suppressive role of androgens in determining the outcome of influenza vaccination as a systems analysis of seasonal trivalent influenza vaccine responses identified a negative relationship between antibody titres and plasma testosterone in males (Furman et al. 2014).

As a live RNA virus LAIV will activate the innate immune system via detection by several PRRs, such as recognition of the double-stranded RNA genome via TLR3,

in addition to ssRNA by TLR7; whereas BNT162b2, as an mRNA vaccine, will activate innate immunity primarily via TLR7.

LAIV was introduced for use in children by the United Kingdom in 2013 and, despite greater antibody titres than the seasonal trivalent influenza vaccine in initial murine models (Lorenzo et al. 2011), no published study has to-date (January 2023) reported any difference in LAIV outcome between sexes. Similarly, despite the relationship between IFN-I and the decreased morbidity and mortality from COVID-19 in females supporting a role for IFN-I in the adaptive immune response to SARS-CoV2 (see Section 1.5.1), a corresponding sex difference in the outcome of BNT162b2 is also not reported in studies in adults (Goel et al. 2021; Guerrera et al. 2021; Michos et al. 2021). No such sex comparisons could be found for studies in children to-date (January 2023).

The immune system of children differs markedly from that of adults (Klein and Flanagan 2016). Importantly, healthy children have higher IFN-I responses than healthy adults and, in the context of natural SARS-CoV2 infection, a greater increase in IFN-I gene signatures within immune cells than adults following infection (Yoshida et al. 2022). SARS-CoV2 is a potent inducer of IFN-I (see Section 1.1.2) and such increased capacity for children to mount an IFN-I response is associated with their capacity to more readily clear the virus than adults (Yoshida et al. 2022).

Reduced COVID-19 symptom severity in children therefore provides a link between IFN-I and immune outcome to SARS-CoV2. Indeed, the early IFN-I response to the live-attenuated Oxford/AstraZeneca ChAdOx1-nCov19 (AZD1222) vaccine is predictive of the neutralising antibody titres 2 months post-vaccination (Shen et al. 2022).

Like SARS-CoV2 infection, a key immunological characteristic of BNT162b2 is a strong early IFN-I response (Arunachalam et al. 2021). The aim of this study was therefore to investigate whether biological sex affects the IFN-I response to BNT162b2 + LAIV co-/vaccination and whether this relates to sex differential outcome of vaccination. The pubertal age range of the cohort studied provided a

unique opportunity to additionally investigate the role of androgens in pDC IFN-I and vaccine outcome.

## 3.3 Materials and Methods

### 3.3.1 Ethics Statement

Blood was sampled from adolescents (median age 14y3m; range 12y0m-16y0m) receiving a primary dose of Pfizer BNT162b2 at schools in Oxfordshire in autumn 2021 and who's parents responded to school-wide invitations for participation in a study of the immunological response to BNT162b2 in adolescents. As part of this national roll-out of SARS-CoV2 vaccination, optional concurrent co-vaccination with intranasal live-attenuated influenza vaccine (LAIV) was offered at the same time. As participants were under 18yrs written, informed consent was obtained from each participant's parents, followed by individual assent at the time of sampling. Participants were excluded if they reported illness in the last 7 days to prevent obfuscation of the true IFN-I response, or if they reported vaccination in the last 28 days to prevent obfuscation of the vaccine response. As this study followed a national roll-out there was no control over experimental design with respect to an individual's choice to receive BNT162b2 alone or BNT162b2 + LAIV co-vaccination, except to address it in analyses post-hoc. Samples were collected in accordance with approval from the University of Oxford Medical Sciences Interdivisional Research Ethics Committee (reference R71346/RE001).

For the LASSO validation cohort, data was used from the same larger cohort as used in the previous chapter (see Section 2.3.1): University of Oxford Medical Sciences Interdivisional Research Ethics Committee (reference R71346/RE001). Written, informed consent was obtained for each participant or, in the case of those under 18yrs, assent with parental consent.

### 3.3.2 Whole blood measurement of pDC IFN-I

Whole blood was collected from adolescents immediately following vaccination directly into heparin vacutainers (BD) containing R10 + Brefeldin + CL097 and maintained at 37°C via a dry block-heater during laboratory transport for further

incubation up to 6hrs, as previously described (see Section 2.3.2). Cells were then stained for flow cytometry as previously described (see Section 2.3.5) and stored at 4°C for 12-48hrs prior to flow cytometry via an LSR II (BD). The assay was repeated in subset of participants the following day.

### 3.3.3 Plasma and serum isolation from whole blood

Blood for plasma isolation was collected in EDTA vacutainers (BD) and preserved at room temperature during laboratory transport. Plasma was separated via Ficoll (Lymphoprep) separation in Leukosep tubes (Greiner) (1000g; 15mins; low deceleration). Plasma was aspirated from the top layer and aliquots stored immediately at -80°C.

Blood for serum was collected in SST II Advance tubes (BD) and preserved at room temperature during laboratory transport. Tubes were centrifuged 2000g 7mins to isolate serum which was then aliquoted for immediate storage at -80°C.

### 3.3.4 Measurement of androgen levels

Testosterone and Dihydrotestosterone (DHT) levels were measured in baseline and day 35 serum samples via Liquid Chromatography Mass Spectrometry through a collaboration with Prof. Wiebke Arlt, Imperial College London, and the average used in analyses. The Lower Limit of Quantification (LLOQ) was 0.35nMol for Testosterone and 0.34nMol for DHT; values below this were set at half the LLOQ as published in Schiffer et al. 2023.

Androgens are typically clinically determined from serum samples as measurements from plasma often underestimate the true concentration (Lachance et al. 2015). However, due to limited serum availability, free testosterone was measured here from baseline plasma samples against a standard curve using a commercial ELISA kit (Abcam; Cat: ab178663). Samples and standards were performed in duplicate.

### 3.3.5 Determination of anti-CoV2-IgG responses and prior infection

Plasma from baseline and day 35 post-vaccination was thawed on ice and IgG against SARS-CoV2 spike, receptor-binding domain (RBD), and nucleocapsid measured via the Meso Scale Discovery V-plex immunoassay 'Coronavirus Panel 3' as detailed in (Payne et al. 2021).

SARS-CoV2 infection was defined as antibody levels against spike (anti-S-IgG) and nucleocapsid (anti-N-IgG) above the cut-offs determined by (Payne et al. 2021); 1160 AU/ml and 3874 AU/ml respectively. Prior infection was defined as anti-S-IgG and/or anti-N-IgG above the cut-off in baseline plasma samples and infection during the study as anti-N-IgG above the cut-off in day 35 samples, due to the presence of S in the vaccine.

### 3.3.6 Determination of anti-HA-IgG influenza responses

Influenza anti-HA-IgG titres were measured by fellow Goulder lab DPhil student Cecilia Jay. Briefly, titres were measured by an in-house ELISA against HA for: influenza A/Victoria (H1N1), A/Cambodia (N3N2), B/Washington, and B/Phuket. Titres were measured by sandwich ELISA with goat anti-human-IgG secondary antibody conjugated to alkaline phosphatase and absorbance at 405nm read to compare with a concurrently measured standard curve of pooled highly reactive sera.

### 3.3.7 Data Analysis & LASSO modelling

Flow cytometry data was analysed with FlowJo v10.7.1 (BD) and pDCs defined as described in Section 2.3.6. Additional gating was undertaken for CD4+ T-cells, defined as: PBMC/Singlet/Live/CD56-/CD19-/CD3+/CD14-/CD11c-/CD4+.

Graphs were plotted and analysed using R Studio running R v4.2.0 via base R and package *ggpubr*; two-group continuous variables were analysed with two-tailed Student's T-test for parametric data or Wilcoxon test for non-parametric data (nb: an unpaired Wilcoxon test is equivalent to Mann Whitney U test). Where appropriate, Welch's correction was applied for unequal variances and Bonferroni correction used for multiple comparisons.

A Least Absolute Shrinkage and Selection Operator (LASSO) model assigns a coefficient to each input covariate and sequentially regresses them within a linear equation to their minimum possible value without affecting a given dependent variable; any coefficients that cannot be regressed to zero therefore influence the dependent variable in the model (Tibshirani 1996). The R package *glmnet* was used to create relaxed-fit LASSO models using lambda.min from model cross-validation.

## 3.4 Results

### 3.4.1 Cohort Demographics

In October 2021 school children of adolescent age in the United Kingdom were offered their primary dose of Pfizer BioNtech BNT162b2 alongside optional co-administered nasal LAIV. Adolescents from three schools in Oxfordshire were enrolled onto our study and their demographics are detailed in Table 3.1. A total of 33 individuals were enrolled, matched for sex (male n=18 & female n=15) and age (median 14y3m; range 12y0m-16y0m). Baseline blood samples were taken immediately after co-/vaccination to determine prior SARS-CoV2 infection and to assess baseline pDC response to TLR7 stimulation via the whole blood assay, as detailed in Section 2.3.2.

A subset of adolescents (n=18) were then sampled the day following co-/vaccination and the whole blood assay repeated to determine the influence of co-/vaccination on the response of pDCs to TLR7 stimulation.

Plasma samples for all 33 individuals were obtained in the fifth week following vaccination (median 35 days; range 33-37 days – henceforth Day 35) to determine the antibody response to the key antigens in the vaccine/s; for BNT162b2: anti-CoV2-Spike-IgG and anti-CoV2-RBD-IgG, and for LAIV: anti-HA-IgG for Phuket, Washington, H3N1, and H1N1 influenza strains.

Lastly, circulating androgen levels were determined to assess whether pDC IFN-I is modulated by male androgens and whether androgen levels relate to sex differential vaccine outcome. Female sex hormones were also considered, but were omitted due to the cyclic nature of their production (see Section 1.6) given the limited number of female participants (n=15).

**Table 3.1:** Adolescent Cohort Demographics

| | **Male** | **Female** | **Total** |
|---|---|---|---|
| Participants | 18 | 15 | 33 |
| Subset Day 1 | 7 | 11 | 18 |
| Age | 14y5m (12y2m-16y0m) | 13y0m (12y0m-15y11m) | 14y3m (12y0m-16y0m) |
| + LAIV | 14 | 11 | 25 |
| Prior CoV2 infection | 11 | 6 | 17 |
| CoV2 infection during | 1 | 2 | 3 |
| CoV2 infection by day 35 | 12 | 8 | 20 |
| Serum Testosterone (nMol) | 14.7 (1.79-24.62) | 0.16 (0.37-1.24) | 2.77 (0.37-24.62) |
| Serum Dihydrotestosterone (nMol) | 0.94 (0.17-1.81) | 0.17 (0.17-0.54) | 0.54 (0.17-1.81) |
| Plasma free Testosterone (pg/ml) | 6.3 (0.2-13.8) | 0.7 (0.1-2.2) | 0.9 (0.1-13.8) |
| Anti-CoV2-S-IgG uninfected (AU/ml) | 62,270 (44,931-171,923) | 36,952 (17,874-58,330) | 44,931 (17,874-171,923) |
| Anti-CoV2-S-IgG infected by day 35 (AU/ml) | 802,891 (129,838-2,062,784) | 574,803 (211,782-1,110,151) | 745,854 (129,838-2,062,784) |
| Anti-CoV2-RBD-IgG uninfected (AU/ml) | 23,861 (16,266-68,122) | 11,443 (8,137-23,377) | 16,402 (8,137-68,122) |
| Anti-CoV2-RBD-IgG infected by day 35 (AU/ml) | 333,313 (77,833-967,962) | 287,958 (73,331-433,284) | 333,313 (73,331-967,962) |

Continuous data show as median with range.

### 3.4.2 High pDC activation and cytokine secretion following co-vaccination

Since IFN-I plays such a central role in the initiation of both the innate and adaptive immune responses, changes to the behaviour of pDCs, as the main IFN-I -producing cell type (Siegal et al. 1999), were first studied between baseline (Day 0; d0) and the day following co-/vaccination (Day 1; d1) in the 18 individuals sampled on both days (Figure 3.1).

Striking proliferation was observed for pDCs between d0 and d1, with the proportion of pDCs of live PBMC increasing significantly from a median of 0.24% to 0.62% ($p=0.00044$) (Figure 3.1a.). Increased pDC activation between d0 and d1 was also reflected in a modest increase of CD123 ($p=0.07$) but was not seen in HLA-DR (Figure 3.1b. & c.).

The percentage of pDCs producing IFN-α increased significantly from a median of 51.5% on d0 to 67.3% on d1 ($p<0.0001$) (Figure 3.1d.), as did the amount of IFN-α produced by each cell; increasing from a median of 9694 to 11937 ($p=0.0097$) (Figure 3.1e.).

Lastly, the change in production of TNF-α showed a mixed pattern in terms of both %TNF-α+ pDCs and TNF-α MFI; levels of both tended to be reduced between d0 and d1 in individuals with high baseline TNF-α and increased for those with lower baseline TNF-α (Figure 3.1f. & g.).

Similar patterns were observed in concurrently collected, unstimulated samples with the notable exception of %TNF-α+ pDCs which increased overnight (Appendix A.1). I have therefore elected to use stimulated data here to focus on differential IFN-I production within, and relative to, baseline samples as unstimulated pDCs expressed little-to-no IFN-α at baseline.

Finally, pDC behaviour was also measured on d0 and d1 in concurrently collected blood from two unvaccinated control individuals for assurance that any observed

phenotype would not be artefactual; Appendix A.2 shows consistency for each measured phenotype between d0 and d1.

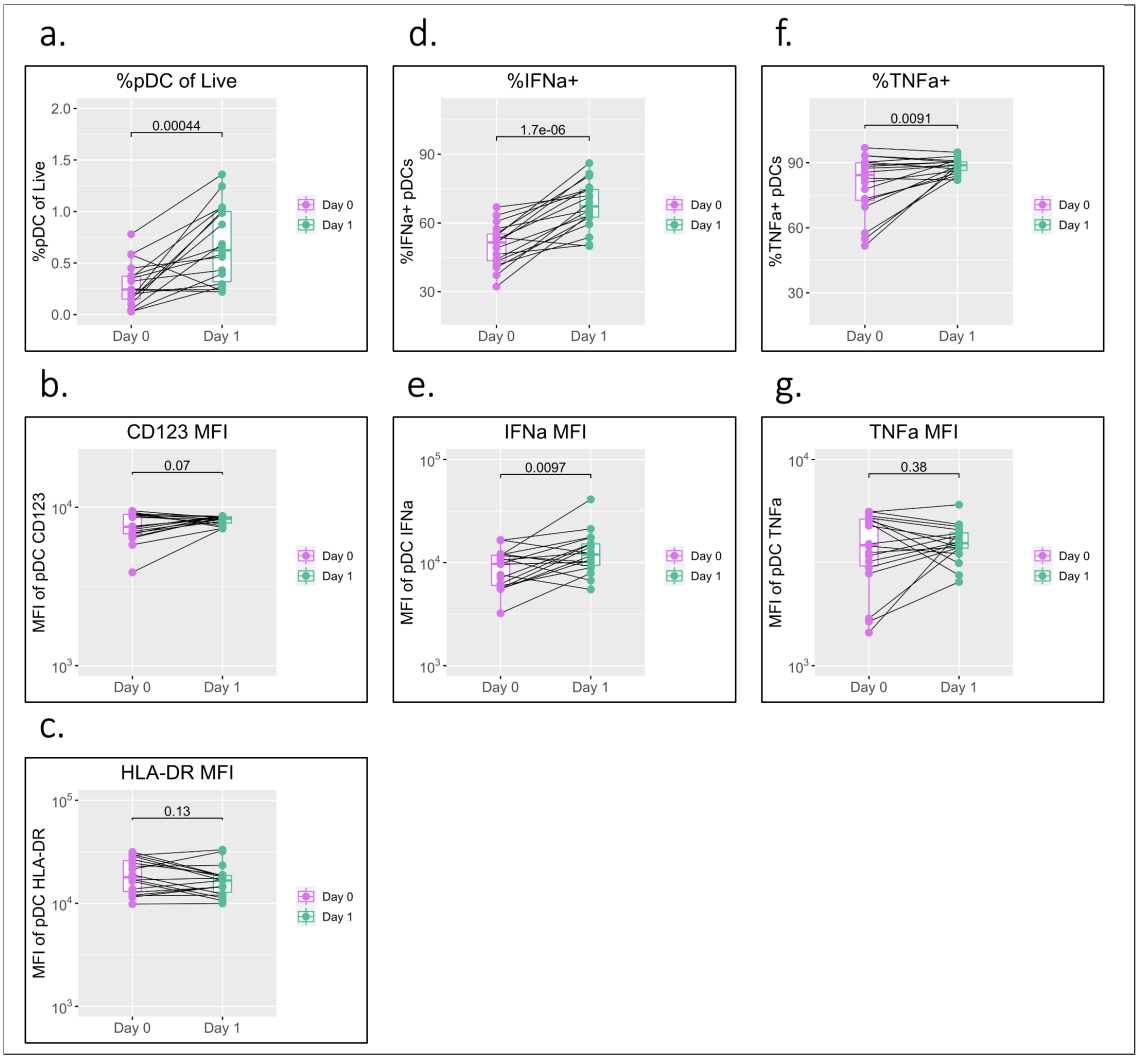



**Figure 3.1: pDC Activation following Co-vaccination.** Paired pDC activation data showing changes in pDC phenotype between Day 0 and Day 1 (n=18). Blood was drawn from adolescents (median age 14y3m) immediately following co-/vaccination with BNT162b2 + LAIV (Day 0; purple) and the following day (Day 1; green). Vacutainers contained R10 + brefeldin + CL097 and were incubated at 37°C for 6hrs as detailed in Section 2.3.2 before analysis via flow cytometry. Samples done in duplicate per donor. a) pDC frequency as percentage of total PBMCs. b), c), e), g) mean fluorescence intensity (MFI) for gated pDCs of: CD123, HLA-DR, IFN-α (IFNa), and TNF-α(TNFa) respectively. d), f) percentage of gated pDCs expressing IFN-α (IFNa) and TNF-α (TNFa) respectively. Pairwise comparisons via Student's paired T-test for equal variance.

### 3.4.3 Delayed activation kinetics and IFN-I production in male pDCs

Since the main cited difference in pDC IFN-I is higher production in females via biallelic TLR7 expression (see Section 1.3), and with data to suggest this results in differential activation kinetics between male and female pDCs (see Section 2.4.5), I next stratified the d0 and d1 pDC data by sex to investigate sex differences in pDC activation kinetics (Figure 3.2).

There were comparable numbers of pDCs as a percentage PMBC between males and females on d0. There were significant increases for both sexes between d0 and d1 but more so in females, increasing from a median of 0.16% to 0.88% ($p<0.001$), whereas males increase from a median of 0.20% to 0.56% ($p=0.015$) (Figure 3.2a.).

Whilst not significant, male pDC activation via CD123 expression appears lower than females on d0 but increases significantly between d0 and d1 ($p=0.023$) whereas female CD123 remains consistent such that no difference is seen between the sexes on d1 (Figure 3.2b.). A similar pattern is also observed for HLA-DR where female expression is higher on d0 but is comparable to male expression on d1 after a modest decrease (Figure 3.2c.).

This work was undertaken before complete analysis of the assay development data, which found no sex difference in pDC IFN-α between pubertal males and females (Figure 2.8d.). Nonetheless, the widely reported significantly higher percentage of IFN-α+ pDCs in females is seen on d0 in this adolescent cohort, with a median of 47.7% for males and 54.4% for females ($p=0.040$) (Figure 3.2d.) There are significant increases in %IFN-α+ pDCs for both sexes between d0 and d1, but more-so for males, increasing to 63.6% for males ($p<0.001$) and to 71.2% for females ($p=0.058$) such that there is no sex difference on d1 (Figure 3.2d.). This pattern is also mirrored for pDC IFN-α MFI (Figure 3.2e.).

Conversely, no significant sex difference is seen for the percentage of TNF-α+ pDCs nor for pDC TNF-α MFI either before or after co-/vaccination (Figure 3.2f. & g.).

The same pattern of sex differences between d0 and d1 was also mirrored by concurrently collected unstimulated control samples (Appendix A.3) but, as before, I elected to use data from stimulated pDCs here to allow consideration of the effect of co-/vaccination on the widely reported sex difference in %IFN-α+ pDCs at baseline.

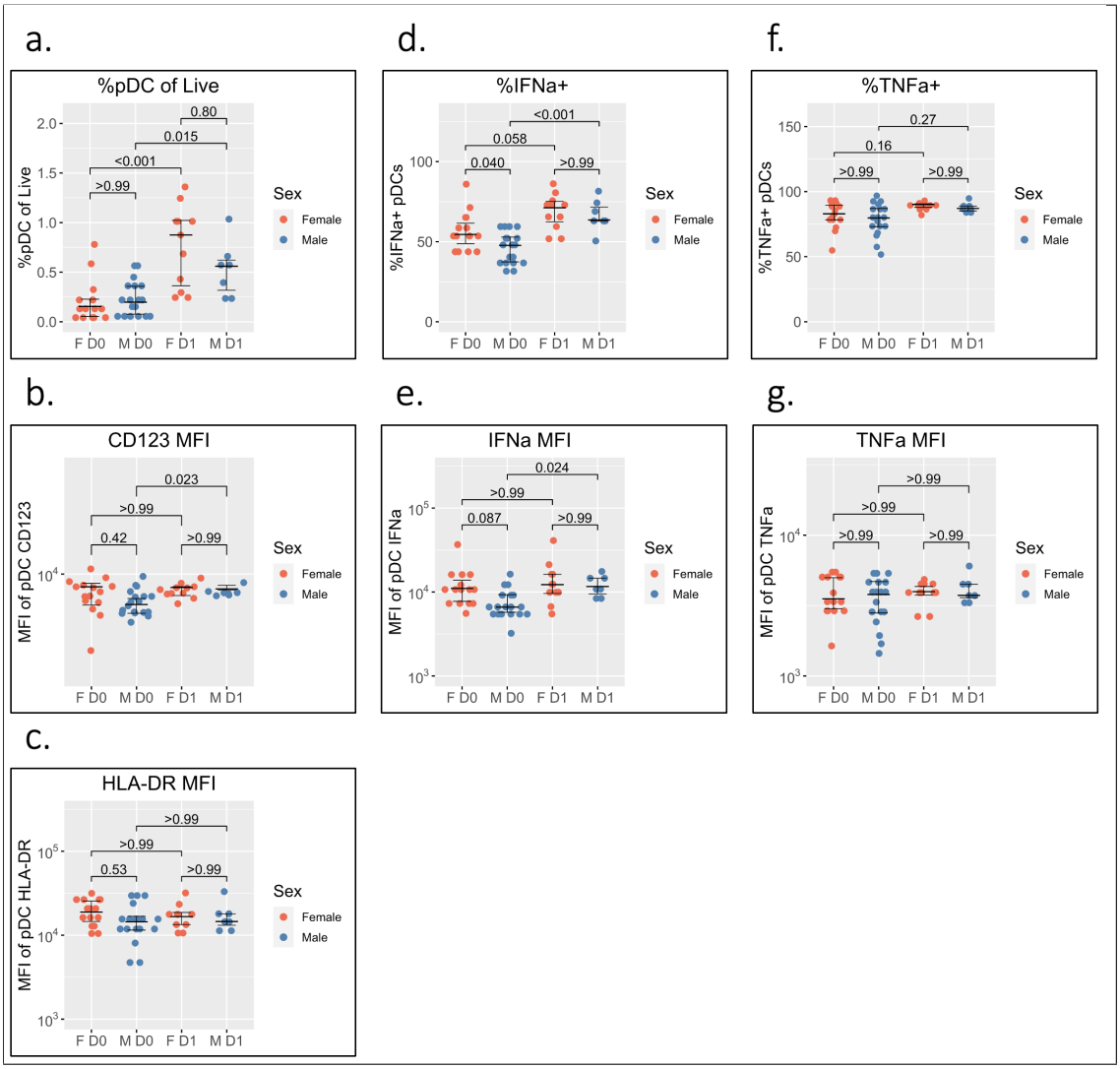



**Figure 3.2: Sex Divergent pDC Activation following Co-vaccination.** Sex-stratified activation data showing changes in pDC phenotype between Day 0 (n=33; male n=17 & female n=16) and Day 1 (n=18; male n=7 & female n=11). Blood was drawn from adolescents (median age 14y3m) immediately following co-/vaccination with BNT162b2 + LAIV (D0) and the following day (D1). Vacutainers contained R10 + brefeldin + CL097 and were incubated at 37°C for 6hrs as detailed in Section 2.3.2 before analysis via flow cytometry. Samples done in duplicate per donor. a) pDC frequency as percentage of total PBMCs. b), c), e), g) mean fluorescence intensity (MFI) for gated pDCs of: CD123, HLA-DR, IFN-α (IFNa), and TNF-α (TNFa) respectively. d), f) percentage of gated pDCs expressing IFN-α (IFNa) and TNF-α (TNFa) respectively. Pairwise comparisons via Student's unpaired T-test with Welch's correction for unequal variance and Bonferroni correction for multiple comparisons. Bars show median with interquartile range.

### 3.4.4 Total testosterone and free testosterone correlate with sex and age in adolescents

Given the body of literature surrounding the role of sex hormones in modulating the innate and adaptive immune response (see Section 1.6) I also wanted to investigate the role of male and female sex hormones in modulating pDC IFN-I. However, as mentioned, with the cyclic nature of oestrogen and progesterone and the small starting number of female participants, it was decided that: i) there would not be measurable levels of either in a meaningful number of females to justify inclusion in any analyses, and ii) it is impossible to control for the timing of an individual measurement within an individuals' cycle without e.g. measuring throughout a month and taking the maxima, which was beyond the scope of the study.

The principal androgen testosterone, and its more bioactive product dihydrotestosterone (DHT), are however produced by both sexes. The majority of circulating androgens are bound by carrier proteins and only the unbound free hormone is biologically available to act on cells in the blood (see Section 1.6.1). Total testosterone and DHT were therefore quantified via Liquid Chromatography Mass Spectrometry whilst free testosterone was determined via ELISA (Figure 3.3). Plasma free DHT concentrations were excluded from the study as they are typically too low to measure without specialist techniques and are accordingly typically only estimated via formulae accounting for levels of sex-hormone binding protein, albumin, and corticosteroid binding protein (Mazer 2009), which was beyond the scope of the study.

Predictably, total serum testosterone was significantly higher in males than females ($p<0.0001$), as were free plasma testosterone ($p=0.00094$) and serum DHT ($p<0.0001$) (Figure 3.3a., b. & c.). Concurrently, the level of total testosterone correlates with age only for males ($r=0.62$, $p=0.0081$), as does free testosterone ($r=0.60$, $p=0.001$) (Figure 3.3b. & d.). DHT is synthesised locally from testosterone only by specialised tissues and unsurprisingly levels of circulating DHT do not therefore correlate with age for males nor females (Figure 3.3e. & f.)

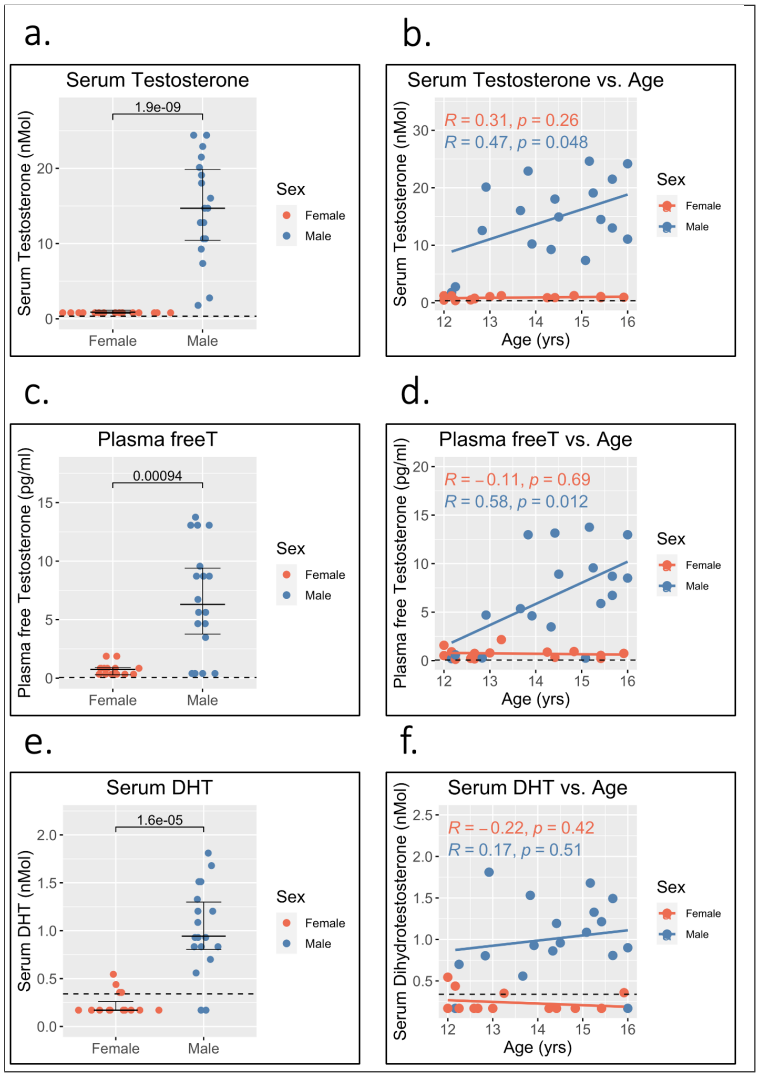



**Figure 3.3: Adolescent androgen measurements.** Androgen measurements in males (n=18) and females (n=15) for serum and plasma measured via Liquid Chromatography Mass Spectrometry and averaged for the day of co-/vaccination and day 35: a) Total Testosterone, c) Dihydrotestosterone (DHT), or via commercial ELISA for: b) free Testosterone. Pairwise comparisons via unpaired Wilcoxon test with Welch's correction for unequal variance. Dashed line represents lower limit of quantification. Bars show median with interquartile range.

### 3.4.5 Sex and age-specific factors influence pDC IFN-I

With the notion of delayed activation kinetics in male pDCs further supported by the sex differences observed following co-/vaccination above (see Section 3.4.3), I next sought to model pDC IFN-α production by pDCs to interrogate the influence thereon of: sex, age, and importantly androgen levels.

Using d0 data for CL097-stimulated pDCs to maximise the number of samples available, and to control for any influence of vaccine-related effects by d1, I constructed a Least Absolute Shrinkage and Selection Operator (LASSO) model setting as the dependent variable: pDC %IFN-α+, and as covariates: sex, age, androgen levels, pDC abundance, pDC activation through CD123 and HLA-DR, and cytokine secretion of TNF-α, plus prior SARS-CoV2 infection and LAIV co-vaccination as negative controls. Coefficients for this adolescent LASSO model are reported alongside a contextual interpretation in Table 3.2a.

**Table 3.2:** Baseline pDC %IFN-α+ LASSO Covariate Coefficients

| | **A) Adolescent LASSO** | | **B) Validation LASSO** | |
|---|---|---|---|---|
| **Covariate** | **Coefficient** | **Interpretation** | **Coefficient** | **Interpretation** |
| Female Sex | 1.22 | +1.22% IFN-α+ pDCs for females | 5.57 | +5.57% IFN-α+ pDCs for females |
| Age(yrs) | -2.53 | -2.53% IFN-α+ pDCs per year | -0.16 | -0.16% IFN-α+ pDCs per year |
| %pDC/Live | -0.97 | -0.097% IFN-α+ pDCs per 0.1% pDC/Live | 0.00 | No Influence |
| CD123 MFI | 0.000219 | +0.2% IFN-α+ pDCs per $10^3$ MFI | 0.002 | +2% IFN-α+ pDCs per $10^3$ MFI |
| HLA-DR MFI | 0.00 | No Influence | 0.00 | No Influence |
| %TNF-α+ | 0.34 | +0.34% IFN-α pDCs per +1% TNF-α | 0.27 | +0.27% IFN-α+ pDCs per +1% TNF-α |
| +/- LAIV | 0.00 | No Influence | N/A | N/A |
| Prior Infection | 0.00 | No Influence | N/A | N/A |
| Plasma Testosterone (nMol) | 0.00 | No Influence | N/A | N/A |
| Plasma free Testosterone (pg/ml) | -0.44 | -0.44% IFN-α+ pDCs per pg/ml | N/A | N/A |
| Plasma DHT (nMol) | -0.44 | -0.44% IFN-α+ pDCs per nMol | N/A | N/A |

Interestingly, the largest effect is a negative association with age; identifying a reduction in %IFN-α+ pDCs with ageing even in the narrow age range of the adolescents studied here.

Concurrent with the flow cytometry data (Figure 3.2) female sex is next identified, with a positive influence on %IFN-α+ pDCs; contributing 1.22% greater IFN-α+ pDCs than male sex.

More importantly, a converse negative influence is identified for free plasma testosterone; reducing %IFN-α+ pDCs by -0.44% per pg/ml; an effect as large as age when considering the 6pg/ml difference in median free testosterone between males (6.72pg/ml) and females (0.75pg/ml) (see Figure 3.3c.). Interestingly, bioavailable free testosterone overshadows total testosterone since total testosterone is identified as negatively influencing %IFN-α+ pDCs when free testosterone is excluded from the model (data not shown). Testosterone is similarly overshadowed by its more bioactive derivative DHT which decreases IFN-α+ by -0.44% per nMol; important considering the ∼0.75nMol difference in median DHT between males (0.94nMol) and females (0.17nMol).

To aid in interpretation of the LASSO model I also plotted a correlation matrix of the input covariates. Pertinently, testosterone, free testosterone, and DHT all correlate negatively with %IFN-α+ pDCs (Appendix A.4).

pDC activation via CD123 expression also increases %IFN-α+ pDCs in the LASSO model (Table 3.2a.), and has a weak positive correlation with %IFN-α+ pDCs but a very strong negative correlation with age (Appendix A.4). Similarly, a weak negative influence on %IFN-α+ pDCs is seen in the LASSO model for the percentage of pDCs of live PBMC (Table 3.2a.), which also correlates with age (Appendix A.4).

Lastly, a weak positive influence is also seen for the %TNF-α+ pDCs (Table 3.2a.), which suggests that high IFN-α production by pDCs is related to their maturation towards the antigen presenting phenotype via TNF-α expression (see Section 1.3).

### 3.4.6 Larger cohort validates pDC IFN-α influences

Aware of the statistical limitations of an n=33 model, I sought to validate the adolescent LASSO model with overlapping data from the larger cohort (n=109) measured in Section 2.4.9. Using the six overlapping parameters as covariates, a second LASSO model was constructed to again investigate how they influence %IFN-α+ pDCs as the dependent variable. Covariate coefficients of this validation LASSO are reported in Table 3.2b.

Of the six overlapping parameters, five are identified as not influential or influential in the same directionality and similar magnitude as they are in the adolescent LASSO. Only the percentage of pDCs of live PBMCs is not also identified in the validation LASSO and this may be explained by increased age range of the validation cohort (6-69yrs) and the tight relationship age has with the parameters identified in the adolescent LASSO (Appendix A.4).

The validation LASSO therefore gives confidence in the adolescent LASSO and lends validity to the coefficients identified for the non-overlapping covariates, namely %IFN-α+ antagonism by plasma free testosterone and DHT.

### 3.4.7 Sex differential outcome of BNT162b2 is masked by prior SARS-CoV2 infection

Having established differential activation kinetics for male and female pDCs and shown through a statistical model for the %IFN-α+ that female sex and free testosterone have some of the highest influence of pDC IFN-α, I next sought to see whether a sex difference is apparent in the outcome of co-/vaccination, beginning with Day 35 (d35) IgG responses to the BNT162b2 antigens Spike and RBD (Figure 3.4).

Since 13 individuals showed no sign of SARS-CoV2 infection by d35 it was necessary to separate the d35 antibody titres according to natural infection to control for the additional antigen exposure of natural infection. Predictably, antibody titres were

markedly higher in the infected group but no difference was apparent between the sexes (Figure 3.4a. & b.). However, the lower antibody titres of the uninfected individuals revealed significantly higher male IgG responses to Spike (p=0.045) and RBD (p=0.054), converse to the direction expected when considering e.g. seasonal influenza responses.

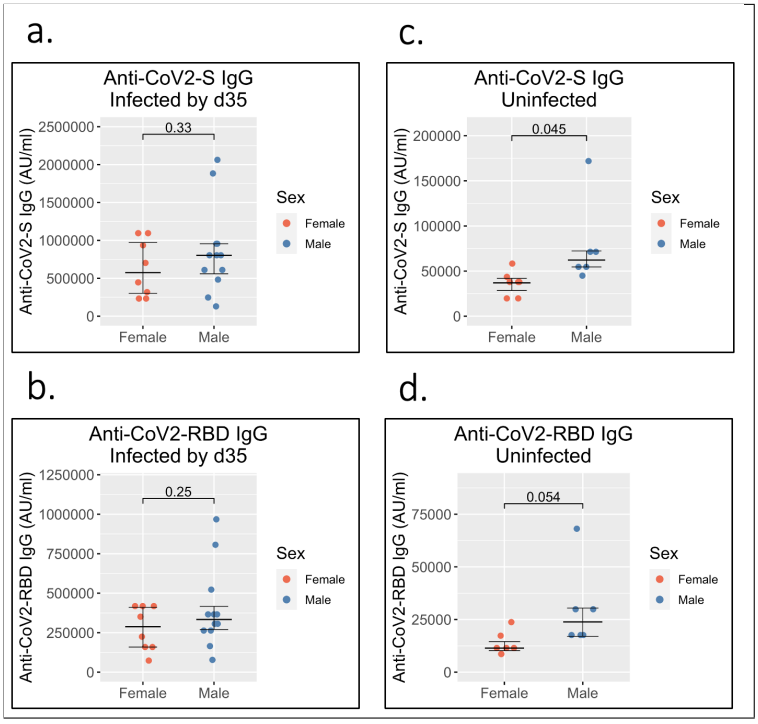



**Figure 3.4: Day 35 IgG responses to SARS-CoV2 antigens.** Sex-stratified MSD data for anti-CoV2-Spike-IgG and anti-CoV2-RBD-IgG titres in plasma from adolescents collected on Day 35 post co-/vaccination with evidence of natural SARS-CoV2 infection (Infected by d35; n=20; male n=12 & female n=8) or without (Uninfected; n=13; male n=6 & female n=7). a), b) Infected by Day 35 anti-Spike-IgG and anti-RBD-IgG, respectively. c), d) Uninfected anti-Spike-IgG and anti-RBD-IgG, respectively. Pairwise comparisons via Student's unpaired T-test for equal variance. Bars show median with interquartile range.

### 3.4.8 LAIV outcome is not affected by sex

It is widely reported that females produce higher antibody titres to trivalent seasonal influenza vaccines than males (see Section 1.5.2) and I therefore wanted to establish whether such a difference is also seen in an adolescent age group, and to LAIV.

Unlike SARS-CoV2, influenza has been circulating for the entire life of an adolescent and each child has therefore been exposed and/or infected multiple times, making it impossible to differentiate participants here by prior natural infection. I therefore compared anti-HA antibody titres between sexes in the cohort as a whole for d0 and d35 time points (Figure 3.5). Despite a modest boost in titres for all four antigens contained in the vaccine, there was surprisingly no difference in antibody titres to all antigens at either baseline (Day 0) or d35 (Day 35) between males and females (Figure 3.5).

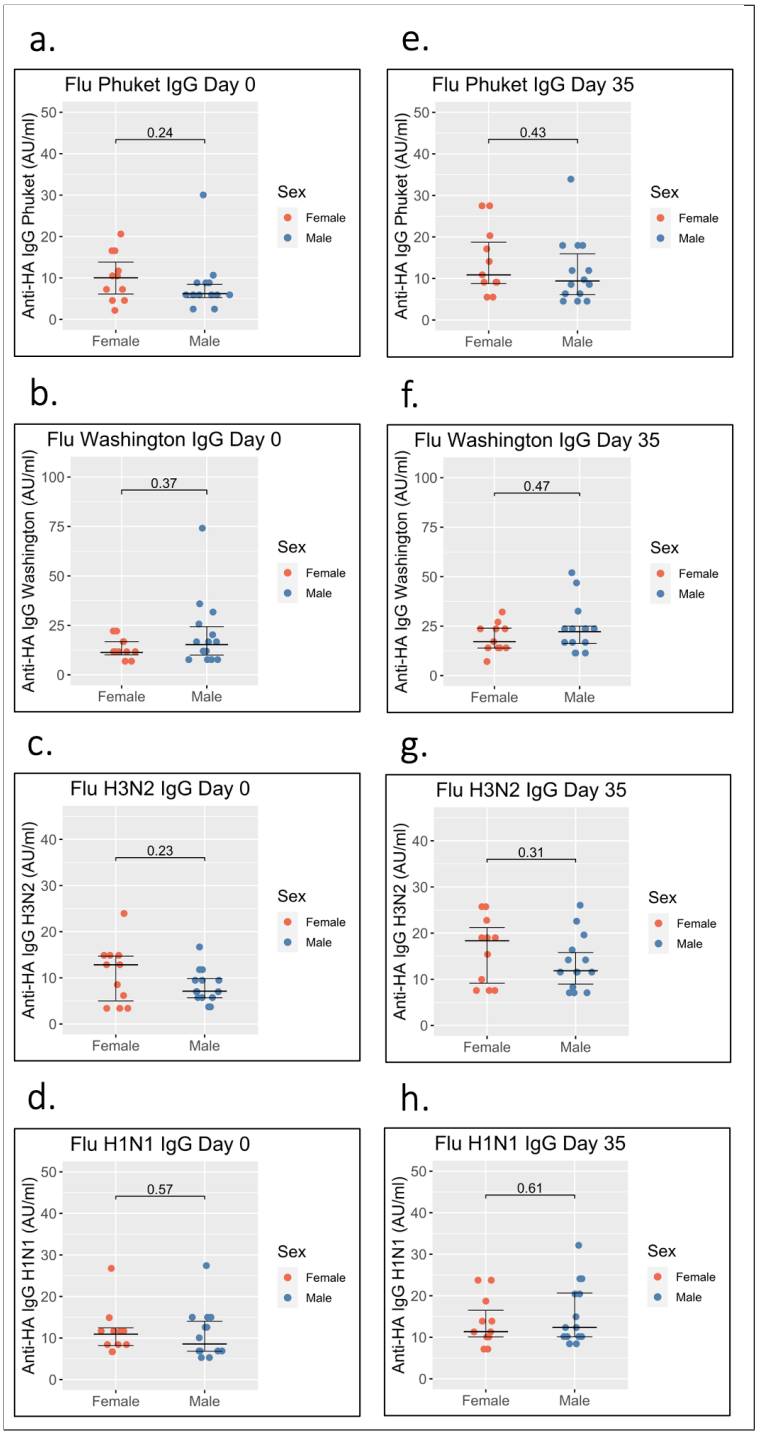



**Figure 3.5: Sex-stratified IgG responses to Influenza HA pre- and post-vaccination.** Sex-stratified IgG responses to Influenza HA from Phuket, Washington, H3N1, and H1N1 strains measured via ELISA in plasma from blood collected on the day of co-/vaccination and from Day 35 post co-/vaccination. Non-parametric pairwise comparisons via unpaired Wilcoxon test with Welch's correction for unequal variance. Bars show median with interquartile range.

### 3.4.9 LAIV co-vaccination increases BNT162b2 response

Many reports in the literature suggest strong IFN-I induction by LAIV, and given the importance of IFN-I in innate and adaptive immune responses I therefore sought to determine whether this would influence the antibody response to BNT162b2 + LAIV co-vaccinated adolescents when compared to adolescents who received only BNT162b2 (Figure 3.6).

After again separating based on natural SARS-CoV2 infection by d35, there were higher antibody titres for BNT162b2 + LAIV co-vaccinated adolescents than for only BNT162b2 vaccination for both Spike (p=0.033) and RBD (p=0.062) (Figure 3.6a. & b.). Interestingly, this difference only appears to take effect only at higher antibody titres as there are no such differences in uninfected individuals (Figure 3.6c. & d.).

### 3.4.10 LAIV increases activation of CD4+ T-cells via IFN-α

Since IFN-I is reported to increase activation of CD4+ T-cells, I turned next to the relationship between pDC IFN-α and CD4 HLA-DR, as a T-cell activation marker that overlapped with the pDC panel used for the whole blood assay. Using data from individuals sampled on both d0 and d1 (n=18) I sought to investigate a mechanism by which LAIV co-vaccination could increase BNT162b2 antibody titres (Figure 3.7).

Despite an increase for both groups, no difference was seen for the %IFN-α+ pDCs between adolescents receiving BNT162b2 + LAIV co-vaccination and BNT162b2 alone either on the day of vaccination (d0) or the following day (d1) (Figure 3.7a. & b.). Neither was there a significant difference for CD4 HLA-DR on either day (Figure 3.7c. & d.).

Interestingly however the %HLA-DR+ CD4 T-cells for BNT162b2 + LAIV co-vaccinated adolescents appears to increase between d0 and d1 from a median of

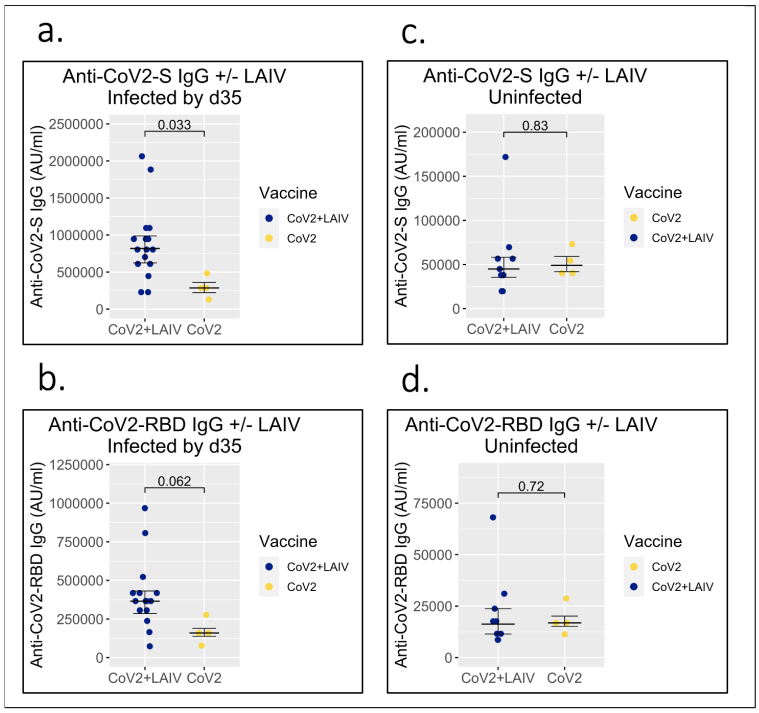



**Figure 3.6: Effect of LAIV co-vaccination on Day 35 IgG responses to SARS-CoV2**. MSD data for anti-CoV2-Spike-IgG and anti-CoV2-RBD-IgG titres in plasma from adolescents collected on Day 35 post co-/vaccination with evidence of natural SARS-CoV2 infection (Infected by d35; n=20; CoV2+LAIV n=16 & CoV2 n=4) or without (Uninfected; n=13; CoV2+LAIV n=9 & COV2 n=4). a), b) Infected by Day 35 anti-Spike-IgG and anti-RBD-IgG, respectively. c), d) Uninfected anti-Spike-IgG and anti-RBD-IgG, respectively. Non-parametric pairwise comparisons via unpaired Wilcoxon test with Welch's correction for unequal variance. Bars show median with interquartile range.

1.89% to 2.90% whereas for BNT162b2 alone there was no change with a median of 2.88% for both (Figure 3.7c. & d.).

With this in mind, I lastly compared the change in CD4 HLA-DR between d0 to d1 to the change in pDC IFN-α. Although not significant in either case, there are opposing relationships in co-vaccination compared to vaccination alone; with a positive correlation between pDC IFN-α and CD4 HLA-DR for BNT162b2 + LAIV co-vaccinated adolescents (r=0.28, p=0.35) opposed to a negative correlation for BNT162b2 alone (r=-0.21, p=0.75) (Figure 3.7e. & f.).

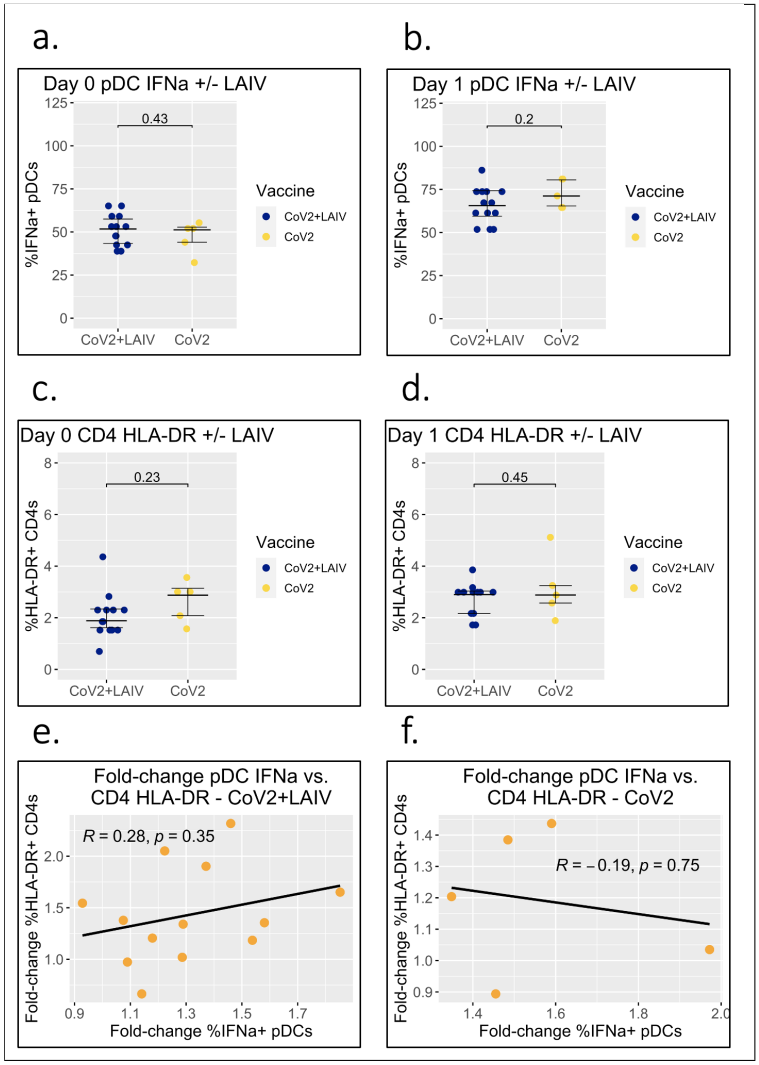



**Figure 3.7: Effect of LAIV Co-vaccination on Early Immune Activation.** Effect of LAIV co-vaccination on pDC IFN-α and CD4 HLA-DR expression for adolescents on the day of co-vaccination (Day 0) and the following day (Day 1) separated by LAIV co-vaccination (CoV2+LAIV n=13 & CoV2 n=5). a), b) %IFN-α+ (IFNa+) pDCs on Day 0 and Day 1, respectively. c), d) %HLA-DR+ CD4 T-cells on Day 0 and Day 1, respectively. e), f) Correlation of fold-change Day 0 to Day 1 of %IFN-α+ (IFNa+) pDCs and %HLA-DR+ CD4 T-cells for CoV2+LAIV and CoV2, respectively. Pairwise comparisons via Student's unpaired T-test for equal variance. Correlation via Pearson's method. Bars show median with interquartile range.

### 3.4.11 LAIV co-vaccination and free testosterone significantly affect BNT162b2 IgG responses

In light of this suggested relationship between IFN-I and the BNT162b2 antibody response, I lastly sought to identify whether a nuanced role for pDCs could be identified by further LASSO modelling of the d35 BNT162b2 antibody titres.

Two final LASSO models were constructed using as the dependent variable: either anti-Spike-IgG or anti-RBD-IgG, and as covariates: sex, age, d0 pDC flow cytometry data, and androgen measurements. Controlling for natural infection precluded modelling of antibody titres for uninfected adolescents due to the small number of individuals (n=13) so models were only possible for antibody titres for infected adolescents (n=20). Covariate coefficients are reported alongside a contextual interpretation for anti-Spike-IgG and anti-RBD-IgG in Table 3.3a. & b., respectively.

Concurrent with the previous comparison (Figure 3.4a. & b.) there is no apparent impact for sex in either anti-Spike-IgG or anti-RBD-IgG models. Strikingly the most influential covariate was indeed LAIV co-vaccination; increasing titres by $3.46\text{x}10^5$ for Spike (Table 3.3a.) and $1.28\text{x}10^5$ for RBD (Table 3.3b.).

Both models also identify a positive influence for free testosterone; increasing titres by $3.9\text{x}10^4$ per pg/ml for Spike (Table 3.3a.) and $2.1\text{x}10^4$ for RBD (Table 3.3b.). This surprisingly opposes previous observations that testosterone antagonises the immune response to trivalent seasonal influenza vaccines (Furman et al. 2014) but indeed positive correlations are seen between free testosterone and both anti-spike-IgG (r=0.43, p=0.060) and anti-RBD-IgG (r=0.46, p=0.042) (Appendix A.5).

**Table 3.3:** anti-CoV2-IgG LASSO Covariate Coefficients

| | **A) anti-Spike-IgG** | | **B) anti-RBD-IgG** | |
|---|---|---|---|---|
| **Covariate** | **Coefficient** | **Interpretation** | **Coefficient** | **Interpretation** |
| Female Sex | 0.00 | No Influence | 0.00 | No Influence |
| Age (yrs) | 0.00 | No Influence | 0.00 | No Influence |
| +/- LAIV | $3.46x10^5$ | $3.46x10^5$ greater AU/ml +LAIV | $1.28x10^5$ | $1.28x10^5$ greater AU/ml +LAIV |
| %pDC/Live | $-1.41x10^4$ | $-1.41x10^4$ per +0.1% pDC/Live | $-0.32x10^4$ | $-0.32x10^4$ per +0.1% pDC/Live |
| CD123 MFI | 67.0 | $+6.7x10^4$ AU/ml per $10^3$ MFI | 41.1 | $+4.1x10^4$ AU/ml per $10^3$ MFI |
| HLA-DR MFI | 0.00 | No Influence | 0.00 | No Influence |
| %IFN-α+ | 0.00 | No Influence | 0.00 | No Influence |
| %TNF-α+ | 0.00 | No Influence | $1.66x10^3$ | $+1.7x10^3$ AU/ml per +1% TNF-α+ |
| Plasma Testosterone (ng/ml) | 0.00 | No Influence | 0.00 | No Influence |
| Plasma free Testosterone (pg/ml) | $3.90x10^4$ | $+3.9x10^4$ AU/ml per pg/ml | $2.09x10^4$ | $+2.1x10^4$ AU/ml per pg/ml |
| Plasma DHT (ng/ml) | 0.00 | No Influence | 0.00 | No Influence |

## 3.5 Discussion

This study sought to identify the behaviour of pDCs with respect to vaccination and investigate whether any role can be attributed to sex differential IFN-I production by pDCs in the widely reported sex differential vaccine outcome (Klein and Flanagan 2016; Klein et al. 2010), specifically to the seasonal trivalent influenza vaccine (Klein et al. 2012; Nakaya et al. 2011; Furman et al. 2014; Klein and Pekosz 2014; Nakaya et al. 2016).

Following BNT162b2 + LAIV co-/vaccination in adolescents, a large increase in pDC abundance is seen between the day of vaccination and the following day, as is a modest increase in cell activation via CD123 expression. This accompanies a larger increase in cytokine production as IFN-α production is significantly increased to the day following vaccination, as is production of TNF-α.

Importantly, differences were seen in these patterns of behaviour between male and female pDCs; pDC abundance increased more for females between the day of vaccination and the following day, whereas cell activation via CD123 expression increased more for males. Further, despite a sex difference on the day of vaccination, male pDCs increased IFN-α production more than female pDCs and the two were statistically comparable the day following vaccination. This suggests differential activation kinetics between male and female pDCs; with greater activation and more ready IFN-α production by female pDCs at baseline, which is caught-up to by male pDCs the following day.

Using baseline flow cytometry data I constructed a LASSO model for pDC IFN-α which found that female sex, cell activation via CD123 expression, and TNF-α production all positively influence pDC IFN-α, whilst pDC abundance, plasma free testosterone, and DHT negatively influence it. Whilst caveated by the relatively small sample size, several covariates were validated in a separate larger cohort, providing confidence in non-overlapping covariates from this smaller model.

The identification of sex importantly adds validity to the model as increased female pDC IFN-α is the most widely-published differential pDC behaviour (see Section 1.4). Whilst this is determined at the chromosomal level by XCI-escape by TLR7 in females, the model identifies an additional sex-associated relationship in the negative influence of plasma free testosterone. The immune-suppressive properties of testosterone have previously been linked with reduced male responses to the seasonal trivalent influenza vaccine (Furman et al. 2014; Flanagan et al. 2017; Jacobsen and Klein 2021), and indeed the model identifies total testosterone as negatively influential of pDC IFN-α when free testosterone is excluded. That the effect of biologically available, free testosterone overshadows that of total testosterone in the model implies a direct antagonistic relationship between testosterone and pDC IFN-α since 97-99% of total plasma testosterone is biologically unavailable when circulating so only the 1-3% unbound testosterone is biologically available to act on cells in the blood (Anderson 1974; Mazer 2009). Likewise, DHT was also identified as negatively influential of pDC IFN-α and is a more potent androgen than testosterone and adds to reports that exogenous DHT has previously been shown to reduce pDC IFN-α *in-vitro* (Wang et al. 2012). This negative association between androgens and pDC IFN-I appears to contrast with the positive reported relationship for female sex hormones as oestrogen had been shown to increase pDC IFN-α in post-menopausal humans and in humanised mouse models (see Section 1.6.4).

The identification of pDC abundance and CD123 expression as influential of pDC IFN-α in the model supports the sex differential flow cytometry data and concurs with my overarching proposal that biallelic TLR7 expression lowers the activation threshold of female pDCs to allow faster IFN-I production than male pDCs. Indeed, CD123 and IFN-α are higher in female pDCs at baseline and CD123 is positively influential of IFN-α in the LASSO model. Likewise, pDC proliferation is greater for female pDCs, and is negatively influential of IFN-α in the LASSO model, supporting a shift away from IFN-α and towards antigen presentation by the day following vaccination for female pDCs. Indeed, Webb et al. 2019 reported higher levels of the

T-cell co-stimulatory molecule CD86 on female pDCs than on male pDCs following 20hrs TLR7 stimulation. Related, TNF-α is seen as the molecular switch for the shift towards antigen presentation (Psarras et al. 2021), and despite no sex differences in the flow cytometry data, is positively related to IFN-α in the LASSO model, suggesting that TNF-α is more readily produced by pDCs that produce high levels of IFN-α so conceivably produce an infection-stunting amount of IFN-I and can afford to begin transitioning to antigen presentation sooner.

IFN-I is important for priming the adaptive immune system by activating CD4+ T-helper cells and B-cells (Teijaro and Farber 2021) and accordingly the female adaptive immune system is predominantly $T_H2$-biased (see Section 1.5). Since the data above confirmed superior IFN-I production by female pDCs in response to BNT162b2 + LAIV co-/vaccination, it was therefore expected that antibody titres against the antigens contained in BNT162b2 would be higher in females. The exact opposite was in fact seen here with males mounting stronger antibody responses to both Spike and RBD. This was however only seen in individuals without evidence of natural SARS-CoV2 infection, and the effect was lost in individuals with natural infection. Importantly, this study was undertaken between October and November 2021 when SARS-CoV2 had been circulating in the UK for nearly two years (Lillie et al. 2020), making it impossible to control for time post-infection or number of infections and/or exposures. Thus it remains that the sex difference seen for uninfected individuals, where the antigen dose was identical, may have been precluded in infected individuals with respect to: different timings of infection, uncontrolled antigen 'dose', and subsequent waning of antibody responses (Townsend et al. 2022). Similarly, no data was collected regarding intrinsic confounding factors such as body mass index, chronic health conditions and co-morbidities, or home dynamics such as family size; all of which have been shown to affect the immune response to vaccination (Zimmermann and Curtis 2019). Likewise, the immune response to LAIV has been reported to differ according to pubertal stage (He et al. 2006) but here only cross-sectional hormonal measurements were used in

place of pubertal stage as the limited sample size precluded separate analyses for adolescents in discrete pubertal stages.

Nonetheless, an unexpected differential BNT162b2 outcome was seen for LAIV co-administration; with both anti-Spike-IgG and anti-RBD-IgG higher in co-vaccinated individuals than those receiving BNT162b2 alone. Conversely to sex, this difference was seen only for individuals with prior SARS-CoV2 infection and not uninfected individuals. This effect is similar to that seen by Sparks et al. 2023 who report higher frequencies of "virtual memory" CD8+ T-cells in COVID-19 recoverees and link their increased frequency in males to increased antibody responses to the seasonal quadrivalent influenza vaccine than females. Such non-specific activation of CD8+ T-cells specific to antigens not relevant to an immune response, so-called "bystander" activation, has also been reported for Modified Vaccinia Ankara (MVA) (Maurice et al. 2019) and Bacillus Calmette-Guerin (BCG) (Parmar et al. 2021), and is attributable to IFN-I induced by the initial vaccine (Tough et al. 1996). LAIV is a potent inducer of IFN-I (Koyama et al. 2010) and IFN-I signatures on day 7 post-vaccination were predictive of neutralising antibody titres to LAIV (Cao et al. 2014). Importantly, this was attributable, in children, to greater numbers of total naïve, memory, and transitional B-cells when compared to the seasonal trivalent influenza vaccine (Cao et al. 2014), which is a weaker inducer of IFN-I relative to LAIV (Koyama et al. 2010).

It follows then that the boosting effect of LAIV co-vaccination seen here may be ascribable to increased levels of systemic IFN-I induced by LAIV leading to a non-specific increase in total numbers of B-cells and bystander activation of SARS-CoV2 -specific immune cells; enabling a greater antibody response to the BNT162b2 antigens than BNT162b2 alone. It is therefore surprising that pDC IFN-$\alpha$ was not identified as influential of BNT162b2 antibody titres by either LASSO model, but this may be explained by the fact that IFN-I induction by LAIV does not reach its' maximum until 7 days post-vaccination (Cao et al. 2014), whereas day 0 pDC data was used in the antibody LASSO models. To this end, a positive correlation

was also seen between the change in pDC IFN-α from the day of vaccination to the following day and expression of the CD4 activation marker HLA-DR in co-vaccinated adolescents.

Related, TLR7 and IFN-I induction have been found essential for a robust adaptive immune response to LAIV in mice (Koyama et al. 2007), and in humans, the IFN-I induced by live-virus influenza vaccination can be attributed, at least in part, to TLR7 signalling via pDCs (Koyama et al. 2010). Whilst IFN-I induction is a powerful vaccine adjuvant, excessive induction leads to hyperinflammation and autoimmunity. Accordingly, mRNA vaccines are formulated to minimise TLR7 activation with highly efficient purification methods like High Pressure Liquid Chromatography and inclusion of the hypo-agonistic synthetic nucleoside 1-methylpseudouridine (Pardi et al. 2018); as is the case for BNT162b2 (Li et al. 2022). Interestingly, mRNA preparations with such modifications display an extended cytoplasmic half-life and translational potential in cells *in-vitro* (Warren et al. 2010; Karikó et al. 2011; Lee and Ryu 2021). It follows that TLR7 activation may therefore influence the rate of clearance of an exogenous mRNA within cells and that differential TLR7 activation between individuals could lead to a differential biological half-life for mRNA vaccines *in-vivo*. The immune-suppressive relationship of both free testosterone and DHT with pDC IFN-α identified by the LASSO model may therefore extend to suggest that local free testosterone and DHT work to reduce TLR7 signalling locally within vaccination sites to increase the duration of antigen availability for the humoral immune response (outlined in Figure 3.8), hence the identification of free testosterone as a positive influence in LASSO models for both measured BNT162b2 antigens.

This deviates from the current understanding of the immune-suppressive role of androgens in reducing vaccine response in males compared to females (Jacobsen and Klein 2021; Flanagan et al. 2017; Furman et al. 2014). However, the positive correlation between free testosterone and IgG response is true here of both antigens studied for BNT162b2 and is supported by the inverse sex difference seen for these antigens in individuals un-confounded by natural SARS-CoV2 infection. Similarly,

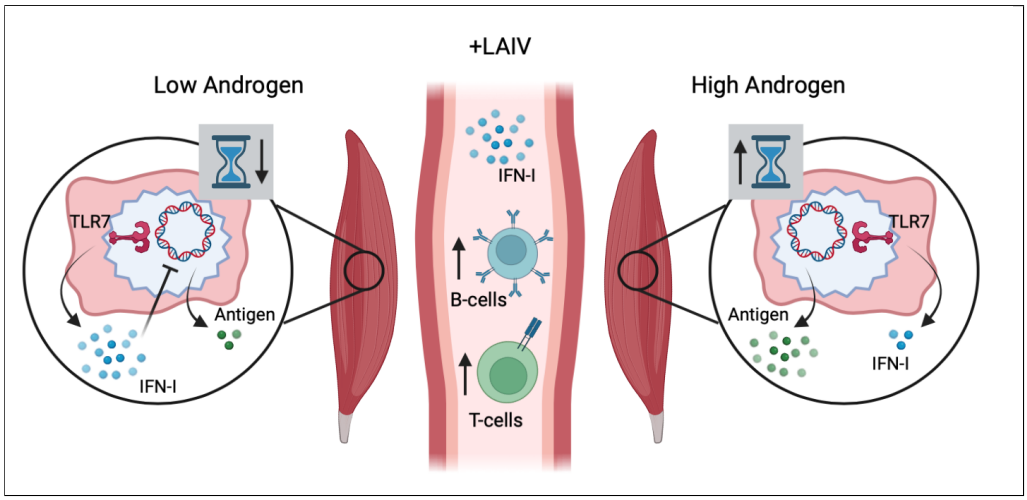



**Figure 3.8: A model for boosting of mRNA vaccine responses by androgens.** Graphical representation of the combination model wherein systemic vaccine-mediated IFN-I boosts general immune activation to increase the vaccine immune response (+LAIV; centre) whilst local reduction of the TLR7 response to mRNA vaccine (circular nucleic acid) in a high androgen environment (right) reduces IFN-I signalling within vaccinated muscle tissue and reduces vaccine clearance, thereby increasing the duration of antigen availability for a more robust adaptive immune response compared to a low androgen environment (left).

despite the widely reported increased female antibody titres to seasonal trivalent influenza vaccines (Nakaya et al. 2011; Klein et al. 2012; Furman et al. 2014; Klein and Pekosz 2014; Nakaya et al. 2016), no sex difference was seen here in the antibody response to LAIV for all four HA serotypes studied, conforming to the absence of reported sex differences for LAIV generally. Thus, the intracellular context introduced by the use of LAIV seasonal influenza vaccines – opposed to the tri-/quadra-valent protein-subunit conjugates – and mRNA-based vaccine technologies like BNT162b2, offers a paradigm shift in the view of the role of androgens in vaccine outcome.

This study is limited in sample size and the number of adolescents recruited was lower than planned due to reduced recruitment resulting from the SARS-CoV2 delta wave in the United Kingdom in autumn 2021 (Eales et al. 2022). This precluded separate analyses of adolescents who received either BNT162b2 alone or BNT162b2 + LAIV co-vaccination, and subsequent division of each group with respect to prior natural SARS-CoV2 infection. Similarly, participants were self-selected from private

schools in Oxfordshire which may introduce bias into the findings as it has been shown that participants engaging with scientific research tend to be more health-conscious, and have higher levels of employment and education which lead to a higher level of general health compared to those who do not participate (Enzenbach et al. 2019). The findings discussed here therefore require further validation in a larger, more representative cohort if they are to be interpreted in the context of public health. Likewise, this study sought to investigate whether a sex difference is apparent in the immune response to BNT162b2, as is reported for seasonal influenza vaccination in adults. The study also sought to additionally investigate whether the sex differential production of IFN-I may contributes to sex differential vaccine outcome but importantly was undertaken in autumn 2021 when the majority of adults in the United Kingdom had already received a primary SARS-CoV2 vaccination. The national roll-out of Pfizer BNT162b2 for adolescents therefore offered the opportunity to study whether the IFN-I response contributes to the immune outcome to primary BNT162b2 vaccination. However, no sex difference has been reported to-date (July 2023) in the outcome of seasonal influenza vaccination in children which limits the power of study to investigate the role of IFN-I in sex differential vaccine outcome.

This study highlights the role played by IFN-I in the outcome to BNT162b2 + LAIV co-/vaccination and identifies sex differences in the behaviour of the primary IFN-I -producing cell type, pDCs. Androgens are identified as important in modulating pDC IFN-I but are conversely beneficial to outcome for both vaccines. As understanding of molecular triggering events that underpin empirically developed vaccine adjuvants increases, so will a need for understanding the nuances surrounding the role played by early IFN-I in determining the outcome of a vaccine response.

# 4

# scRNA-seq finds similar expression for IFN-I genes and classic pDC markers between males and females but differential cytokine response and antigen presentation following TLR7 stimulation

This chapter builds on the protein expression data of the previous two chapters and looks to investigate whether similar sex differences between male and female pDCs exist at the transcriptional level both at baseline and following TLR7 stimulation via CL097.

## 4.1 Abstract

Single cell RNA sequencing (scRNA-seq) is fast replacing conventional analysis of protein expression and allows massively-parallel analysis of transcription across the entire genome within cells individually. Plasmacytoid dendritic cells (pDCs) are critical to innate and adaptive immunity and are the main source of Type I interferon (IFN-I). There are many reports detailing increased production of IFN-I by female pDCs compared to male pDCs via biallelic expression of the upstream single-stranded RNA receptor, TLR7, in females. To these, previous chapters in this thesis add data to suggest differential activation kinetics between male and female pDCs; with a higher activation threshold for male pDCs driving delayed IFN-I production and requiring greater activation through expression of CD123 and HLA-DR. The scarcity of pDCs has thus-far limited their description within scRNA-seq literature to studies of dendritic cell ontology and one small study of their response to influenza virus *in-vitro*. The impact of sex on pDC biology has yet to be investigated via scRNA-seq.

Here, a method for reliably isolating pDCs from lysed whole blood to high purity is developed and SeqWell is employed to generate the largest pDC scRNA-seq dataset to-date. Containing pDCs from five male and five female donors, homeostatic behaviour is described for 27,451 pDCs at baseline in addition to the response to TLR7 stimulation for 10,609 CL097-stimulated pDCs. The majority of unstimulated pDCs cluster together at baseline and show minor polarisation between sexes with evidence for higher baseline activation in males. Such polarisation is not seen for stimulated pDCs as they converge on IFN-I production and no difference is detected in IFN-I gene transcription between males and females. Nonetheless, subtle differences are seen within differentially-expressed genes that suggest greater focus on signalling by female pDCs and greater focus on antigen presentation by male pDCs.

## 4.2 Introduction

Single cell RNA sequencing (scRNA-seq) has transformed the understanding of cell functionality. Analysis of protein expression by traditional methods like flow cytometry are powerful but are limited by the number of proteins that can be analysed simultaneously. Likewise, gene expression analysis via micro-array or bulk transcriptome sequencing typically requires prior cell sorting to separate cell populations or can only provide estimated gene expression profiles for cell types without accounting for heterogeneous expression at the individual cell level (Andrade Barbosa et al. 2021). Cells typically express thousands of genes and scRNA-seq offers unprecedented granularity to the understanding of individual cell functionality by allowing analysis of transcription across the entire genome in each cell (Haque et al. 2017).

Differential production of IFN-I is a widely cited phenotypic difference between male and female pDCs (see Section 1.4) and is corroborated by data in Chapter 2 and Chapter 3. Data from these chapters additionally suggest a difference in the activation kinetics between pDCs from males and females (see Section 2.4.4 and Section 3.4.3).

Little of the published literature surrounds the behaviour of pDCs beyond IFN-I production and scRNA-seq therefore offers the opportunity to: understand in detail the homeostatic behaviour of pDCs, investigate the mechanisms that underpin the sex difference in IFN-I production, and see whether sex differences extend to other aspects of pDC biology.

Only two studies to-date (March 2023) have reported scRNA-seq analysis for pDCs specifically; the first in the context of *in-vitro* exposure of human pDCs to influenza virus (Ghanem et al. 2022), and the second in the context of chronic simian immunodeficiency virus (SIV) infection in Rhesus Macaques (RMs) compared to Sootey Mangabeys (Lee et al. 2021). Neither considered the impact of sex on pDC behaviour, and notably the human influenza study consisted of pDCs from three exclusively female donors.

Prior to incubation with influenza virus, Ghanem et al. 2022 reported that *ex-vivo* human pDCs formed a single scRNA-seq cluster which sub-clustered into nine but without any discerning phenotypes. Following *in-vitro* incubation with influenza virus for 6 or 24 hours, pDCs formed five and seven clusters, respectively. Importantly, these were wholly distinct from the baseline cluster, suggesting all pDCs respond to viral infection at the transcriptional level. Notably, only a single cluster of IFN-I -producing pDCs was present at 6 and 24 hours and appeared dedicated entirely to IFN-I production. These cells had limited transcriptional diversity – additionally expressing only notably *NK-κB* – and had little expression of the classic pDC markers *CD123* and *BDCA2* (Ghanem et al. 2022), suggesting differentiation from baseline. Similar down-regulation of pDC-specific transcripts, such as the transcription factor *TCF4*, was seen amongst the other 6 and 24 hour clusters and was accompanied by upregulation of the T-cell co-stimulatory molecules *CD80* and *CD86*, plus the lymph node -homing receptor *CCR7* (Ghanem et al. 2022); suggesting that antigen presentation represents an alternative terminal differentiation for pDCs distinct from IFN-I production.

One of the 24-hour clusters showed high expression of *CD123*, *BDCA2*, and *TCF4*, and was thought to represent cells that were either refractory to stimulation or, since this cluster was not present at 6 hours, more likely a return to baseline (Ghanem et al. 2022). This stands in opposition to the short measured half-life of pDCs and observed apoptosis following stimulation (see Section 1.3) so could represent an artefact of *ex-vivo* culture, or potential aborted activation which may then explain why the percentage of pDCs producing IFN-I following TLR7 stimulation is never 100% (see Chapter 2 and Section 3.4.3).

Protein secretion was also analysed following the 24 hour influenza incubation, and in addition to the expected IFN-α subtypes, IFN-β, and TNF-α, secretion of the additional IFN-I IFN-ω was also detected, as was secretion of the IFN-λ subtypes (Type III IFN; IFN-III), ISG15, and the chemoattractant CXCL10 (Ghanem et al. 2022). Interestingly, granzyme B (GZB) was also amongst the

proteins more highly secreted by pDCs following influenza exposure, but was also secreted at baseline (Ghanem et al. 2022).

Likewise, despite the absence of a baseline for comparison, similar *IFNA* transcription patterns were observed for pDCs following chronic infection of RMs (Lee et al. 2021), which is both pathogenic and characterised by high levels of immune activation driven, at least in part, by pDC IFN-I (see Section 5.2). *IFNA* transcription was also accompanied by upregulation of *CXCL10*, *ISG15*, and *CCR7*. Further, *HLA-DRA* was identified as the second most highly expressed transcript in pDCs from chronic RM SIV infection and was seen alongside the co-stimulatory molecule *CD86* (Lee et al. 2021) which, in this context of chronic stimulation, supports activation of pDCs progressing from IFN-I production to antigen presentation.

Due to their relative scarcity, pDCs are rarely detected in PBMC scRNA-seq experiments and seldom in sufficient numbers to justify detailed analysis. Their description within the wider scRNA-seq literature is therefore limited to DC-specific ontological analyses which report a nuanced transcriptional profile that makes their delineation from other DCs difficult (Villani et al. 2017; See et al. 2017).

For example, it has been argued that the proportion of pDCs that adopt the antigen-presenting phenotype following stimulation represent contamination with so-called "pre-DCs" which branch during development from the same progenitor as pDCs, and still therefore express pDC-defining markers like CD123 and BDCA2, but have not yet fully differentiated into cDCs (See et al. 2017). This is undermined by their reported frequency of ∼0.001% – 10 to 50 -fold lower than pDCs – given the magnitude of HLA-DR upregulation seen in, for example, Section 2.4.4. Villani et al. 2017 also reported a DC population which overlaps both conventional pDC and cDC transcriptional profiles; these so-called "AS-DCs" were named because of their unique expression of *AXL* and *SIGLEC6* but were also found to express low levels of *CD123* and *BDCA2*. Interestingly, pre-DCs were also shown to express *SIGLEC6* (See et al. 2017) and the populations described by both studies also uniquely express *CD2*, *CD5*, *SIGLEC3*, and *CX3CR1* (Villani et al. 2017; See

et al. 2017), so likely concern the same population of cells separate to pDCs with higher antigen-presenting potential.

Regardless, after excluding AS-DCs Villani et al. 2017 still found pDCs to express *CD86* which suggests at least some capacity for antigen presentation by pDCs as their pDC population was confirmed to also express upstream genes for IFN-I production like *IRF7* and *TLR7*, and the pDC-specific transcription factor *TCF4*. Interestingly, *GZB* was also detected within pDCs (Villani et al. 2017).

Separately, scRNA-seq analysis of DC subsets within human umbilical cord blood described two separate pDC clusters; one expressing classic pDC markers like *CD123*, *BDCA2*, *TCF4*, and also *GZB*, and a unique second cluster dominated by megakaryocyte-like genes such as *PPBP*, *PF4* and *CD9* (Jin et al. 2019). If also detected in adults, this would introduce an additional homeostatic dimension to pDCs in terms of platelet activation and clotting.

None of these scRNA-seq studies however investigated whether a transcriptional difference exists between pDCs from males and females. Indeed, very few phenotypic studies of pDCs consider sex differences in their behaviour beyond IFN-I production.

At the individual cell level, the pDC response to stimulation is heterogeneous. The widely-cited increased production of IFN-I by female pDCs (see Section 1.4) for example is detectable because not 100% of pDCs produce IFN-I following TLR7 stimulation (see Chapter 2 and Section 3.4.3). Indeed, this percentage of pDCs that produce IFN-I following stimulation was shown to be unaltered by increasing TLR ligand concentration, and was attributed to undefined bottlenecks within the trafficking of uptaken ligands to endosomes (Wimmers et al. 2018). Further, in addition to the IFN-I producing phenotype, two additional phenotypes are defined via CD80/PD-L1 within *ex-vivo* human pDCs following incubation with influenza virus and are thought to represent distinct stages of differentiation after IFN-I production towards antigen presentation (Alculumbre et al. 2017). Differences in the proportions of these populations may underpin the observed sex difference in IFN-I between males and females but the factor driving differentiation between

the three phenotypes was reported to be TNF-α (Alculumbre et al. 2017; Psarras et al. 2021); the production of which has been shown not to differ between male and female pDCs (Meier et al. 2009; Wang et al. 2012; Webb et al. 2019).

Elsewhere, levels of co-stimulatory CD86, importantly shown to increase following stimulation in pDC scRNA-seq (Lee et al. 2021; Ghanem et al. 2022), are reportedly higher on female pDCs following TLR7 stimulation than male pDCs (Webb et al. 2019). Alternatively, female pDCs have been shown to express higher levels of *IRF5*, which fulfils a similar role to IRF7 in TLR7 signal transduction (see Section 1.2.3), and differential expression of *IRF5* has been shown to contribute to increased IFN-α production by female pDCs (Griesbeck et al. 2015).

Such scarce reports of the differences in biology between male and female pDCs beyond the TLR7/IFN-I axis (see Section 1.4) highlight the large gaps missing from our understanding of basic pDC behaviour. scRNA-seq offers a platform through which to conduct large scale analyses to understand the behaviour of individual pDCs both at baseline and following activation. Reports thus far have however been limited to descriptions of pDCs in semantic comparisons to minor other DC subsets, or have been conducted on a small scale without the scope to consider differences between biological sexes.

The aim of this chapter was therefore to utilise scRNA-seq to analyse a large number of pDCs isolated to high purity from similar numbers of male and female donors to understand whether their functionality differs during homeostatic conditions, and whether sex-differential production of IFN-I following TLR7 stimulation extends to further aspects of pDC biology. To this end, pDCs were isolated from healthy donors before and after stimulation with CL097 and 38,060 cells analysed from ten individuals matched equally for biological sex.

## 4.3 Materials and Methods

### 4.3.1 Ethics Statement

Whole blood was taken in sodium heparin vacutainers (BD) from healthy donors (median age 25yrs; range 24-36yrs) in accordance with Human Study Protocols approved by the Research Ethics Committee (REC) at Yorkshire & The Humber – Sheffield (GI Biobank Study 16/YH/0247). Written, informed consent was obtained for each participant.

Donors were recruited anonymously from a pool of healthy adults and the youngest six selected for each sex to allow closer comparison to the protein expression data in Chapter 2 and Chapter 3. Donors were excluded if they reported illness or vaccination in the last 7 days to prevent obfuscation of the true IFN-I response.

One male was excluded on technical experimental grounds after an array failed to seal and thus their cells were not reliable isolated from each other during RNA capture, precluding single-cell resolution. One female was excluded during data cleanup as their unstimulated sample yielded zero cells post-cleanup (see Section 4.4.2).

### 4.3.2 Confirmation of BDCA2 Expression by pDCs following TLR7 Stimulation

Whole blood was stimulated using the whole-blood assay as Sampson et al. 2022 (see also Section 2.3.2) with a reduced incubation time of 4hrs and an additional condition omitting brefeldin, as proposed for the single-cell experiment (see Section 4.3.3).

Samples were stained for flow cytometry as Sampson et al. 2022 (see also Section 2.3.5) with a modified antibody panel containing CD14-PE-Cy5 (BioLegend, Cat: 301864) to accommodate BDCA2-BV421 (BioLegend, Cat: 354212).

### 4.3.3 pDC Enrichment from Whole Blood before and after TLR7 Stimulation

TLR7 stimulation of pDCs was performed within whole blood with adaptations to Sampson et al. 2022. Four 50ml Falcon tubes per donor were prepared in advance to contain 5mls R10 + CL097 (2ug/ml) and 5mls whole blood mixed with each (final conc. CL097 1ug/ml) for incubation for 4hrs in a 37°C tissue culture incubator. Samples incubated within 45mins of blood draw.

For unstimulated samples, and stimulated samples following 4 hours incubation, red blood cells were lysed by addition of 40mls RBC lysis buffer (BioLegend) to each tube for 20mins at room temperature. White blood cells were pelleted via centrifugation (500g; 3mins) and washed in 45mls PBS + 1% FBS + 20mM EDTA (FACS Wash Buffer; FWB). Tubes were then pooled 2-into-1 and washed again with 45mls FWB before a final resuspension in 1ml FWB each and further pooling 2-into-1 into a single 15ml Falcon tube per donor.

pDC enrichment was then performed via EasySep pDC Isolation Kit (StemCell): 30ul Fc-γR -blocking antibody and 60ul each of Component A and B were added to each sample for 30min incubation at 4°C before incubation with 200ul magnetic beads for a further 10mins at 4°C.

Tubes were then placed in pre-cooled EasySep magnets (StemCell) for 5mins at 4°C and supernatant decanted into a new 15ml Falcon for a second 5min incubation at 4°C after which supernatant was decanted into a new 15ml Falcon.

Cells were pelleted by centrifugation (500g; 3mins) and resuspended with 100ul Far-IR Live/Dead (Thermo) diluted 1/500 in FWB, plus 5ul BDCA2-BV421 (BioLegend, Cat: 354212), plus 5ul of either: CD45-FITC, CD45-APC, CD45-PE-Cy7, or CD45-BV605 (BioLegend, Cat: 304006, 304012, 304016, 304042, respectively). Samples were incubated at 4°C for 20mins before addition of 1ml FWB and centrifugation. Cells were resuspended in 10mls FWB and passed through a 0.45µm filter into a new 15ml Falcon.

Cells were pelleted by centrifugation, aspirated, and resuspended in residual volume ($\sim$ 200µl) and pooled into a single 1.5ml polypropylene tube. Sample was transported to the Cell Sorting Facility on ice (under 5mins).

### 4.3.4 pDC isolation via Fluorescence-Activated Cell Sorting

Fluorescence-Activated Cell Sorting (FACS) was performed via Sony MA9000 for four donors per sort; matched in number for sex to control against batch effects introducing artificial sex differences. Pooled, stained pDCs were sorted into 5ml FACS tubes containing 400ul R10 media. Both sample and collection chambers were maintained at 4°C for the duration of the sort.

After gating to remove debris, doublets, and dead cells, pDCs were defined as BDCA2+ and sorted according to donor via differentially labelled CD45. See Section 4.4.1 for representative gating strategy.

### 4.3.5 Single-Cell Gene Expression Measurement via SeqWell

FACS-isolated pDCs were immediately diluted with R10, or concentrated via centrifugation and aspiration, to 75,000 cells/ml and single cell RNA sequencing (scRNA-seq) gene expression analysis via SeqWell (Gierahn et al. 2017) undertaken by fellow DPhil Student Nicholas Lim with minor contributions from myself.

Briefly, cells were allowed to settle via gravity into microwells on the SeqWell array – one array per sample. Each well contains a uniquely-barcoded RNA capture bead. The array was sealed and the cells lysed before bead removal and reverse transcription of bead-bound RNA (Maxima H RT; Thermo), followed by exonuclease digestion to remove remaining single-strand overhangs (ExoI; NEB). Whole transcriptome amplification was performed using KAPPA HiFi (Roche) and PCR products size-selected twice (0.6X then 1.0X) via AMPure XP SPRI

(Beckman). After quantification via QBit High Sensitivity DNA kit (Thermo), appropriate dilutions were used for library preparation via Nextera XT using a custom P5 oligo. Tagmented libraries were size-selected once more (0.6X) and quantified via TapeStation D5000 High Sensitivity (Agilent) prior to sequencing.

Quantified libraries were sequenced via NextSeq using NextSeq500/550 v2 (75 cycles) kits (Illumina) set for a 20 base custom Read 1 primer and 50 base reverse primer.

### 4.3.6 Single-Cell Data Processing

Single-cell sequence data was downloaded from BaseSpace (Illumina) as *.fasta* files and reads aligned to the GRCh38 human genome via *STARsolo* (Kaminow et al. 2021). Samples were demultiplexed by Nextera index and cell-by-gene matrices were created via *STARsolo* without UMI-collapsing, and unfiltered (*raw*) files downloaded for local analysis.

### 4.3.7 Data Analysis

Flow cytometry data was analysed with FlowJo v10.7.1 (BD) and pDCs defined as described in Section 2.3.6, or simply as BDCA2+ for FACS.

Graphs were plotted and analysed using R Studio running R v4.2.0 via base R and package *ggpubr*; two-group continuous variables were analysed with two-tailed Student's T-test for parametric data or Wilcoxon test for non-parametric data (nb: an unpaired Wilcoxon test is equivalent to Mann Whitney U test). Where appropriate, Welch's correction was applied for unequal variances and Bonferroni correction used for multiple comparisons.

Single cell data was analysed via the R package *Seurat – v4* (Hao et al. 2021). Doublets and low-quality cells were filtered out via: high/low total gene count, high/low individual transcript count, and high percentage of mitochondrial gene

reads. Gene expression data was then Log2-normalised and centred via the inbuilt *ScaleData()* function and the top principal components identified via the inbuilt *ElbowPlot()* function for unsupervised clustering via Uniform Manifold Approximation and Projection (UMAP).

UMAP is a dimensionality reduction technique that approximates the topology and weights the closeness of data points in multi-dimensional space via Riemannian geometry – here the number of selected PCAs defined the number of dimensions – then uses the closeness weights to preserve topology as the data is collapsed into two dimensions (McInnes et al. 2020). UMAP was selected as it better preserves global topology during collapsing compared to contemporary methods, such as t-distributed stochastic neighbour embedding (t-SNE), which reduce dimensions by individual data points and therefore preserve local topology at the expense of global topology (Luecken and Theis 2019).

Contaminating clusters were identified using the top 25 differentially-expressed (DE) genes by cluster calculated via the inbuilt *FindVariableFeatures()* function and removed. Data for remaining clusters was re-centred before repeated unsupervised clustering via UMAP.

Upregulated pathways within clusters were identified using the top 50 DE genes per cluster via Gene Set Enrichment Analysis (GSEA) (Subramanian et al. 2005) to search the MSigDB Hallmark dataset (Liberzon et al. 2015) and curated KEGG pathways (Kanehisa and Goto 2000) using a minimum cut-off of three index genes per pathway.

Data was sub-setted via sex and stimulation and co-expressed gene modules within each group identified via Weighted Gene Correlation Network Analysis (WGCNA) (Langfelder and Horvath 2008). Upregulated pathways within WGCNA gene modules were identified via GSEA as above. GSEA was also performed on the top 50 DE genes per group as identified via Seurat's inbuilt *FindVariableFeatures()* function. For visualisation via Volcano Plot, infinite p-values (ie expression in one

group compared to zero expression in the other), -Log10(p-adjusted) was assigned an arbitrary value of 300.

Module scores were added via Seurat's inbuilt *AddModuleScore()* function for manually-curated modules of: IFN-I subtypes, MHC, and hormone modules; constructed using MSigDB Hallmark pathways for androgen and oestrogen responses (Liberzon et al. 2015).

## 4.4 Results

### 4.4.1 BDCA2 allows high purity pDC isolation from multiple donors simultaneously

The statistical power of an scRNA-seq investigation is determined by the number of cells from which gene expression data is collected (Haque et al. 2017) but the expense of scRNA-seq places limitations on the size of each investigation. In order to study the underlying biology of male and female pDCs, it was therefore important to develop a method wherein pDCs could be isolated to almost 100% purity prior to their loading into scRNA-seq arrays.

Human pDC enrichments kits are commercially available from two companies: a column-based negative isolation kit (Miltenyi) and a bead-based negative isolation kit (StemCell). To avoid the inherent loss of sample retained within sorting columns, the bead-based kit was trialled for the isolation of pDCs from lysed whole blood, before and after stimulation, using the marker BDCA2 to identify pDCs (Table 4.1), as was used for scRNA-seq of human pDCs before (Ghanem et al. 2022).

The commercial pDC enrichment kit proved to be inconsistent and could not be relied upon to yield highly pure pDC populations, especially from large blood volumes (Table 4.1). It was therefore decided to add a second enrichment via Fluorescence-Activated Cell Sorting (FACS) using BDCA2. The low frequency of pDCs within PBMC ruled out FACS straight from lysed whole blood as the increased sorting time raised concerns regarding loss of pDC biology with increased time *ex-vivo* seen by Meier et al. 2008 and in Chapter 2.

The Sony MA9000 can sort up to four conditions simultaneously so to increase throughput, and increase consistency for donors sampled on the same day, separate CD45 antibodies were introduced to allow sorting of pDCs from four donors simultaneously. Donor separation was reliable as the sum of the CD45-separated cells did not exceed 100% of BDCA2+ cells (Figure 4.1).

Staining and post-enrichment sorting via FACS added an additional two hours to the processing time. In the interests of maintaining viability for CL097-stimulated cells with respect to the large-scale apoptosis following activation (Swiecki et al. 2011), the decision was taken to reduce the CL097-stimulation to 4 hours. This decision was supported by the detection of IFN-α protien production by both sexes following 4 hours incubation in Section 2.4.4.

**Table 4.1:** StemCell EasySep pDC Enrichment Trials

| **Experiment** | **Donors** | **Starting blood Vol.** | **Stimulation** | **BDCA2+ gate via flow cytometry** |
|---|---|---|---|---|
| Trial 1 | 2 | 10mls | Unstim | 1 = 46.3%<br>2 = 78.6% |
| Trial 1 | 2 | 10mls | CL097 | 1 = 49.3%<br>2 = 58.5% |
| Small Vol. 1 | 4; pooled | 10mls | Unstim | 69.9% |
| Small Vol. 2 | 4; pooled | 10mls | CL097 | 78.2% |
| Large Vol. 1 | 4; pooled | 25mls | Unstim | 23.0% |
| Large Vol. 1 | 4; pooled | 25mls | CL097 | 32.0% |
| Large Vol. 2 | 1 | 25mls | Unstim | 9.60% |
| Large Vol. 3 | 1 | 25mls | Unstim | 74.9% |
| Large Vol. 4 | 1 | 25mls | Unstim | 10.0% |
| Large Vol. 4 | 1 | 25mls | CL097 | 50.4% |

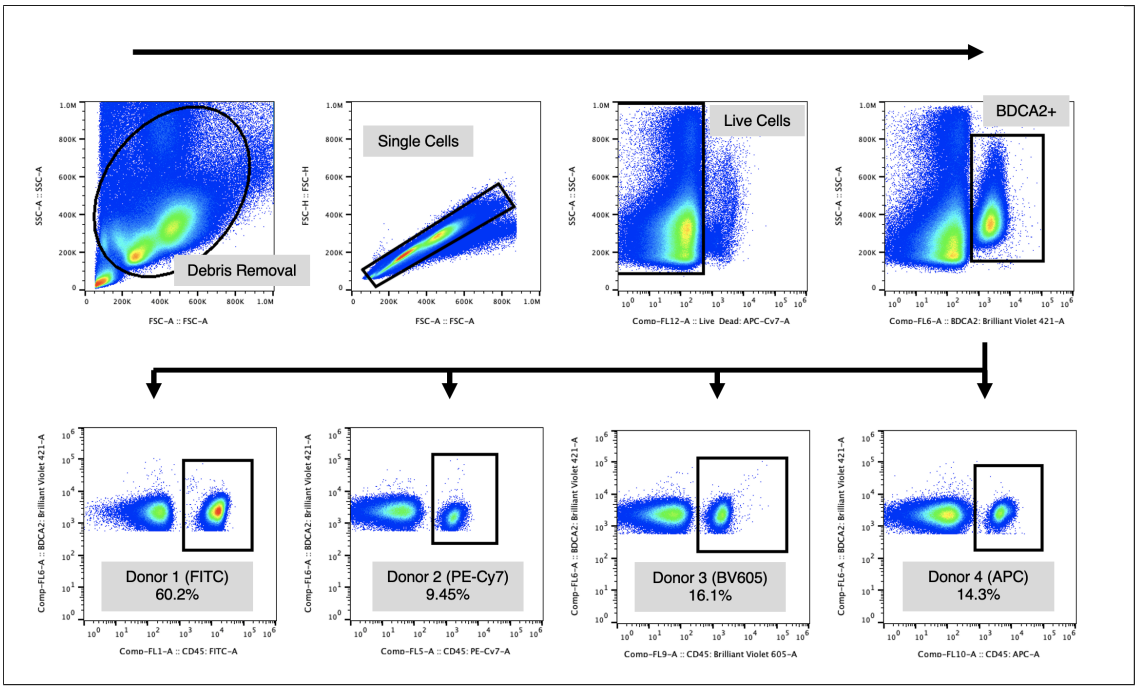



**Figure 4.1: Example of simultaneous 4-donor pDC enrichment via BDCA2.** Lysed whole blood was enriched for pDCs via EasySep (StemCell) prior to labelling with BDCA2 plus donor-specific CD45 and sorted via MA9000 (Sony). After gating to remove debris, doublets, and dead cells, pDCs were defined as BDCA2+ and sorted according to individually-labelled donor CD45.

Lastly, given the reported down-regulation of *BDCA2* by stimulated pDCs (Ghanem et al. 2022), surface expression of BDCA2 was confirmed for CL097-stimulated pDCs to ensure all phenotypes would be captured by FACS using BDCA2 (Figure 4.2). The experiment was initially conducted with only minor adaptation to the whole blood assay (see Section 2.3.2). The scRNA-seq CL097 stimulation was planned without brefeldin to allow for IFN-I feedback mechanisms, so the experiment was repeated with the exclusion of brefeldin to control for similar feedback loops negatively affecting BDCA2 expression. Neither condition showed significant alteration to surface BDCA2 expression post- CL097-stimulation (Figure 4.2).

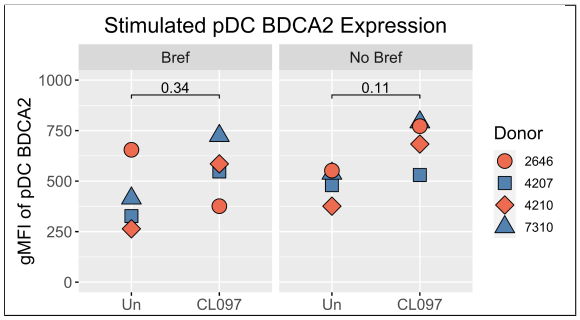



**Figure 4.2: BDCA2 Expression in Unstimulated and CL097-stimulated pDCs.** Blood from four healthy donors was stimulated with adaptation to the whole blood assay (see Section 2.3.2); blood was stimulated for 4 hours at 37°C in the presence (a.) and absence (b.) of brefeldin A (5µg/ml) and stained with a modified antibody panel to include BDCA2 in the surface stain. Pairwise comparisons via Student's paired T-test for equal variance.

### 4.4.2 Data Cleanup post- scRNA-seq

With a method for reliably sorting high-purity pDCs from both unstimulated and CL097-stimulated whole blood, blood was taken from four healthy donors for each of three experiments. Batch effects were controlled for by sampling equal numbers of males and females for each experiment, and undertaking unstimulated and CL097-stimulated experiments on the same day.

The time constraints of enrichment and sorting for unstimulated samples then CL097-stimulated samples in the same day prevented use of the whole blood assay to confirm CL097-stimulation. Instead, a multi-subtype IFN-α ELISA was later performed for plasma collected prior to RBC lysis of unstimulated and CL097-stimulated samples. IFN-α was detected in CL097-stimulated samples for all individuals, and not for unstimulated samples. Median secretion was higher for females (3,180pg/ml) than males (1,692pg/ml) which was not statistically significant (p=0.55) as one male had high IFN-α secretion (Appendix A.6).

Purified pDCs were loaded into SeqWell arrays for scRNA-seq (Gierahn et al. 2017) and subsequent gene expression matrices generated from *.fasta* files via STARsolo (Kaminow et al. 2021). Data was then cleaned to remove low quality cells and artefacts. Figure 4.3 shows data pre-cleanup.

An important feature of low quality cells is a high percentage of mitochondrial transcript reads, which must be balanced against the higher proportion of mitochondrial genes in respirationally-active cells (Luecken and Theis 2019). Likewise, high numbers of total transcripts or unique genes may indicate cell doublets (Griffiths et al. 2018; Luecken and Theis 2019). STARsolo does not collapse like-barcodes as other scRNA-seq analysis packages, so low numbers of total transcripts and unique genes may indicate artefacts of this alignment process (Kaminow et al. 2021). Lastly, a low ratio of total transcripts-to-genes is used to identify cells with poor gene coverage where RNA was likely incompletely captured (Ilicic et al. 2016). These parameters were used to define cut-offs and the data filtered; Figure 4.3 shows data post-cleanup. See Appendix A.7 for summary data of cell numbers by array.

Zero cells remained for the CL097-stimulated sample for donor 7308 post-cleanup so the decision was taken to also remove the corresponding unstimulated sample for 7308 from future analyses. The dataset taken forward for analysis consisted of 38,415 cells.

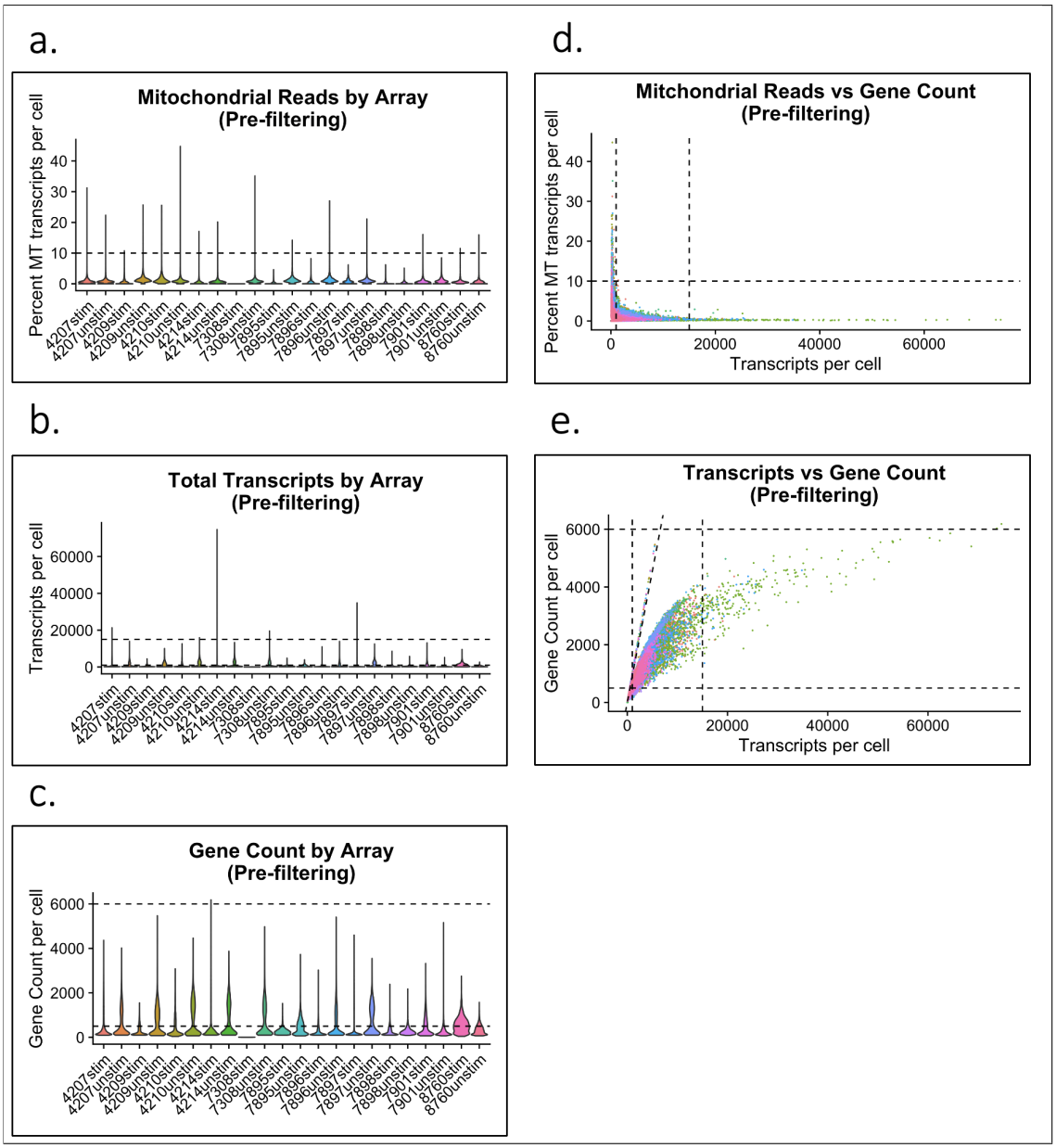



**Figure 4.3: Quality Control Metrics for Unclean scRNA-seq Data.** QC Metrics from uncleaned single cell transcript expression data from purified unstimulated and CL097-stimulated pDC populations. Each donor and condition was analysed via single SeqWell array. a) Percentage of mitochondrial reads (%MT) per cell by array, b) Total Transcripts per cell by array, c) Total unique Genes per cell by array, d) Comparison of %MT against Total Transcripts per cell for all arrays, e) Comparison of Total unique Genes against Total Transcripts per cell for all arrays. Dashed line represents cutoff values for low quality cells.

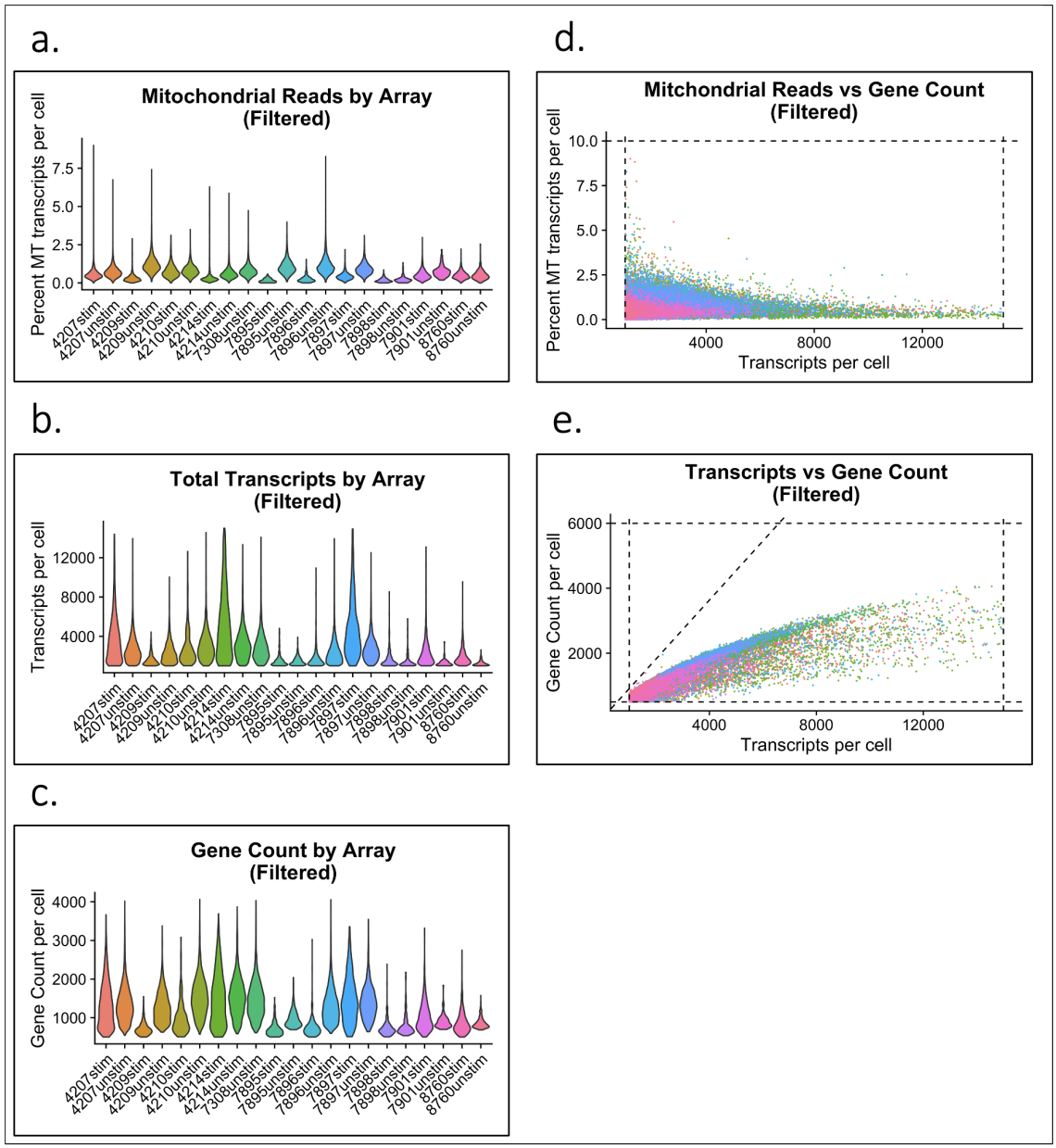



**Figure 4.4: Quality Control Metrics for Cleaned scRNA-seq Data.** QC Metrics from cleaned single cell transcript expression data from purified unstimulated and CL097-stimulated pDC populations. Each donor and condition was analysed via single SeqWell array. a) Percentage of mitochondrial reads (%MT) per cell by array, b) Total Transcripts per cell by array, c) Total unique Genes per cell by array, d) Comparison of %MT against Total Transcripts per cell for all arrays, e) Comparison of Total unique Genes against Total Transcripts per cell for all arrays. Dashed line represents cutoff values.

### 4.4.3 Identification of a small population of "AS-DCs"

Following data cleanup, gene expression counts were Log2-normalised and centred. The 14 most influential principal components (PCs) identified via principal component analysis (PCA) were selected for unsupervised cell clustering via UMAP which yielded six clusters (Figure 4.5a.). The UMAP was coloured by array to ensure no cluster was driven by a single array (Figure 4.5b.). Likewise, mitochondrial reads, total transcripts, and unique gene count were also used to ensure low cell quality was not responsible for any cluster (Figure 4.5c., d. & e.).

A plot of the 25 most differentially-expressed (DE) genes across all cells featured myeloid markers such as lysozyme *LYZ*, *S100A8*, and *S100A9* (Figure 4.6). The top 25 most DE genes per cluster (see Appendix A.8) revealed these originated from Cluster 5 which also contained *AXL* and *SIGLEC6*. Cluster 5, consisting of 355 cells, therefore likely represented AS-DCs (Villani et al. 2017) and was excluded from further analyses.

The top 25 DE genes across the remaining 38,060 cells were then dominated by IFN-I and other inflammatory markers, including the IFN-III (IFN-λ) subtypes (Figure 4.7).

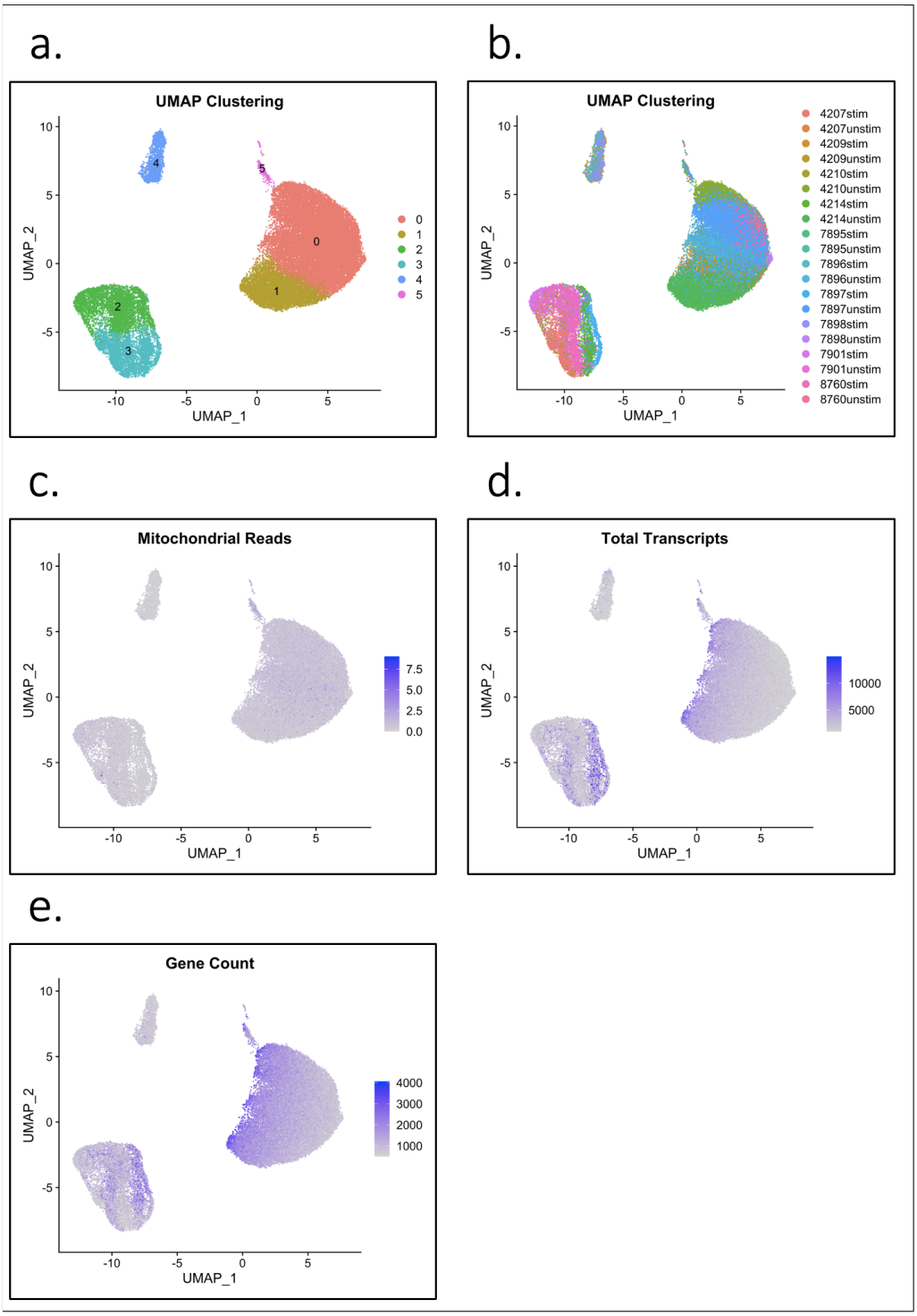



**Figure 4.5: UMAP clusters of pDC scRNA-seq data pre- AS-DC exclusion.** Seurat clusters for unstimulated and CL097-stimulated pDCs defined by unsupervised UMAP. Coloured by: a) cluster number, b) array, c) percentage of mitochondrial reads per cell, d) total transcript count per cell, e) total unique gene count per cell.

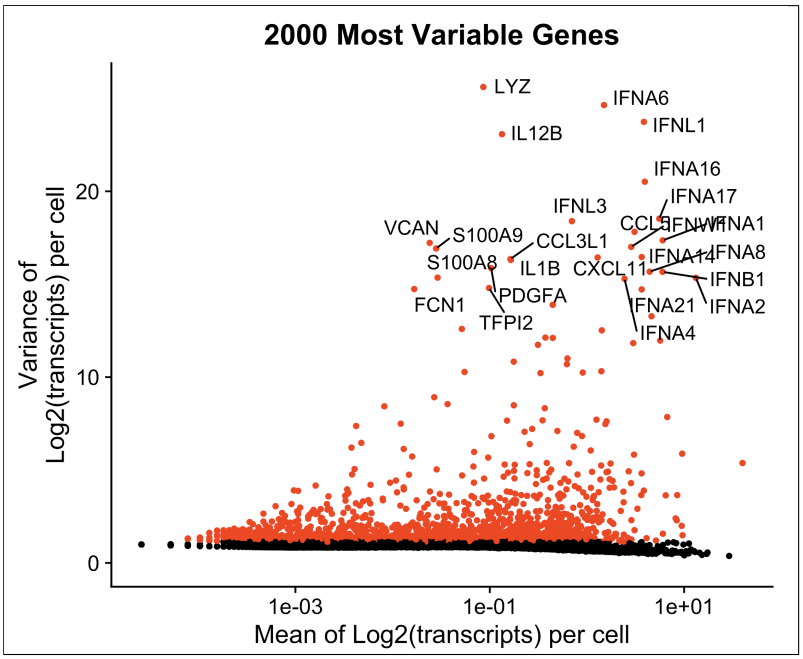



**Figure 4.6: Top 2000 Most Variable Genes pre-AS-DC exclusion.** Variance of transcripts per cell plotted against the mean number of transcripts per cell. The 2000 genes with the highest variance are coloured red; the top 25 are labelled.

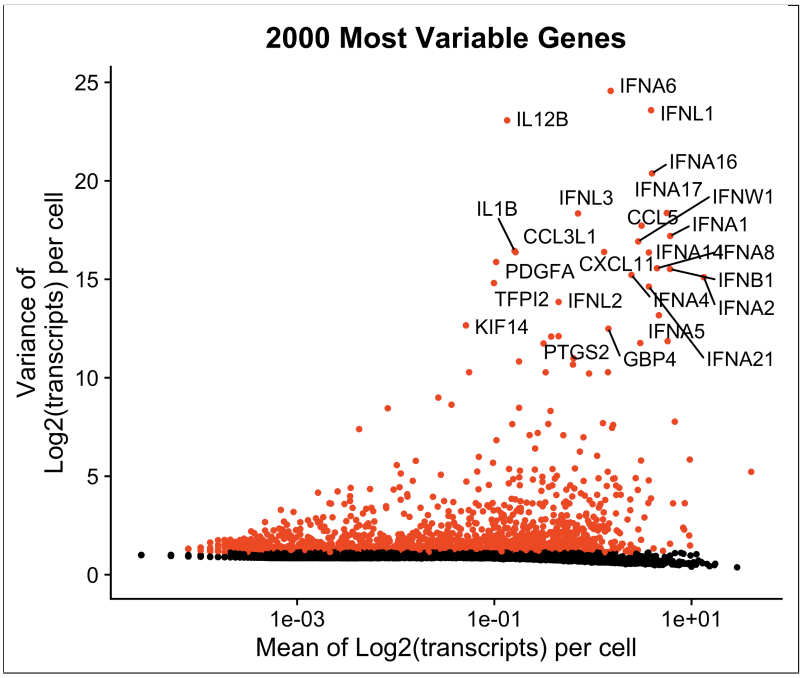



**Figure 4.7: Top 2000 Most Variable Genes post-AS-DC exclusion.** Variance of transcripts per cell plotted against the mean number of transcripts per cell. The 2000 genes with the highest variance are coloured red; the top 25 are labelled.

Following the exclusion of Cluster 5, data was re-centred and the top 13 most influential PCs from a repeated PCA were selected for unsupervised clustering via UMAP which re-identified 5 clusters. (Figure 4.8a.). Again no cluster was defined by a single array (Figure 4.8b.). Cell numbers by cluster are reported in Table 4.2.

**Table 4.2:** Cell Numbers per UMAP Cluster

| **Cluster** | **Cell Number** |
|---|---|
| 0 | 19,179 |
| 1 | 8,272 |
| 2 | 4,692 |
| 3 | 4,117 |
| 4 | 1,800 |
| Total | 38,060 |

Colouring the UMAP by stimulation revealed complete segregation of unstimulated and CL097-stimulated pDCs (Figure 4.8c.), suggesting a global change in gene expression following CL097-stimulation.

Interestingly, unstimulated pDCs in Clusters 0 and 1 appear polarised into female and male sex, respectively, whereas CL097-stimulated pDCs in Clusters 2, 3 and 4, show no clear delineation between sexes (Figure 4.8d.).

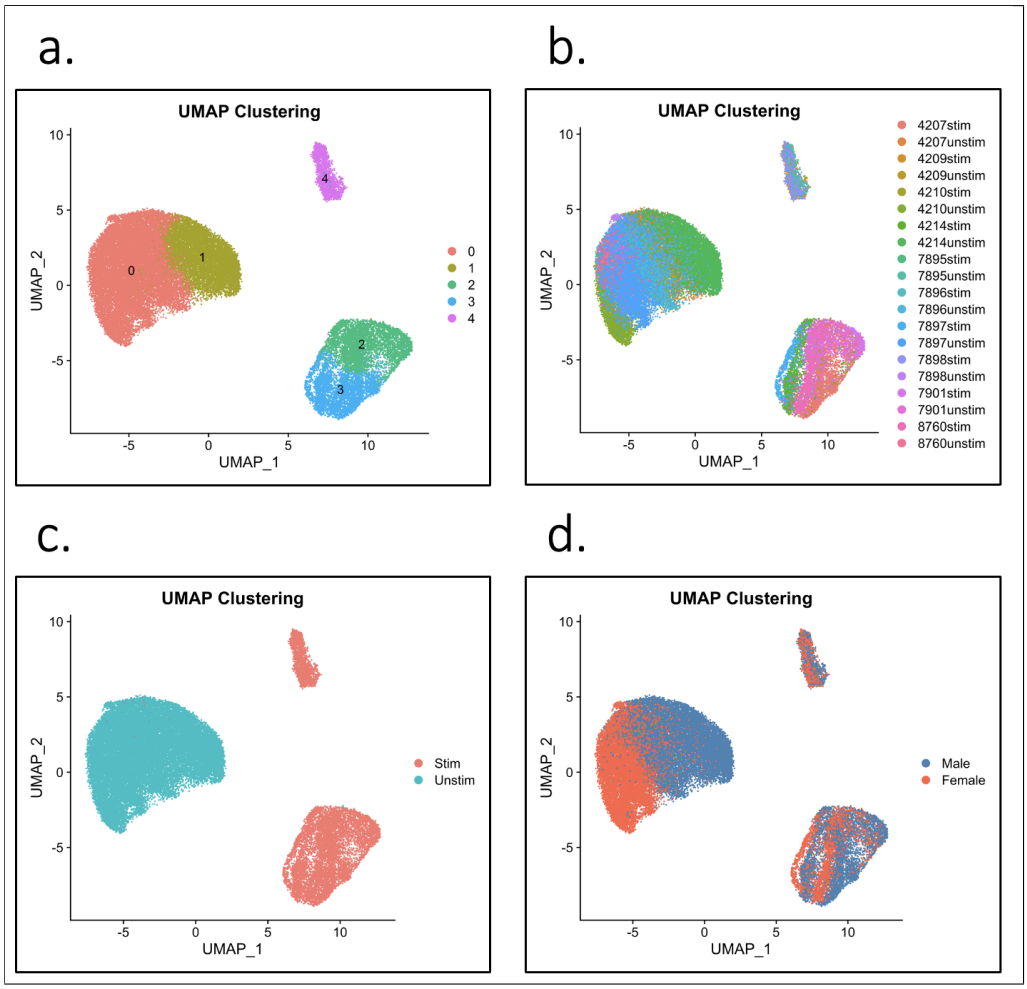



**Figure 4.8: UMAP clusters of pDC scRNA-seq data post- AS-DC exclusion.** Seurat clusters for unstimulated and CL097-stimulated pDCs defined by unsupervised UMAP. Coloured by: a) cluster number, b) array, c) stimulation, d) sex.

### 4.4.4 Functional Dichotomy within Unstimulated and CL097-stimulated pDCs

UMAP clustering produced two clusters for unstimulated pDCs and three for CL097-stimulated pDCs (Figure 4.8a.). To understand the biological processes of each cluster Gene Set Enrichment Analysis (GSEA) was used to search the top 50 DE genes per cluster (see Appendix A.9) for pathways from either the MSigDB Hallmark dataset or curated KEGG pathway database (Figure 4.9). See Appendix A.10 for visualisation of pathway index genes identified by GSEA.

Unstimulated Cluster 0 appears to be the least activated cluster with enrichment for homeostatic pathways such as KEGG_LEUKOCYTE_TRANSENDOTHELIAL_MIGRATION whilst HALLMARK_HEME_METABOLISM also suggests a role for iron uptake (Figure 4.9). Unstimulated Cluster 1 appears to be more activated with the KEGG_RIBOSOME pathway suggesting active protein translation and HALLMARK_TNFA_SIGNALLING_VIA_NFKB suggesting a level of immune activation which may be offset by the HALLMARK_TGF_BETA_SIGNALLING pathway (Figure 4.9).

Cluster 2 is the only stimulated cluster also with enrichment for the HALLMARK_TNFA_SIGNALLING_VIA_NFKB pathway and may therefore correspond to unstimulated Cluster 1. Cluster 2 however is also enriched for the HALLMARK_INTERFERON_ALPHA_RESPONSE and HALLMARK_APOPTOSIS pathways which may instead suggest the TNF-α response in these cells represents a later stage of differentiation away from IFN-I production towards antigen presentation and is supported by their enrichment for HALLMARK_IL2_STAT5_SIGNALLING (Figure 4.9).

Stimulated Clusters 3 and 4 show remarkably similar enrichment with almost complete overlap. Signalling pathways like KEGG_TOLL_LIKE_RECEPTOR_SIGNALLING_PATHWAY, KEGG_JAK_STAT_SIGNALLING_PATHWAY and KEGG_CYTOKINE_CYTOKINE_RECEPTOR_INTERACTION suggest cells within this cluster are in earlier stages of activation and may not yet have been

influenced by autocrine IFN-I signalling compared to Cluster 2. Clusters 3 and 4 also both show enrichment for the KEGG_ANTIGEN_PROCESSING_AND_PRESENTATION pathway which may represent preparation for antigen presentation (Figure 4.9). The only distinguishing genes between Clusters 3 and 4 appear to be the redox protein Thioredoxin *TXN* and anti-apoptotic *MTRNR2L1* (Appendix A.11).

Interestingly, hormone response pathways are identified within unstimulated Clusters 0 and 1; with HALLMARK_ANDROGEN_RESPONSE present in Cluster 0 and both HALLMARK_ESTROGEN_RESPONSE_EARLY and HALLMARK_ESTROGEN_RESPONSE_LATE in Cluster 1.

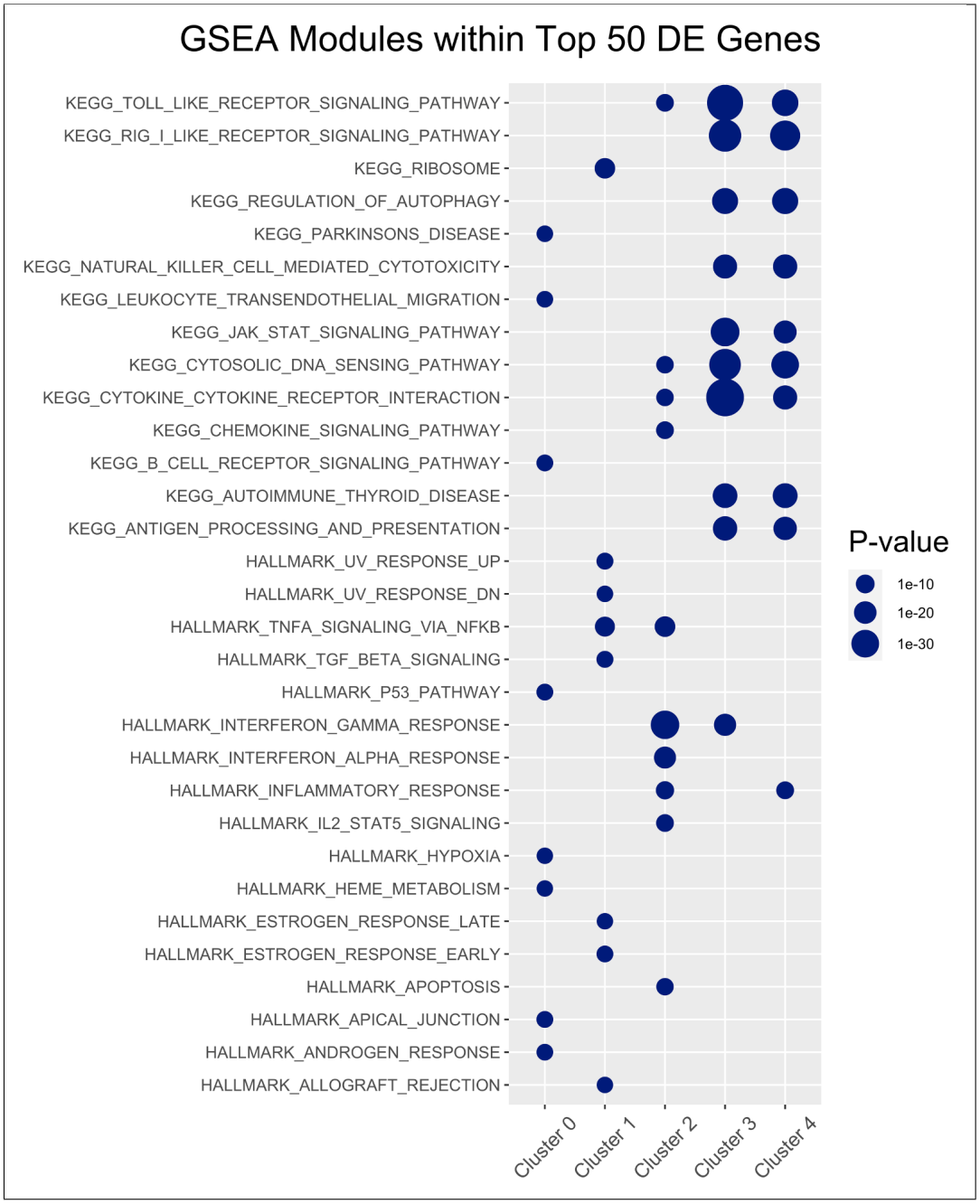



**Figure 4.9: GSEA Module Identification for Individual Clusters.** Pathways identified by GSEA for the top 50 differentially-expressed (DE) genes per cluster. A purple dot indicates identification by GSEA, size corresponds the p-value of the identification.

### 4.4.5 Convergence of Male and Female pDCs following CL097-stimulation

Since differential IFN-I production is the most commonly cited difference between male and female pDCs (see Section 1.4) the data was next stratified by sex and stimulation to compare the relative contribution of the four groups to the UMAP clusters (Figure 4.10).

In contrast to what was expected, there appears to be equal contribution by both sexes to each cluster, with the exception of unstimulated Cluster 1 which is exclusively comprised of male arrays (Figure 4.10).

To understand whether gene expression patterns therefore differ between male and female pDCs before and after CL097-stimulation, Weighted Gene Correlation Network Analysis (WGCNA) was used to search for modules of co-expressed genes within each of the four stratified groups. WGCNA identified zero modules within both unstimulated groups and only a single module for both stimulated groups. GSEA was again used to search for pathways within the co-expressed genes for male and female CL097-stimulated pDC groups within the MSigDB Hallmark dataset and curated KEGG pathway database (Figure 4.11).

See Appendix A.12 for the co-expressed genes identified via WGCNA. See also Appendix A.13 for visualisation of pathway index genes identified by GSEA.

Identical pathways were identified in both and included: KEGG_TOLL_LIKE_RECEPTOR_SIGNALLING_PATHWAY, KEGG_JAK_STAT_SIGNALLING_PATHWAY, KEGG_CYTOKINE_CYTOKINE_RECEPTOR_INTERACTION, and KEGG_ANTIGEN_PROCESSING_AND_PRESENTATION (Figure 4.11); as were seen for Clusters 3 and 4 (Figure 4.9). Both sexes also showed enrichment for the HALLMARK_TNFA_SIGNALLING_VIA_NFKB pathway (Figure 4.11) which suggests that TNF-α -mediated IFN-I antagonsim may not differ between male and female pDCs.

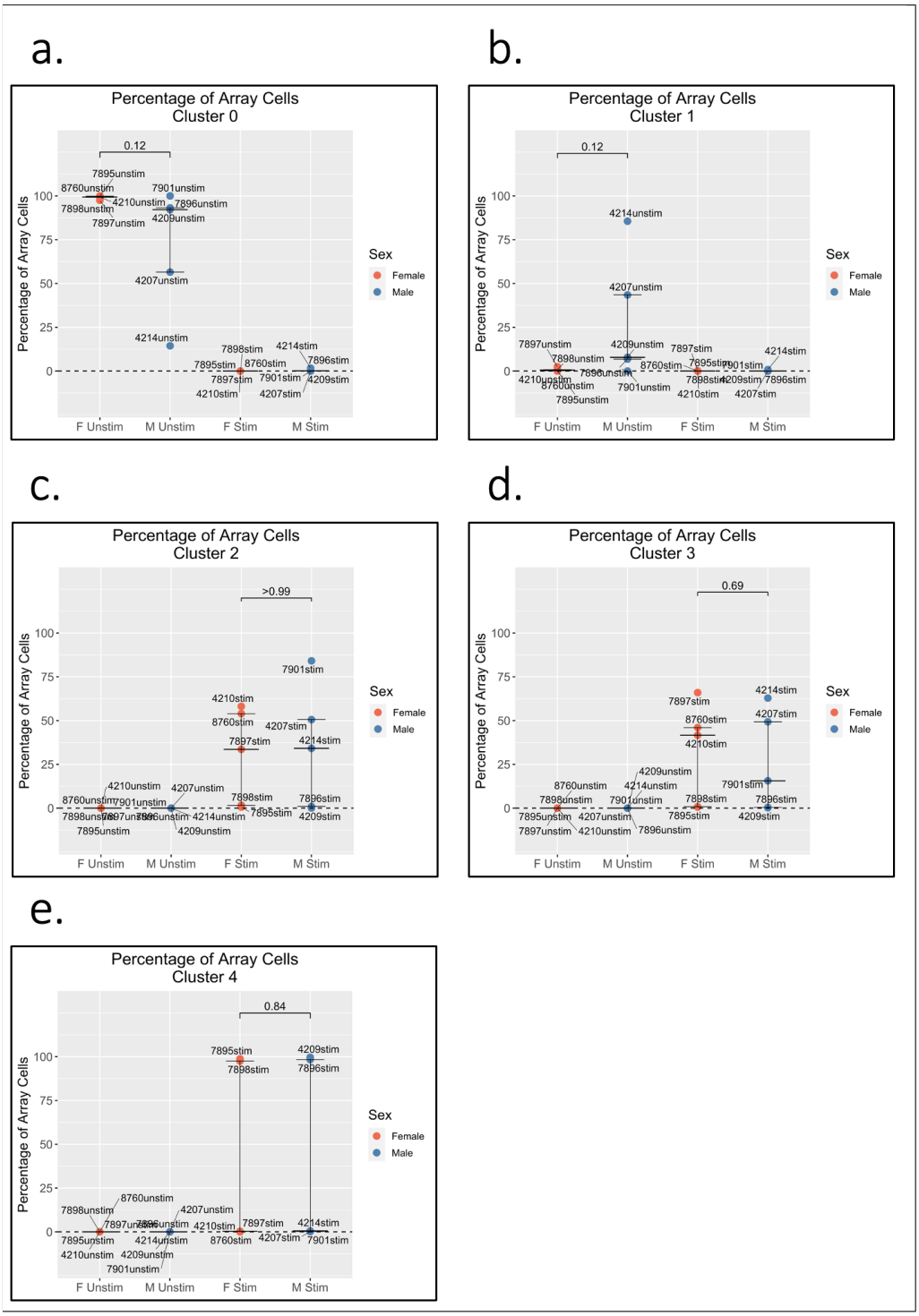



**Figure 4.10: Distribution of Arrays by Cluster.** Labelled plots showing the percentage of individual arrays present in individual clusters. Dashed line shows 0%. Pairwise comparisons via unpaired Wilcoxon test with Welch's correction for unequal variance. Bars show median with interquartile range for each group.

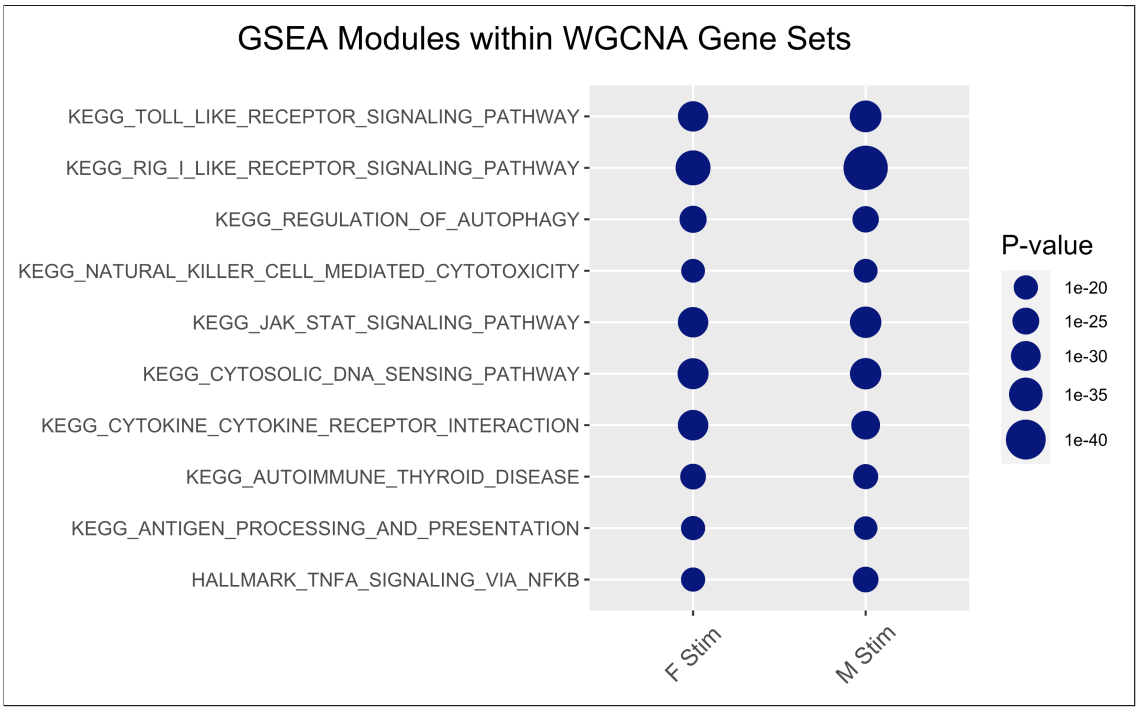



**Figure 4.11: GSEA Pathway Identification for WGCNA co-expressed Genes.** WGCNA was used to identify co-expressed genes within unstimulated and CL097-stimulated pDCs for both sexes and GSEA used to identify enriched pathways within the resulting WGCNA co-expression modules. A purple dot indicates identification by GSEA, size indicates the p-value of the identification.

### 4.4.6 Sex differential pDC IFN production is not mirrored at the transcriptional level

With identical enriched pathways identified within the WGCNA co-expressed gene modules for male and female CL097-stimulated pDCs, the percentage of cells expressing a transcript for the *IFNA* subtypes or *TNF* was next calculated to identify whether the sex difference in protein-level IFN-I production was mirrored at the transcriptional level (Figure 4.12).

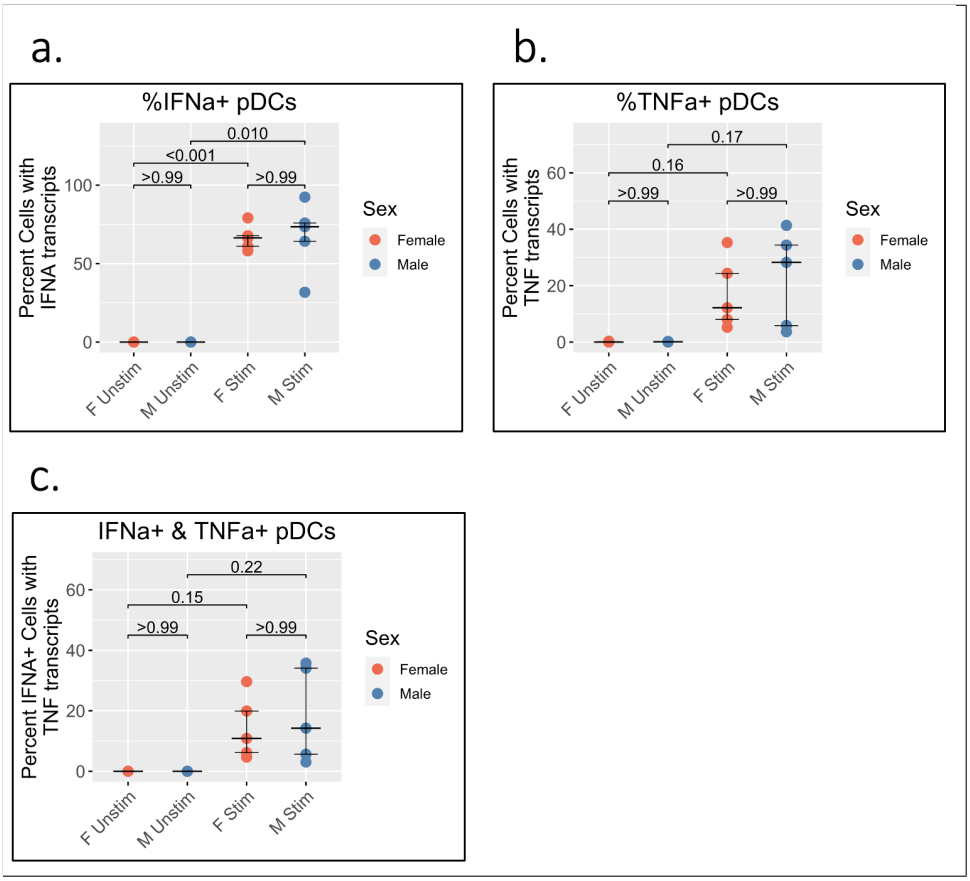



**Figure 4.12: Percentage Expression of *IFNA* and *TNF* transcripts between sexes.** The percentage of total pDCs per array expressing: a) any *IFNA* transcript, b) the *TNF* transcript, and c) the percentage of *IFNA*+ cells also expressing the *TNF* transcript, grouped by sex and stimulation. Pairwise comparisons via unpaired Student's unpaired T-test with Bonferroni correction for multiple comparisons. Bars show median with interquartile range for each group.

Expectedly, both sexes have a significantly higher percentage of *IFNA*+ cells following CL097-stimulation, but unexpectedly there was no difference between the median for stimulated male pDCs (73.5%) and stimulated female pDCs (66.4%) (p=0.93 before adjusting) (Figure 4.12a.).

The percentage of cells expressing the *TNF* transcript was also compared since TNF-α is antagonistic of IFN-α (Psarras et al. 2021). Expectedly a greater percentage of CL097-stimulated pDCs expressed *TNF* for both sexes but this was not significant compared to unstimulated pDCs. The percentage of *TNF*+ cells following stimulation was higher for males (28.5%) than females (17.0%) but again this was not significant (p=0.57 before adjusting) (Figure 4.12b.).

Lastly, the percentage of IFN-α+ cells also expressing *TNF* was compared to account for autocrine TNF-α signalling and again no difference was seen between stimulated pDCs from males (14.3%) and females (10.9%) (p=0.59 before adjusting) (Figure 4.12c.).

### 4.4.7 Expression of canonical pDC markers does not differ between males and females

Whilst the percentage expression of transcripts for the *IFNA* subtypes unexpectedly did not differ between male and female pDCs following CL097-stimulation, data from previous chapters supports a model for differential activation kinetics between male and female pDCs (see Section 2.4.4 and Section 3.4.3). Expression scores were therefore assigned to individual cells for a module consisting of the 13 *IFNA* transcripts to compare whether the level of expression differed between sexes. Expression of *IFNB1* and *TLR7* were also compared, as was expression for a module containing the *IFNL* subtypes, as identified within Section 4.4.3 in the present study (Figure 4.13).

Despite significant upregulation of the *IFNA* module and *IFNB1*, there was surprisingly no significant difference between sexes following CL097-stimulation (Figure 4.13a. & b.). The *IFNL* module followed same pattern (Figure 4.13c.).

Lastly, biallelic TLR7 expresion is reported to underpin the increased production of IFN-I by female pDCs (see Section 1.4). Unexpectedly the expression *TLR7* was not statistically different between male and female pDCs and decreased following CL097-stimulation for both sexes (Figure 4.13d.).

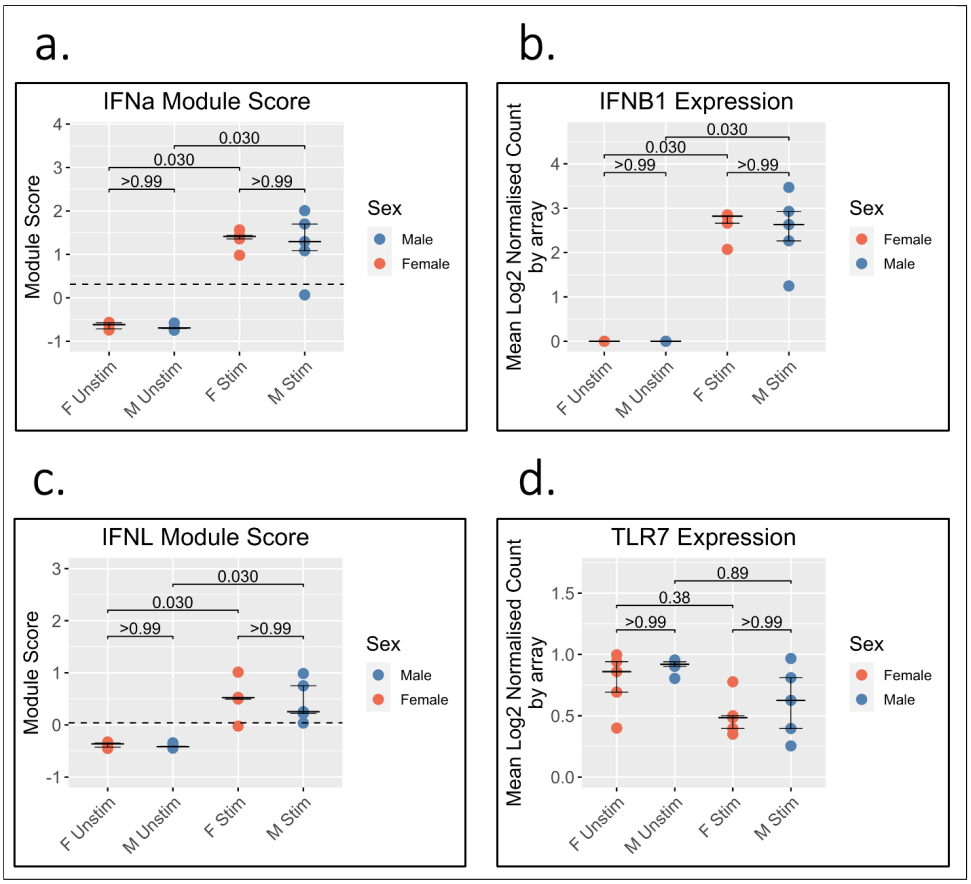



**Figure 4.13: pDC Expression of IFN-I and *TLR7*.** Seurat *AddModuleScore()* was used to score module expression within individual cells then averaged by array for modules consisting of: a) the 13 *IFNA* subtypes, and c) the 3 *IFNL* subtypes. Module score is given representative of the mean across the dataset (dashed line) and grouped according to sex and CL097 stimulation. Log2 Normalised gene counts were averaged across cells within arrays for individual genes: b) *IFNB1* and d) *TLR7*. Pairwise comparisons via unpaired Wilcoxon test with Welch's correction for unequal variance and Bonferroni correction for multiple comparisons. Bars show median with interquartile range for each group.

The data from previous chapters supporting differential activation kinetics between male and female pDCs included differential upregulation of CD123 and HLA-DR at the protein level (see Section 2.4.4 and Section 3.4.3). Expression was therefore compared for canonical pDC markers and other markers of cell activation (Figure 4.14).

Despite consistent surface expression of BDCA2 following CL097-stimulation (Figure 4.2), transcriptional expression of *BDCA2* decreased significantly for both sexes following CL097-stimulation, and did not differ between male and female pDCs. Though not significantly down-regulated upon stimulation, *CD123* also follows a similar pattern (Figure 4.14b.).

Consistent with the notion of antigen presentation by activated pDCs, expression of *HLA-DRA*, the gene for HLA-DR, increases for both sexes following CL097-stimulation, but again shows no significant difference between male and female pDCs (Figure 4.14c.). Lesser upregulation is seen for the wider MHC-II module, but this likewise does not differ between sexes (Figure 4.14d.).

The median MHC-I module score increases slightly following CL097-stimulation but appears to decrease in some individuals. Again no difference is seen between male and female pDCs (Figure 4.14e.).

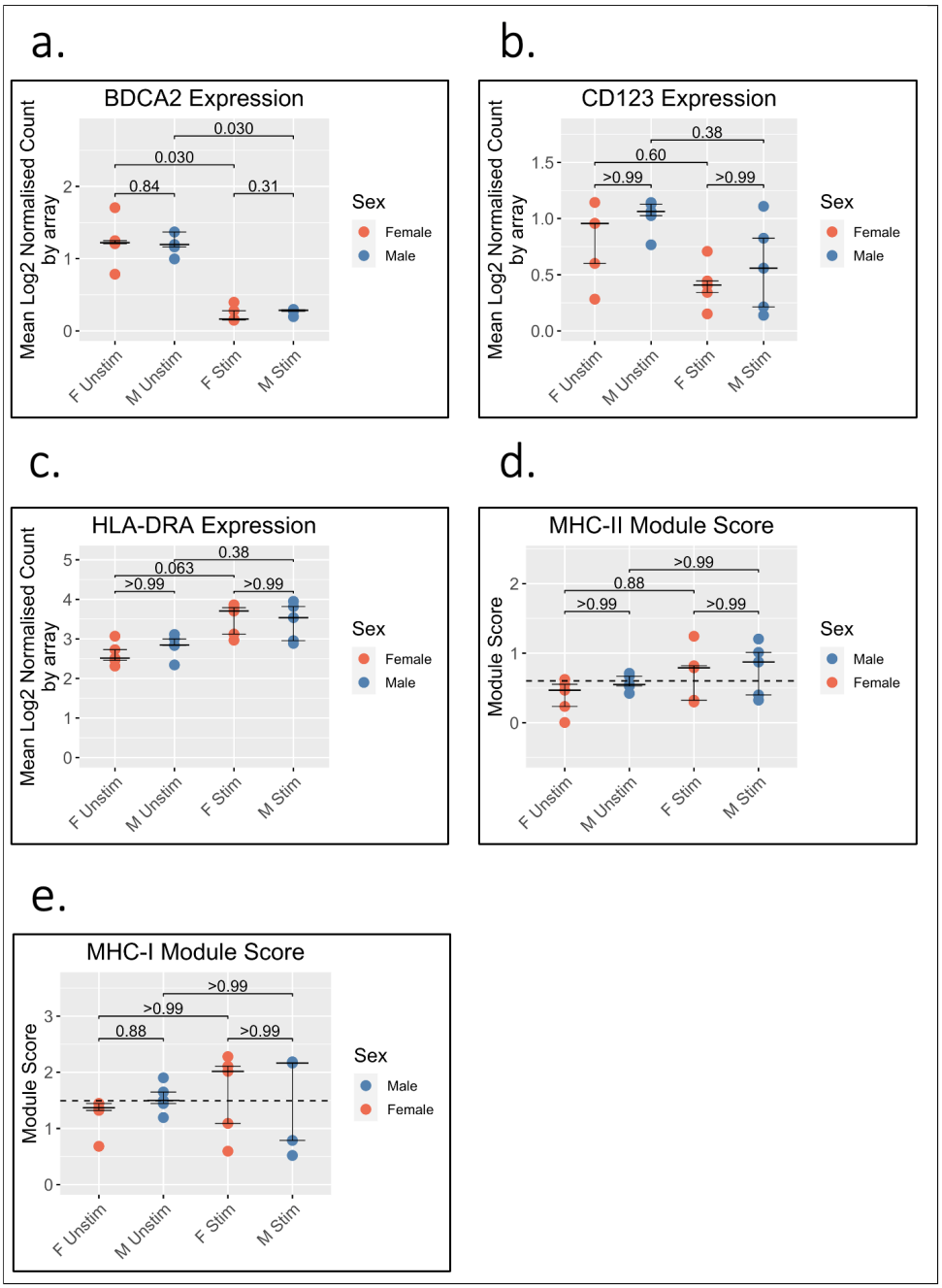



**Figure 4.14: pDC Expression of canonical markers and markers of activation.** Log2 Normalised gene counts were averaged across cells within arrays for individual genes: a) *BDCA2*, b) *CD123*, and c) *HLA-DRA*. Seurat *AddModuleScore()* was used to score module expression within individual cells then averaged by array for modules consisting of: d) MHC-II genes, and e) MHC-I genes. Module score is given representative of the mean across the dataset (dashed line) and grouped according to sex and CL097 stimulation. Pairwise comparisons via unpaired Wilcoxon test with Welch's correction for unequal variance and Bonferroni correction for multiple comparisons. Bars show median with interquartile range for each group.

Lastly, a module score was assigned for ribosomal genes as a measure of the translational activity within the cells, and the percentage of mitochondrial transcripts as a proxy for cellular respiration (Figure 4.15).

Ribosomal module score and percentage of mitochondrial genes decrease in both sexes following CL097-stimulation, but this was only significant for male pDCs (ribosomal p=0.008 & mitochondrial p=0.008, before adjusting). Despite this, there was no statistical difference between the sexes for either unstimulated or stimulated pDCs (Figure 4.15).

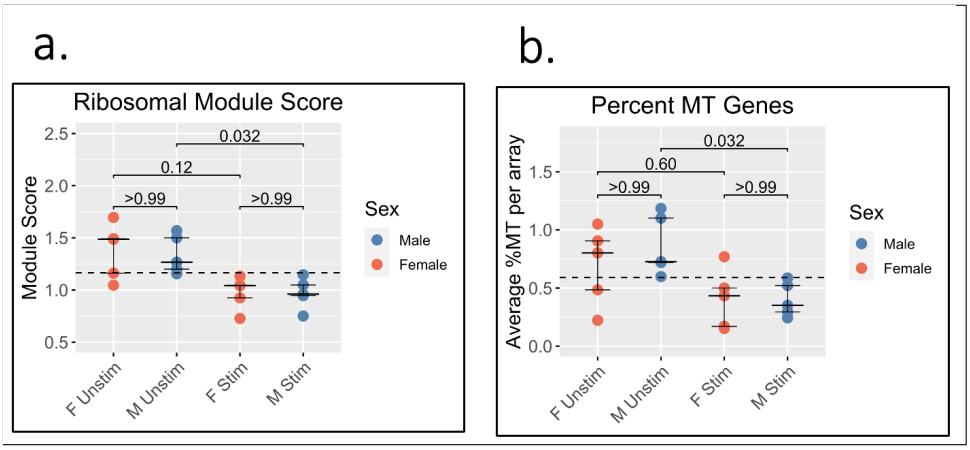



**Figure 4.15: Seurat Module Scores for pDC activity.** Seurat *AddModuleScore()* was used to score module expression within individual cells then averaged by array for modules consisting of: a) ribosomal genes, and b) percentage of mitochondrial (MT) transcripts per cell. Score is given representative of the mean across the dataset (dashed line) and grouped according to sex and CL097 stimulation. Pairwise comparisons via unpaired Wilcoxon test with Welch's correction for unequal variance and Bonferroni correction for multiple comparisons. Bars show median with interquartile range for each group.

### 4.4.8 Sex Hormone Module Scores Correlate with pDC Phenotypes

The role played by sex hormones in modulating pDC function remains to be wholly elucidated (see Section 1.6) but data from Chapter 3 supports immunosuppression of pDC IFN-I by androgens and hormone response modules were identified within the unstimulated clusters in this chapter (see Figure 4.9). Final module scores were therefore added for the genes listed in the MSigDB Hallmark pathways for androgen and oestrogen responses (Figure 4.16). Oestrogen gene sets are differentiated within MSigDB into early and late expression; detectable from 3 and 12 hours post-oestrogen stimulation respectively (Carroll et al. 2006). A corresponding gene set was not available for progesterone.

Expression for the androgen response module increases for both sexes following CL097-stimulation, which is significant for male pDCs (p=0.032). Interestingly, there is not a difference between the sexes (Figure 4.16a.).

Although not significant the early oestrogen response module appears higher in unstimulated male pDCs than unstimulated female pDCs. The module score increases for both sexes following stimulation and no difference is seen between males and females (Figure 4.16b.).

The late oestrogen response conversely shows no difference between unstimulated pDCs but is similarly upregulated following CL097-stimulation and appears higher in females compared to males (Figure 4.16c.).

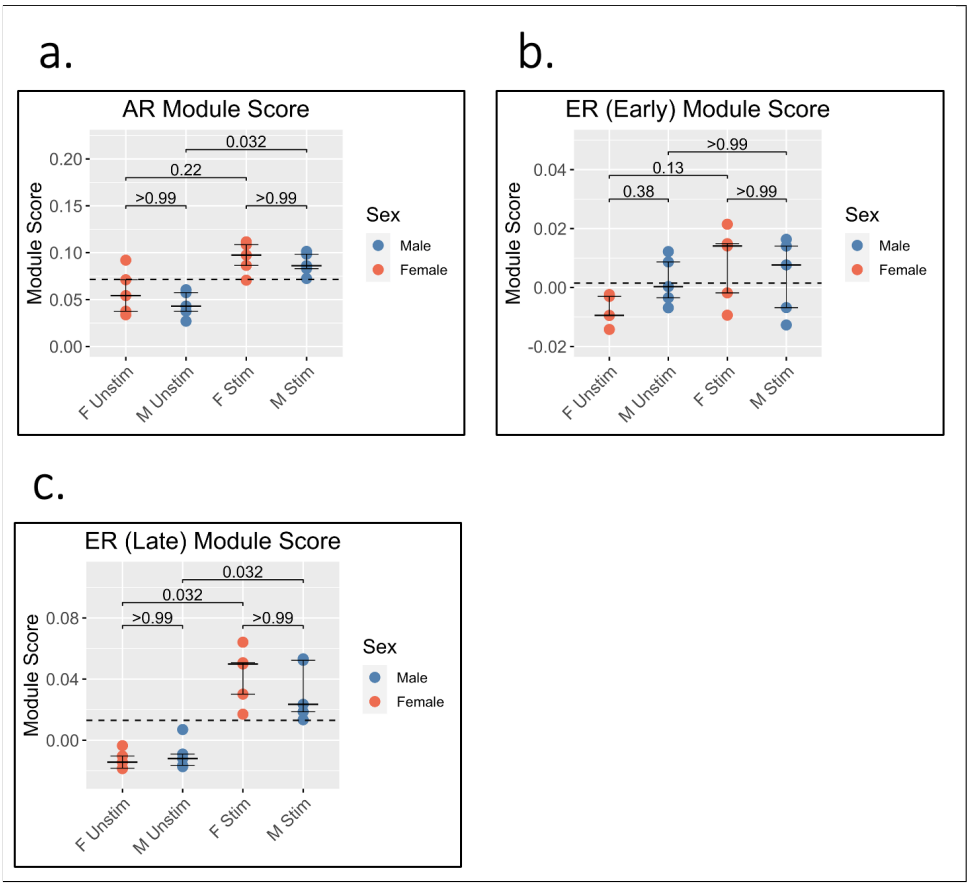



**Figure 4.16: Seurat Module Scores for GSEA Sex Hormone Modules.** Seurat *AddModuleScore()* was used to score module expression within individual cells then averaged by array for GSEA hallmark modules for: a) androgen response, b) oestrogen response (early), c) oestrogen response (late). Score is given representative of the mean across the dataset (dashed line) and grouped according to sex and CL097 stimulation. Pairwise comparisons via unpaired Wilcoxon test with Welch's correction for unequal variance and Bonferroni correction for multiple comparisons. Bars show median with interquartile range for each group.

In order to understand the impact, if any, the patterns of sex hormone response modules have on pDC phenotype, a correlation matrix was constructed using the module scores calculated for IFN modules and average expression for canonical pDC markers (Figure 4.17).

Significant positive correlations were seen for the three IFN modules, which all negatively correlated with the module scores for the classic pDC genes *TLR7*, *BDCA2*, and *CD123*. (Figure 4.17).

Conversely to that expected by the immunosuppressive role of androgens (see Section 1.6.2), the androgen response module correlated positively with all three IFN modules but did correlate negatively with the module scores for *TLR7*, *BDCA2*, and *CD123* (Figure 4.17).

Interestingly, this pattern is mirrored by the late oestrogen response module, though the correlations with *TLR7* and *CD123* are not significant. Indeed the androgen response module score correlates with the late but not early oestrogen response module scores.

The oestrogen response module scores correlate positively with each other though, and both positively correlate with MHC-II and MHC-I (Figure 4.17).

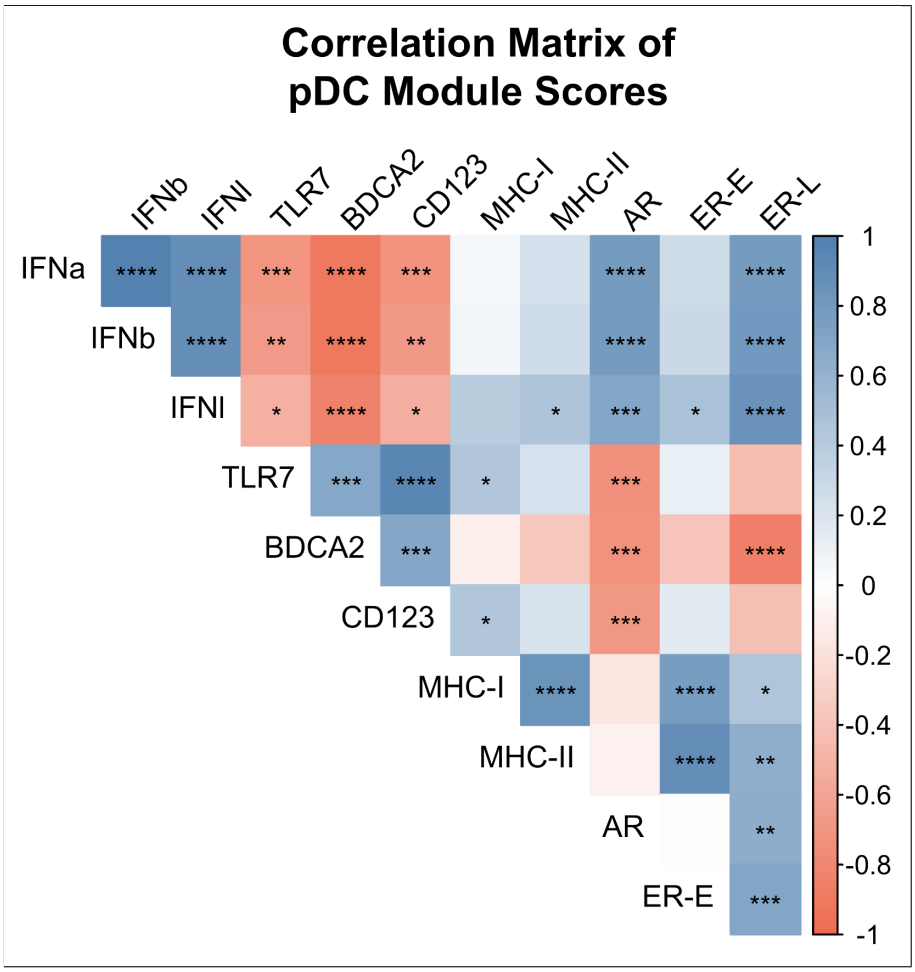



**Figure 4.17: Correlation matrix for Seurat Module Scores.** Seurat *AddModuleScore()* was used to score module expression within individual cells then averaged by array for: *IFNA* subtypes, *IFNL* subtypes, MHC-I, MHC-II, GSEA androgen genes, GSEA oestrogen genes (E = early; L = late). Log2 Normalised gene counts were averaged across cells within arrays for individual genes: *INFB1*, *TLR7*, *BDCA2*, *CD123*. A matrix of individual pairwise correlations was then constructed. Colour represents r-value and stars represent unadjusted p-value.

### 4.4.9 Differentially-expressed Genes reveal differences in the biology of male and female pDCs

With the previously observed sex differences in protein expression (see Section 2.4.4 and Section 3.4.3) seemingly not reflected at the transcript level, the gene expression data was separated by stimulation and differential gene gene expression performed via Seurat's inbuilt *FindVariableFeatures()* function to identify the genes most differentially expressed between males and females in unstimulated pDCs (Figure 4.18) and CL097-stimulated pDCs (Figure 4.19). Interestingly, the magnitude of differential expression is decreased following CL097-stimulation, further supporting the convergence of male and female pDCs following activaiton.

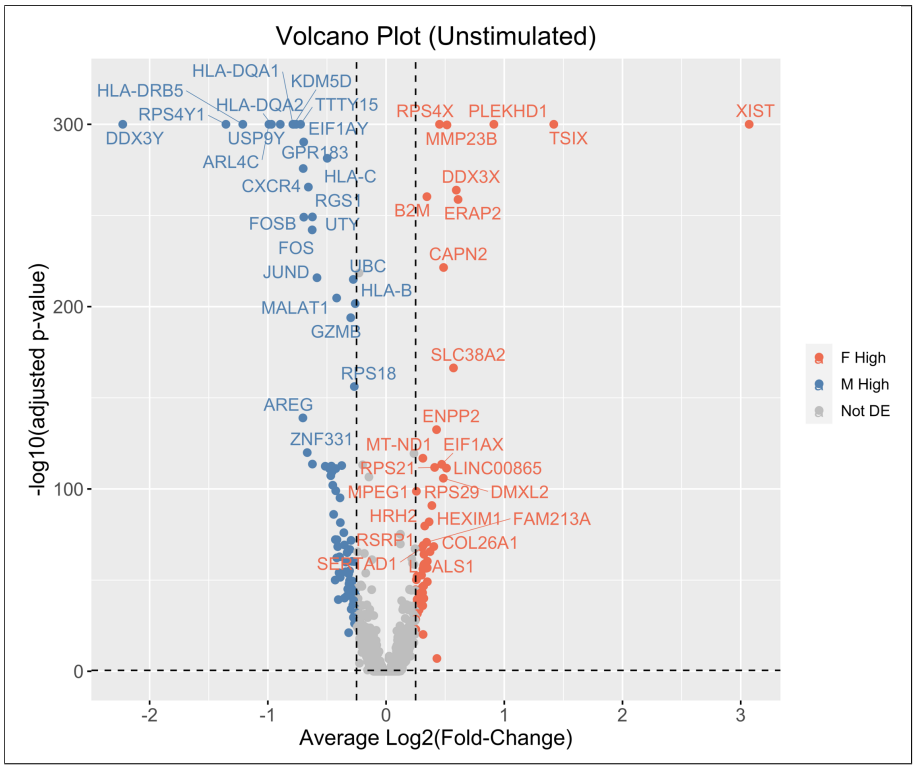



**Figure 4.18: Volcano Plot of Differentially-Expressed Genes by Sex for Unstimulated pDCs.** Volcano plot showing the average Log2(fold-change) of expression between unstimulated male and female pDCs per gene against the adjusted p-value. Horizontal dashed line shows cut off of p-adjusted=0.05 and vertical dashed lines show cut offs for Log2(fold-change) of -0.25 for genes significantly more expressed in males (blue) and +0.25 for genes significantly more expressed in females (red). Labels identify the top 25 differentially-expressed genes for each sex.

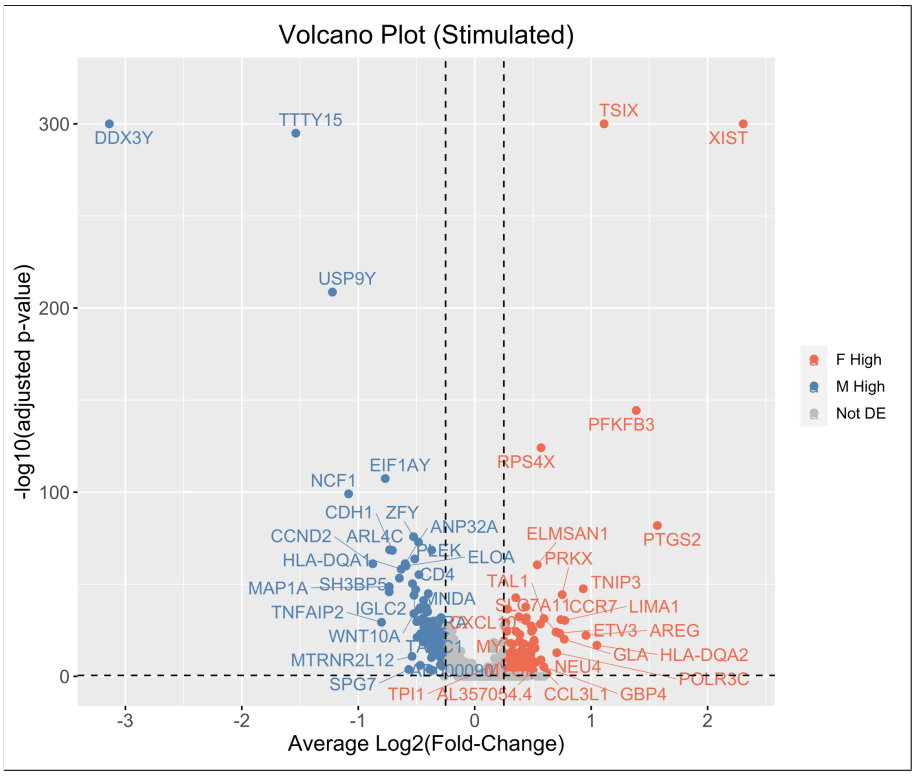



**Figure 4.19: Volcano Plot of Differentially-Expressed Genes by Sex for CL097-stimulated pDCs.** Volcano plot showing the average Log2(fold-change) of expression between CL097-stimulated male and female pDCs per gene against the adjusted p-value. Horizontal dashed line shows cut off of p-adjusted=0.05 and vertical dashed lines show cut offs for Log2(fold-change) of -0.25 for genes significantly more expressed in males (blue) and +0.25 for genes significantly more expressed in females (red). Labels identify the top 25 differentially-expressed genes for each sex.

GSEA was then used to search the top 50 DE genes found for unstimulated and CL097-stimulated male and female pDCs for pathways in the MSigDB Hallmark dataset and curated KEGG pathway database (Figure 4.20).

See Appendix A.14 for the top 50 DE genes in each group. See also Appendix A.15 for visualisation of pathway index genes identified by GSEA.

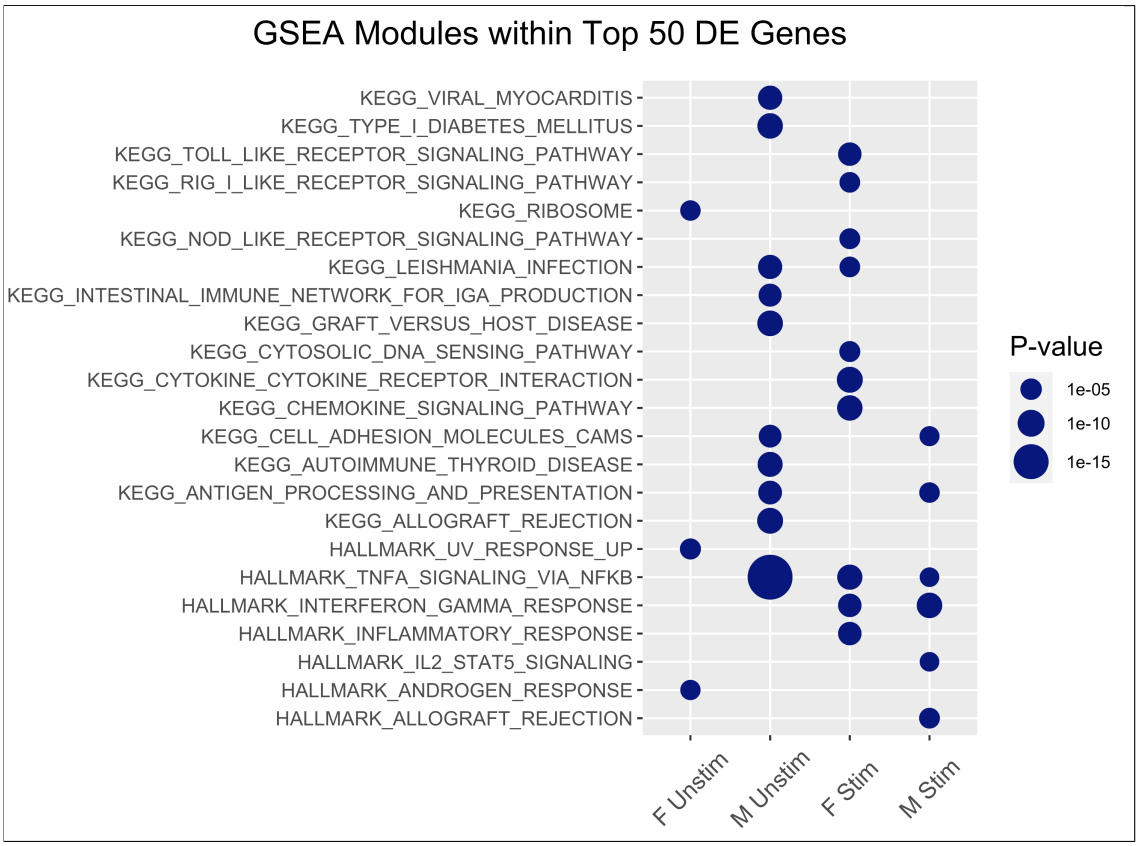



**Figure 4.20: GSEA Pathway Identification for top 50 sex-DE genes in unstimulated and CL097-stimulated pDCs.** GSEA was used to identify pathways enriched in the top 50 DE genes between males and females for unstimulated and CL097-stimulated pDCs. A purple dot indicates identification by GSEA, size corresponds the p-value of the identification.

Very few pathways are identified within unstimulated female pDCs; notably the only group to show enrichment for the KEGG_RIBOSOME pathway (Figure 4.20) despite there being no statistical difference in the ribosomal gene module score to the other three groups (Figure 4.15).

Unstimulated male pDCs show enrichment for general inflammatory pathways, the index genes for which are mostly MHC-II (see Appendix A.15). The only enriched pathway in unstimulated male pDCs with non- MHC-II index genes was HALLMARK_TNFA_SIGNALLING_VIA_NFKB; as seen for Cluster 1 (see Figure 4.9).

Interestingly, despite broadly comparable module scores for classic metrics of pDC behaviour (see Section 4.4.7), there appears to be little overlap amongst the DE genes between male and female CL097-stimulated pDCs.

Stimulated female pDCs show enrichment for several TLR-like receptor pathways like KEGG_TOLL_LIKE_RECEPTOR_SIGNALLING_PATHWAY, KEGG_RIG_I_LIKE_RECEPTOR_SIGNALLING_PATHWAY, and KEGG_NODD_LIKE_RECEPTOR_SIGNALLING_PATHWAY, and also show enrichment for the cytokine production pathways KEGG_CYTOKINE_CYTOKINE_RECEPTOR_INTERACTION and KEGG_CHEMOKINE_SIGNALLING_PATHWAY (Figure 4.15), which align with the more pro-inflammatory nature of female pDCs compared to male pDCs.

These are notably absent from stimulated male pDCs which instead show enrichment for antigen presentation with the KEGG_ANTIGEN_PROCESSING_AND_PRESENTATION pathway alongside the KEGG_CELL_ADHESION_MOLECULES_CAMS pathway and HALLMARK_IL2_STAT5_SIGNALLING (Figure 4.15). Together these support a transcriptional profile directed towards increasing presentation of antigen to the adaptive immune response.

## 4.5 Discussion

IFN-I production by pDCs is a critical component of the immune system and differs between males and females. That the significance of this difference is still not wholly understood exposes the limits in the current understanding of basic pDC biology. scRNA-seq offers a window through which to analyse transcriptional patterns across the entire genome within individual cells to allow unparalleled detail in understanding the behaviour of each cell.

The aim of this chapter was therefore to investigate the difference in IFN-I production between male and female pDCs at the transcriptional level via scRNA-seq, and whether sex differences are apparent in other aspects of pDC biology. A compound method of pDC enrichment followed by Flow cytometry Assisted Cell Sorting was developed for the isolation of pDCs from lysed whole blood to high purity. Through whole transcriptome analysis of pDCs via SeqWell (Gierahn et al. 2017) from 10 healthy donors matched for sex, the homeostatic behaviour of 27,451 unstimulated pDCs was described alongside the response to TLR7 stimulation in 10,609 CL097-stimulated pDCs. This is the largest scRNA-seq study of pDCs to-date (March 2023) and the first to consider differences between pDCs from males and females.

Understanding of pDC behaviour beyond IFN-I production is limited and it has been proposed that some of the biology ascribed to pDCs following their standard classification via canonical markers like CD123 and BDCA2 represents contamination with so-called "pre-DCs". These were found to branch from the same progenitor as pDCs but have yet to fully differentiate into cDCs and were proposed to be responsible for pDC antigen-presenting behaviour (See et al. 2017). Villani et al. 2017 describe an overlapping gene expression profile for their "AS-DCs", so-called because of their unique expression of *AXL* and *SIGLEC6*, which they showed were functionally distinct from pDCs. A small but distinct cluster with corresponding expression of *AXL* and *SIGLEC6* was also identified amongst the pDCs analysed here and so was removed to prevent their obfuscation of true pDC biology. That

MHC-II upregulation was still observed in this study supports antigen-presenting behaviour within pDCs.

Following AS-DC removal, the top differentially-expressed (DE) genes across the dataset were those elicited by stimulation; expectedly the *IFNA* subtypes, but also the alternative IFN-I *IFNW*, and interestingly also *IFNL* subtypes. IFN-λ is reportedly expressed by pDCs with the highest IFN-α expression and was shown to increase survival through autocrine signalling via IFNAR (Yin et al. 2012). Further, high *IFNA* and *IFNL* expression was shown to directly correspond to protein expression as both families of proteins featured heavily amongst the proteins secreted by pDCs following stimulation with influenza virus (Ghanem et al. 2022).

Unsupervised clustering of our dataset via UMAP grouped pDCs into five clusters. Over two thirds of unstimulated cells formed a single cluster, Cluster 0, which suggests limited functional diversity at baseline. Indeed, Gene Set Enrichment Analysis (GSEA) of the top DE genes within Cluster 0 identified relatively few discerning pathways and concurs with Ghanem et al. 2022 who reported no discerning phenotype within their unstimulated pDCs. Cluster 0 nonetheless showed enrichment for transendothelial migration which supports the short half-life and continued renewal of pDCs from bone marrow (Zhan et al. 2016) and was used to identify these cells as naïve, unstimulated pDCs. Interestingly, Cluster 0 also showed enrichment for heme metabolism which may highlight a role for iron in pDC homeostasis; as also suggested by their uniquely high expression of the transferrin receptor (Lippitsch et al. 2017).

Genes present in Cluster 0 aligned with those reported by Jin et al. 2019 in their C1 cluster of "classic" pDCs identified within umbilical cord blood and suggests that pDCs fulfil similar functions *in-utero* as they do in adults. None of the clusters here however correspond to their C2 cluster of "megakaryocyte-like" pDCs which therefore either represent an artefact of platelet contamination or a real population of pDCs present *in-utero* and lost before adulthood.

The remaining unstimulated pDCs formed a second cluster, Cluster 1, which consisted entirely of male cells and appeared more active than Cluster 0 with enrichment for NFκB signalling and the TGF-β pathway. TGF-β has been shown to inhibit TNF-α production (Finkel-Jimenez et al. 2002) and to down-regulate the TNF-α receptor (Weiss et al. 1999) which together may suggest a basal level of activation in some male pDCs that is controlled by TGF-β to maintain a state of readiness.

CL097-stimulated pDCs formed three clusters that were entirely separated from unstimulated pDCs despite not all expressing IFN-I. Likewise, Ghanem et al. 2022 reported complete separation between their unstimulated pDC cluster and clusters of influenza-stimulated pDCs and that only a subset express IFN-I. Together these suggest that all pDCs respond to stimulation and some fulfil a role other than IFN-I production.

Indeed, Stimulated pDCs in Cluster 2 appeared to already have progressed past IFN-I production and showed enrichment for pathways relating to cytokine and chemokine responses. Cluster 2 was also the only cluster to show enrichment for the interferon alpha response specifically which was indicative of a later stage of activation following autocrine or paracrine IFNAR signalling. Further, Cluster 2 was the only stimulated cluster to show enrichment for TNF alpha signalling which supports a later stage of activation as TNF-α drives differentiation of stimulated pDCs (Alculumbre et al. 2017; Psarras et al. 2021). However, the three populations of pDCs described by Alculumbre et al. 2017 via surface expression of PD-L1 and CD80 are not recapitulated here at the transcriptional level. The IL-2/STAT5 pathway was also enriched within Cluster 2 and lends support to previous reports of IL-2 as an autocrine survival signal since IL-2R is detectable on pDCs following TLR stimulation and enhances TNF-α production (Naranjo-Gómez et al. 2007).

The remaining stimulated pDCs formed Clusters 3 and 4 which were identified as early activated pDCs still in the process of producing IFN-I and in which autocrine or paracrine IFNAR signalling has yet to impact transcription. Both clusters

show remarkably similar enrichment for several nucleic acid sensing and signalling pathways and the only discernible difference between them was expression of *TXN*, involved in redox, and *MTRNR2L1*, which is predicted to inhibit apoptosis (Stelzer et al. 2016). Large scale apoptosis within activated pDCs is understood to prevent perpetuation of the IFN-I response (Swiecki et al. 2011) so differentiation of Cluster 4 by an anti-apoptotic marker would suggest a mechanism through which selected cells survive IFN-I production to differentiate into alternative functions.

Related, none of the stimulated pDC clusters here exhibit the 'return-to-baseline' seen following 24 hours incubation with influenza virus and characterised by similar expression of *CD123* and *BDCA2* to baseline (Ghanem et al. 2022). CL097-stimulation here was only 4 hours and suggests 'return-to-baseline' happens only after prolonged activation. Cluster 4 may therefore alternatively represent pDCs in the process of aborting IFN-I production which upregulate survival markers to return to baseline. The terminal fate of stimulated pDCs has yet to be resolved (Reizis 2019) and this would challenge the dispensability of individual pDCs as implied by their short half-life.

Further understanding of the interplay between the different pDC clusters awaits more complex computational investigation through techniques like trajectory inference (Van den Berge et al. 2020).

Unexpectedly, broadly similar behaviour was seen for pDCs when separated by sex. The protein-level difference in the percentage of IFN-α+ pDCs following TLR7 stimulation (see Section 1.4, Chapter 2, and Section 3.4.3) was not seen at the transcriptional level. No sex difference was likewise seen for the percentage of cells expressing *TNF* which discounts a possible role for TNF-α -mediated differentiation in different rates of pDC differentiation (Alculumbre et al. 2017; Psarras et al. 2021). Accordingly, TNF-α has been shown not to differ at the protein level between sexes (Meier et al. 2009; Wang et al. 2012; Webb et al. 2019).

The expression level of IFN-I transcripts also did not differ between males and females. This contradicts previous reports that mRNA expression was higher in

female pDCs than male pDCs for all *IFNA* transcripts following CL097 stimulation (Ziegler et al. 2017; Hagen et al. 2020). In both studies however mRNA was measured after only 2 hours stimulation. That we do not see a difference in cells stimulated for 4 hours supports the model wherein female pDCs respond to TLR7 more readily and males catch up after a delay.

The proposed involvement of TLR7 XCI in this model is however undermined here as no difference was seen in *TLR7* expression between sexes before or after stimulation. Of note, *TLR7* XCI was observed for only an average of 30% of immune cells (Souyris et al. 2018b) and transcript levels were only significantly higher for female pDCs sorted beforehand for biallelic *TLR7* expression from donors with a *TLR7* SNP which allowed identification of biallelic expression via heterozygosity (Hagen et al. 2020). This study was not designed to consider *TLR7* specifically and without such donor selection, biallelic *TLR7* in the females studied may have been subject to sufficient noise to mask the expected difference.

Regardless, *TLR7* was interestingly downregulated within pDCs from both sexes following CL097-stimulation, as were other the classic pDC markers *CD123* and *BDCA2*, which are discordant with the protein expression data in Chapter 2 and Section 4.4.1, respectively. CD123 expression did however decrease below baseline after overnight incubation (see Section 2.4.4) which suggests a lag between decreasing transcript expression and decreased protein expression. Downregulation of *CD123* and *BDCA2* transcription was also seen by Ghanem et al. 2022 and thus may represent a streamlining of pDC transcription towards IFN-I following activation; as evidenced by the overlap of male and female cells within stimulated clusters and identical pathways within co-expressed genes identified via WGCNA.

Considering the DE genes between male and female pDCs following CL097-stimulation did however reveal differential enrichment for immune pathways. Nucleic acid sensing and cytokine signalling pathways were identified within female pDCs and antigen presentation and cell adhesion were identified within male pDCs.

The absence of IFN-I pathways from the sex-DE genes of stimulated pDCs concurs with the discordance seen between the transcriptional data here and protein data of previous chapters which all together suggest that sex-differential IFN-I production is regulated at the post-transcriptional level. One such example is the increased expression of IRF5 shown for female pDCs which fulfils a similar role to IRF7 in TLR7 signal transduction (see Section 1.2.3) and was shown to increase female IFN-I production through increased TLR7 signal transduction (Griesbeck et al. 2015).

Likewise, the half-life of an *IFNA* mRNA was reported to be ∼5hrs, and was increased by an antisense microRNA (Kimura et al. 2013). Indeed, microRNAs are heavily implicated in the control of both translation and transcription of *IFNA* transcripts (Savan 2014) with one reported microRNA, mi-R4661, able to repress translation of nine of the thirteen *IFNA* mRNAs (Li et al. 2012). Over 100 microRNAs are encoded by the X-chromosome and only 2 by the Y-chromosome (Sharma and Eghbali 2014). Differential expression of microRNAs has been described between males and females under both homeostatic conditions and in response to viral infection, and their expression is influenced by sex hormones (Sharma and Eghbali 2014). Differential post-transcriptional regulation of IFN-I transcripts therefore offers one possible explanation to the discord between phenotypic observations and transcriptional data.

Further, the top DE genes in unstimulated female cells were enriched for the ribosomal pathway and female pDCs may therefore translate IFN-I mRNAs more efficiently following activation. Similarly, downregulation of the ribosomal gene module following stimulation was significant for males but not females. Differential translation would also support the model wherein female cells more readily activate and may explain the need for greater MHC transcription by males following stimulation but more importantly also at baseline. Indeed, despite lower HLA-DR protein expression at baseline (see Section 3.4.3) unstimulated male pDCs showed enrichment for MHC transcription here and corresponded to Cluster 1 wherein NFκB may be suppressed by TGF-β (Weiss et al. 1999; Finkel-Jimenez et al. 2002).

The male immune system is overall less inflammatory than for females (see Section 1.5) and baseline modulation by anti-inflammatory proteins like TGF-β could add another layer to potential post-transcriptional IFN-I control in male pDCs.

Lastly, expression scores for hormone response modules increased in both male and female pDCs following stimulation. The androgen module score negatively correlated with classic pDC markers and supports the idea of immune suppression by androgens (see Section 1.6.2) through downregulation of their homeostatic phenotype. Paradoxically oestrogen module scores positively correlate with MHC which was enriched within the male DE genes. This may be explained by the GSEA index gene *FOS* representing convergence of the transcription factors STAT3, shown to upregulate MHC-I (Kida et al. 2013) and AP-1, upregulated by oestrogen receptor signalling (Björnström and Sjöberg 2005).

A caveat of this study is the limited sample size possible due to the expense of scRNA-seq, and the experimental time constraints of SeqWell precluding concurrent measurement of protein expression via the whole blood assay for comparison. Likewise, this study considered only a single time-point and would benefit from a future quantitative PCR (qPCR) time series to measure expression specific key genes, such as the *IFNA* subtypes, *CD123*, and *HLA-DRA* immediately following CL097 stimulation to identify whether expression kinetics differ between males and females before 4hrs, or do not as presented here at 4hrs. Whilst the whole blood assay was developed to best retain *in-vivo* pDC activity, the compound use of magnetic bead separation followed by FACS for pDC isolation was necessary because of their rarity and the delay from ending the incubation to cell lysis may have allowed time for the loss of true pDC biology. Further investigation of post-transcriptional regulation of the aforementioned key genes may yet provide an explanation for the discordance between protein expression data see in Chapter 2 and Chapter 3 and the gene expression data presented in this Chapter.

The aim of this study was to investigate the protein-level sex difference in IFN-I production by pDCs at the transcriptional level, and whether other aspects of pDC

biology differ by sex. No differences were seen in expression of IFN-I transcripts, classic pDC markers, or markers of activation between male and female pDCs at baseline or following CL097-stimulation. Such convergence of function likely represents the essentiality of the primary function of pDCs to produce IFN-I for both innate and adaptive immunity. Nonetheless, differential gene expression supports greater focus on cytokine signalling for stimulated female pDCs and antigen presentation for stimulated male pDCs. Differences in IFN-I production are therefore likely to occur after transcription. To this end, unstimulated cells showed some polarisation for sex and unstimulated female pDCs were enriched for the ribosomal pathway.

Overall there is considerable overlap in the transcription of genes relating to the primary function of pDCs between males and females which highlights their importance to immunity. Subtle differences in differentially-expressed genes suggest minor sex differences in the pDC response to TLR7 stimulation and at baseline.

# 5

# The HIV-1 Clade C transmission bottleneck is different for heterosexual adult-to-adult transmission than *in-utero* mother-to-child transmission

Building on work from the Goulder group showing sex-differences in the HIV-1 Clade C transmission bottleneck for *in-utero* mother-to-child transmission with respect to IFN-I resistance and viral replicative capacity (Adland et al. 2020), this chapter details the investigation into whether similar sex-differences are also present at the transmission bottleneck for heterosexual transmission between adults.

## 5.1 Abstract

A strong selection bottleneck is imposed on transmission of HIV-1 and infection is typically established by a single genotype in the recipient. Many factors have been proposed to underpin this selection and data surrounding Clade C HIV-1 transmission between adults is conflicting; with increased viral replicative capacity (VRC) and increased resistance to IFN-I reported by some studies and not others. *In-utero* mother-to-child transmission (MTCT) of HIV-1 preferentially selects for lower VRC virus than the dominant maternal virus, and was recently reported to differ according to sex; with females receiving lower VRC virus relative to males. Increased IFN-I resistance relative to maternal virus was also reported for *in-utero* transmission to females but not males. IFN-I is an important component of the anti- HIV-1 innate immune response and pDCs have a confirmed role therein. Sex differential IFN-I production by pDCs therefore offers one mechanism by which this selection occurs during MTCT. Only one *in-silico* study of heterosexual adult-to-adult Clade C HIV-1 transmission has to-date examined whether such a difference in selection exists according to the sex of donor and recipient.

Following the same method as for MTCT, NL4-3::*gag-pro* chimeric viruses were generated to investigate whether VRC is differentially selected for during male-to-female and female-to-male transmission of Clade C HIV-1 between matched adult-to-adult transmission pairs. No difference was seen between donors and recipients for transmission in either direction and strong amino acid conservation was seen between donor and recipient Gag-Pro amino acid sequences. A range of VRC values was nonetheless recorded which allowed Random Forest prediction of amino acids within Gag-Pro which significantly affect VRC. These grouped towards Gag protein C-termini and principally concerned alterations to hydrophobicity. Two sequence duplications, 155insGQVSQNA, near the p17 C-terminus, and 483insPYR/KE, at the p6 C-terminus, were found to have the strongest association with high VRC and were faithfully transmitted between donor and recipient.

Overall, there was no significant selection for Gag-Pro -related phenotypes during heterosexual adult-to-adult transmission and it remains that the Clade C HIV-1 transmission bottleneck is different for adults than for *in-utero* MTCT.

## 5.2 Introduction

Transmission of HIV-1 is remarkably inefficient and occurs in less than 1% of sexual encounters (Patel et al. 2014). A strict selection bottleneck is imposed on the transmitted virus and typically only a single genotype from the donor quasispecies is responsible for establishing infection in the recipient (Zhu et al. 1993; Poss et al. 1995). Importantly, this so-called 'transmitter-founder' (TF) virus is almost invariably not the dominant genotype circulating in the donor (Boeras et al. 2011; Deymier et al. 2015) and transmission in fact appears to select for the so-called 'ancestral' genotype similar to that responsible for the donor's own historic infection (Redd et al. 2012; Sagar et al. 2009).

The factors that define this selection bottleneck remain incompletely resolved despite many reports of phenotypic properties common to TF viruses. The frequency of target activated CD4+ T-cells in the sub-epithelial tissue is predictive of HIV-1 transmission (Hladik et al. 2007), but an important obstacle to successful transmission for the incoming virus is separation by the epithelial layer of the recipient genital tract (Joseph et al. 2015). Accordingly, many reports of the phenotypic properties of TF viruses centre on increased efficiency of CD4 engagement by viral Envelope (Env) through: the shortening Env variable loops, reduction in Env N-linked glycosylation sites, and increased Env count per virion (Derdeyn et al. 2004; Li et al. 2006; Liu et al. 2008; Parrish et al. 2013). Env is a key target for neutralising antibodies during chronic infection and such TF phenotypes show selection for ancestral viruses without escape mutations – which can be presumed dispensable during transmission to a naïve host (Nawaz et al. 2011). Similar selection is seen for ancestral co-receptor usage as TF virus Env invariably binds CCR5 and not CXCR4 (Keele et al. 2008; Van't Wout et al. 1994). This is thought to be defined by the initial cell type supportive of productive infection but whether they are CD4+ T-cells or CD4-expressing myeloid cells like macrophages remains a subject of intense discussion (Joseph et al. 2015).

Epidemiologically, HIV-1 can be separated into clades and Env-related TF characteristics hold true for Clade B viruses, which predominate in Europe and America, but may be less applicable to Clade C viruses, which predominate Southern Africa (Parrish et al. 2013; Iyer et al. 2017). An important difference between the clades is their capacity to replicate and the viral replicative capacity (VRC) of Clade C viruses is substantially lower than Clade B viruses (Kiguoya et al. 2017). VRC is strongly associated with the *gag-protease* (*gag-pro*) region of HIV-1 (Kiguoya et al. 2017; Kapaata et al. 2021); for example CD8+ cytotoxic T-cell escape mutations within Gag result in decreased VRC (Goulder and Watkins 2008).

Several studies support a role for VRC in selection at the Clade C transmission bottleneck. Low VRC virus is preferentially transmitted during *in-utero* mother-to-child transmission (MTCT) (Naidoo et al. 2017). Conversely, the VRC of TF viruses following adult-to-adult transmission is reported to be significantly higher than corresponding donor viruses (Iyer et al. 2017). Indeed, viral fitness, predicted computationally using clinical data relating to VRC, was also found in a study of 137 linked heterosexual Clade C transmission pairs to be higher in recipients than corresponding donors (Carlson et al. 2014). This selection was stronger in males as fitness was higher in viruses transmitted to male recipients than female recipients (Carlson et al. 2014). A similar effect was also reported for *in-utero* MTCT where the VRC of the virus transmitted to females was significantly lower than that transmitted to males (Adland et al. 2020).

Importantly this may relate to IFN-I as the virus transmitted *in-utero* to females showed significantly higher resistance to IFN-I (IFN-resistance) than that transmitted to males (Adland et al. 2020). Further, selection for high fitness virus in adults was strongest for male recipients without genital inflammation compared to male recipients with genital inflammation and female recipients regardless of genital inflammation which provides a link between inflammation and selection for lower VRC virus during transmission to females (Carlson et al. 2014).

One of the major consequences of HIV-1 infection is a strong early IFN-I response (see Section 1.1.1). HIV-1 has evolved multiple mechanisms which specifically antagonise interferon-stimulated genes in order to overcome the antiviral effects of IFN-I and establish an infection in a new host (see Section 1.2.5). This ability of a HIV-1 isolate to replicate in the presence of IFN-I, or "IFN-resistance", is therefore a critical consideration when studying the transmission bottleneck. There are however major technical and ethical obstacles in detecting transmission in humans immediately following transmission, before the virus begins to diversify, and the majority of inflammation research surrounding HIV-1 TF viruses has therefore been conducted in non-human primate models using infection with Simian Immunodeficiency Virus (SIV) (Deeks et al. 2015). Infection of the natural host of SIV, Sooty Mangabeys (SMs) results in a non-pathogenic infection characterised by resolution of the IFN-I response within weeks of infection, which is not seen in the pathogenic SIV infection experienced by Rhesus Macaques (RMs) (Silvestri et al. 2003). Strikingly, the very early IFN-I response in SMs most closely resembles that of human HIV-1 non-progressors, who remain healthy despite high viral loads, and in RMs most closely resembles human progressive HIV-1 infection (Rotger et al. 2011; Lee et al. 2021). Through this relationship with the outcome of infection, the very early IFN-I response can therefore be expected to contribute to selection of the incoming virus at, or shortly after, transmission of HIV-1 in humans.

Resistance of TF viruses to IFN-I can also be expected since vaginal infection of female macaques by humanised SIV (SHIV) is prevented by topical IFN-β (Veazey et al. 2016). IFN-resistance is indeed found to be the “most important” transmission determinant for HIV-1 in humans by Iyer et al. 2017 who reported increased IFN-resistance amongst TF viruses compared to corresponding donor viruses. Likewise, increased IFN-resistance is also reported for TF viruses compared to viruses from the same individuals during chronic infection (Fenton-May et al. 2013; Parrish et al. 2013; Gondim et al. 2021).

Related, HIV-1 transmission between adults is most likely when the donor themselves has recently been infected which confirms the importance of the TF phenotype in determining transmission (Deeks et al. 2015). Similarly, Adland et al. 2020 also reported that sex-differential selection for VRC and IFN-resistance *in-utero* is only significant for recently infected mothers and not for chronically infected mothers. The implication that the virus transmitted *in-utero* to females but not males is pre-adapted to the female immune environment through selection during transmission to an acutely infected mother suggests both VRC and IFN-resistance are important transmission determinants for Clade C HIV-1.

Through the IFN-I/TLR7 axis it can be expected that females produce more IFN-I in response to HIV-1 (see Section 1.4). The role of IFN-I in determining HIV-1 transmission is however multifaceted as the protection from SHIV achieved by topical IFN-β was attributed to a protective IFN-I phenotype in vaginal myeloid cells, but was accompanied by a concurrent increase in HIV-1 -permissible CD4+CCR5+ T-cells (Veazey et al. 2016). An increased number of CD4+CCR5+ T-cells was previously associated with increased transmission risk for SIV and their recruitment was attributed to IFN-I production by pDCs at the site of infection (Li et al. 2009). pDC IFN-I has also been shown to differentially affect the disputed initially-infected cell type; enhancing infection of CD4+ T-cells and restricting infection in CD4+ myeloid cells (Tong et al. 2021).

This chapter therefore investigates the contribution of sex differences in selection of VRC at the heterosexual adult-to-adult Clade C HIV-1 transmission bottleneck. Comparison of IFN-resistance was planned but was disrupted by the COVID-19 pandemic and then by technical difficulties.

## 5.3 Materials and Methods

### 5.3.1 Study Participants

Plasma samples were provided by the Zambia-Emory HIV Research Project (ZEHRP); collected from Clade C HIV-1 -infected, antiretroviral therapy (ART) -naïve matched heterosexual transmission partners enrolled in the International AIDS Vaccine Initiative (IAVI) Protocol C early-infection cohort. Ethical approval was granted by both the University of Zambia Research Ethics Committee and the Emory University Institutional Review Board. See (Deymier et al. 2015).

Protocol C was established in 1994 to offer voluntary HIV-1 testing and safer-sex counselling to cohabitating couples in Lusaka, Zambia, and was successful in it's aim to reduce the risk of transmission between serodiscordant couples in the pre-ART era (Trask et al. 2002). Samples used here were collected between 2000 and 2011 when, despite the availability of ART, the continued stigmatisation, fear of disclosure, and intolerable side effects precluded ART acceptance in a third of HIV-1 positive individuals in Lusaka (Sasaki et al. 2012). Study participants not taking ART at the time of sampling therefore did so against the advice of clinicians and counsellors. Written, informed consent was obtained for each participant after an interview with a counsellor, and participation in the study was voluntary.

### 5.3.2 Generation of chimeric NL4-3::*gag-pro* viruses

Viral RNA was extracted from patient plasma and *gag-protease* (henceforth *gag-pro*) cloned into an NL4-3Δ*gag-pro* construct as detailed in Adland et al. 2020. Briefly, *gag-pro* was amplified from extracted viral RNA via a two-round *gag-pro* -specific PCR and electroporated with pNL4-3Δ*gag-pro* into a CEM T-cell line with a HIV-1 trans-activator of transcription (TAT) -driven green fluorescence protein (GFP) reporter, GXR25 (see Brockman et al. 2006). GFP expression was monitored via flow cytometry for expression of >15% in viable cells whence viruses were harvested

by collecting supernatant after centrifugation to remove cells (2000g, 10mins) and aliquots frozen immediately at -80°C.

### 5.3.3 Confirmation of transmission pairs

Chimeric NL4-3::*gag-pro* viruses were deep sequenced courtesy of Prof. David Bonsall, University of Oxford and aligned to HXB2 (Genbank accession: K03455) by Dr. Nicholas Grayson, University of Oxford. *.fasta* files for p17/p24 nucleotide sequences were then re-aligned to a Clade C reference genome (Genbank accession: AB254141) via AliView (Larsson 2014) and phylogenetic trees constructed via Neighbour Joining using JalView (Waterhouse et al. 2009).

Pairwise alignment for transmission pair amino acid sequences was performed using translated consensus deep sequence data via NCBI BLAST (Altschul et al. 1990).

### 5.3.4 Determination of stock viral concentrations

400ul virus was plated with 1x10$^6$ GXR25 cells for 48hrs in a tissue culture incubator and GFP in viable cells measured by flow cytometry. Samples performed in duplicate.

The volume required for a desired percentage of infection by 48hrs for future experiments was calculated using the following formula:

$$\frac{400\mu l}{\%GFP+_{48hrs}} \times \%GFP+_{desired} \times \frac{\text{Total Vol.}_{desired}}{400\mu l} = \text{Virus Vol.}$$

### 5.3.5 Determination of viral replicative capacity of chimeric NL4-3::*gag-pro* virus

Viral replicative capacity (VRC) was determined as in Adland et al. 2020. Briefly, GXR25 cells were infected in triplicate with low concentration chimeric NL4-3::*gag-pro* virus (%GFP+$_{\text{desired}} = 0.03$) and the mean slope of exponential growth (between 48hrs and 168hrs) calculated using the semi-log method in Excel (Microsoft). Results were divided by the slope of concurrently run wild-type NL4-3 infection to generate a normalised VRC relative to NL4-3.

### 5.3.6 Data Analysis and phenotype prediction via Random Forest

Graphs were plotted and analysed using R Studio running R v4.2.0 via base R and package *ggpubr*; two-group continuous variables were analysed with two-tailed Student's T-test for parametric data or Wilcoxon test for non-parametric data (nb: an unpaired Wilcoxon test is equivalent to Mann Whitney U test). Where appropriate, Welch's correction was applied for unequal variances and Bonferroni correction used for multiple comparisons.

Amino acid positions with the greatest influence on the VRC of generated NL4-3::*gag-pro* chimeric viruses were identified via Random Forest as detailed in Segal et al. 2004, using the R package *randomForest* for translated consensus *gag-pro* deep sequence data (see Section 5.3.3).

The Random Forest is a so-called 'recursive partitioning' machine learning algorithm wherein the input samples are repeatedly randomly subsetted, or 'bootstrapped', to generate a tree wherein each bifurcating node represents a group of amino acid positions that significantly alters VRC relative to the mean for the subset. The process is repeated $n$ times and the recurrence of each amino acid at nodes within trees of the resulting 'forest' is used to determine the most influential of VRC.

## 5.4 Results

### 5.4.1 Cohort Demographics

Study participants of the ZEHRP early-infection cohort consist of HIV-1 serodiscordant heterosexual couples who wish to remain ART-naïve following voluntary HIV-1 testing and safer-sex counselling. HIV-1 negative partners are therefore tested monthly as transmission is considered likely. If transmission occurs, plasma samples are stored from both donor and recipient for the time of identified transmission to allow study of early genotypes to better understand transmission determinants for HIV-1. 27 such transmission pairs were included in this study: male-to-female transmission (n=11) and female-to-male transmission (n=16) as detailed in Table 5.1.

Data from three transmission pairs was included from pilot work undertaken by Dr. Emily Adland, University of Oxford, and are identified in Table 5.1.

**Table 5.1:** HIV-1 Heterosexual Transmission Pairs

| Donor | Lab ID | Recipient | Lab ID | Sexual Transmission | Sampling delay from EDI | Ran by? |
|---|---|---|---|---|---|---|
| 239020 | No26 | 235020 | No32 | MtF | 46 | OS |
| 239047 | No16 | 235047 | No25 | MtF | 40 | OS |
| 239213 | No19 | 235213 | No24 | MtF | 56 | OS |
| 239218 | No10 | 235218 | No36 | MtF | 32 | OS |
| 249001 | No27 | 245001 | No21 | MtF | 81 | OS |
| 249002 | No45 | 245002 | No8 | MtF | 49 | OS |
| 249003 | No48 | 245003 | No20 | MtF | 46 | OS |
| 309144 | No40 | 305144 | No60 | MtF | 26 | OS |
| 309147 | No12 | 305147 | No47 | MtF | 23 | OS |
| 309153 | No31 | 305153 | No59 | MtF | 23 | OS |
| 309156 | No22 | 305156 | No52 | MtF | 17 | OS |
| 239013 | No14 | 235013 | No37 | FtM | 76 | OS |
| 239014 | No57 | 235014 | No1 | FtM | 46 | OS |
| 239030 | No5 | 235030 | No56 | FtM | 96 | OS |
| 239054 | No42 | 235054 | No51 | FtM | 44 | OS |
| 239055 | No34 | 235055 | No53 | FtM | 91 | OS |
| 239214 | No39 | 235214 | No18 | FtM | 24 | OS |
| 239239 | No17 | 235239 | No7 | FtM | 21 | OS |
| 249005 | No29 | 245005 | No11 | FtM | 21 | OS |
| 249006 | No4 | 245006 | No44 | FtM | 21 | OS |
| 249007 | No43 | 245007 | No46 | FtM | 32 | OS |
| 309139 | No38 | 305139 | No50 | FtM | 47 | OS |
| 309146 | No58 | 305146 | No55 | FtM | 46 | OS |
| 309160 | No3 | 305160 | No49 | FtM | 47 | OS |
| Z3410F | N/A | Z3410M | N/A | FtM | N/A | EA |
| Z3470F | N/A | Z3470M | N/A | FtM | N/A | EA |
| Z4298F | N/A | Z4298M | N/A | FtM | N/A | EA |

Sampling delay given in days. EDI = estimated date of infection; provided by Prof. Eric Hunter, Emory University. MtF = male-to-female transmission; FtM female-to-male transmission. OS = myself; EA = Emily Adland.

### 5.4.2 Transmission pairs cluster phylogenetically

Recombinant NL4-3 virus chimeric for donor *gag-pro* has previously been shown to identify differences in IFN-resistance and VRC surrounding transmission events (Adland et al. 2020). Here, plasma sampled from participants after identified transmission was used to similarly generate NL4-3::*gag-pro* chimeric viruses.

To first confirm the relationship between donor and recipient samples, viruses were deep sequenced courtesy of Prof. David Bonsall and aligned *.fasta* files returned by his group's bioinformatician Dr. Nicholas Grayson. Nucleotide sequences for *gag* p17/p24 were then re-aligned to a Clade C reference sequence (Genbank accession: AB254141) and used to construct a phylogenetic tree (Figure 5.1).

Sequences from the viruses of each transmission pair cluster together in the tree exactly as expected from Table 5.1; no sequences are mis-matched, nor are any sequences unpaired. This confirms the linkage of donor and recipient viruses.

A Clade C reference sequence (Genbank accession: AB254141) was included and sits within the donor pairings which all importantly cluster separately from the outgroup sequence of the Clade B reference genome HXB2 (Genbank accession: K03455), to provide certainty that all studied transmission pairs concerned Clade C virus.

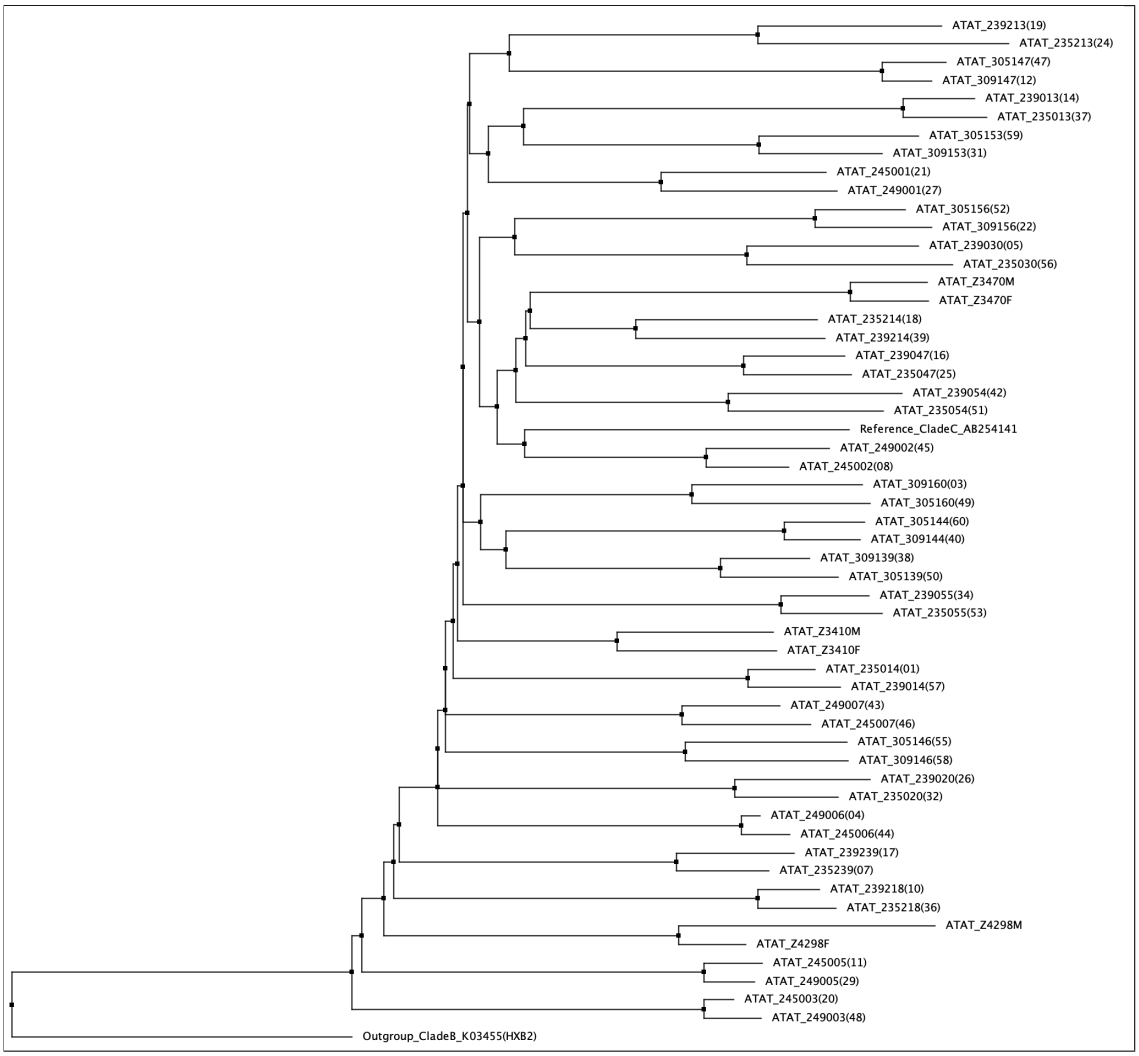



**Figure 5.1: Phylogenetic tree for p17/p24 of HIV-1 heterosexual transmission pairs.** Chimeric NL4-3::*gag-pro* viruses were deep sequenced and p17/p24 consensus sequences used to construct a Neighbour Joining phylogenetic tree. A Clade C reference sequence (Genbank accession: AB254141) was included and the tree was rooted using Clade B HXB2 sequence (Genbank accession: K03455).

### 5.4.3 VRC does not vary according to donor or recipient sex in adults

It has also been reported that viral fitness is a strong transmission determinant for heterosexual adult-to-adult transmission and *in-utero* MTCT of Clade C HIV-1 (Carlson et al. 2014; Iyer et al. 2017; Naidoo et al. 2017; Adland et al. 2020). VRC relative to wild-type NL4-3 was therefore measured for the participant NL4-3::*gag-pro* viruses generated here (Figure 5.2).

VRC data was included for non-overlapping transmission pairs measured separately during pilot studies by Dr. Emily Adland after confirmation that VRC values for overlapping participant viruses showed consistency with ones generated by myself (Appendix A.16).

Overall there was no difference between donor and recipient viruses; median 0.851 for donor and 0.816 for recipient (paired T-test p=0.193) and converse to the difference expected, the VRC of the virus transmitted to male recipients was no higher than that transmitted to female recipients (Figure 5.2a.).

Likewise, in contrast to the decrease in VRC seen between maternal and infant virus for *in-utero* MTCT to females (Adland et al. 2020), no such difference was seen here for transmission from male-to-female, nor was there a difference for transmission from female-to-male (Figure 5.2a.), both of which were confirmed by individual paired analyses (Figure 5.2b. & c.).

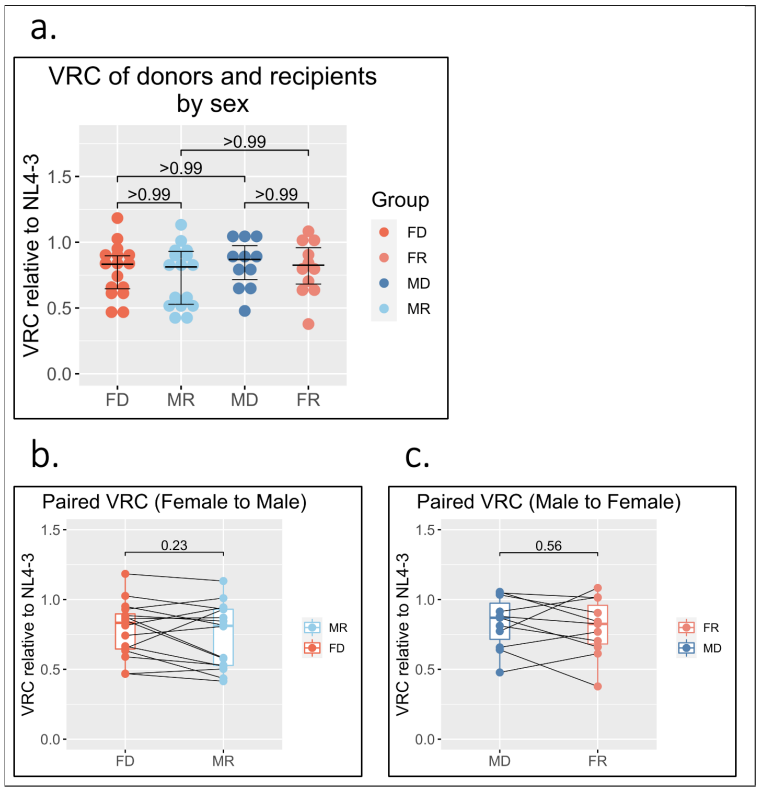



**Figure 5.2: VRC of Donor and Recipient Viruses by Sex.** VRC of donor and recipient NL4-3::*gag-pro* chimeric viruses calculated relative to growth of wild-type NL4-3 in the GXR25 cell line over 7 days. a) separated according to sex of donor and recipient; pairwise comparisons via Student's unpaired T-test with Bonferroni correction for multiple comparisons. b), c) paired analyses separated according to direction of transmission; pairwise comparisons via Student's paired T-test. Bars show median with interquartile range. FD = Female Donor (red), MR = Male Recipient (light blue), MD = male donor (blue), FR = female recipient (pink).

### 5.4.4 Recipient VRC is determined by donor VRC in adults

Since no difference was seen in the VRC of viruses transmitted to males or females or their corresponding donors (Figure 5.2), I next sought to understand whether a non- sex-specific VRC-related transmission bottleneck exists by examining the relationship between donor and recipient virus (Figure 5.3).

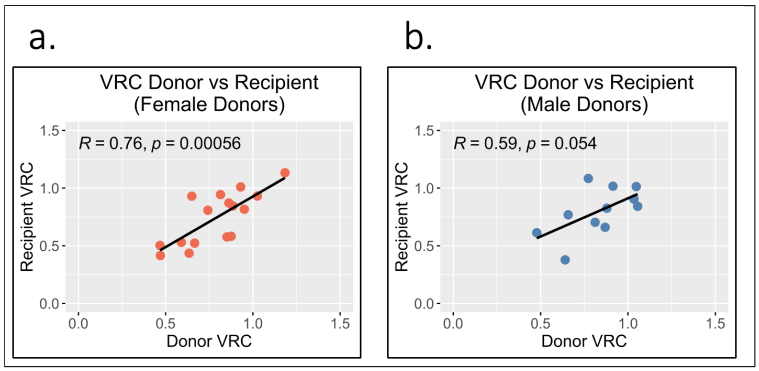



**Figure 5.3: Relationship between Donor and Recipient Virus VRC.** VRC of donor and recipient NL4-3::*gag-pro* chimeric viruses calculated relative to growth of wild-type NL4-3 in the GXR25 cell line over 7 days separated for paired analyses for transmission: a) from female-to-male, b) male-to-female.

Strikingly, the VRC of viruses from donors and recipients have strong positive correlations for both transmission from female-to-male (Figure 5.3a.) and from male-to-female (Figure 5.3b.), suggesting that VRC may not contribute to the transmission bottleneck for heterosexual adult-to-adult transmission.

### 5.4.5 TF VRC is not affected by sampling delay

The phenotypic properties of TF viruses are reportedly overshadowed as viral diversity increases in the months following infection (Parrish et al. 2013; Fenton-May et al. 2013; Gondim et al. 2021). Since no difference was seen in the VRC of viruses transmitted to males and females (Figure 5.2), I sought to rule out the time since estimated date of infection (EDI) as a confounding factor for transmission pairs where an EDI was provided (Figure 5.4; see Table 5.1).

Importantly, the time between sampling and EDI did not differ between male-to-female and female-to-male transmission (median 40 days vs. 46 days; p=0.7054).

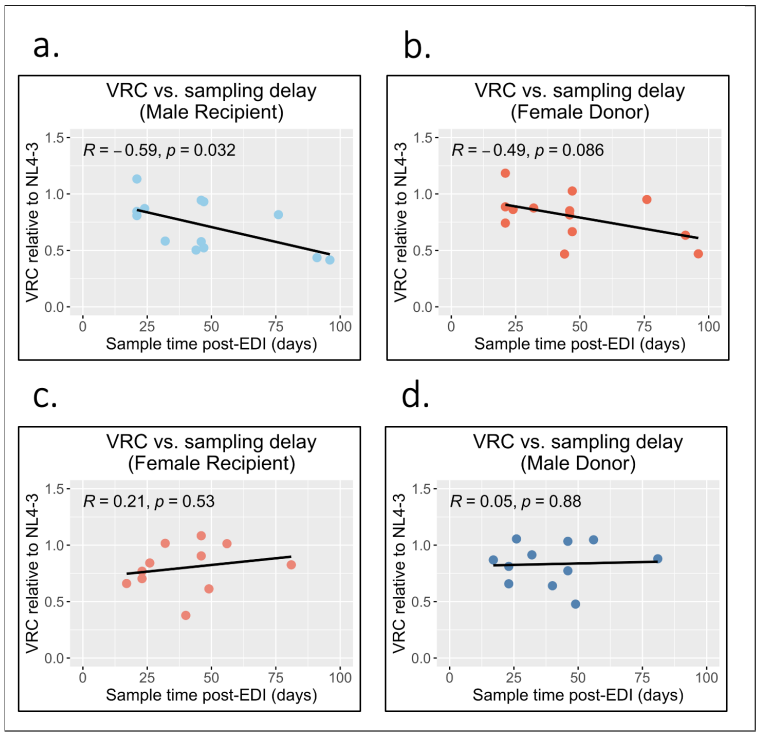



**Figure 5.4: Relationship between recipient VRC and time post-EDI.** VRC of recipient and donor NL4-3::*gag-pro* chimeric viruses calculated relative to growth of wild-type NL4-3 in the GXR25 cell line over 7 days compared to the time post- estimated date of infection (EDI) of recipients. a) male recipients, b) corresponding female donors, c) female recipients, d) corresponding male donors. Correlation via Pearson's method.

Interestingly, VRC for the viruses transmitted to male recipients decreases significantly with time post-EDI (Figure 5.4a.) which may suggest evolution away from the TF phenotype in the male immune environment if not for the fact that the same pattern is seen in the corresponding female donors (Figure 5.4b.).

The VRC of the viruses transmitted to female recipients has no such correlation with time post-EDI (Figure 5.4c.), which is similarly reflected in the corresponding male donors (Figure 5.4d.).

### 5.4.6 Gag-Pro amino acid sequence is conserved between donor and recipient in adults

Having excluded timing post-EDI as a confounding factor, the strong correlation between recipient and donor VRC still raised the question of whether recipient

virus was genotypically distinct from the donor plasma virus. The percentage of amino acid conservation between recipient and donor virus of both Gag and Pro was therefore compared for each transmission pair (Figure 5.5).

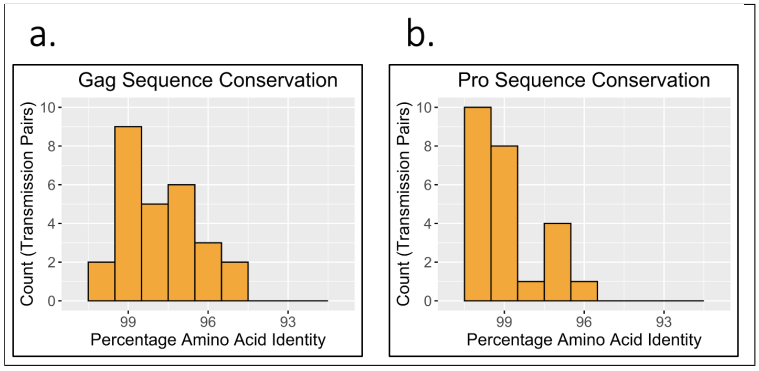



**Figure 5.5: Conservation of Amino Acid sequence between recipient and donor virus.** Percentage of identical amino acid positions between donor and recipient NL4-3::*gag-pro* chimeric virus. Translated consensus deep sequence data aligned for each transmission pair via NCBI BLAST for: a) the Gag polyprotein, b) Pro.

Remarkable sequence similarity is seen between donor and recipient virus and both Gag and Pro exhibit a minimum of 95% amino acid homology (Figure 5.5).

Gag exhibited slightly more variation between donor and recipient with a median of 98% and 16/27 transmission pairs below 99% identity (Figure 5.5a.).

Pro amino acid sequence data was not available for the transmission pairs provided courtesy of Dr. Emily Adland (see Table 5.1), but for remaining participants was conserved to an even greater extent than Gag; with a median of 99% and only 6/24 below 99% identity (Figure 5.5b.).

This conservation of amino acid sequence following heterosexual adult-to-adult transmission of HIV-1 therefore indicates a lack of selection for phenotypic variation within Gag-Pro at the transmission bottleneck and that the Gag-Pro associated phenotype of the recipient virus is comparable to that of the donor quasispecies consensus sequence.

### 5.4.7 Random Forest prediction identifies C-terminal mutations that influence VRC

Lastly, despite not identifying any differences in the VRC of donor and recipient viruses for either female-to-male or male-to-female transmission, the range of VRCs measured offered an opportunity to probe specific sequence changes that affect VRC.

Deep sequence consensus nucleotide data for each participant was translated into amino acid sequence for *gag* and *pro* separately then combined into a single sequence for prediction of amino acid positions relevant to VRC via Random Forest machine learning.

A Random Forest was constructed via regression using a subset size of 16 sequences (1/3 total sequences) per tree and a default terminal node size of 5, as defined in Segal et al. 2004. An optimal forest size of 408 trees was found to offer the minimal mean squared error (MSE) for model-predicted VRC compared to experimental VRC, see Appendix A.17.

For each position the model reports a value for the increase in 'purity' for the node when containing that position versus without – that is, how much more accurately the node can discriminate VRC when including that position – and a value for the increase in MSE for randomly shuffling the amino acids in that position. Those with high values of either are therefore more directly linked to VRC. Cut-offs were set arbitrarily to capture points separated from the main cluster of conserved amino acids. Using values of +0.025% for increased node purity and 0.25% for increased MSE, 29 such positions were identified (Figure 5.6).

Amongst the 29 positions are 27 within Gag and two within Pro. Two sites in particular appear to be most influential of VRC; Gag_134 and Gag_391.

The VRC for viruses carrying each amino acid polymorphism was then compared to the median VRC to identify those with significant relationships with VRC; summarised in Table 5.2 (see also Appendix A.18).

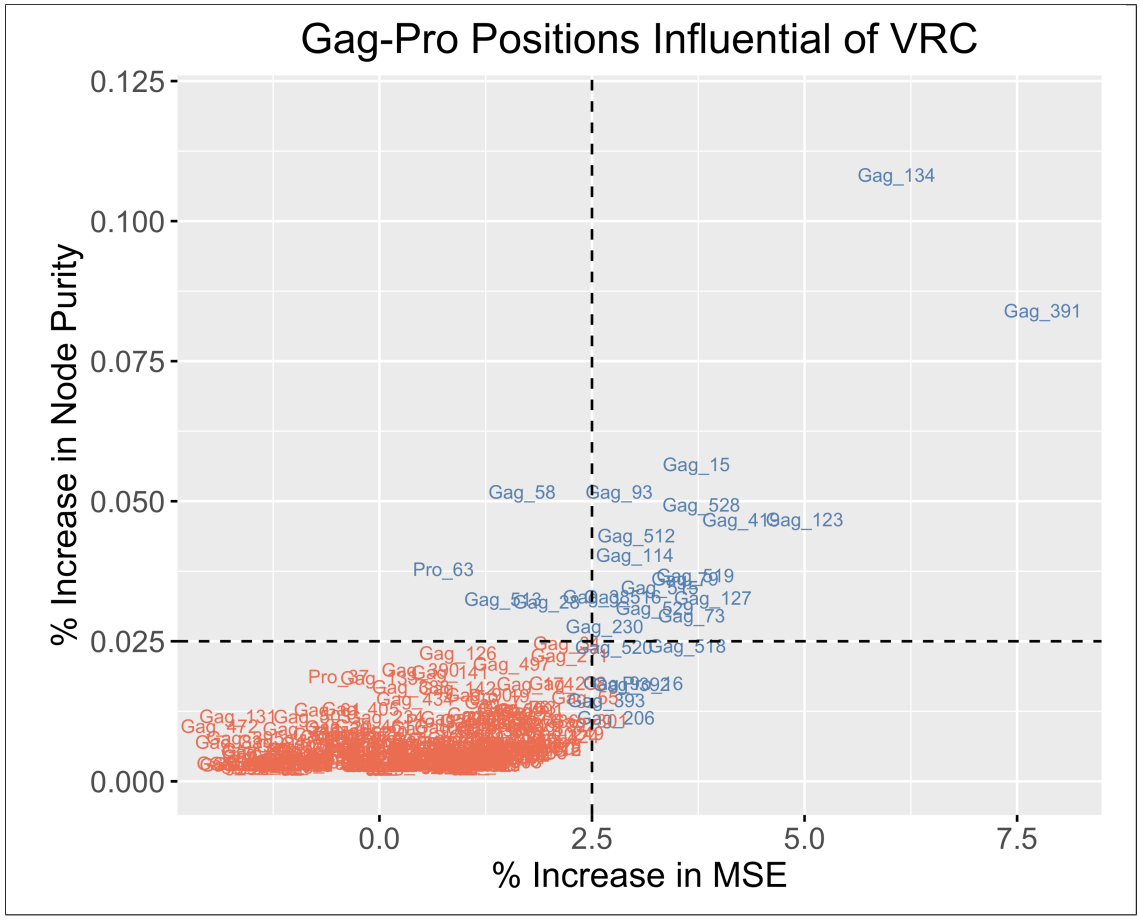



**Figure 5.6: Gag-Pro amino acids predicted to influence VRC via Random Forest.** The percentage Increase in Node Purity plotted against the percentage Increase in Mean Squared Error (MSE) for VRC prediction via Random Forest for each amino acid position for Gag and Pro of NL4-3::*gag-pro* chimeric viruses. Dashed lines represent cut-off for positions not considered influential (red) and influential (blue).

**Table 5.2:** Gag-Pro Amino Acid Positions identified by Random Forest

| **Position (RF)** | **Position (HXB2)** | **Reference (Clade C)** | **RF Mutation** | **VRC Correlation** |
|---|---|---|---|---|
| Gag9 | Gag9; p17 | R | R9K | Increase |
| Gag15 | Gag15; p17 | A | Multiple | Unidentifiable |
| Gag28 | Gag28; p17 | Q | Multiple | Unidentifiable |
| Gag58 | Gag58; p17 | K | K58R | Decrease |
| Gag73 | Gag73; p17 | E | E73K | Decrease |
| Gag79 | Gag79; p17 | Y | Y79F | Increase |
| Gag93 | Gag93; p17 | E | Multiple | Unidentifiable |
| Gag114 | Gag111; p17 | C | C111V | Decrease |
| Gag123 | Gag115; p17 | I | I115T | Increase |
| Gag127 | Gag119; p17 | Q | Q119G | Increase |
| Gag134 | Gag122; p17 | - | GQVSQNA insertion | Increase |
| Gag206 | Gag191; p24 | V | V191I | Decrease |
| Gag230 | Gag215; p24 | L | Multiple | Unidentifiable |
| Gag 385 | Gag370; p7 | A | Multiple | Unidentifiable |
| Gag391 | Gag376; p2/p7 | I | I376V | Increase |
| Gag392 | Gag377; p2/p7 | M | M377L | Increase |
| Gag393 | Gag378; p2/p7 | M | M378I | Decrease |
| Gag419 | Gag403; p7 | R | R403K | Increase |
| Gag512 | Gag478; p6 | P | Multiple | Unidentifiable |
| Gag513 | Gag479; p6 | K | Multiple | Unidentifiable |
| Gag520 | Gag481; p6 | R | R481Q | Decrease |
| Gag515 | Gag483; p6 | - | PYR/KE insertion | Increase |
| Gag516 | " | - | | Increase |
| Gag518 | " | - | | Increase |
| Gag519 | " | - | | Increase |
| Gag528 | Gag487; p6/end | I | I487P | Decrease |
| Gag529 | Gag488; p6/end | S | S488A | Increase |
| Pro16 | Pro16 | G | Multiple | Unidentifiable |
| Pro63 | Pro63 | P | Multiple | Unidentifiable |

NB: indels for my alignment alter position number of amino acids so provided are their relative positions with respect to the HIV-1 reference genome HXB2 (Genbank accession: K03455). Clade C reference Genbank accession: AB254141.

Despite the identification of two positions within Pro by the Random Forest (Figure 5.6), neither had a discernible impact on VRC (Table 5.2; Appendix A.18). The majority of Pro was otherwise markedly conserved (Appendix A.19) and the remainder of the VCR-related mutations occurred within Gag; except notably within p24 (Figure 5.7).

Interestingly many mutations appear to group together towards the C-termini of the proteins (Figure 5.7). Hydrophobicity towards the end of p17 is associated with decreased VRC; with C111V associated with a reduction and I115T with an increase. Similarly, the 122 GQVSQNA insertion is associated with increased VRC (see also Appendix A.20.1).

Conversely, hydrophobicity at the p2/p7 cleavage site (I376V & M377L) is associated with increased VRC but decreased VRC if this impacts the start of p7 (M378I) (see also Appendix A.20.2). Interestingly, M377L only appears concurrently with I376V (see Appendix A.20.2).

Additionally, alterations to hydrophobicity at the p6 N-terminus (R481Q & I487P) are associated with decreased VRC whilst the 483 PYK/RE insertion is associated with increased VRC (Figure5.7; Table 5.2). Indeed, all six viruses carrying this insertion sit within the top quartile for VRC (see also Appendix A.20.3).

The remaining substitutions mostly concern substitutions between R and K, with the notable exception of a charge-reversal K73E and dehydroxylation of Y79F.

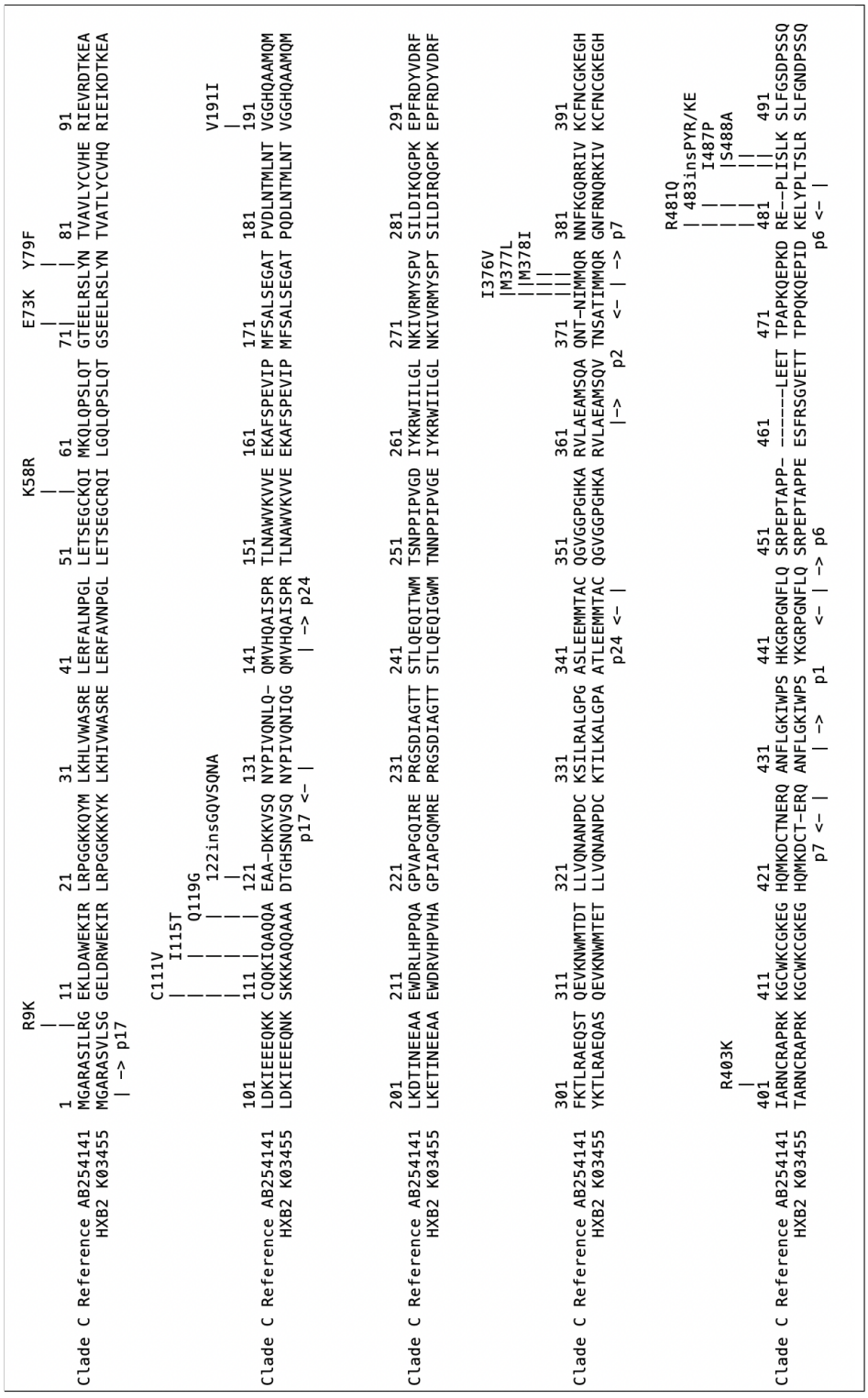



**Figure 5.7: Positions of VRC-related amino acids within Gag polyprotein.** Positions of VRC-related amino acids identified by Random Forest marked on the Gag polyprotein. Positions numbered with respect to HXB2 (Genbank accession: K03455) and mutations relative to Clade C reference (Genbank accession: AB154141). Start and end positions are given for: p17 (matrix), p24 (capsid), p2 (spacer protein), p7 (nucleocapsid), p1 (spacer protein), and p6 (budding protein), as Genbank annotation for K03455.

## 5.5 Discussion

Sex differential selection of HIV-1 at the transmission bottleneck has been reported for *in-utero* MTCT where females are infected by lower VRC virus with increased IFN-resistance relative to males (Adland et al. 2020). Likewise it was reported that selection for computed viral fitness differs between males and females during heterosexual transmission between adults and TF viruses in male recipients had higher fitness compared to female recipients (Carlson et al. 2014). Selection for VRC and fitness were related to IFN-resistance and inflammation, respectively (Carlson et al. 2014; Adland et al. 2020). Differential IFN-I production between males and females provides one mechanism for distinct HIV-1 selection bottlenecks between sexes. This study therefore sought to investigate whether there is a sex difference in the selection for VRC during adult-to-adult transmission of HIV-1 from male-to-female and female-to-male.

Many studies have investigated the role of VRC in selection of HIV-1 during transmission. In adults, Iyer et al. 2017 reported higher replicative capacity amongst TF viruses for four Clade C female-to-male transmission pairs. This is supported by Carlson et al. 2014 who reported that computed viral fitness is increased in recipients compared to donors for 137 transmission pairs. However, no such selection is reported by Deymier et al. 2015 in a study of six heterosexual transmission pairs – the majority of which (5/6) were female-to-male – from the same cohort as the present study. Likewise, no difference in the VRC of TF viruses was seen for between males or females in a mixed study of Clade B MSM / Clade C heterosexual pairs which contained similar numbers of female-to-male and male-to-female Clade C pairs (Parrish et al. 2013).

Only one study has considered a sex difference in selection for VRC for heterosexual adult-to-adult HIV-1 transmission and reports significantly higher computed fitness for TF viruses transmitted to males compared to females (Carlson et al. 2014).

These reports in adults contrast to that seen for *in-utero* MTCT where selection is seen for lower VRC (Naidoo et al. 2017) and differed by sex, with females

receiving significantly lower VRC virus than males (Adland et al. 2020). Both studies measured VRC using NL4-3::*gag-pro* chimeric viruses, which was favoured for the present investigation to allow the comparison of the adult-to-adult and MTCT bottleneck. Additionally by generating chimeric viruses this study was able to include a greater number of transmission pairs than achieved previously with outgrowth of infectious molecular clones (IMCs) (Deymier et al. 2015) which allowed the consideration of differences in the transmission bottleneck between the sexes.

Likewise, the insertion of Clade C *gag-pro* into a Clade B NL4-3 backbone raises concerns over the representativeness of chimeric viruses to the true *in-vivo* virus. However, similarly grown NL4-3::*gag-pro* chimeric viruses have been shown to faithfully represent the consensus Gag-Pro amino acid sequence of plasma virus (Adland et al. 2015) and have been used extensively elsewhere in the study of Clade C virus VRC (Miura et al. 2009; Miura et al. 2010; Brockman et al. 2010; Wright et al. 2010; Wright et al. 2011; Wright et al. 2012a; Wright et al. 2012b; Nomura et al. 2013; Payne et al. 2014; Kiguoya et al. 2017). Moreover, their *in-vitro* activity has been confirmed to correlate with the clinical markers of HIV-1 disease progression (Miura et al. 2009; Wright et al. 2010; Brockman et al. 2010; Nomura et al. 2013; Payne et al. 2014; Kiguoya et al. 2017) which supports the representativeness of their behaviour to wild-type virus. The HIV-1 genome has a high mutation rate and the NL4-3::*gag-pro* system therefore provides a limited window through which to study the genetic background of VRC without the biological noise across the enitre genome. *Gag-pro* was selected over alternative immune targets such as envelope since previous studies of CD8+ T-cell escape variants have identified a close link between *gag-pro* mutations and VRC (Goulder and Watkins 2008). To this end, NL4-3::*gag-pro* chimeric viruses have most recently been used to investigate the role of VRC in Clade C HIV-1 MTCT bottleneck by Naidoo et al. 2017 and Adland et al. 2020 which were precursors to this project.

Through generation of NL4-3::*gag-pro* chimeric viruses, the VRC was measured here for donor and recipient viruses for 27 transmission pairs – 11 male-to-female and 16 female-to-male – and no difference was seen between donors, recipients, or donor-recipient pairs. This contradicts the hypothesis that increased VRC is selected for in transmission to males compared to females, as suggested by Carlson et al. 2014; Naidoo et al. 2017; Adland et al. 2020. It is however noted that the sex differences reported for *in-utero* MTCT are only apparent in recently infected mothers and not for chronically infected mothers (Adland et al. 2020). Data regarding the timing of infection for the donors in the transmission pairs of this study has not been made available and may therefore contain an explanation for the discordance between MTCT and the present study if for example donors were largely chronically infected.

Two studies conversely also found no selection for VRC during HIV-1 transmission between adults (Parrish et al. 2013; Deymier et al. 2015). The latter also reported no selection for IFN-resistance during transmission and this aligns with a recent study comparing a TF IMC with one of similar replicative capacity from the same participant during chronic infection, albeit Clade B infection and from a single participant (Sugrue et al. 2022). Through *in-silico* modelling after measuring *in-vitro* growth of both IMCs in the presence of IFN-α14 and 10 separate anti-HIV-1 ISGs, the authors demonstrated that even minor differences in replicative capacity were capable of inducing large differences in measurable IFN-'resistance', concluding that the apparent IFN-resistance of TF viruses over chronic viruses reported previously (Fenton-May et al. 2013; Parrish et al. 2013; Iyer et al. 2017) may indeed be an artefact of statistically non-significant, marginally increased replicative capacity within the particular TF viruses measured (Sugrue et al. 2022).

The relative resistance to IFN-I of viruses transmitted *in-utero* to females during MTCT appears not to conform to this finding as an inverse correlation is seen between VRC and IFN-resistance. Thus overall the transmission bottleneck for heterosexual adult-to-adult transmission of Clade C HIV-1 appears: 1) not to differ

between male-to-female and female-to-male transmission, and 2) more importantly to differ from that for HIV-1 Clade C *in-utero* MTCT.

Nonetheless, the range of VRC values obtained here across the transmission pairs allowed interrogation of the sequence data of the cloned participant *gag-pro* sequences to identify amino acid changes within Gag-Pro that may relate to VRC. Through Random Forest machine learning 29 such sites were identified. Several sites were discounted as they contained many amino acid variants without any that significantly altered VRC from the mean and were likely artefacts of artificial inflation of node purity due to the entropy increase introduced by their shuffling. The remaining positions occurred entirely within Gag and predominantly around protein C-termini.

Many such mutations have been linked with resistance to protease inhibitors and, as compensatory mutations to enable more efficient proteolysis by mutant protease, are reported to confer an increase in replicative capacity (Peters et al. 2001; Myint et al. 2004; Tamiya et al. 2004; Parry et al. 2011; Kožíšek et al. 2012; Sutherland et al. 2016; van Domselaar et al. 2019).

Common to the groups of C-termini mutations identified by the Random Forest is alteration of hydrophobicity. The preservation of polarity at the p17 C-terminus appears beneficial to VRC since C111V (polar-to-hydrophobic) is associated with decreased VRC whereas I115T (hydrophobic-to-polar) and Q119G (polar-to-polar) are both associated with increased VRC. Importantly, mutations that preserved polarity at position 111 or introduced acidity to position 119 were previously shown to increase VRC (Prince et al. 2012).

Conversely, disruption to polarity appears important within p17 itself as Y79F (polar-to-hydrophobic) is associated with an increase in VRC and was previously linked with protease inhibitor resistance and increased VRC (Parry et al. 2011; Sutherland et al. 2016). This gives confidence to the additional identification of an association for a charge-reversal within the same region, E73K (acidic-to-basic), with a reduction in VRC.

Hydrophobicity at the p2/p7 cleavage site similarly appears to benefit VRC as both I376V (hydrophobic-to-hydrophobic) and M377L (polar-to-hydrophobic) are associated with increased VRC. M377I (polar-to-hydrophobic) was previously shown to increase p2/p7 cleavage efficiency (Kožíšek et al. 2012) and I376V has been linked to protease resistance (Sutherland et al. 2016; Codoñer et al. 2017), and was in fact one of the two strongest positions identified by the Random Forest, Gag_391; providing understanding for the mechanism behind such observations. Such an impact on VRC lends credence to the additional mutations identified in the p2/p7 cleavage site, including M378I (polar-to-hydrophobic), which is associated with decreased VRC and may be explained in relation to shifted hydrophobicity or by disruption of the p7 start codon.

The final region in which amino acid positions identified by the Random Forest appear to group is the C-terminus of p6 where increases in hydrophobicity, R481Q (basic-to-polar) and I487P (hydrophobic increase), are associated with reduced VRC. Most significant however is the 483 PYR/KE insertion which is shared by three donor and recipient pairs with a VRC in the top quartile and appears linked with S488A (polar-to-hydrophobic), which occurs only in these viruses (see Appendix A.20.3) but was previously independently associated with decreased VRC (Myint et al. 2004; Votteler et al. 2011). However, it's relationship with increased VRC here is supported as position 488 is reportedly associated with recruitment of ALG-2-interacting protein X (ALIX) by p6 (Votteler et al. 2011). p6 is an important packaging protein for HIV-1 assembly and mechanistically PYR/KE multiplication has been shown to improve recruitment of both ALIX and endosomal sorting complexes required for transport (ESCRT) and to increase VRC through enhanced viral exocytosis (Votteler et al. 2011; Aralaguppe et al. 2017; Ajasin et al. 2019; van Domselaar et al. 2019).

One of these transmission pairs 249006 and 245006, had the two highest VRCs measured and also carried a 122 GQVSQNA insertion at the p17 C-terminus (see Appendix A.20.1). An SQVN p17 C-terminal insertion was previously shown to

reduce VRC *in-vitro* (Tamiya et al. 2004) but was here the second of the two strongest positions identified by the Random Forest (Gag_134) which supports its role in increasing VRC within the transmission pair.

Of note, whilst all positions of the PYR/KE insertion were identified by the Random Forest (Gag_515 to Gag_519), only the start position was identified for the GQVSQNA as the other sequences did not have amino acids at the other positions against which to compare VRC and an $n$ of 2 was not sufficient for their identification, testament to the resilience of the model.

Not detected by the model was however, the duplication of the 455 PTAPP motif which has been linked by multiple studies to increased VRC *in-vitro* (Peters et al. 2001; Sharma et al. 2018), though was not detected in a targeted p6 sequence analysis of 117 Clade C HIV-1 infections (Flys et al. 2005). PTAPP duplication appears randomly distributed across the full range of VRC within this study of *n=48* viruses (see Appendix A.20.3) which supports this lack of influence on VRC.

Overall, it appears that the factors which govern the adult-to-adult HIV-1 Clade C transmission bottleneck cannot be attributed to polymorphisms within Gag-Pro as remarkable sequence conservation was seen between donor and recipient sequences and VRC of NL4-3::*gag-pro* chimeric viruses was strongly correlated. Indeed, insertions associated with high VRC via Random Forest were faithfully transmitted from donor to recipient. VRC-related mutations occurred mainly at protein C-termini and commonly concerned alterations to hydrophobicity within the Gag polyprotein proteolysis sites.

Lastly, unlike that reported for *in-utero* MTCT (Adland et al. 2020), there was no apparent sex difference in the transmission bottleneck and no selection for increased VRC was seen for transmission to males. It is therefore apparent that the heterosexual adult-to-adult HIV-1 Clade C transmission bottleneck differs from the *in-utero* MTCT bottleneck.

# 6

# Conclusion: a model for sex differential pDC IFN-I via delayed activation kinetics in males

There is growing recognition of the impact of immune sex differences on a broad range of disease outcomes from infection, vaccination, inflammatory conditions, autoimmune disease, and cancers. The female immune system is generally more pro-inflammatory and has a greater $T_H2$-skew whilst the male immune system is generally more tolerant and $T_H1$-skewed. This has wide-reaching consequences in the outcome of infection and vaccination, which this thesis focuses on. Females respond better than males to viral infections and vaccination but the underlying inflammation can be detrimental in chronic infection and results in a higher incidence of autoimmunity and adverse reactions following vaccination.

Central to this difference is increased IFN-I production by female pDCs resulting from biallelic expression of the upstream receptor TLR7 in ∼30% of female immune cells through escape from X-chromosome inactivation. The aim of this thesis was to further investigate the role of sex in pDC behaviour and the impact of differential IFN-I production in the context of vaccination outcome and heterosexual HIV-1 transmission.

Study of pDCs has been historically challenging as they constitute only 0.1-0.5% of peripheral blood mononuclear cells and their activity declines rapidly *ex-vivo*.Through development of an assay to stimulate pDCs with a TLR7 agonist within whole blood immediately *ex-vivo* to best preserve their *in-vivo* activity, it was noted that upregulation of the pDC activation markers HLA-DR and CD123 was higher for male pDCs than female pDCs despite lower IFN-I production.

Further study of pDCs in a cohort of adolescents receiving BNT162b2 + LAIV co-vaccination revealed that IFN-I production by male pDCs was reduced by androgens and, whilst lower than female pDCs on the day of vaccination, caught up by the following day. Further, free testosterone was identified as positively influential of IgG titres to BNT162b2, contrary to published findings for seasonal influenza vaccination, and suggests that local modulation of the IFN-I response at vaccination sites may be beneficial to new mRNA vaccine technologies.

Investigation of transcriptional differences between male and female pDCs identified no differences in the transcription of IFN-I genes or markers of activation at baseline or in response to TLR7 stimulation. Differential gene expression (DGE) did however reveal a focus on transcription of antigen presentation genes in male pDCs and cytokine signalling genes in female pDCs.

Together, these data support a model wherein biallelic expression of TLR7 lowers the activation threshold of female pDCs relative to male pDCs, such that female pDCs produce IFN-I more readily and progress sooner to additional functions than male pDCs; which lag behind and activate to a greater extent than female pDCs to produce similar quantities of IFN-I. That no difference was seen at the transcriptional level suggests this process is regulated at the post-transcriptional level. DGE, for example, revealed enrichment of ribosomal genes in female pDCs at baseline which may indicate differences in protein translation and is supported by enrichment for MHC-II in DGE for male pDCs at baseline despite comparable protein expression of HLA-DR to female pDCs.

Lastly, a sex difference has been reported in selection for IFN-resistance and VRC for *in-utero* mother-to-child transmission of HIV-1. Here strong amino acid sequence conservation was seen for heterosexual transmission of HIV-1 between adults, and no difference was seen in VRC between donor and recipient viruses regardless of sex. This would suggest that the mechanism that governs the HIV-1 selection bottleneck for heterosexual transmission between adults is distinct from that for *in-utero* mother-to-child transmission.

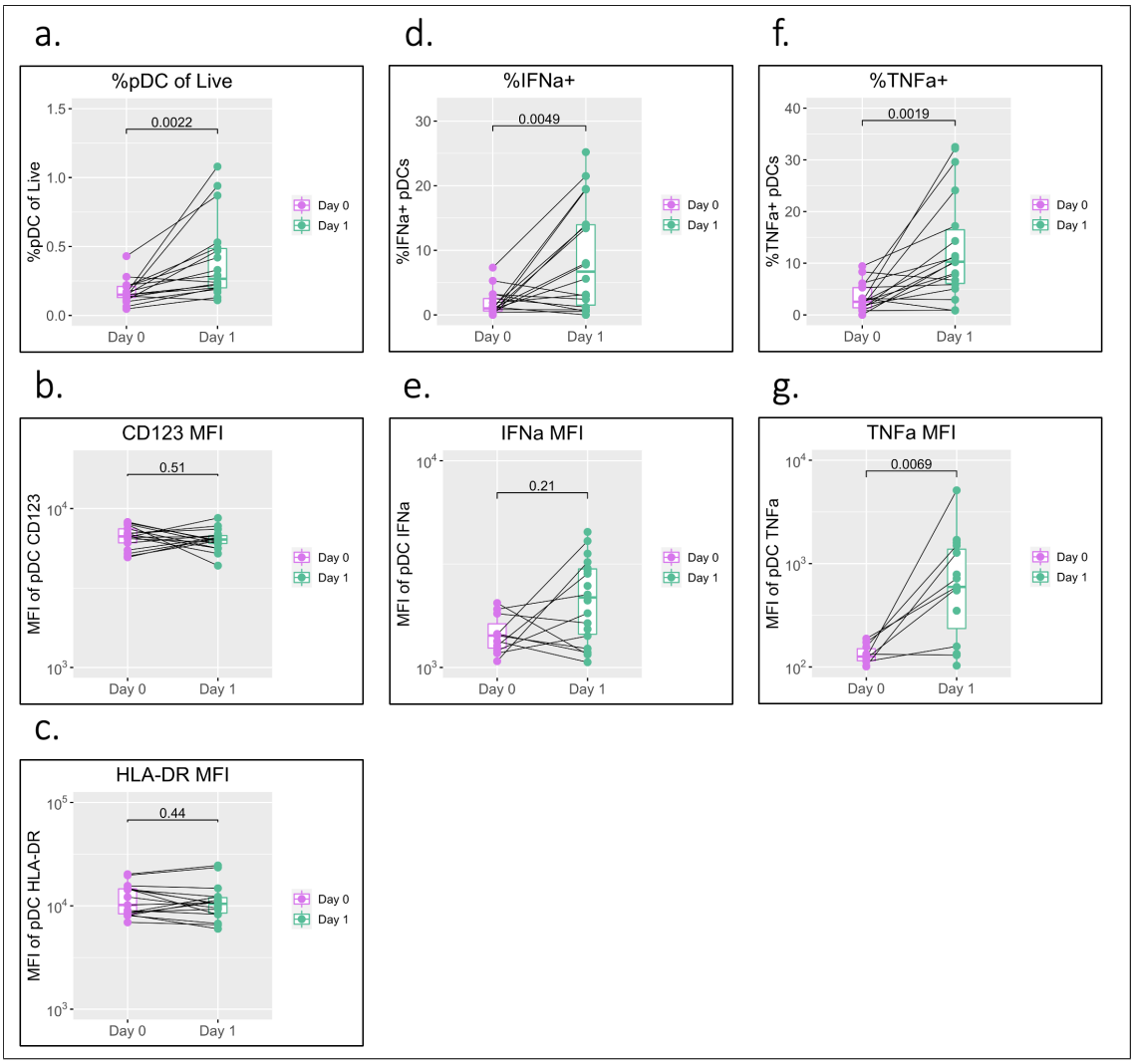
# Appendices

# A

# Appendix

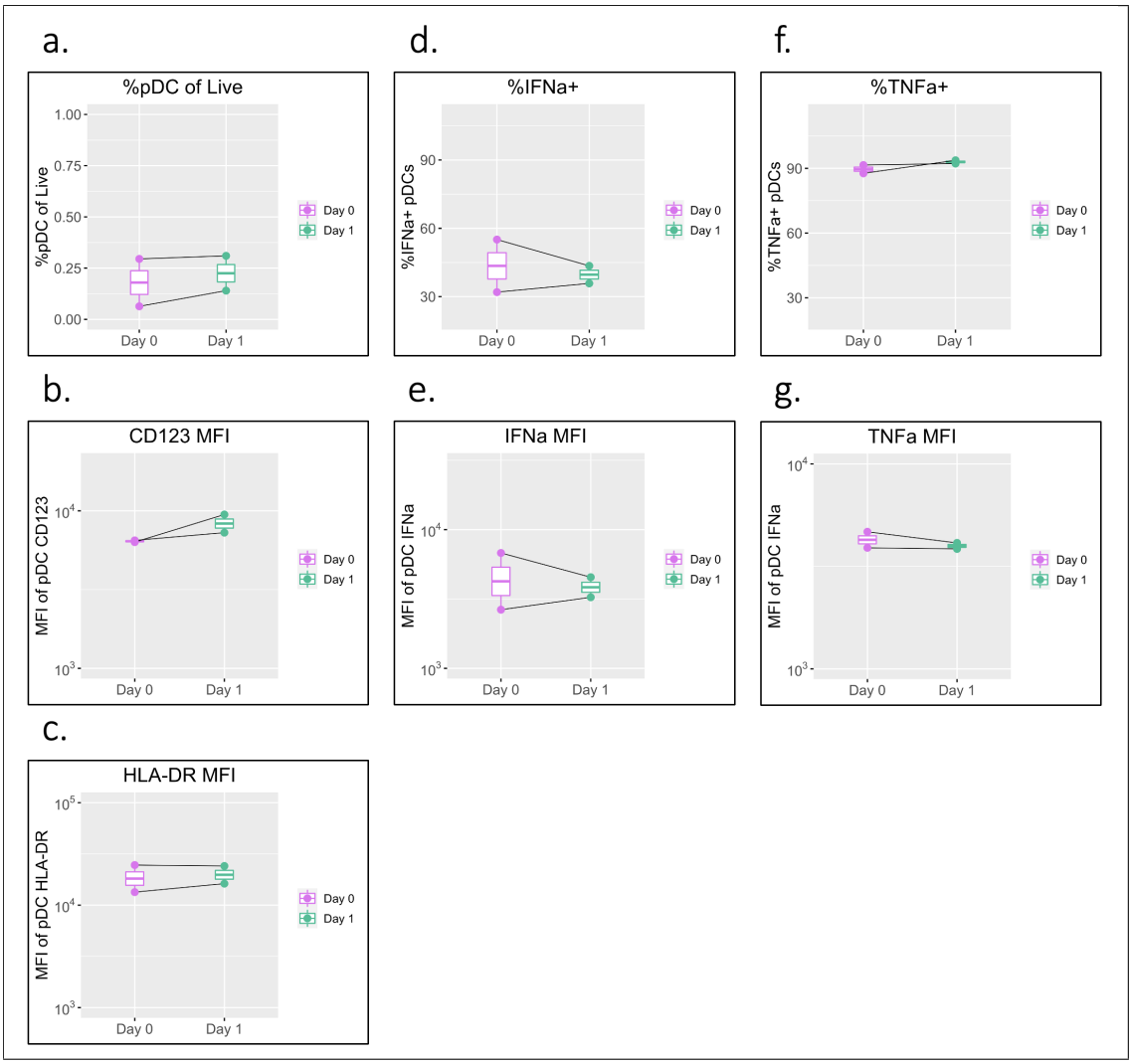
# A.1 Unstimulated Adolescent pDCs Day 0 to Day 1

Paired data showing changes in unstimulated pDC phenotype between Day 0 and Day 1 (n=18). Blood was drawn from adolescents (median age 14y3m) immediately following co-/vaccination with BNT162b2 + LAIV (Day 0; purple) and the following day (Day 1; green). Vacutainers contained R10 + brefeldin and were incubated at 37°C for 6hrs as detailed in Section 2.3.2 before analysis via flow cytometry. Samples done in duplicate per donor. a) pDC frequency as percentage of total PBMCs. b), c), e), g) mean fluorescence intensity (MFI) for gated pDCs of: CD123, HLA-DR, IFN-α (IFNa), and TNF-α (TNFa) respectively. d), f) percentage of gated pDCs expressing IFN-α (IFNa) and TNF-α (TNFa) respectively. Pairwise comparisons via Student's paired T-test for equal variance.


a.
%pDC of Live
%pDC of Live
0.0022
Day 0
Day 1
b.
CD123 MFI
MFI of pDC CD123
0.51
c.
HLA-DR MFI
MFI of pDC HLA-DR
0.44
d.
%IFNa+
%IFNa+ pDCs
0.0049
e.
IFNa MFI
MFI of pDC IFNa
0.21
f.
%TNFa+
%TNFa+ pDCs
0.0019
g.
TNFa MFI
MFI of pDC TNFa
0.0069

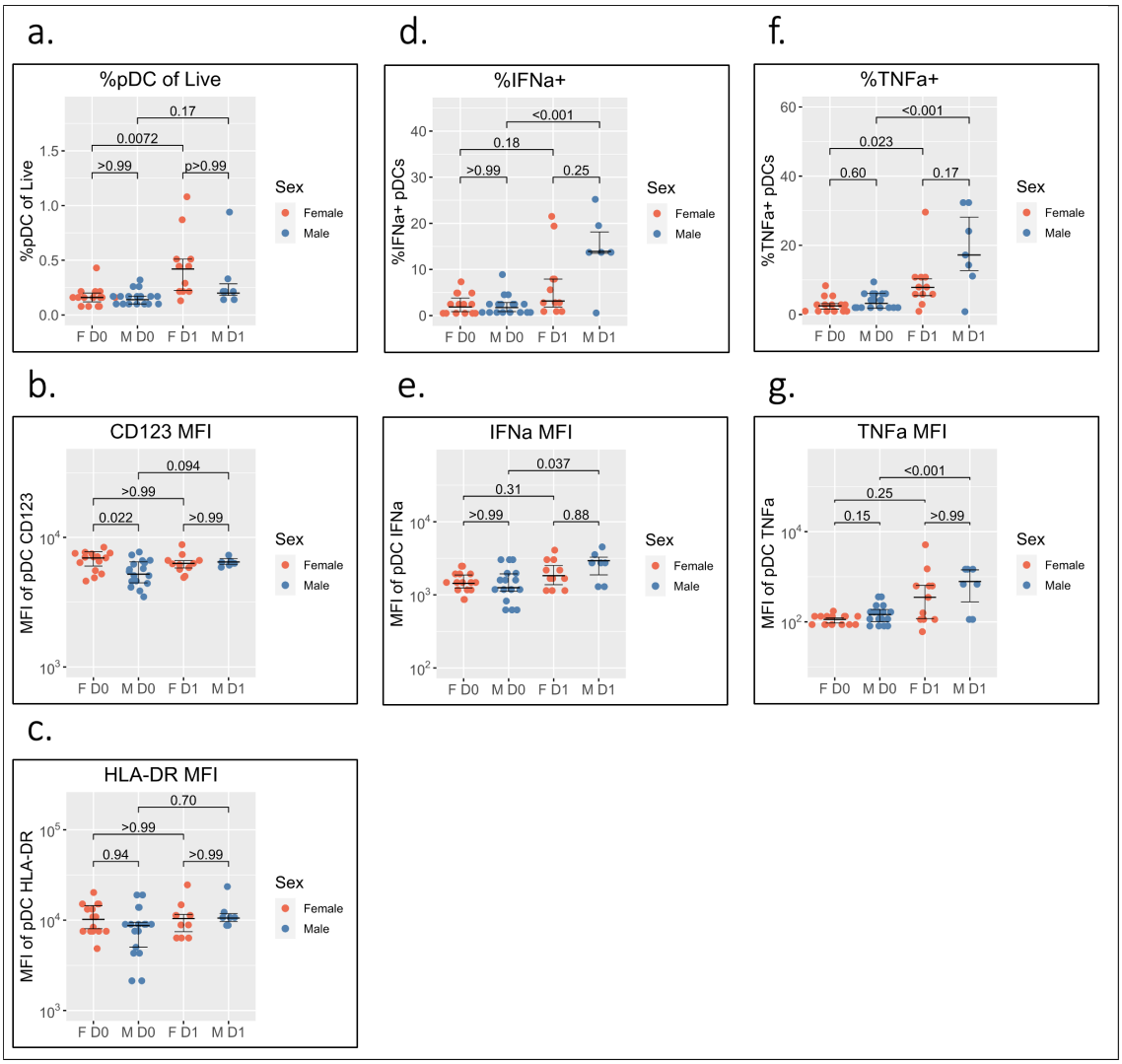
## A.2 Stimulated Unvaccinated Control Donor pDCs Day 0 to Day 1

Paired pDC activation data for unvaccinated control donors between Day 0 and Day 1 (n=2). Blood was drawn concurrently to adolescent samples on the day of co-/vaccination with BNT162b2 + LAIV (Day 0; purple) and the following day (Day 1; green). Vacutainers contained R10 + brefeldin and were incubated at 37°C for 6hrs as detailed in Section 2.3.2 before analysis via flow cytometry. Samples done in duplicate per donor. a) pDC frequency as percentage of total PBMCs. b), c), e), g) mean fluorescence intensity (MFI) for gated pDCs of: CD123, HLA-DR, IFN-α (IFNa), and TNF-α (TNFa) respectively. d), f) percentage of gated pDCs expressing IFN-α (IFNa) and TNF-α (TNFa) respectively.


a.
%pDC of Live
%pDC of Live
1.00
0.75
0.50
0.25
0.00
Day 0
Day 1
Day 0
Day 1
d.
%IFNa+
%IFNa+ pDCs
90
60
30
Day 0
Day 1
Day 0
Day 1
f.
%TNFa+
%TNFa+ pDCs
90
60
30
Day 0
Day 1
Day 0
Day 1
b.
CD123 MFI
MFI of pDC CD123
$10^4$
$10^3$
Day 0
Day 1
Day 0
Day 1
e.
IFNa MFI
MFI of pDC IFNa
$10^4$
$10^3$
Day 0
Day 1
Day 0
Day 1
g.
TNFa MFI
MFI of pDC IFNa
$10^4$
$10^3$
Day 0
Day 1
Day 0
Day 1
c.
HLA-DR MFI
MFI of pDC HLA-DR
$10^5$
$10^4$
$10^3$
Day 0
Day 1
Day 0
Day 1

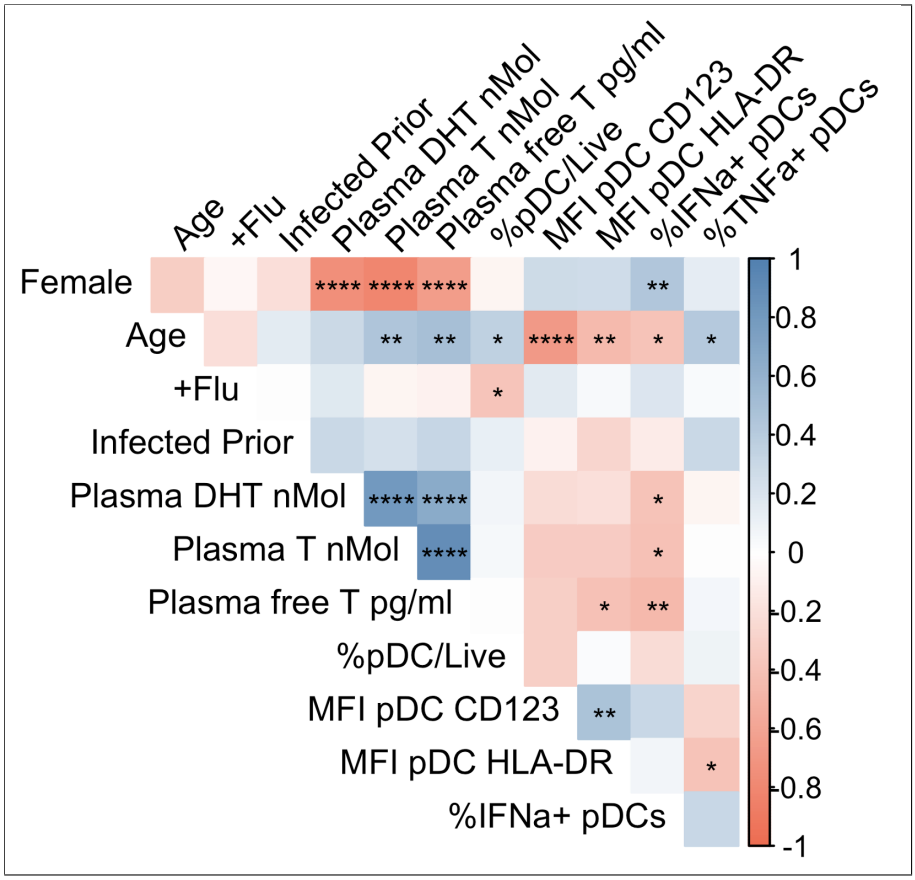
## A.3 Sex-stratified Unstimulated Adolescent pDCs Day 0 to Day 1

Sex-stratified data showing changes in unstimulated pDC phenotype between Day 0 (n=33; male n=17 & female n=16) and Day 1 (n=18; male n=7 & female n=11). Blood was drawn from adolescents (median age 14y3m) immediately following co-/vaccination with BNT162b2 + LAIV (D0) and the following day (D1). Vacutainers contained R10 + brefeldin and were incubated at 37°C for 6hrs as detailed in Section 2.3.2 before analysis via flow cytometry. Samples done in duplicate per donor. a) pDC frequency as percentage of total PBMCs. b), c), e), g) mean fluorescence intensity (MFI) for gated pDCs of: CD123, HLA-DR, IFN-α (IFNa), and TNF-α (TNFa) respectively. d), f) percentage of gated pDCs expressing IFN-α (IFNa) and TNF-α (TNFa) respectively. Pairwise comparisons via Student's unpaired T-test with Welch's correction for unequal variance and Bonferroni correction for multiple comparisons. Bars show median with interquartile range.


a.
%pDC of Live
%pDC of Live
0.17
0.0072
>0.99
p>0.99
F D0
M D0
F D1
M D1
Sex
Female
Male
d.
%IFNa+
%IFNa+ pDCs
<0.001
0.18
>0.99
0.25
f.
%TNFa+
%TNFa+ pDCs
<0.001
0.023
0.60
0.17
b.
CD123 MFI
MFI of pDC CD123
0.094
>0.99
0.022
>0.99
e.
IFNa MFI
MFI of pDC IFNa
0.037
0.31
>0.99
0.88
g.
TNFa MFI
MFI of pDC TNFa
<0.001
0.25
0.15
>0.99
c.
HLA-DR MFI
MFI of pDC HLA-DR
0.70
>0.99
0.94
>0.99

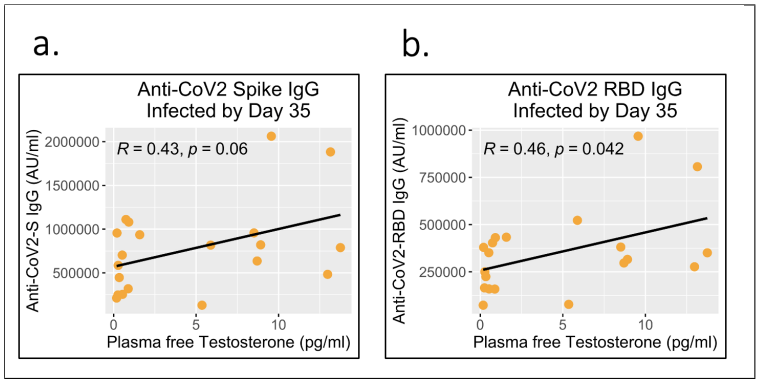
## A.4 Adolescent pDC IFN-α LASSO Correlation Matrix

Individual pairwise Pearson correlations between input covariates of the adolescent LASSO model. Colour represents Pearson's r-value. Stars represent unadjusted p-values.



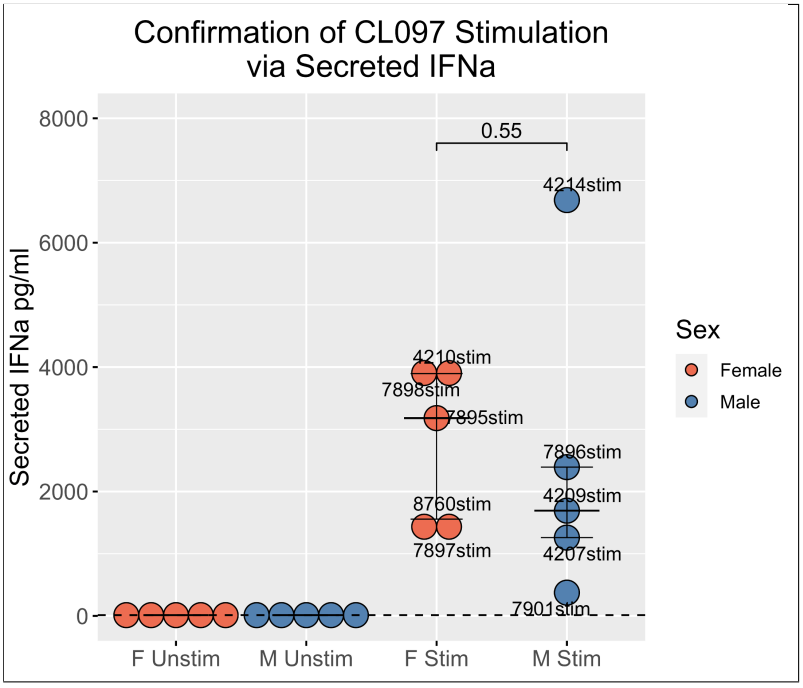
## A.5 Adolescent Day 35 anti-CoV2 IgG correlated with plasma free Testosterone

Relationship between plasma free testosterone and Day 35 MSD data for a) anti-Spike-IgG and b) anti-RBD-IgG for adolescents with evidence of natural SARS-CoV2 infection (n=20). Correlation via Pearson's method.



## A.6 scRNA-seq Confirmation of TLR7 Stimulation via IFN-α ELISA

Plasma was collected from whole blood prior to pDC enrichment for all donors pre- and post- CL097-stimulation and IFN-α (IFNa) concentration ascertained via Human IFN Alpha multi-subtype ELISA (PBL Bioscience) as per manufacturers instruction.



## A.7 Summary Table of Cell Numbers pre- and post- data Cleanup

**Table A.1:** scRNA-seq pDC Numbers

| **Array** | **Sex** | **Age** | **Pre-filter** | **Post-filter** | **Array** | **Sex** | **Age** | **Pre-filter** | **Post-filter** |
|---|---|---|---|---|---|---|---|---|---|
| 4210unstim | Female | 36 | 7390 | 3454 | 4207unstim | Male | 25 | 17112 | 6020 |
| 7308unstim | Female | 24 | 14755 | 6114 | 4209unstim | Male | 25 | 6021 | 2684 |
| 7895unstim | Female | 28 | 3425 | 688 | 4214unstim | Male | 26 | 14372 | 6020 |
| 7897unstim | Female | 24 | 11201 | 5064 | 7896unstim | Male | 24 | 10582 | 3328 |
| 7898unstim | Female | 33 | 2930 | 126 | 7901unstim | Male | 24 | 4038 | 74 |
| 8760unstim | Female | 29 | 6600 | 300 | | | | | |
| Mean | | 29 | 7940 | 1926 | | | 24.8 | 10425 | 3625 |
| Total | | | 46301 | 15746 | | | | 52125 | 18126 |
| **Array** | **Sex** | **Age** | **Pre-filter** | **Post-filter** | **Array** | **Sex** | **Age** | **Pre-filter** | **Post-filter** |
| 4210stim | Female | 36 | 1843 | 425 | 4207stim | Male | 25 | 18937 | 3355 |
| 7308stim | Female | 24 | 17 | 0 | 4209stim | Male | 25 | 7166 | 850 |
| 7895stim | Female | 28 | 5425 | 162 | 4214stim | Male | 26 | 12911 | 1706 |
| 7897stim | Female | 24 | 5729 | 700 | 7896stim | Male | 24 | 5287 | 427 |
| 7898stim | Female | 33 | 6047 | 363 | 7901stim | Male | 24 | 5079 | 1523 |
| 8760stim | Female | 29 | 2548 | 1146 | | | | | |
| Mean | | 29 | 3812 | 559 | | | 24.8 | 9876 | 1572 |
| Total | | | 21609 | 2796 | | | | 49380 | 7861 |

## A.8 pDC scRNA-Seq Top 25 Genes per cluster pre-exclusion

**Table A.2:** scRNA-Seq Top 25 Genes by Cluster pre-exclusion

| **Cluster 0** | **Cluster 1** | **Cluster 2** | **Cluster 3** | **Cluster 4** | **Cluster 5** |
|---|---|---|---|---|---|
| SYK | ZNF331 | CCND2 | IFNL1 | IFNA4 | LYZ |
| XIST | RGS2 | CCR7 | IFNA1 | MTRNR2L1 | ANXA1 |
| SLC38A1 | ARL4C | FAM129A | IFNA2 | TXN | COTL1 |
| TGFBI | CXCR4 | CCL4 | IFNW1 | IFNA7 | FGL2 |
| MAPKAPK2 | FOSB | CD44 | IFNA5 | IFNA17 | CAPN2 |
| UBE2J1 | AREG | TNFSF10 | IFNA16 | IFNA21 | AXL |
| CCDC69 | DUSP1 | CD83 | IFNA14 | IFNA10 | SIGLEC6 |
| APP | JUNB | MX1 | IFNB1 | NMI | S100A10 |
| SULF2 | NR4A2 | BIRC3 | IFNA8 | BCL2A1 | CTSH |
| PECAM1 | GPR183 | CALCRL | IFNA17 | IFNB1 | S100A4 |
| PRKCB | ZFP36L2 | NABP1 | IFNA6 | IFNA8 | FLNA |
| SPIB | FOS | CDH1 | IFNA21 | PMAIP1 | MYO1F |
| SMPD3 | SOX4 | CXCL10 | IFNA10 | IFNA13 | VSIR |
| IQGAP2 | EGLN3 | SLAMF7 | CCL5 | IFNA14 | ITGB2 |
| ETS1 | THBD | NFKB1 | IFNL3 | IFNA2 | ANXA2 |
| ABHD15 | KLF4 | CXCL9 | GBP4 | IFNA16 | RAB31 |
| FAM213A | HLA-DRB5 | RSAD2 | OASL | MIR155HG | KLF4 |
| UGCG | ZBTB18 | RAB29 | IFIT2 | SUB1 | TNFRSF1B |
| SELPLG | TSC22D3 | CD40 | POLR3C | IFNA5 | VASH1 |
| CNPY3 | GPR65 | SWAP70 | IFNL2 | GPM6A | LTK |
| SNX18 | FTH1 | HSPA1A | IFIT3 | PSMA2 | MT-CYB |
| SAMHD1 | MED26 | ISG15 | GPR34 | POMP | AHNAK |
| PTPRE | RPS4Y1 | IFI44L | PPP1R15A | ENY2 | DUSP1 |
| LAIR1 | KLF10 | XAF1 | TAL1 | MTRNR2L8 | JUN |
| SERPINF1 | TCL1A | PDE7A | IFNA4 | CXCL8 | IGHM |

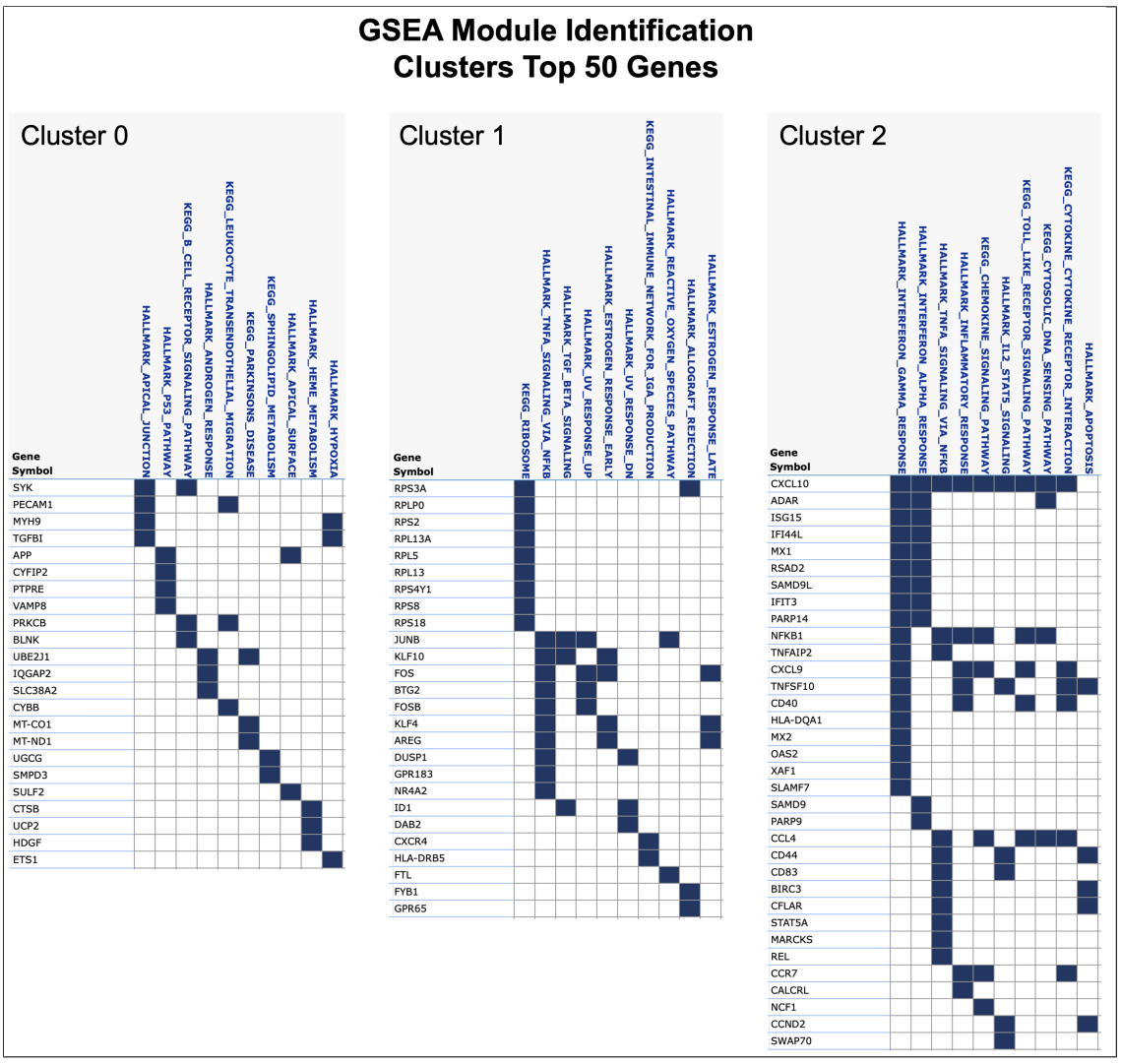
## A.9 scRNA-Seq Top 50 Genes by Cluster post-exclusion; as used for GSEA

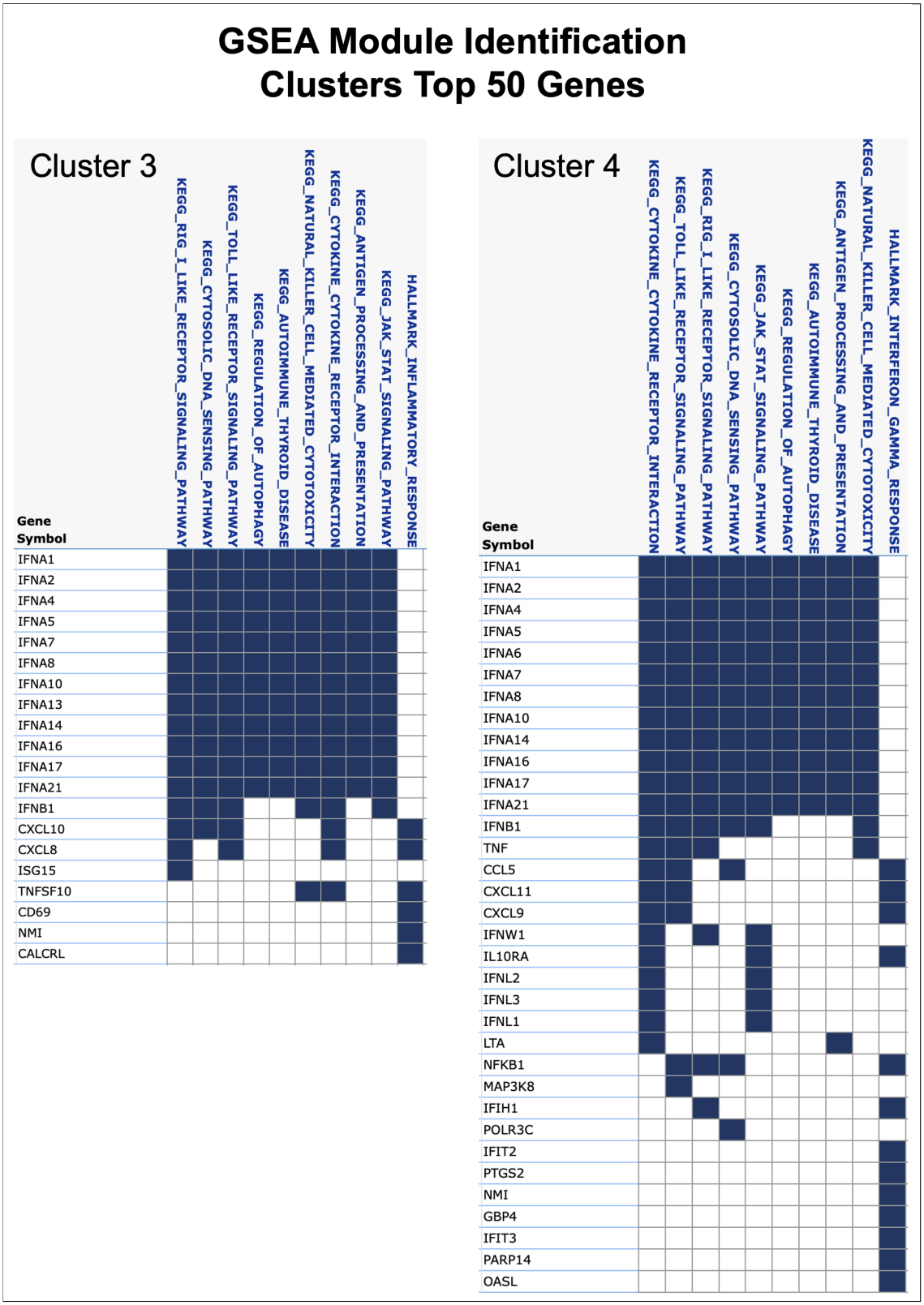
**Table A.3:** scRNA-Seq Top 50 Genes by Cluster post-exclusion

| Cluster 0 | Cluster 1 | Cluster 2 | Cluster 3 | Cluster 4 |
|---|---|---|---|---|
| XIST | ZNF331 | CCND2 | IFNL1 | IFNA4 |
| SYK | RGS2 | CCR7 | IFNA1 | MTRNR2L1 |
| SLC38A1 | ARL4C | FAM129A | IFNA2 | TXN |
| TGFBI | CXCR4 | CD44 | IFNW1 | IFNA7 |
| UBE2J1 | FOSB | CCL4 | IFNA5 | IFNA17 |
| MAPKAPK2 | AREG | TNFSF10 | IFNA16 | IFNA21 |
| APP | JUNB | CD83 | IFNA14 | IFNA10 |
| SULF2 | GPR183 | MX1 | IFNA8 | NMI |
| PECAM1 | ZFP36L2 | CALCRL | IFNB1 | BCL2A1 |
| CCDC69 | NR4A2 | CDH1 | IFNA17 | IFNB1 |
| PRKCB | EGLN3 | BIRC3 | IFNA6 | IFNA8 |
| ETS1 | FOS | NABP1 | IFNA10 | PMAIP1 |
| MT-ND1 | DUSP1 | CXCL10 | IFNA21 | IFNA13 |
| SNX18 | ZBTB18 | SLAMF7 | CCL5 | IFNA14 |
| SPIB | THBD | NFKB1 | IFNL3 | IFNA2 |
| RUNX2 | SOX4 | RSAD2 | GBP4 | IFNA16 |
| SAMHD1 | TSC22D3 | RAB29 | OASL | MIR155HG |
| FAM213A | RPS4Y1 | CXCL9 | IFIT2 | SUB1 |
| LAIR1 | FTH1 | SWAP70 | POLR3C | IFNA5 |
| BLNK | RPS18 | CD40 | IFNL2 | GPM6A |
| UGCG | MED26 | HSPA1A | IFIT3 | PSMA2 |
| SMPD3 | RPS8 | PDE7A | GPR34 | POMP |
| SEL1L3 | KLF10 | ISG15 | TAL1 | ENY2 |
| ABHD15 | KLF4 | XAF1 | PPP1R15A | MTRNR2L8 |
| CNPY3 | GPR65 | IFI44L | IFNA4 | CXCL8 |
| SERPINF1 | ID1 | RGL1 | IFIH1 | ISG15 |
| IGHM | HLA-DRB5 | SLFN5 | IFNA7 | RPS29 |
| EIF4B | RPLP0 | OAS2 | PTGS2 | AL035078.1 |
| IQGAP2 | ACTG1 | TNFAIP2 | TNF | NT5C3A |
| NUMA1 | DAB2 | IGFBP4 | HERC5 | RPL36A |
| CORO1C | FYB1 | HLA-DQA1 | PLEKHA4 | SRGN |
| CYTH4 | GAPT | OPTN | DBF4 | MTRNR2L12 |
| IRF2BP2 | RPL13A | TSPAN13 | NFKB1 | CXCL10 |
| CYBB | MS4A6A | SAMD9L | NR4A3 | SELENOK |
| PTPRE | GNA15 | FSCN1 | CEP126 | CD69 |
| SELPLG | BTG2 | CFLAR | PARP14 | RPL21 |
| MT-CO1 | CCDC186 | NCF1 | FAM111A | CREM |
| UCP2 | AKAP9 | PARP14 | RNF144B | TNFSF10 |
| CTSB | RPS14 | IFIT3 | IGFBP4 | REL |
| CYFIP2 | EIF4A3 | TFRC | NMI | HERC5 |
| PSAP | RPS2 | STAT5A | UBALD2 | ZFP36L1 |
| SLC38A2 | PPP1R14B | ADAR | BCL2A1 | LINC01641 |
| Sep-09 | GRASP | MX2 | AL357054.4 | ENAM |
| SCRN1 | MYADM | ECE1 | MAP3K8 | IFNA1 |
| USF2 | VEGFB | MARCKS | MIR155HG | BIRC3 |
| HDGF | RPS3A | ELOA | CXCL9 | COX17 |
| ELMSAN1 | RPL5 | SAMD9 | IL10RA | CALCRL |
| VAMP8 | FTL | NCF2 | CXCL11 | SEC61G |
| CORO1A | JUND | REL | AC073957.3 | TIPIN |
| MYH9 | RPL13 | PARP9 | LTA | TMA7 |

## A.10 scRNA-seq GSEA Index Genes for GSEA Pathways Identified within Clusters

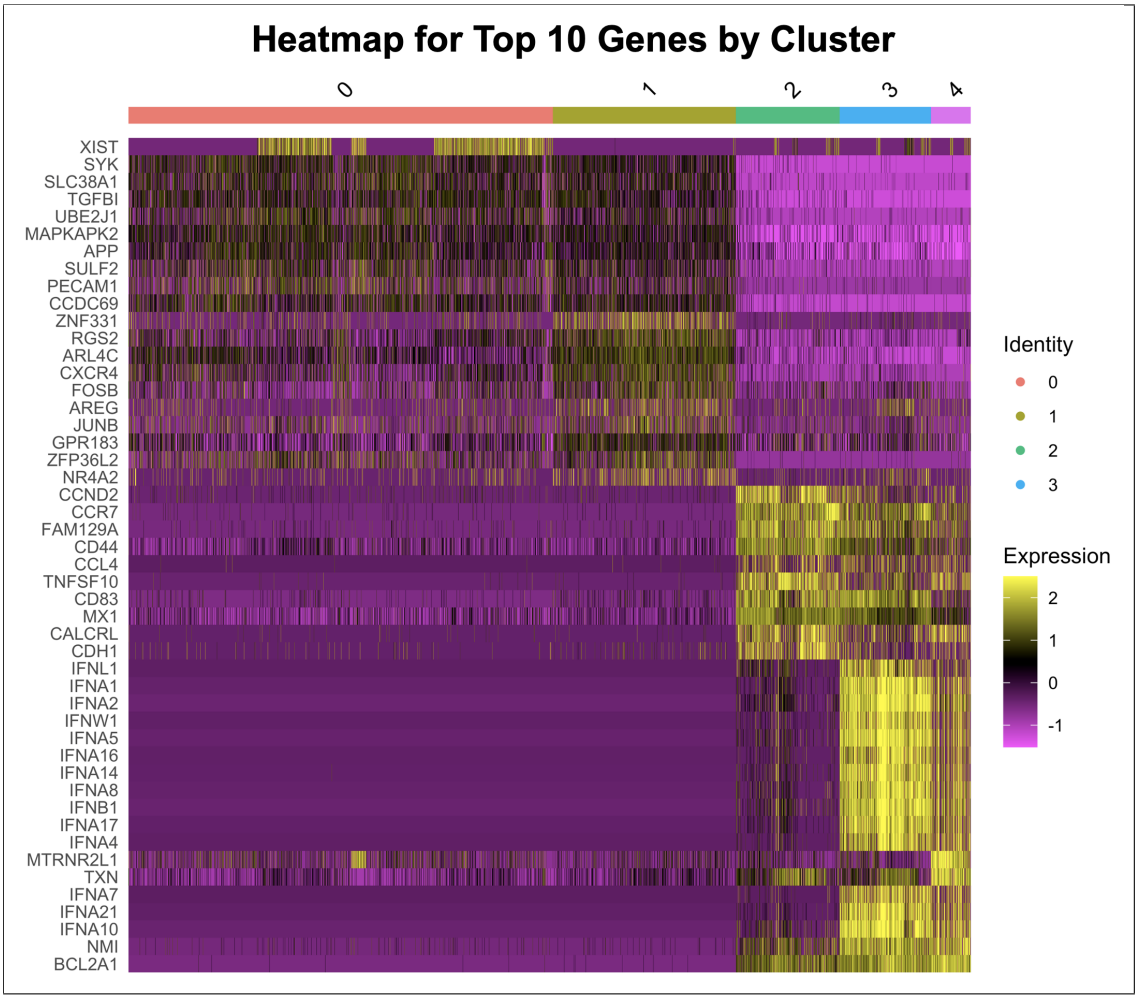
The top 50 differentially-expressed genes for each cluster identified via Seurat *FindVariableFeatures()* (listed in Appendix A.9) were used to search via GSEA (Subramanian et al. 2005) for enriched pathways within the MSigDB Hallmark dataset (Liberzon et al. 2015) and curated KEGG pathways (Kanehisa and Goto 2000) using a minimum cut-off of three index genes per pathway. GSEA reports genes (x-axis) responsible for identification of enriched pathways (y-axis). Blue squares indicate such index genes.




GSEA Module Identification
Clusters Top 50 Genes
Cluster 3
Gene Symbol
KEGG_RIG_I_LIKE_RECEPTOR_SIGNALING_PATHWAY
KEGG_CYTOSOLIC_DNA_SENSING_PATHWAY
KEGG_TOLL_LIKE_RECEPTOR_SIGNALING_PATHWAY
KEGG_REGULATION_OF_AUTOPHAGY
KEGG_AUTOIMMUNE_THYROID_DISEASE
KEGG_NATURAL_KILLER_CELL_MEDIATED_CYTOTOXICITY
KEGG_CYTOKINE_CYTOKINE_RECEPTOR_INTERACTION
KEGG_ANTIGEN_PROCESSING_AND_PRESENTATION
KEGG_JAK_STAT_SIGNALING_PATHWAY
HALLMARK_INFLAMMATORY_RESPONSE
IFNA1
IFNA2
IFNA4
IFNA5
IFNA7
IFNA8
IFNA10
IFNA13
IFNA14
IFNA16
IFNA17
IFNA21
IFNB1
CXCL10
CXCL8
ISG15
TNFSF10
CD69
NMI
CALCRL
Cluster 4
Gene Symbol
KEGG_CYTOKINE_CYTOKINE_RECEPTOR_INTERACTION
KEGG_TOLL_LIKE_RECEPTOR_SIGNALING_PATHWAY
KEGG_RIG_I_LIKE_RECEPTOR_SIGNALING_PATHWAY
KEGG_CYTOSOLIC_DNA_SENSING_PATHWAY
KEGG_JAK_STAT_SIGNALING_PATHWAY
KEGG_REGULATION_OF_AUTOPHAGY
KEGG_AUTOIMMUNE_THYROID_DISEASE
KEGG_ANTIGEN_PROCESSING_AND_PRESENTATION
KEGG_NATURAL_KILLER_CELL_MEDIATED_CYTOTOXICITY
HALLMARK_INTERFERON_GAMMA_RESPONSE
IFNA1
IFNA2
IFNA4
IFNA5
IFNA6
IFNA7
IFNA8
IFNA10
IFNA14
IFNA16
IFNA17
IFNA21
IFNB1
TNF
CCL5
CXCL11
CXCL9
IFNW1
IL10RA
IFNL2
IFNL3
IFNL1
LTA
NFKB1
MAP3K8
IFIH1
POLR3C
IFIT2
PTGS2
NMI
GBP4
IFIT3
PARP14
OASL

## A.11 scRNA-seq Heatmap of Top 10 DE Genes per Cluster

Heatmap showing expression of the top 10 genes per cluster for every cell. Each vertical line represents one cell. Colour represents Log2(expression) relative to the mean of the dataset. Identity corresponds to cluster.



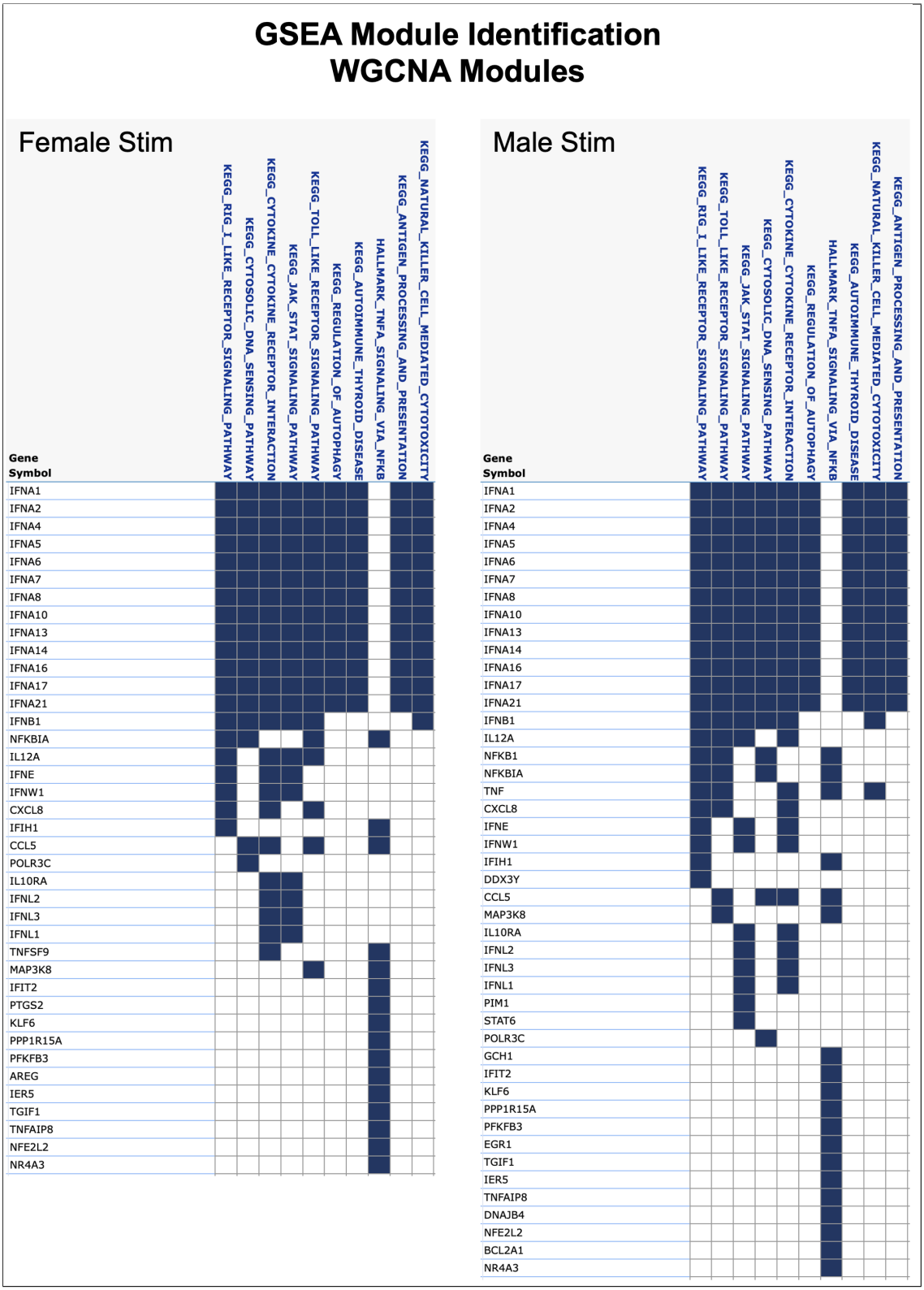
## A.12 WGCNA Gene Modules; as used for GSEA

**Table A.4:** scRNA-Seq WGCNA Gene Modules

| **Male Stim** | | | **Female Stim** | |
|---|---|---|---|---|
| TAL1 | MAFK | WARS | MACF1 | IFNA21 |
| AL135960.1 | SLC25A40 | TRIM69 | TAL1 | IFNA4 |
| NEXN | DBF4 | MYO1E | NEXN | IFNA7 |
| DNAJB4 | BET1 | BCL2A1 | GBP7 | IFNA10 |
| GBP4 | SRPK2 | IGF1R | GBP4 | IFNA16 |
| POLR3C | GPR34 | NOMO1 | POLR3C | IFNA17 |
| IER5 | SH2D4A | HYDIN | IER5 | IFNA14 |
| NR5A2 | ENPP2 | AC092723.3 | PTGS2 | IFNA5 |
| SIPA1L2 | IFNB1 | MIR22HG | NR5A2 | IFNA6 |
| GCSAML | IFNW1 | ZZEF1 | SIPA1L2 | IFNA13 |
| PUS10 | IFNA21 | CCL5 | RBKS | IFNA2 |
| ARID5A | IFNA4 | IGFBP4 | PUS10 | IFNA8 |
| MAP4K4 | IFNA7 | LRRC59 | SLC35F5 | IFNA1 |
| SLC35F5 | IFNA10 | MRPS7 | NIFK-AS1 | IFNE |
| NIFK-AS1 | IFNA16 | UBALD2 | NMI | NR4A3 |
| NMI | IFNA17 | TGIF1 | IFIH1 | FAM111A |
| IFIH1 | IFNA14 | RNMT | NFE2L2 | CEP126 |
| NFE2L2 | IFNA5 | ZNFX1 | HECW2 | IL10RA |
| HECW2 | IFNA6 | IFNL3 | NEU4 | KLF6 |
| NEU4 | IFNA13 | IFNL2 | SELENOK | PFKFB3 |
| RAB5A | IFNA2 | IFNL1 | NFKBIZ | MAP3K8 |
| SELENOK | IFNA8 | PLEKHA4 | IL12A | SLC29A3 |
| CGGBP1 | IFNA1 | PPP1R15A | CXCL8 | IFIT2 |
| NFKBIZ | IFNE | TTTY15 | AREG | NEMP1 |
| IL12A | NR4A3 | DDX3Y | HERC5 | CSRP2 |
| CXCL8 | SPTY2D1 | ASPHD2 | SLC7A11 | OASL |
| FRAS1 | LMO2 | HSPA13 | RANBP3L | PDS5B |
| HERC5 | FAM111A | | TMEM267 | NFKBIA |
| NFKB1 | CEP126 | | TNFAIP8 | FOXA1 |
| SLC7A11 | IL10RA | | HARS | BMP4 |
| FAM198B | KLF6 | | AL357054.4 | HIF1A |
| RANBP3L | PFKFB3 | | FOXC1 | TRIM69 |
| TMEM267 | ARL5B | | RNF144B | MYO1E |
| ELL2 | MAP3K8 | | TENT5A | IGF1R |
| TNFAIP8 | SLC29A3 | | CITED2 | NOMO1 |
| EGR1 | IFIT2 | | IGF2R | HYDIN |
| HARS | IFIT3 | | AC073957.3 | AC092723.3 |
| AL357054.4 | FGFBP3 | | ADAP1 | MIR22HG |
| FOXC1 | NEMP1 | | MAFK | CCL5 |
| SERPINB9P1 | STAT6 | | SLC25A40 | SP6 |
| JARID2 | THAP2 | | DBF4 | MRPS7 |
| RNF144B | CSRP2 | | BET1 | UBALD2 |
| TNF | OASL | | SRPK2 | TGIF1 |
| PIM1 | PDS5B | | GPR34 | RNMT |
| TENT5A | BAZ1A | | GLA | TNFSF9 |
| CITED2 | NFKBIA | | NXT2 | IFNL3 |
| IGF2R | FOXA1 | | SH2D4A | IFNL2 |
| CAHM | BMP4 | | ENPP2 | IFNL1 |
| AC073957.3 | GCH1 | | IFNB1 | PLEKHA4 |
| ADAP1 | HIF1A | | IFNW1 | PPP1R15A |

## A.13 scRNA-seq GSEA Pathway Enrichment within WGCNA Gene Modules

The co-expressed genes identified for groups via WGCNA (Langfelder and Horvath 2008) (listed in Appendix A.12) were used to search via GSEA (Subramanian et al. 2005) for enriched pathways within the MSigDB Hallmark dataset (Liberzon et al. 2015) and curated KEGG pathways (Kanehisa and Goto 2000) using a minimum cut-off of three index genes per pathway. GSEA reports genes (x-axis) responsible for identification of enriched pathways (y-axis). Blue squares indicate such index genes.


GSEA Module Identification
WGCNA Modules
Female Stim
Gene Symbol
KEGG_RIG_I_LIKE_RECEPTOR_SIGNALING_PATHWAY
KEGG_CYTOSOLIC_DNA_SENSING_PATHWAY
KEGG_CYTOKINE_CYTOKINE_RECEPTOR_INTERACTION
KEGG_JAK_STAT_SIGNALING_PATHWAY
KEGG_TOLL_LIKE_RECEPTOR_SIGNALING_PATHWAY
KEGG_REGULATION_OF_AUTOPHAGY
KEGG_AUTOIMMUNE_THYROID_DISEASE
HALLMARK_TNFA_SIGNALING_VIA_NFKB
KEGG_ANTIGEN_PROCESSING_AND_PRESENTATION
KEGG_NATURAL_KILLER_CELL_MEDIATED_CYTOTOXICITY
IFNA1
IFNA2
IFNA4
IFNA5
IFNA6
IFNA7
IFNA8
IFNA10
IFNA13
IFNA14
IFNA16
IFNA17
IFNA21
IFNB1
NFKBIA
IL12A
IFNE
IFNW1
CXCL8
IFIH1
CCL5
POLR3C
IL10RA
IFNL2
IFNL3
IFNL1
TNFSF9
MAP3K8
IFIT2
PTGS2
KLF6
PPP1R15A
PFKFB3
AREG
IER5
TGIF1
TNFAIP8
NFE2L2
NR4A3
Male Stim
Gene Symbol
KEGG_RIG_I_LIKE_RECEPTOR_SIGNALING_PATHWAY
KEGG_TOLL_LIKE_RECEPTOR_SIGNALING_PATHWAY
KEGG_JAK_STAT_SIGNALING_PATHWAY
KEGG_CYTOSOLIC_DNA_SENSING_PATHWAY
KEGG_CYTOKINE_CYTOKINE_RECEPTOR_INTERACTION
KEGG_REGULATION_OF_AUTOPHAGY
HALLMARK_TNFA_SIGNALING_VIA_NFKB
KEGG_AUTOIMMUNE_THYROID_DISEASE
KEGG_NATURAL_KILLER_CELL_MEDIATED_CYTOTOXICITY
KEGG_ANTIGEN_PROCESSING_AND_PRESENTATION
IFNA1
IFNA2
IFNA4
IFNA5
IFNA6
IFNA7
IFNA8
IFNA10
IFNA13
IFNA14
IFNA16
IFNA17
IFNA21
IFNB1
IL12A
NFKB1
NFKBIA
TNF
CXCL8
IFNE
IFNW1
IFIH1
DDX3Y
CCL5
MAP3K8
IL10RA
IFNL2
IFNL3
IFNL1
PIM1
STAT6
POLR3C
GCH1
IFIT2
KLF6
PPP1R15A
PFKFB3
EGR1
TGIF1
IER5
TNFAIP8
DNAJB4
NFE2L2
BCL2A1
NR4A3

## A.14 scRNA-Seq Top 50 DE Genes by Sex and Stimulation; as used for GSEA

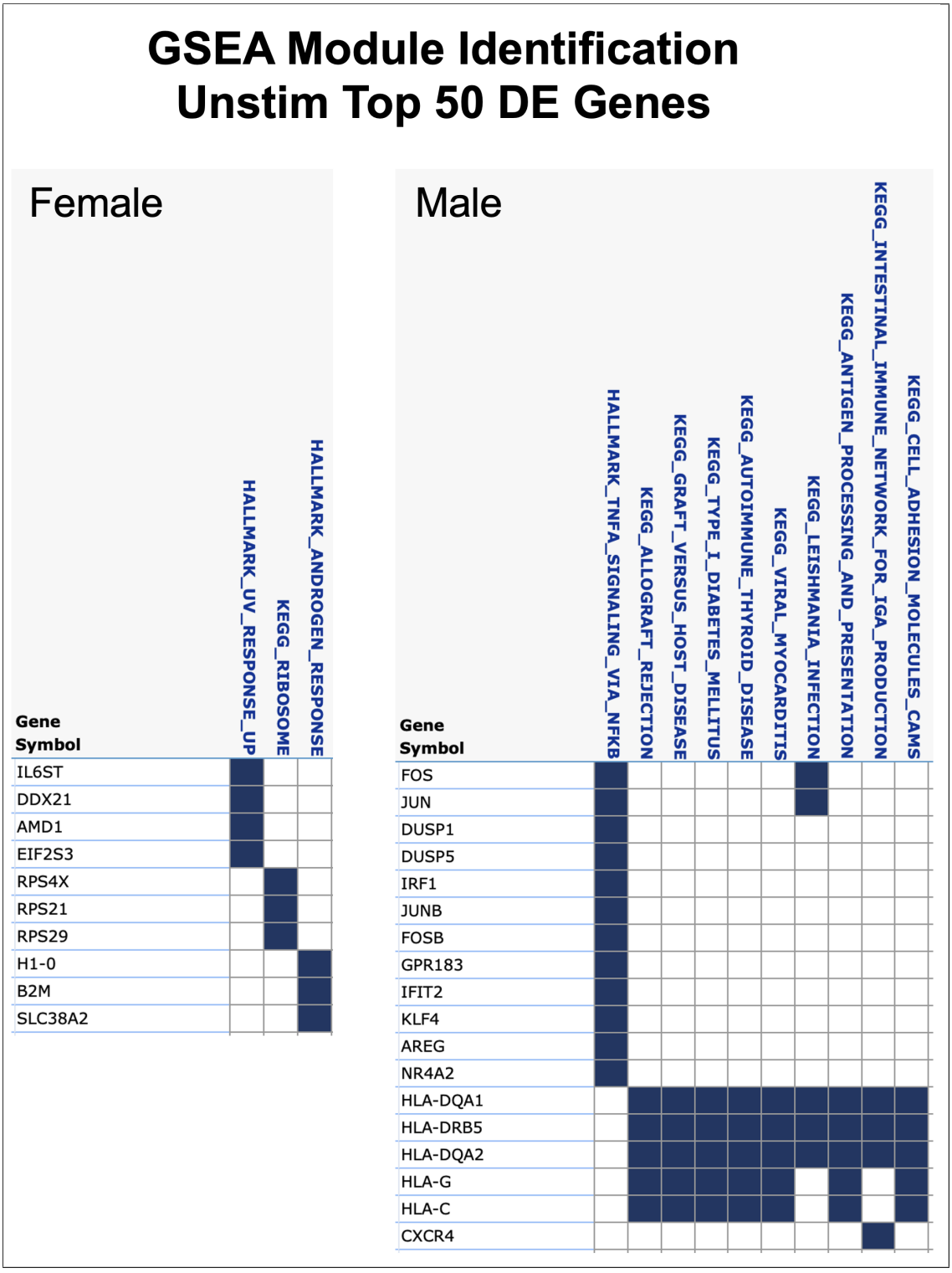
**Table A.5:** scRNA-Seq Top 50 DE Genes by Sex and Stimulation

| **Female Unstim** | **Male Unstim** | **Female Stim** | **Male Stim** |
|---|---|---|---|
| XIST | DDX3Y | XIST | DDX3Y |
| TSIX | RPS4Y1 | PTGS2 | TTTY15 |
| PLEKHD1 | HLA-DRB5 | PFKFB3 | USP9Y |
| ERAP2 | ARL4C | TSIX | NCF1 |
| DDX3X | HLA-DQA2 | HLA-DQA2 | CCND2 |
| SLC38A2 | USP9Y | AREG | TNFAIP2 |
| MMP23B | HLA-DQA1 | TNIP3 | EIF1AY |
| LINC00865 | KDM5D | LIMA1 | IGLC2 |
| CAPN2 | EIF1AY | GLA | MAP1A |
| DMXL2 | TTTY15 | PRKX | ARL4C |
| EIF1AX | AREG | CCR7 | CDH1 |
| RPS4X | CXCR4 | ETV3 | SH3BP5 |
| MTRNR2L1 | GPR183 | POLR3C | HLA-DQA1 |
| ENPP2 | FOSB | SLC7A11 | ANP32A |
| RPS21 | ZNF331 | CCL3L1 | ELOA |
| COL26A1 | RGS1 | IFNL3 | SPG7 |
| RPS29 | FOS | TAL1 | MTRNR2L12 |
| LGALS1 | UTY | GBP4 | CD4 |
| HEXIM1 | RGS2 | RPS4X | ZFY |
| IL6ST | JUND | NEU4 | WNT10A |
| H1F0 | NBPF19 | SH2D4A | IL3RA |
| C12orf57 | HLA-C | CXCL10 | PLEK |
| B2M | FYB1 | ELMSAN1 | MNDA |
| FAM213A | KLF4 | CCL5 | TACC1 |
| COMMD6 | SORL1 | MYOF | AD000090.1 |
| HRH2 | AJAP1 | TPI1 | RPS4Y1 |
| RLF | DUSP1 | MYO1G | XAF1 |
| GPCPD1 | SHD | AL357054.4 | FMNL3 |
| SUSD1 | IFIT2 | ACSL1 | RNF213 |
| DUSP6 | NR4A2 | PTPN1 | MTRNR2L1 |
| RSRP1 | DUSP5 | BIRC2 | TYW3 |
| AD000090.1 | ZBTB18 | FOSL2 | MDN1 |
| Sep-11 | MALAT1 | AC093484.3 | BTG1 |
| MT-ND1 | GPR65 | CXCL8 | FP671120.4 |
| STK17B | RRP7A | GPR171 | MGLL |
| IGFBP3 | SOX4 | CMTM6 | ARHGAP24 |
| RUNX2 | JUN | LMNB1 | CYB561A3 |
| SERTAD1 | JUNB | BATF3 | RAB11FIP1 |
| SUB1 | THBD | FOXC1 | MALAT1 |
| TSPAN13 | KDM5A | RNF115 | MTRNR2L8 |
| HIST1H4C | KRT5 | GPR34 | VPS13C |
| DYNLL1 | RPS26 | INSIG1 | MX2 |
| DDX21 | HLA-DQB2 | TMEM267 | SLC43A3 |
| KDM6A | GRASP | SLC25A19 | CIITA |
| KCTD12 | DDX24 | HNRNPLL | SWAP70 |
| ZBTB11 | IRF1 | IL12A | PNN |
| GRAMD1B | TNFRSF1B | CXCL9 | BCL11A |
| EIF2S3 | SLC18A2 | ENPP2 | TEX14 |
| USP24 | EGLN3 | GBP7 | GTF2I |
| AMD1 | HLA-G | RNF144B | GZMB |

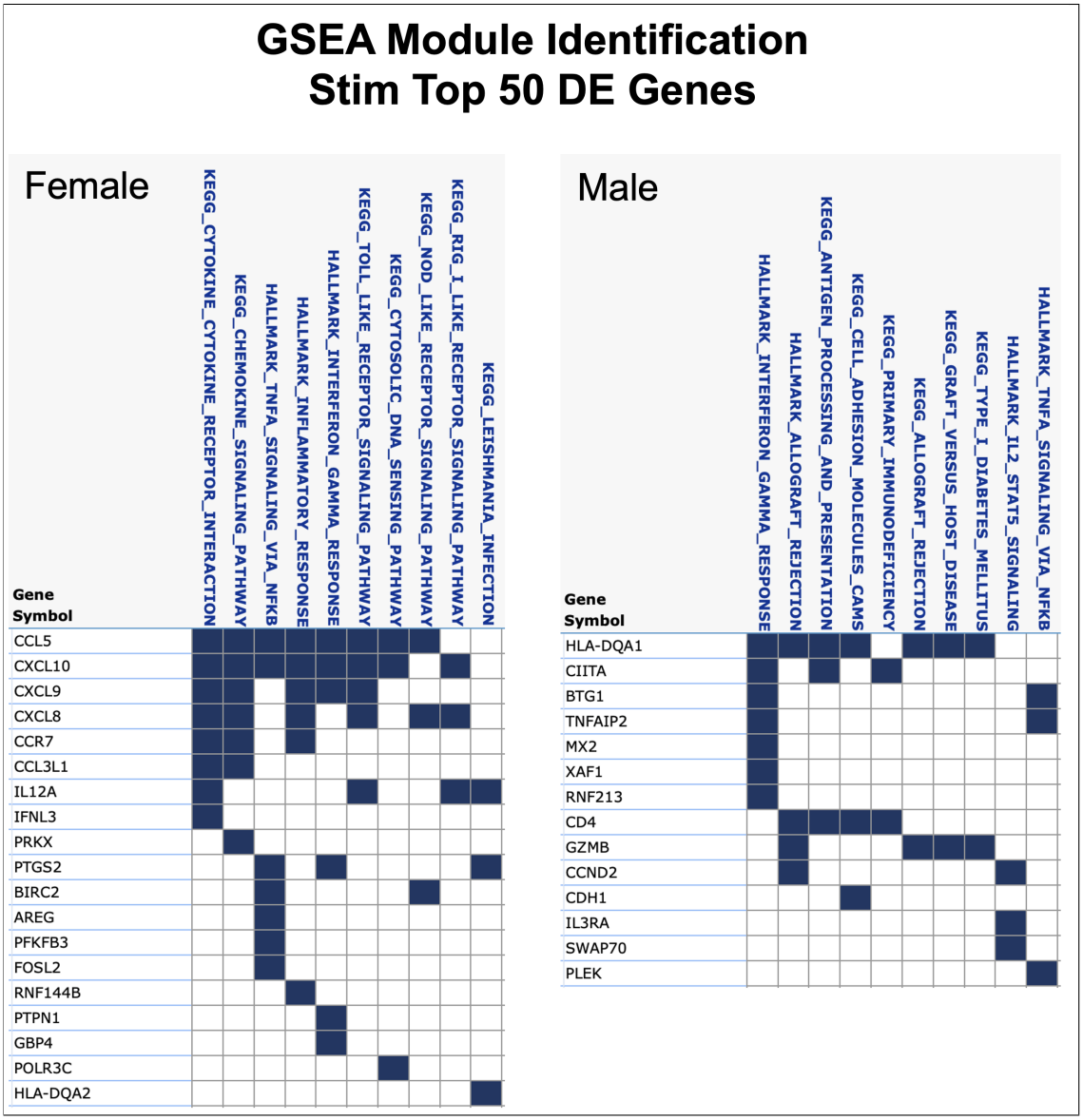
## A.15 scRNA-seq GSEA Pathway Enrichment within Top50 Differentially-expressed Genes between Males and Females

The top 50 differentially-expressed genes for each cluster identified via Seurat *FindVariableFeatures()* (listed in Appendix A.9) were used to search via GSEA (Subramanian et al. 2005) for enriched pathways within the MSigDB Hallmark dataset (Liberzon et al. 2015) and curated KEGG pathways (Kanehisa and Goto 2000) using a minimum cut-off of three index genes per pathway. GSEA reports genes (x-axis) responsible for identification of enriched pathways (y-axis). Blue squares indicate such index genes.

### A.15.1 Unstimulated pDCs

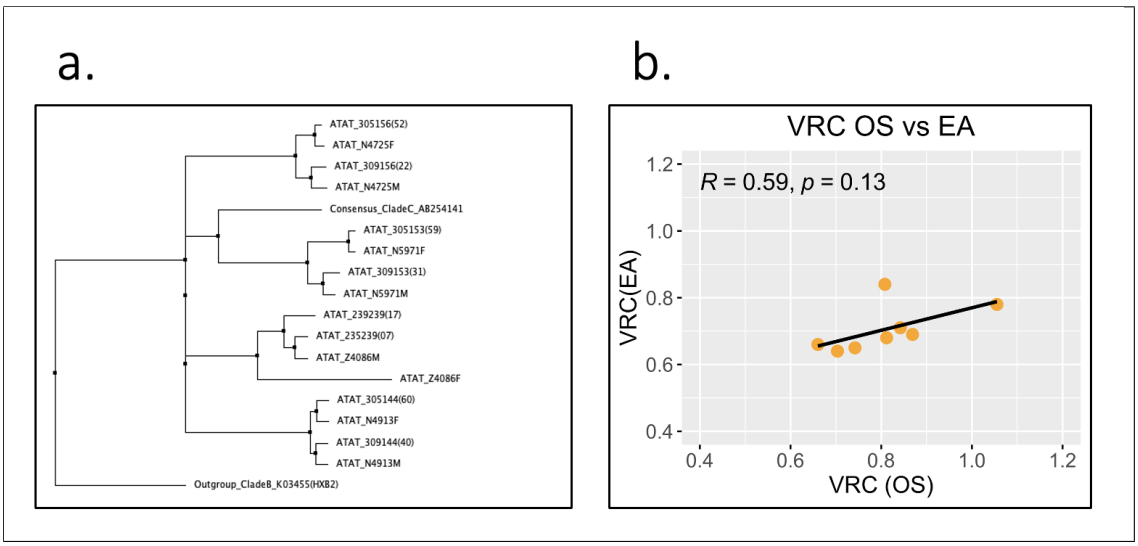


### A.15.2 CL097-stimulated pDCs



## A.16 Confirmation that VRC for overlapping chimeric NL4-3::*gag-pro* viruses correlate for two investigators

Chimeric NL4-3::*gag-pro* viruses were produced and VRC measured for pilot work in 2018 by Dr. Emily Adland (EA) before other viruses were generated anew by myself (OS); some happened to overlap so were used to confirm merging of VRC data for non-overlapping samples. a) Phylogenetic tree of p17 sequence for viruses from the four transmission pairs that overlapped. b) Scatter plot of the VRCs measured by EA compared to OS. Correlation via Pearson's method.

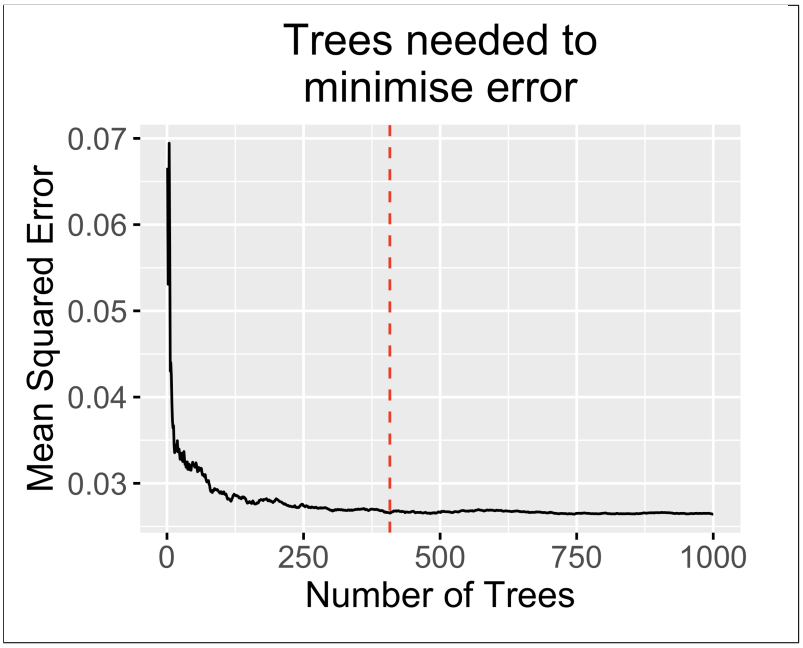


## A.17 Determination of optimal tree number for Random Forest

Using amino acid sequences for donor NL4-3::*gag-pro* chimeric viruses, positions relevant to VRC were predicted using a Random Forest constructed via regression using a subset size of 16 sequences (1/3 total sequences) per tree and a default terminal node size of 5, as defined in Segal et al. 2004.

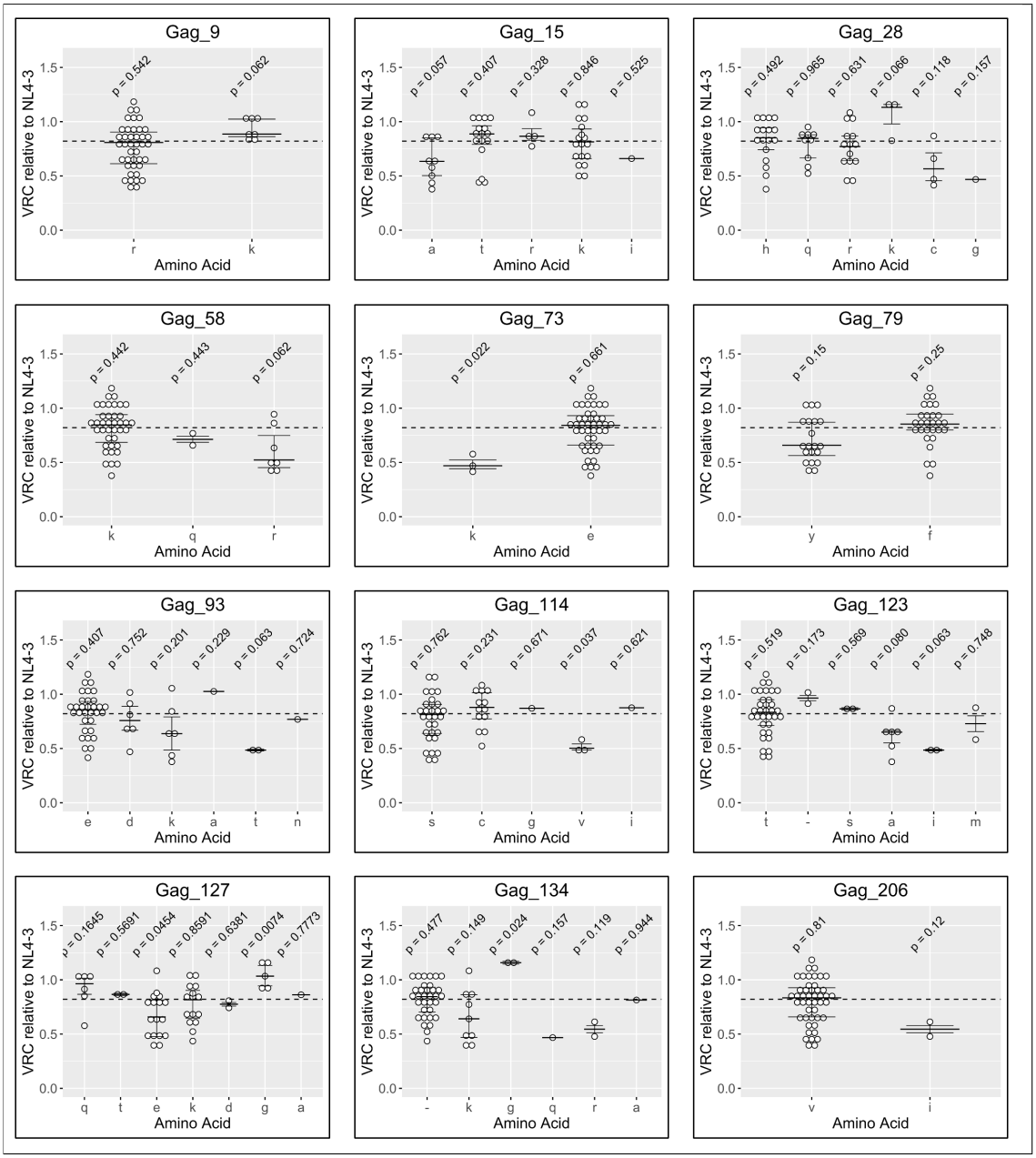
To identify the optimal number of trees, forests of 1-1,000 trees were constructed and the Mean squared error (MSE) for each calculated for the difference in VRCs predicted by that forest and the true VRC values.

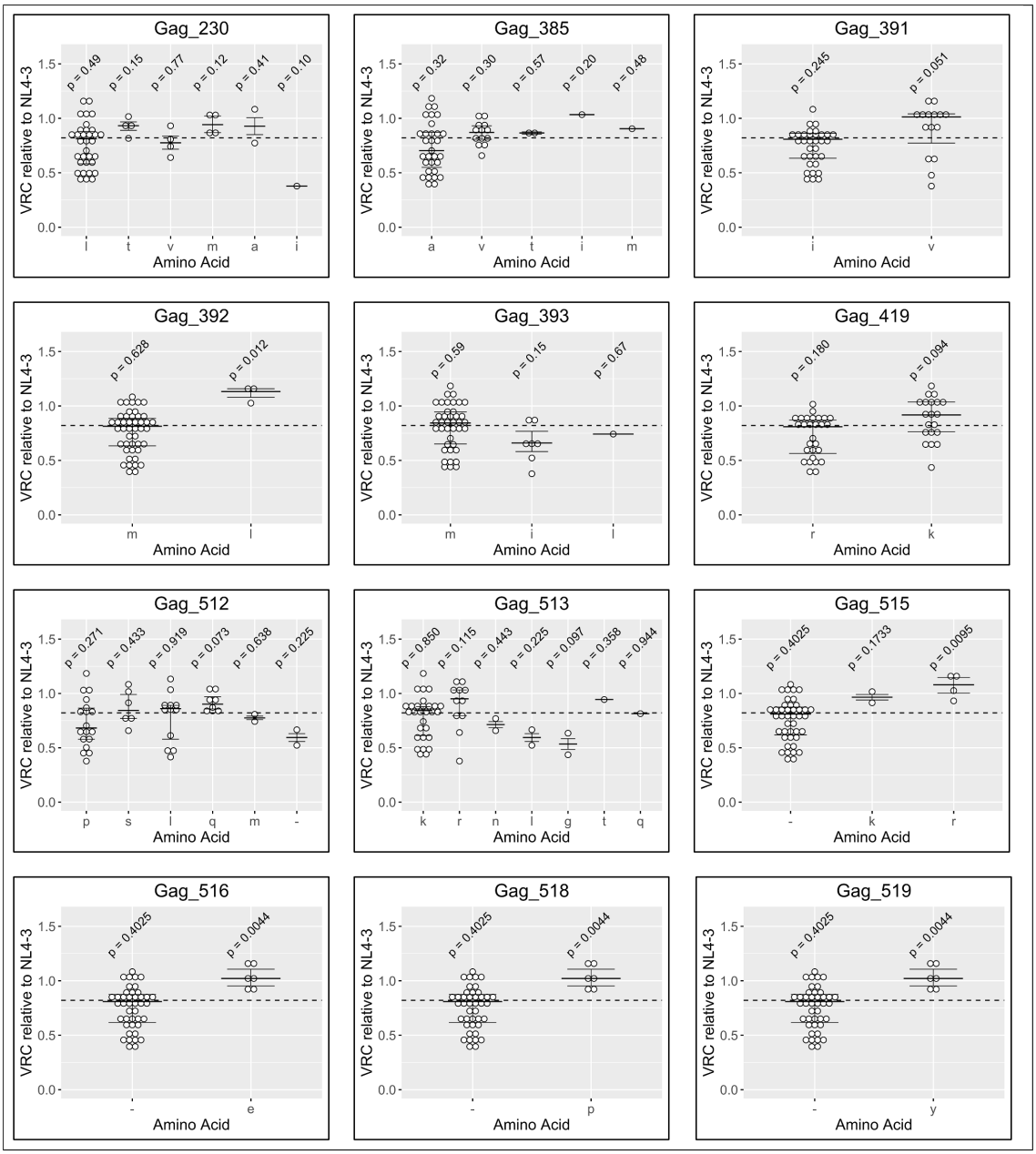
The optimum is the nadir following the stabilisation of the error rate; 408 in this case (red dashed line).

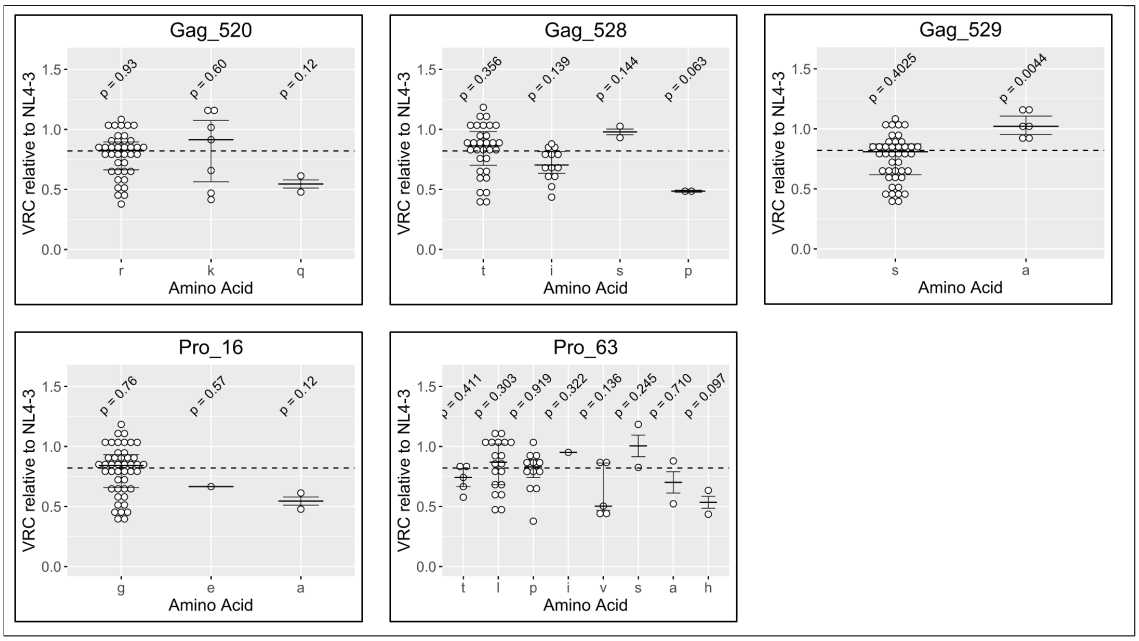


## A.18 VRC of NL4-3::*gag-pro* chimeric viruses by amino acid for positions identified by Random Forest

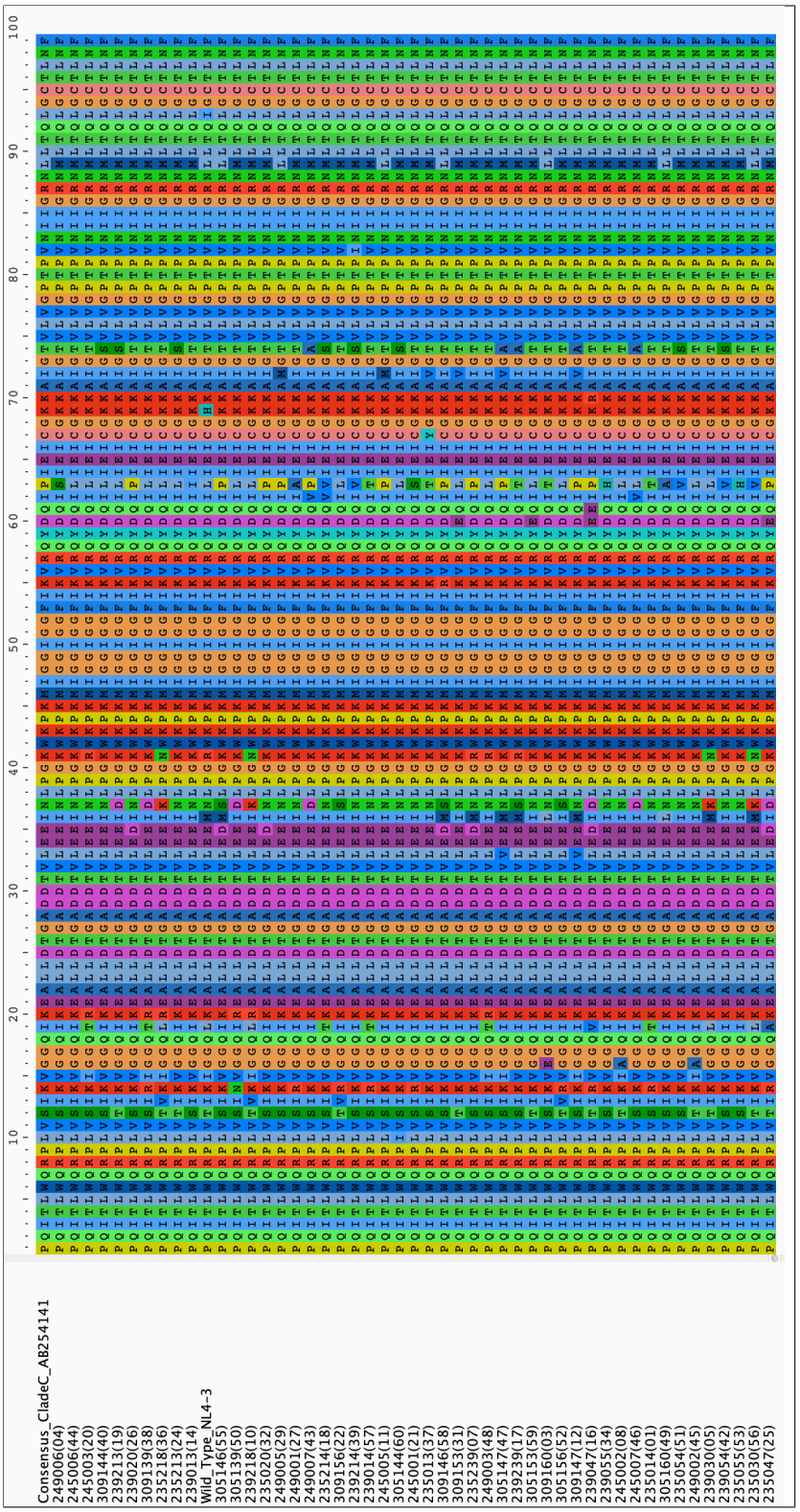
VRC data for NL4-3::*gag-pro* chimeric viruses generated from donor and recipient virus from heterosexual adult-to-adult transmission pairs. Stratified by amino acid for Gag-Pro positions with the greatest influence on the VRC of generated NL4-3::*gag-pro* chimeric viruses as identified via Random Forest (Section 5.3.6). Bars show median with interquartile range.


Gag_9
p = 0.542
p = 0.062
r
k
Gag_15
p = 0.057
p = 0.407
p = 0.328
p = 0.846
p = 0.525
a
t
r
k
i
Gag_28
p = 0.492
p = 0.965
p = 0.631
p = 0.066
p = 0.118
p = 0.157
h
q
r
k
c
g
Gag_58
p = 0.442
p = 0.443
p = 0.062
k
q
r
Gag_73
p = 0.022
p = 0.661
k
e
Gag_79
p = 0.15
p = 0.25
y
f
Gag_93
p = 0.407
p = 0.752
p = 0.201
p = 0.229
p = 0.063
p = 0.724
e
d
k
a
t
n
Gag_114
p = 0.762
p = 0.231
p = 0.671
p = 0.037
p = 0.621
s
c
g
v
i
Gag_123
p = 0.519
p = 0.173
p = 0.569
p = 0.080
p = 0.063
p = 0.748
t
-
s
a
i
m
Gag_127
p = 0.1645
p = 0.5691
p = 0.0454
p = 0.8591
p = 0.6381
p = 0.0074
p = 0.7773
q
t
e
k
d
g
a
Gag_134
p = 0.477
p = 0.149
p = 0.024
p = 0.157
p = 0.119
p = 0.944
-
k
g
q
r
a
Gag_206
p = 0.81
p = 0.12
v
i
VRC relative to NL4-3
Amino Acid
0.0
0.5
1.0
1.5


Gag_230
p = 0.49
p = 0.15
p = 0.77
p = 0.12
p = 0.41
p = 0.10
l t v m a i
Gag_385
p = 0.32
p = 0.30
p = 0.57
p = 0.20
p = 0.48
a v t i m
Gag_391
p = 0.245
p = 0.051
i v
Gag_392
p = 0.628
p = 0.012
m l
Gag_393
p = 0.59
p = 0.15
p = 0.67
m i l
Gag_419
p = 0.180
p = 0.094
r k
Gag_512
p = 0.271
p = 0.433
p = 0.919
p = 0.073
p = 0.638
p = 0.225
p s l q m -
Gag_513
p = 0.850
p = 0.115
p = 0.443
p = 0.225
p = 0.097
p = 0.358
p = 0.944
k r n l g t q
Gag_515
p = 0.4025
p = 0.1733
p = 0.0095
- k r
Gag_516
p = 0.4025
p = 0.0044
- e
Gag_518
p = 0.4025
p = 0.0044
- p
Gag_519
p = 0.4025
p = 0.0044
- y
VRC relative to NL4-3
Amino Acid
0.0
0.5
1.0
1.5


Gag_520
p = 0.93
p = 0.60
p = 0.12
r
k
q
Gag_528
p = 0.356
p = 0.139
p = 0.144
p = 0.063
t
i
s
p
Gag_529
p = 0.4025
p = 0.0044
s
a
Pro_16
p = 0.76
p = 0.57
p = 0.12
g
e
a
Pro_63
p = 0.411
p = 0.303
p = 0.919
p = 0.322
p = 0.136
p = 0.245
p = 0.710
p = 0.097
t
l
p
i
v
s
a
h
VRC relative to NL4-3
Amino Acid
0.0
0.5
1.0
1.5

## A.19 Protease alignment

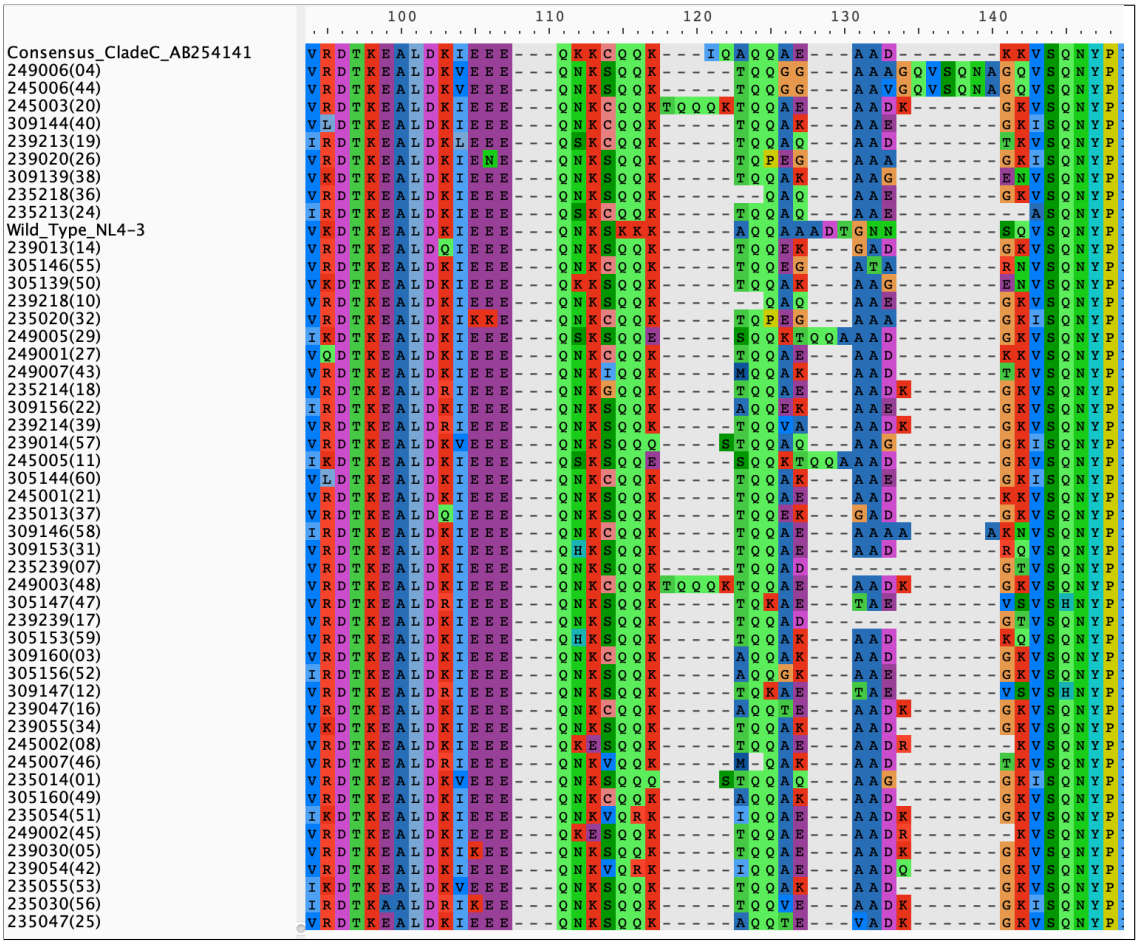


# A.20 N-terminal Gag-polyprotein alignments

Alignments of Gag polyprotein amino acid sequences for donor and recipient NL4-3::*gag-pro* chimeric viruses ordered by VRC. As VRC was measured relative to wild-type NL4-3, sequence for NL4-3 (Genbank accession: MN685337 is included for reference at VRC=1.0.

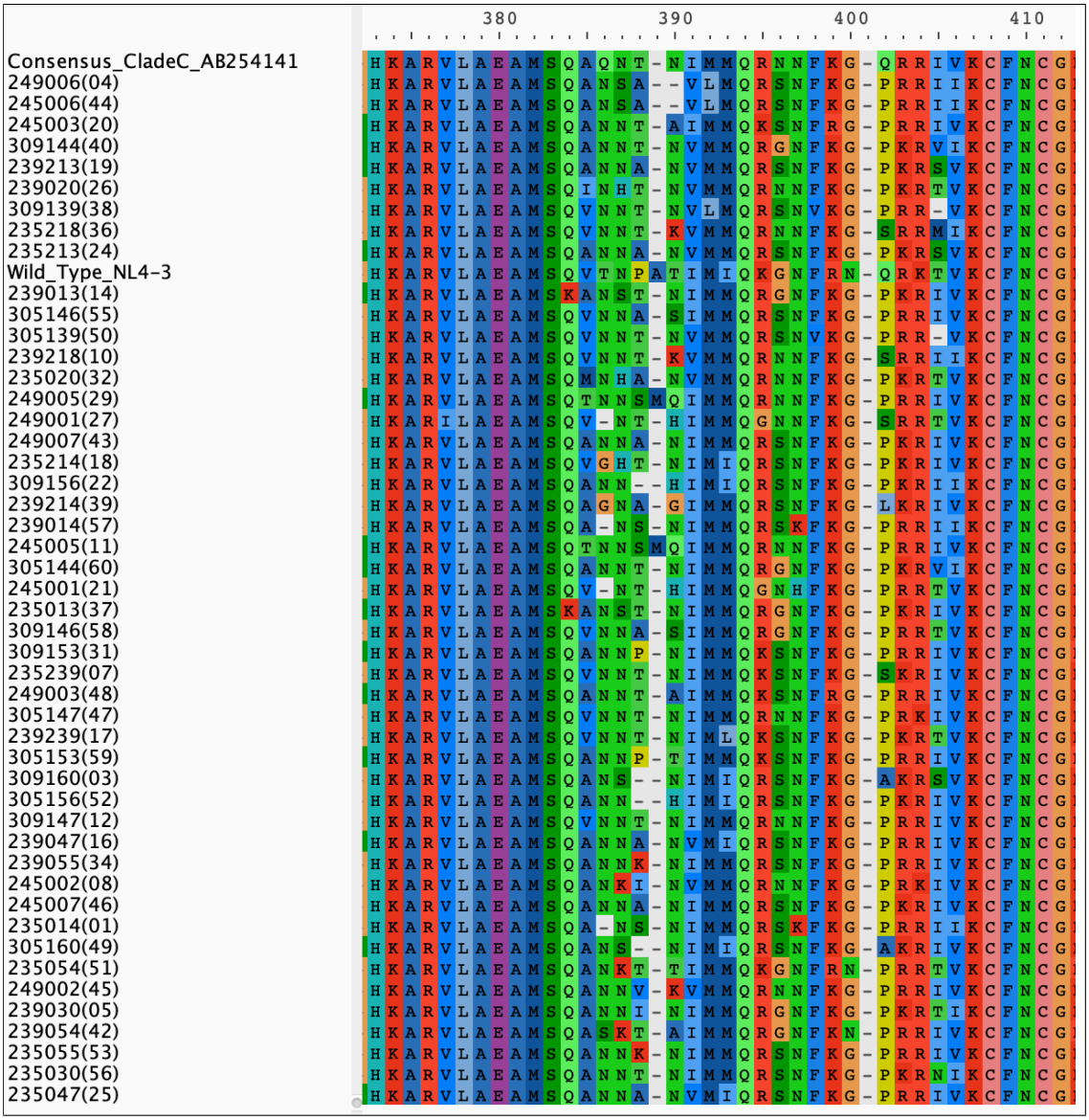
## A.20.1 Gag p17 N-terminus

NB: position 100 corresponds to 100 of HXB2; and position 145 to 130 of HXB2.



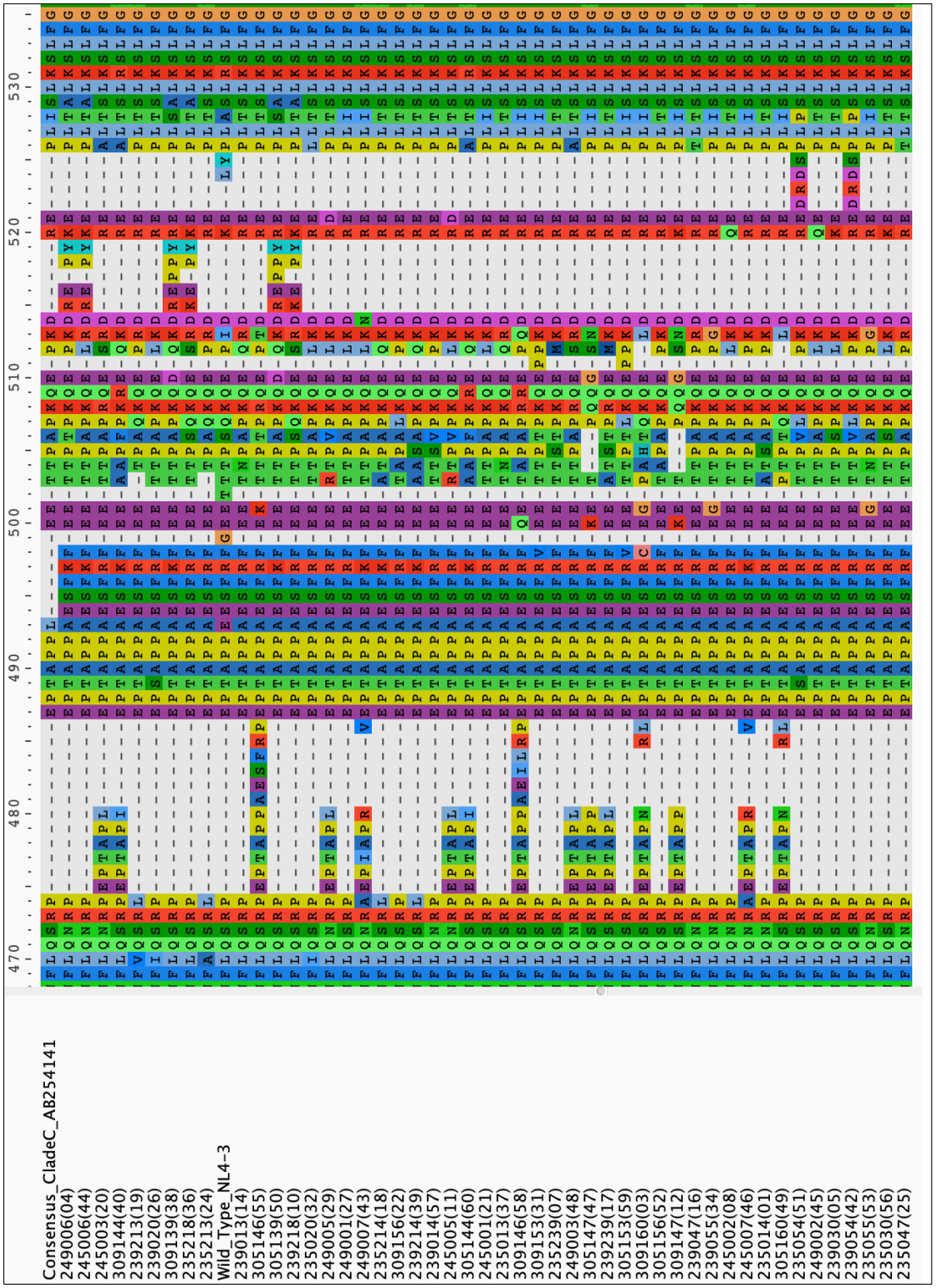
## A.20.2 Gag p2/p7 cleavage site

NB: position 380 corresponds to 365 of HXB2; and 410 to 385 of HXB2.



### A.20.3 Gag p6 N-terminus

NB: position 470 corresponds to 449 of HXB2; and 530 to 489 of HXB2.



# References


Abbas, Flora, et al. 2022. "HIV-1 infection enhances innate function and TLR7 expression in female plasmacytoid dendritic cells". *Life Science Alliance* 5 (10): e202201452. doi:10.26508/lsa.202201452.

Abraham, Guy E. 1974. "Ovarian and Adrenal Contribution to Peripheral Androgens During the Menstrual Cycle". *The Journal of Clinical Endocrinology & Metabolism* 39 (2): 340–346. doi:10.1210/jcem-39-2-340.

Adland, Emily, et al. 2015. "Discordant Impact of HLA on Viral Replicative Capacity and Disease Progression in Pediatric and Adult HIV Infection". *PLOS Pathogens* 11 (6): 1–26. doi:10.1371/journal.ppat.1004954.

Adland, Emily, et al. 2020. "Sex-specific innate immune selection of HIV-1 in utero is associated with increased female susceptibility to infection". *Nature Communications* 11:1767. doi:10.1038/s41467-020-15632-y.

Aiello, Alessandra, et al. 2018. "The involvement of plasmacytoid cells in HIV infection and pathogenesis". *Cytokine  Growth Factor Reviews* 40:77–89. doi:10.1016/j.cytogfr.2018.03.009.

Ajasin, David O, et al. 2019. "CCL2 mobilizes ALIX to facilitate Gag-p6 mediated HIV-1 virion release". *eLife* 8:e35546. doi:10.7554/eLife.35546.

Akira, Shizuo, and Kiyoshi Takeda. 2004. "Toll-like receptor signalling". *Nature Reviews Immunology* 4 (7): 499–511. doi:10.1038/nri1391.

Alculumbre, Solana G., et al. 2017. "Diversification of human plasmacytoid predendritic cells in response to a single stimulus". *Nature Immunology* 19 (1): 63–75. doi:10.1038/s41590-017-0012-z.

Altschul, Stephen F., et al. 1990. "Basic local alignment search tool". *Journal of Molecular Biology* 215 (3): 403–410. doi:10.1016/S0022-2836(05)80360-2.

Amenyogbe, Eric, et al. 2020. "A review on sex steroid hormone estrogen receptors in mammals and fish". *International Journal of Endocrinology* 2020:1–9. doi:10.1155/2020/5386193.

Anderson, David C. 1974. "SEX-HORMONE-BINDING GLOBULIN". *Clinical Endocrinology* 3 (1): 69–96. doi:10.1111/j.1365-2265.1974.tb03298.x.

Andrade Barbosa, Bárbara, et al. 2021. "Bayesian log-normal deconvolution for enhanced in silico microdissection of bulk gene expression data". *Nature communications* 12 (1): e6106. doi:10.1038/s41467-021-26328-2.

Aralaguppe, Shambhu G., et al. 2017. “Increased replication capacity following evolution of PYxE insertion in Gag-p6 is associated with enhanced virulence in HIV-1 subtype C from East Africa”. *Journal of Medical Virology* 89 (1): 106–111. doi:10.1002/jmv.24610.

Arnold, Cosby G., et al. 2022. “Immune mechanisms associated with sex-based differences in severe COVID-19 clinical outcomes”. *Biology of Sex Differences* 13 (1). doi:10.1186/s13293-022-00417-3.

Arunachalam, Prabhu S, et al. 2021. “Systems vaccinology of the BNT162b2 mRNA vaccine in humans”. *Nature* 596 (7872): 410–416. doi:10.1038/s41586-021-03791-x.

Asano, Takaki, et al. 2021. “X-linked recessive TLR7 deficiency in 1% of men under 60 years old with life-threatening COVID-19”. *Science Immunology* 6 (62): eabl4348. doi:10.1126/sciimmunol.abl4348.

Asselin-Paturel, Carine, et al. 2001. “Mouse type I IFN-producing cells are immature apcs with plasmacytoid morphology”. *Nature Immunology* 2 (12): 1144–1150. doi:10.1038/ni736.

Azeez, Juberiya M, et al. 2021. “New insights into the functions of progesterone receptor (PR) isoforms and progesterone signaling”. *American Journal of Cancer Research* 11 (11): 5214–5232.

Bastard, Paul, et al. 2021a. “Autoantibodies neutralizing type I IFNs are present in 4% of uninfected individuals over 70 years old and account for 20% of COVID-19 deaths”. *Science Immunology* 6 (62): eabl4340. doi:10.1126/sciimmunol.abl4340.

— . 2021b. “Autoantibodies neutralizing type I IFNs are present in 4% of uninfected individuals over 70 years old and account for 20% of COVID-19 deaths”. *Science Immunology* 6 (62): eabl4340. doi:10.1126/sciimmunol.abl4340.

Ben-Batalla, Isabel, et al. 2020. “Influence of androgens on immunity to self and foreign: effects on immunity and cancer”. *Frontiers in immunology* 11:e1184. doi:10.3389/fimmu.2020.01184.

Berghöfer, Beate, et al. 2006. “TLR7 Ligands Induce Higher IFN-α Production in Females”. *The Journal of Immunology* 177 (4): 2088–2096. doi:10.4049/jimmunol.177.4.2088.

Björnström, Linda, and Maria Sjöberg. 2005. “Mechanisms of Estrogen Receptor Signaling: Convergence of Genomic and Nongenomic Actions on Target Genes”. *Molecular Endocrinology* 19 (4): 833–842. doi:10.1210/me.2004-0486.

Bobjer, Johannes, et al. 2013. “Negative Association between Testosterone Concentration and Inflammatory Markers in Young Men: A Nested Cross-Sectional Study”. *PLOS ONE* 8 (4): 1–8. doi:10.1371/journal.pone.0061466.

Boeras, Debrah I., et al. 2011. “Role of donor genital tract HIV-1 diversity in the transmission bottleneck”. *Proceedings of the National Academy of Sciences* 108 (46): E1156–E1163. doi:10.1073/pnas.1103764108.

Brockman, Mark A., et al. 2006. “Use of a novel GFP reporter cell line to examine replication capacity of CXCR4- and CCR5-tropic HIV-1 by flow cytometry”. *Journal of Virological Methods* 131 (2): 134–142. doi:10.1016/j.jviromet.2005.08.003.

Brockman, Mark A., et al. 2010. "Early Selection in Gag by Protective HLA Alleles Contributes to Reduced HIV-1 Replication Capacity That May Be Largely Compensated for in Chronic Infection". *Journal of Virology* 84 (22): 11937–11949. doi:10.1128/JVI.01086-10.

Brundin, Peik M. A., et al. 2021. "Expression of Sex Hormone Receptor and Immune Response Genes in Peripheral Blood Mononuclear Cells During the Menstrual Cycle". *Frontiers in Endocrinology* 12. doi:10.3389/fendo.2021.721813.

Bruni, Daniela, et al. 2015. "Viral entry route determines how human plasmacytoid dendritic cells produce type I interferons". *Science Signaling* 8 (366): ra25–ra25. doi:10.1126/scisignal.aaa1552.

Bucasas, Kristine L., et al. 2011. "Early Patterns of Gene Expression Correlate With the Humoral Immune Response to Influenza Vaccination in Humans". *The Journal of Infectious Diseases* 203 (7): 921–929. doi:10.1093/infdis/jiq156.

Bui, Hong N., et al. 2013. "Dynamics of serum testosterone during the menstrual cycle evaluated by daily measurements with an ID-LC–MS/MS method and a 2nd generation automated immunoassay". *Steroids* 78 (1): 96–101. doi:10.1016/j.steroids.2012.10.010.

Burger, Henry G. 2002. "Androgen production in women". *Fertility and Sterility* 77:3–5. doi:10.1016/S0015-0282(02)02985-0.

Buyon, Jill P., et al. 2005. "The Effect of Combined Estrogen and Progesterone Hormone Replacement Therapy on Disease Activity in Systemic Lupus Erythematosus: A Randomized Trial". *Annals of Internal Medicine* 142 (12_Part_1): 953–962. doi:10.7326/0003-4819-142-12_Part_1-200506210-00004.

Cao, Raquel G., et al. 2014. "Differences in Antibody Responses Between Trivalent Inactivated Influenza Vaccine and Live Attenuated Influenza Vaccine Correlate With the Kinetics and Magnitude of Interferon Signaling in Children". *The Journal of Infectious Diseases* 210 (2): 224–233. doi:10.1093/infdis/jiu079.

Carlson, Jonathan M., et al. 2014. "Selection bias at the heterosexual HIV-1 transmission bottleneck". *Science* 345 (6193): 1254031. doi:10.1126/science.1254031.

Carroll, Jason S, et al. 2006. "Genome-wide analysis of estrogen receptor binding sites". *Nature genetics* 38 (11): 1289–1297. doi:10.1038/ng1901.

Cevik, Muge, et al. 2021. "SARS-CoV-2, SARS-CoV, and MERS-CoV viral load dynamics, duration of viral shedding, and infectiousness: a systematic review and meta-analysis". *The Lancet Microbe* 2 (1): E13–E22. doi:10.1016/S2666-5247(20)30172-5.

Chahroudi, Ann, et al. 2012. "Natural SIV Hosts: Showing AIDS the Door". *Science* 335 (6073): 1188–1193. doi:10.1126/science.1217550.

Chung, Eugene, et al. 2005. "Characterization of Virus-Responsive Plasmacytoid Dendritic Cells in the Rhesus Macaque". *Clinical and Vaccine Immunology* 12 (3): 426–435. doi:10.1128/CDLI.12.3.426-435.2005.

Clemens, Michael J., and Bryan R.G. Williams. 1978. "Inhibition of cell-free protein synthesis by pppA2 p5 A2 p5 A: a novel oligonucleotide synthesized by interferon-treated L cell extracts". *Cell* 13 (3): 565–572. doi:10.1016/0092-8674(78)90329-X.

Coch, Christoph, et al. 2013. "A Human In Vitro Whole Blood Assay to Predict the Systemic Cytokine Response to Therapeutic Oligonucleotides Including siRNA". *PLoS ONE* 8 (8): 1–10. doi:10.1371/journal.pone.0071057.

Codoñer, Francisco M, et al. 2017. "Gag-protease coevolution analyses define novel structural surfaces in the HIV-1 matrix and capsid involved in resistance to protease inhibitors". *Scientific Reports* 7 (1). doi:10.1038/s41598-017-03260-4.

Corcoran, Michael P, et al. 2010. "Sex hormone modulation of proinflammatory cytokine and CRP expression in macrophages from older men and postmenopausal women". *The Journal of endocrinology* 206 (2): 217.

Corrales, Juan José, et al. 2009. "Persistence of androgenic effects on the production of proinflammatory cytokines by circulating antigen-presenting cells after withdrawal of testosterone treatment in aging type 2 diabetic men with partial androgen deficiency". *Fertility and sterility* 92 (1): 311–319.

Crozat, Karine, et al. 2010. "Comparative genomics as a tool to reveal functional equivalences between human and mouse dendritic cell subsets". *Immunological Reviews* 234 (1): 177–198. doi:10.1111/j.0105-2896.2009.00868.x.

D'agostino, P, et al. 1999. "Sex hormones modulate inflammatory mediators produced by macrophages a". *Annals of the New York Academy of Sciences* 876 (1): 426–429.

Davey, Rachael A., and Mathis Grossmann. 2016. "Androgen Receptor Structure, Function and Biology: From Bench to Bedside". *Clin Biochem Rev.* 37 (1): 3–15.

Davidson, Sophia, et al. 2014. "Pathogenic potential of interferon αβ in acute influenza infection". *Nature Communications* 5:e3864. doi:10.1038/ncomms4864.

De Abreu Costa, Lucas, et al. 2017. "Dimethyl Sulfoxide (DMSO) Decreases Cell Proliferation and TNF-α, IFN-γ, and IL-2 Cytokines Production in Cultures of Peripheral Blood Lymphocytes". *Molecules* 22 (11). doi:10.3390/molecules22111789.

De Weerd, Nicole A, et al. 2013. "Structural basis of a unique interferon-$\beta$ signaling axis mediated via the receptor IFNAR1". *Nature immunology* 14 (9): 901–907. doi:10.1038/ni.2667.

Deeks, Steven G., et al. 2015. "HIV infection". *Nature Reviews Disease Primers* 1 (15035). doi:10.1038/nrdp.2015.35.

Deitch, Edwin A., et al. 2006. "Neutrophil activation is modulated by sex hormones after trauma-hemorrhagic shock and burn injuries". *American Journal of Physiology-Heart and Circulatory Physiology* 291 (3): H1456–H1465. doi:10.1152/ajpheart.00694.2005.

Der, Evan, et al. 2014. "Gr1+ cells suppress T-dependent antibody responses in (NZB× NZW) F1 male mice through inhibition of T follicular helper cells and germinal center formation". *The Journal of Immunology* 192 (4): 1570–1576.

Derdeyn, Cynthia A., et al. 2004. "Envelope-Constrained Neutralization-Sensitive HIV-1 After Heterosexual Transmission". *Science* 303 (5666): 2019–2022. doi:10.1126/science.1093137.

Deymier, Martin J., et al. 2015. "Heterosexual Transmission of Subtype C HIV-1 Selects Consensus-Like Variants without Increased Replicative Capacity or Interferon-α Resistance". *PLOS Pathogens* 11, no. 9 (): 1–22. doi:10.1371/journal.ppat.1005154.

Diebold, Sandra S., et al. 2004. "Innate Antiviral Responses by Means of TLR7-Mediated Recognition of Single-Stranded RNA". *Science* 303 (5663): 1529–1531. doi:10.1126/science.1093616.

Dong, Ensheng, Hongru Du, and Lauren Gardner. 2020. "An interactive web-based dashboard to track COVID-19 in real time". *The Lancet Infectious Diseases* 20 (5): 533–534. doi:10.1016/S1473-3099(20)30120-1.

Dou, Dan, et al. 2018. "Influenza A virus cell entry, replication, Virion Assembly and Movement". *Frontiers in Immunology* 9. doi:10.3389/fimmu.2018.01581.

Doyle, Tomas, Caroline Goujon, and Michael H. Malim. 2015. "HIV-1 and interferons: Who's interfering with whom?" *Nature Reviews Microbiology* 13 (7): 403–413. doi:10.1038/nrmicro3449.

Dunning, Jake, et al. 2018. "Progression of whole-blood transcriptional signatures from interferon-induced to neutrophil-associated patterns in severe influenza". *Nature Immunology* 19 (6): 625–635. doi:10.1038/s41590-018-0111-5.

Eales, Oliver, et al. 2022. "SARS-CoV-2 lineage dynamics in England from September to November 2021: high diversity of Delta sub-lineages and increased transmissibility of AY. 4.2". *BMC infectious diseases* 22 (1): 647. doi:10.1186/s12879-022-07628-4.

Engler, Renata J. M., et al. 2008. "Half- vs Full-Dose Trivalent Inactivated Influenza Vaccine (2004-2005): Age, Dose, and Sex Effects on Immune Responses". *Archives of Internal Medicine* 168 (22): 2405–2414. doi:10.1001/archinternmed.2008.513.

Enzenbach, Cornelia, et al. 2019. "Evaluating selection bias in a population-based cohort study with low baseline participation: the LIFE-Adult-Study". *BMC medical research methodology* 19:1–14. doi:10.1186/s12874-019-0779-8.

"Estrogen receptors regulate innate immune cells and signaling pathways". 2015. *Cellular Immunology* 294 (2): 63–69. doi:10.1016/j.cellimm.2015.01.018.

Fenton-May, Angharad E, et al. 2013. "Relative resistance of HIV-1 founder viruses to control by interferon-alpha". *Retrovirology* 10 (1): 1–18. doi:10.1186/1742-4690-10-146.

Finkel-Jimenez, Beatriz, Marcel Wüthrich, and Bruce S. Klein. 2002. "BAD1, an Essential Virulence Factor of Blastomyces dermatitidis, Suppresses Host TNF-α Production Through TGF-β-Dependent and -Independent Mechanisms1". *The Journal of Immunology* 168 (11): 5746–5755. doi:10.4049/jimmunol.168.11.5746.

Flanagan, Katie L., et al. 2017. "Sex and Gender Differences in the Outcomes of Vaccination over the Life Course". *Annual Review of Cell and Developmental Biology* 33 (1): 577–599. doi:10.1146/annurev-cellbio-100616-060718.

Flys, Tamara, et al. 2005. "Analysis of PTAP Duplications in the gag p6 Region of Subtype C HIV Type 1". *AIDS Research and Human Retroviruses* 21 (8): 739–741. doi:10.1089/aid.2005.21.739.

Frankel, Alan D., and John A. T. Young. 1998. "HIV-1: Fifteen Proteins and an RNA". *Annual Review of Biochemistry* 67 (1): 1–25. doi:10.1146/annurev.biochem.67.1.1.

Freed, Eric O. 2015. "HIV-1 assembly, release and maturation". *Nature Reviews Microbiology* 13 (8): 484–496. doi:10.1038/nrmicro3490.

Freitas, Raul S., Tyler F. Crum, and Kislay Parvatiyar. 2022. "SARS-CoV-2 Spike Antagonizes Innate Antiviral Immunity by Targeting Interferon Regulatory Factor 3". *Frontiers in Cellular and Infection Microbiology* 11. doi:10.3389/fcimb.2021.789462.

Fung, Sin-Yee, et al. 2021. "SARS-CoV-2 main protease suppresses type I interferon production by preventing nuclear translocation of phosphorylated IRF3". *Int J Biol Sci* 17:1547–1554. doi:10.7150/ijbs.59943.

Furman, David, et al. 2014. "Systems analysis of sex differences reveals an immunosuppressive role for testosterone in the response to influenza vaccination". *Proceedings of the National Academy of Sciences* 111 (2): 869–874. doi:10.1073/pnas.1321060111.

Gandhi, Monica, et al. 2002. "Does Patient Sex Affect Human Immunodeficiency Virus Levels?" *Clinical Infectious Diseases* 35 (3): 313–322. doi:10.1086/341249.

García-Sastre, Adolfo. 2017. "Ten Strategies of Interferon Evasion by Viruses". *Cell Host & Microbe* 22 (2): 176–184. doi:10.1016/j.chom.2017.07.012.

Gavin, Amanda L., et al. 2006. "Adjuvant-Enhanced Antibody Responses in the Absence of Toll-Like Receptor Signaling". *Science* 314 (5807): 1936–1938. doi:10.1126/science.1135299.

Ghanem, Mustafa H., et al. 2022. "Proteomic and Single-Cell Transcriptomic Dissection of Human Plasmacytoid Dendritic Cell Response to Influenza Virus". *Frontiers in Immunology* 13. doi:10.3389/fimmu.2022.814627.

Gibbert, K, et al. 2013. "IFN-α subtypes: distinct biological activities in anti-viral therapy". *British Journal of Pharmacology* 168 (5): 1048–1058. doi:10.1111/bph.12010.

Gierahn, Todd M, et al. 2017. "SEQ-well: Portable, low-cost RNA sequencing of single cells at high throughput". *Nature Methods* 14 (4): 395–398. doi:10.1038/nmeth.4179.

Goel, Rishi R., et al. 2021. "Distinct antibody and memory B cell responses in SARS-CoV-2 naïve and recovered individuals after mRNA vaccination". *Science Immunology* 6 (58): eabi6950. doi:10.1126/sciimmunol.abi6950.

Gondim, Marcos V. P., et al. 2021. "Heightened resistance to host type 1 interferons characterizes HIV-1 at transmission and after antiretroviral therapy interruption". *Science Translational Medicine* 13 (576): eabd8179. doi:10.1126/scitranslmed.abd8179.

Goujon, Caroline, et al. 2013. "Human MX2 is an interferon-induced post-entry inhibitor of HIV-1 infection". *Nature* 502 (7472): 559–562. doi:10.1038/nature12542.

Goulder, Philip, and Steven G. Deeks. 2018. "HIV control: Is getting there the same as staying there?" *PLOS Pathogens* 14 (11): 1–18. doi:10.1371/journal.ppat.1007222.

Goulder, Philip JR, and David I Watkins. 2008. "Impact of MHC class I diversity on immune control of immunodeficiency virus replication". *Nature Reviews Immunology* 8 (8): 619–630. doi:10.1038/nri2357.

Griesbeck, Morgane, et al. 2015. "Sex Differences in Plasmacytoid Dendritic Cell Levels of IRF5 Drive Higher IFN-α Production in Women". *The Journal of Immunology* 195 (11): 5327–5336. doi:10.4049/jimmunol.1501684.

Griffiths, Jonathan A, Antonio Scialdone, and John C Marioni. 2018. "Using single-cell genomics to understand developmental processes and cell fate decisions". *Molecular Systems Biology* 14 (4): e8046. doi:10.15252/msb.20178046.

Grino, Placido B., James E. Griffin, and Jean D. Wilson. 1990. "Testosterone at High Concentrations Interacts with the Human Androgen Receptor Similarly to Dihydrotestosterone*". *Endocrinology* 126 (2): 1165–1172. doi:10.1210/endo-126-2-1165.

Grouard, Géraldine, et al. 1997. "The Enigmatic Plasmacytoid T Cells Develop into Dendritic Cells with Interleukin (IL)-3 and CD40-Ligand". *Journal of Experimental Medicine* 185 (6): 1101–1112. doi:10.1084/jem.185.6.1101.

Gubbels Bupp, Melanie R, and Trine N Jorgensen. 2018. "Androgen-induced immunosuppression". *Frontiers in immunology* 9:e794. doi:10.3389/fimmu.2018.00794.

Guerrera, Gisella, et al. 2021. "BNT162b2 vaccination induces durable SARS-CoV-2–specific T cells with a stem cell memory phenotype". *Science Immunology* 6 (66): eabl5344. doi:10.1126/sciimmunol.abl5344.

Guiducci, Cristiana, et al. 2006. "Properties regulating the nature of the plasmacytoid dendritic cell response to Toll-like receptor 9 activation ". *Journal of Experimental Medicine* 203 (8): 1999–2008. doi:10.1084/jem.20060401.

Hagen, Sven Hendrik, et al. 2020. "Heterogeneous Escape from X Chromosome Inactivation Results in Sex Differences in Type I IFN Responses at the Single Human pDC Level". *Cell Reports* 33 (10): 108485. doi:10.1016/j.celrep.2020.108485.

Han, Lulu, et al. 2021. "SARS-CoV-2 ORF9b antagonizes type I and III interferons by targeting multiple components of the RIG-I/MDA-5–MAVS, TLR3–TRIF, and cGAS–STING signaling pathways". *Journal of Medical Virology* 93 (9): 5376–5389. doi:10.1002/jmv.27050.

Hannah, Michele F., Vladimir B. Bajic, and Sabra L. Klein. 2008. "Sex differences in the recognition of and innate antiviral responses to Seoul virus in Norway rats". *Brain, Behavior, and Immunity* 22 (4): 503–516. doi:10.1016/j.bbi.2007.10.005.

Hao, Yuhan, et al. 2021. "Integrated analysis of multimodal single-cell data". *Cell* 184 (13): 3573–3587. doi:10.1016/j.cell.2021.04.048.

Haque, Ashraful, et al. 2017. "A practical guide to single-cell RNA-sequencing for biomedical research and clinical applications". *Genome medicine* 9:e75. doi:10.1186/s13073-017-0467-4.

Hardy, Gareth A. D., et al. 2013. "Interferon-α Is the Primary Plasma Type-I IFN in HIV-1 Infection and Correlates with Immune Activation and Disease Markers". *PLOS ONE* 8 (2): 1–9. doi:10.1371/journal.pone.0056527.

He, Xiao-Song, et al. 2006. "Cellular Immune Responses in Children and Adults Receiving Inactivated or Live Attenuated Influenza Vaccines". *Journal of Virology* 80 (23): 11756–11766. doi:10.1128/jvi.01460-06.

Hedrick, Stephen H. 2004. "The Acquired Immune System: A Vantage from Beneath". *Immunity* 21:607–615. doi:10.1016/j.immuni.2004.08.020.

Hepworth, Matthew R, Matthew J Hardman, and Richard K Grencis. 2010. "The role of sex hormones in the development of Th2 immunity in a gender-biased model of Trichuris muris infection". *European journal of immunology* 40 (2): 406–416.

Hertzog, Jonny, and Jan Rehwinkel. 2020. "Regulation and inhibition of the DNA sensor cgas". *EMBO reports* 21 (12). doi:10.15252/embr.202051345.

Hladik, Florian, et al. 2007. "Initial Events in Establishing Vaginal Entry and Infection by Human Immunodeficiency Virus Type-1". *Immunity* 26 (2): 257–270. doi:10.1016/j.immuni.2007.01.007.

Honda, Kenya, Akinori Takaoka, and Tadatsugu Taniguchi. 2006. "Type I Inteferon Gene Induction by the Interferon Regulatory Factor Family of Transcription Factors". *Immunity* 25 (3): 349–360. doi:10.1016/j.immuni.2006.08.009.

Honda, Kenya, et al. 2005. "Spatiotemporal regulation of myd88–IRF-7 signalling for robust type-I interferon induction". *Nature* 434 (7036): 1035–1040. doi:10.1038/nature03547.

Hou, Jun, and Fei Zheng Wu. 1988. "Effect of sex hormones on NK and ADDC activity of mice". *International journal of immunopharmacology* 10 (1): 15–22.

Howard, Leigh M., et al. 2017. "Cell-Based Systems Biology Analysis of Human AS03-Adjuvanted H5N1 Avian Influenza Vaccine Responses: A Phase I Randomized Controlled Trial". *PLOS ONE* 12 (1): 1–34. doi:10.1371/journal.pone.0167488.

Huang, Bin, et al. 2021. "Sex-based clinical and immunological differences in COVID-19". *BMC Infectious Diseases* 21 (1). doi:10.1186/s12879-021-06313-2.

Hughes, Grant C., et al. 2008. "Cutting Edge: Progesterone Regulates IFN-α Production by Plasmacytoid Dendritic Cells1". *The Journal of Immunology* 180 (4): 2029–2033. doi:10.4049/jimmunol.180.4.2029.

Ida, James A., et al. 2006. "A whole blood assay to assess peripheral blood dendritic cell function in response to Toll-like receptor stimulation". *Journal of Immunological Methods* 310 (1): 86–99. doi:10.1016/j.jim.2005.12.008.

Ilicic, Tomislav, et al. 2016. "Classification of low quality cells from single-cell RNA-seq data". *Genome Biology* 17:e29. doi:10.1186/s13059-016-0888-1.

Isaacs, Alick, and J. Lindenmann. 1957. "Virus interference. i. the Interferon". *Proceedings of the Royal Society of London. Series B - Biological Sciences* 147 (927): 258–267. doi:10.1098/rspb.1957.0048.

Iwasaki, Akiko, and Padmini S. Pillai. 2014. "Innate immunity to influenza virus infection". *Nature Reviews Immunology* 14 (5): 315–328. doi:10.1038/nri3665.

Iyer, Shilpa S., et al. 2017. "Resistance to type 1 interferons is a major determinant of HIV-1 transmission fitness". *Proceedings of the National Academy of Sciences* 114 (4): E590–E599. doi:10.1073/pnas.1620144114.

Jacobsen, Henning, and Sabra L. Klein. 2021. "Sex Differences in Immunity to Viral Infections". *Frontiers in Immunology* 12. doi:10.3389/fimmu.2021.720952.

Jaillon, Sébastien, Kevin Berthenet, and Cecilia Garlanda. 2017. "Sexual dimorphism in innate immunity". *Clinical Reviews in Allergy & Immunology* 56 (3): 308–321. doi:10.1007/s12016-017-8648-x.

Jewell, Nancy A., et al. 2007. "Differential Type I Interferon Induction by Respiratory Syncytial Virus and Influenza A Virus In Vivo". *Journal of Virology* 81 (18): 9790–9800. doi:10.1128/JVI.00530-07.

Jin, Xiaoyang, et al. 2019. "Characterization of dendritic cell subtypes in human cord blood by single-cell sequencing". *Biophysics Reports* 5:199–208. doi:10.1007/s41048-019-00096-5\left(.

Jing, Yu, et al. 2009. "Aging is associated with a numerical and functional decline in plasmacytoid dendritic cells, whereas myeloid dendritic cells are relatively unaltered in human peripheral blood". *Human immunology* 70 (10): 777–784. doi:10.1016/j.humimm.2009.07.005.

Joseph, Sarah B., et al. 2015. "Bottlenecks in HIV-1 transmission: insights from the study of founder viruses". *Nature Reviews Microbiology* 13:414–425. doi:10.1038/nrmicro3471.

Kaminow, Benjamin, Dinar Yunusov, and Alexander Dobin. 2021. "STARsolo: accurate, fast and versatile mapping/quantification of single-cell and single-nucleus RNA-seq data". *bioRxiv*. doi:10.1101/2021.05.05.442755.

Kanehisa, Minoru, and Susumu Goto. 2000. "KEGG: Kyoto Encyclopedia of Genes and Genomes". *Nucleic Acids Research* 28, no. 1 (): 27–30. doi:10.1093/nar/28.1.27.

Kapaata, Anne, et al. 2021. "HIV-1 Gag-Pol Sequences from Ugandan Early Infections Reveal Sequence Variants Associated with Elevated Replication Capacity". *Viruses* 13 (171). doi:10.3390/v13020171.

Karaba, Andrew H, et al. 2021. "Differential Cytokine Signatures of Severe Acute Respiratory Syndrome Coronavirus 2 (SARS-CoV-2) and Influenza Infection Highlight Key Differences in Pathobiology". *Clinical Infectious Diseases* 74 (2): 254–262. doi:10.1093/cid/ciab376.

Karikó, Katalin, et al. 2011. "Generating the optimal mRNA for therapy: HPLC purification eliminates immune activation and improves translation of nucleoside-modified, protein-encoding mRNA". *Nucleic Acids Research* 39 (21): e142–e142. doi:10.1093/nar/gkr695.

Kaul, Arvind, et al. 2016. "Systemic lupus erythematosus". *Nature Reviews Disease Primers* 2 (1). doi:10.1038/nrdp.2016.39.

Kawai, Taro, and Shizuo Akira. 2010. "The role of pattern-recognition receptors in innate immunity: Update on toll-like receptors". *Nature Immunology* 11 (5): 373–384. doi:10.1038/ni.1863.

Keele, Brandon F., et al. 2008. "Identification and characterization of transmitted and early founder virus envelopes in primary HIV-1 infection". *Proceedings of the National Academy of Sciences* 105 (21): 7552–7557. doi:10.1073/pnas.0802203105.

Kida, Hiroshi, Shoichi Ihara, and Atsushi Kumanogoh. 2013. "Involvement of STAT3 in immune evasion during lung tumorigenesis". *OncoImmunology* 2 (1): e22653. doi:10.4161/onci.22653.

Kiguoya, Marion W., et al. 2017. "Subtype-Specific Differences in Gag-Protease-Driven Replication Capacity Are Consistent with Intersubtype Differences in HIV-1 Disease Progression". *Journal of Virology* 91 (13): e00253–17. doi:10.1128/JVI.00253-17.

Kimura, Tominori, et al. 2013. "Stabilization of human interferon-$\alpha$1 mRNA by its antisense RNA". *Cellular and Molecular Life Sciences* 70:1451–1467. doi:10.1007/s00018-012-1216-x.

Kioon, Marie Dominique Ah, et al. 2018. "Plasmacytoid dendritic cells promote systemic sclerosis with a key role for TLR8". *Science Translational Medicine* 10 (423): eaam8458. doi:10.1126/scitranslmed.aam8458.

Kirchner, H., Ch. Kleinicke, and W. Digel. 1982. "A whole-blood technique for testing production of human interferon by leukocytes". *Journal of Immunological Methods* 48 (2): 213–219. doi:10.1016/0022-1759(82)90195-8.

Kissick, Haydn T, et al. 2014. "Androgens alter T-cell immunity by inhibiting T-helper 1 differentiation". *Proceedings of the National Academy of Sciences* 111 (27): 9887–9892.

Klein, Sabra L, Anne Jedlicka, and Andrew Pekosz. 2010. "The Xs and Y of immune responses to viral vaccines". *The Lancet Infectious Diseases* 10 (5): 338–349. doi:10.1016/S1473-3099(10)70049-9.

Klein, Sabra L. 2012. "Immune Cells Have Sex and So Should Journal Articles". *Endocrinology* 153 (6): 2544–2550. doi:10.1210/en.2011-2120.

Klein, Sabra L., and Katie L. Flanagan. 2016. "Sex differences in immune responses". *Nature Reviews Immunology* 16 (10): 626–638. doi:10.1038/nri.2016.90.

Klein, Sabra L., Andrea Hodgson, and Dionne P. Robinson. 2012. "Mechanisms of sex disparities in influenza pathogenesis". *Journal of Leukocyte Biology* 92 (1): 67–73. doi:10.1189/jlb.0811427.

Klein, Sabra L., and Andrew Pekosz. 2014. "Sex-based Biology and the Rational Design of Influenza Vaccination Strategies". *The Journal of Infectious Diseases* 209 (suppl$_3$): S114–S119. doi:10.1093/infdis/jiu066.

Kocar, IH, et al. 2000. "The effect of testosterone replacement treatment on immunological features of patients with Klinefelter's syndrome". *Clinical & Experimental Immunology* 121 (3): 448–452.

Koonin, Eugene V., Mart Krupovic, and Vadim I. Agol. 2021. "The Baltimore Classification of Viruses 50 Years Later: How Does It Stand in the Light of Virus Evolution?" *Microbiology and Molecular Biology Reviews* 85 (3): e00053–21. doi:10.1128/MMBR.00053-21.

Koyama, Shohei, et al. 2007. "Differential Role of TLR- and RLR-Signaling in the Immune Responses to Influenza A Virus Infection and Vaccination". *The Journal of Immunology* 179 (7): 4711–4720. doi:10.4049/jimmunol.179.7.4711.

Koyama, Shohei, et al. 2010. "Plasmacytoid Dendritic Cells Delineate Immunogenicity of Influenza Vaccine Subtypes". *Science Translational Medicine* 2 (25): 25ra24–25ra24. doi:10.1126/scitranslmed.3000759.

Kožíšek, Milan, et al. 2012. "Mutations in HIV-1 gag and pol Compensate for the Loss of Viral Fitness Caused by a Highly Mutated Protease". *Antimicrobial Agents and Chemotherapy* 56 (8): 4320–4330. doi:10.1128/AAC.00465-12.

Krammer, Florian, et al. 2018. "Influenza". *Nature Reviews Disease Primers* 4 (3). doi:10.1038/s41572-018-0002-y.

Kulle, A. E., et al. 2010. "A Novel Ultrapressure Liquid Chromatography Tandem Mass Spectrometry Method for the Simultaneous Determination of Androstenedione, Testosterone, and Dihydrotestosterone in Pediatric Blood Samples: Age- and Sex-Specific Reference Data". *The Journal of Clinical Endocrinology & Metabolism* 95 (5): 2399–2409. doi:10.1210/jc.2009-1670.

Lachance, Sylvain, et al. 2015. "Importance of measuring testosterone in enzyme-inhibited plasma for oral testosterone undecanoate androgen replacement therapy clinical trials". *Future Science OA* 1 (4). doi:10.4155/fso.15.55.

Laffont, Sophie, et al. 2014. "X-Chromosome Complement and Estrogen Receptor Signaling Independently Contribute to the Enhanced TLR7-Mediated IFN-α Production of Plasmacytoid Dendritic Cells from Women". *The Journal of Immunology* 193 (11): 5444–5452. doi:10.4049/jimmunol.1303400.

Langfelder, Peter, and Steve Horvath. 2008. "WGCNA: an R package for weighted correlation network analysis". *BMC Bioinformatics* 9:e559. doi:10.1186/1471-2105-9-559.

Lanser, Lukas, et al. 2021. "Testosterone deficiency is a risk factor for severe COVID-19". *Frontiers in Endocrinology* 12:694083.

Larcombe, Alexander N., et al. 2011. "Sexual dimorphism in lung function responses to acute influenza A infection". *Influenza and Other Respiratory Viruses* 5:334–342. doi:10.1111/j.1750-2659.2011.00236.x.

Larsson, Anders. 2014. "AliView: a fast and lightweight alignment viewer and editor for large datasets". *Bioinformatics* 30 (22): 3276–3278. doi:10.1093/bioinformatics/btu531.

Laurent, Paôline, et al. 2022. "Sensing of SARS-COV-2 by pDCs and their subsequent production of IFN-I contribute to macrophage-induced cytokine storm during COVID-19". *Science Immunology* 7 (75). doi:10.1126/sciimmunol.add4906.

Lazear, Helen M, John W Schoggins, and Michael S Diamond. 2019. "Shared and distinct functions of type I and type III interferons". *Immunity* 50 (4): 907–923. doi:10.1016/j.immuni.2019.03.025.

Lee, Heung Kyu, et al. 2007. "Autophagy-Dependent Viral Recognition by Plasmacytoid Dendritic Cells". *Science* 315 (5817): 1398–1401. doi:10.1126/science.1136880.

Lee, Michelle Y.-H., et al. 2021. "Tissue-specific transcriptional profiling of plasmacytoid dendritic cells reveals a hyperactivated state in chronic SIV infection". *PLOS Pathogens* 17 (6): 1–32. doi:10.1371/journal.ppat.1009674.

Lee, SangJoon, and Jin-Hyeob Ryu. 2021. "Influenza Viruses: Innate Immunity and mRNA Vaccines". *Frontiers in Immunology* 12. doi:10.3389/fimmu.2021.710647.

Lei, Xiaobo, et al. 2020. "Activation and evasion of type I interferon responses by SARS-COV-2". *Nature Communications* 11 (1). doi:10.1038/s41467-020-17665-9.

Li, Bing, et al. 2006. "Evidence for Potent Autologous Neutralizing Antibody Titers and Compact Envelopes in Early Infection with Subtype C Human Immunodeficiency Virus Type 1". *Journal of Virology* 80 (11): 5211–5218. doi:10.1128/JVI.00201-06.

Li, Chunfeng, et al. 2022. "Mechanisms of innate and adaptive immunity to the Pfizer-BioNTech BNT162b2 vaccine". *Nature Immunology* 23 (4): 543–555. doi:10.1038/s41590-022-01163-9.

Li, Guangming, et al. 2014. "Plasmacytoid Dendritic Cells Suppress HIV-1 Replication but Contribute to HIV-1 Induced Immunopathogenesis in Humanized Mice". *PLOS Pathogens* 10, no. 7 (): 1–12. doi:10.1371/journal.ppat.1004291.

Li, Qingsheng, et al. 2009. "Glycerol monolaurate prevents mucosal SIV transmission". *Nature* 458 (7241): 1034–1038. doi:10.1038/nature07831.

Li, Yingke, et al. 2012. "MicroRNA-466l inhibits antiviral innate immune response by targeting interferon-alpha". *Cellular & molecular immunology* 9 (6): 497–502. doi:10.1038/cmi.2012.35.

Liberzon, Arthur, et al. 2015. "The Molecular Signatures Database Hallmark Gene Set Collection". *Cell Systems* 1 (6): 417–425. doi:10.1016/j.cels.2015.12.004.

Lillie, Patrick J, et al. 2020. "Novel coronavirus disease (Covid-19): the first two patients in the UK with person to person transmission". *Journal of Infection* 80 (5): 578–606. doi:10.1016/j.jinf.2020.02.020.

Lin, Dawn S., et al. 2018. "DiSNE Movie Visualization and Assessment of Clonal Kinetics Reveal Multiple Trajectories of Dendritic Cell Development". *Cell Reports* 22 (10): 2557–2566. doi:10.1016/j.celrep.2018.02.046.

Lindholt, Marie Fly, et al. 2021. "Public acceptance of COVID-19 vaccines: cross-national evidence on levels and individual-level predictors using observational data". *BMJ open* 11 (6): e048172. doi:10.1136/bmjopen-2020-048172.

Lippitsch, Anne, et al. 2017. "Unique high and homogenous surface expression of the transferrin receptor CD71 on murine plasmacytoid dendritic cells in different tissues". *Cellular Immunology* 316:41–52. doi:10.1016/j.cellimm.2017.03.005.

Liu, Yi, et al. 2008. "Env length and N-linked glycosylation following transmission of human immunodeficiency virus Type 1 subtype B viruses". *Virology* 374 (2): 229–233. doi:10.1016/j.virol.2008.01.029.

Liva, Stephanie M, and Rhonda R Voskuhl. 2001. "Testosterone acts directly on CD4+ T lymphocytes to increase IL-10 production". *The Journal of Immunology* 167 (4): 2060–2067.

Lopez, Jonathan, et al. 2021. "Early nasal type I IFN immunity against SARS-CoV-2 is compromised in patients with autoantibodies against type I IFNsImpact of nasal IFN-I autoantibodies in COVID-19". *Journal of Experimental Medicine* 218 (10). doi:10.1084/jem.20211211.

Lorenzo, Maria E, et al. 2011. "Antibody responses and cross protection against lethal influenza A viruses differ between the sexes in C57BL/6 mice". *Vaccine* 29 (49): 9246–9255. doi:10.1016/j.vaccine.2011.09.110.

Lü, FX, et al. 2002. "The strength of B cell immunity in female rhesus macaques is controlled by CD8+ T cells under the influence of ovarian steroid hormones". *Clinical & Experimental Immunology* 128 (1): 10–20. doi:10.1046/j.1365-2249.2002.01780.x.

Luecken, Malte D, and Fabian J Theis. 2019. "Current best practices in single-cell RNA-seq analysis: a tutorial". *Molecular Systems Biology* 15 (6): e8746. doi:10.15252/msb.20188746.

Malone, Brandon, et al. 2021. "Structures and functions of coronavirus replication–transcription complexes and their relevance for SARS-CoV-2 drug design". *Nature Reviews Molecular Cell Biology* 23:21–39. doi:10.1038/s41580-021-00432-z.

Maurice, Nicholas J, et al. 2019. "CXCR3 enables recruitment and site-specific bystander activation of memory CD8+ T cells". *Nature communications* 10 (1): 4987. doi:10.1038/s41467-019-12980-2.

Mazer, Norman A. 2009. "A novel spreadsheet method for calculating the free serum concentrations of testosterone, dihydrotestosterone, estradiol, estrone and cortisol: With illustrative examples from male and female populations". *Steroids* 74 (6): 512–519. doi:10.1016/j.steroids.2009.01.008.

McInnes, Leland, John Healy, and James Melville. 2020. "UMAP: Uniform Manifold Approximation and Projection for Dimension Reduction". *arXiv*. doi:10.48550/arXiv.1802.03426.

McNab, Finlay, et al. 2015. "Type I interferons in infectious disease". *Nature Reviews Immunology* 15:87–103. doi:10.1038/nri3787.

McNerlan, S.E, I.M Rea, and H.D Alexander. 2002. "A whole blood method for measurement of intracellular TNF-α, IFN-γ and IL-2 expression in stimulated CD3+ lymphocytes: differences between young and elderly subjects". *Experimental Gerontology* 37 (2): 227–234. doi:10.1016/S0531-5565(01)00188-7.

Meier, Angela, et al. 2008. "Rapid loss of dendritic cell and monocyte responses to TLR ligands following venipuncture". *Journal of Immunological Methods* 339 (2): 132–140. doi:10.1016/j.jim.2008.09.007.

Meier, Angela, et al. 2009. "Sex differences in the toll-like receptor–mediated response of plasmacytoid dendritic cells to HIV-1". *Nature Medicine* 15 (8): 955–959. doi:10.1038/nm.2004.

Mendel, Carl M. 1989. "The Free Hormone Hypothesis: A Physiologically Based Mathematical Model*". *Endocrine Reviews* 10 (3): 232–274. doi:10.1210/edrv-10-3-232.

Meyer-Wentrup, Friederike, et al. 2008. "Targeting DCIR on human plasmacytoid dendritic cells results in antigen presentation and inhibits IFN-α production". *Blood* 111 (8): 4245–4253. doi:10.1182/blood-2007-03-081398.

Michos, Athanasios, et al. 2021. "Association of total and neutralizing SARS-CoV-2 spike -receptor binding domain antibodies with epidemiological and clinical characteristics after immunization with the 1st and 2nd doses of the BNT162b2 vaccine". *Vaccine* 39 (40): 5963–5967. doi:10.1016/j.vaccine.2021.07.067.

Miura, Toshiyuki, et al. 2009. "HLA-Associated Alterations in Replication Capacity of Chimeric NL4-3 Viruses Carrying gag-protease from Elite Controllers of Human Immunodeficiency Virus Type 1". *Journal of Virology* 83 (1): 140–149. doi:10.1128/JVI.01471-08.

Miura, Toshiyuki, et al. 2010. "Impaired Replication Capacity of Acute/Early Viruses in Persons Who Become HIV Controllers". *Journal of Virology* 84 (15): 7581–7591. doi:10.1128/JVI.00286-10.

Moll, Herwig P., et al. 2011. "The differential activity of interferon-α subtypes is consistent among distinct target genes and cell types". *Cytokine* 53 (1): 52–59. doi:10.1016/j.cyto.2010.09.006.

Morley, John E., et al. 1997. "Longitudinal changes in testosterone, luteinizing hormone, and follicle-stimulating hormone in healthy older men". *Metabolism* 46 (4): 410–413. doi:10.1016/S0026-0495(97)90057-3.

Moss, P. 2022. "The T cell immune response against SARS-CoV-2". *Nature Immunology* 23:186–193. doi:10.1038/s41590-021-01122-w.

Musabak, U, et al. 2003. "Gonadotropin treatment restores in vitro interleukin-1β and tumour necrosis factor-α production by stimulated peripheral blood mononuclear cells from patients with idiopathic hypogonadotropic hypogonadism". *Clinical and Experimental Immunology* 132 (2): 265–270. doi:10.1046/j.1365-2249.2003.02141.x.

Myers, Michael P, et al. 2001. "TYK2 and JAK2 are substrates of protein-tyrosine phosphatase 1B". *Journal of Biological Chemistry* 276 (51): 47771–47774.

Myint, Lay, et al. 2004. "Gag Non-Cleavage Site Mutations Contribute to Full Recovery of Viral Fitness in Protease Inhibitor-Resistant Human Immunodeficiency Virus Type 1". *Antimicrobial Agents and Chemotherapy* 48 (2): 444–452. doi:10.1128/AAC.48.2.444-452.2004.

Naidoo, Vanessa L., et al. 2017. "Mother-to-Child HIV Transmission Bottleneck Selects for Consensus Virus with Lower Gag-Protease-Driven Replication Capacity". *Journal of Virology* 91 (17): e00518–17. doi:10.1128/JVI.00518-17.

Nakaya, Helder I, et al. 2011. "Systems biology of vaccination for seasonal influenza in humans". *Nature Immunology* 12 (8): 786–795. doi:10.1038/ni.2067.

Nakaya, Helder I., et al. 2016. "Systems biology of immunity to MF59-adjuvanted versus nonadjuvanted trivalent seasonal influenza vaccines in early childhood". *Proceedings of the National Academy of Sciences* 113 (7): 1853–1858. doi:10.1073/pnas.1519690113.

Naranjo-Gómez, Mar, et al. 2007. "Expression and function of the IL-2 receptor in activated human plasmacytoid dendritic cells". *European Journal of Immunology* 37 (7): 1764–1772. doi:10.1002/eji.200636980.

Nawaz, Fatima, et al. 2011. "The Genotype of Early-Transmitting HIV gp120s Promotes α4β7 –Reactivity, Revealing α4β7+/CD4+ T cells As Key Targets in Mucosal Transmission". *PLOS Pathogens* 7 (2): 1–14. doi:10.1371/journal.ppat.1001301.

Nomura, Shigeru, et al. 2013. "Significant Reductions in Gag-Protease-Mediated HIV-1 Replication Capacity during the Course of the Epidemic in Japan". *Journal of Virology* 87 (3): 1465–1476. doi:10.1128/JVI.02122-12.

Oertelt-Prigione, Sabine. 2012. "Immunology and the menstrual cycle". *Autoimmunity Reviews* 11 (6): A486–A492. doi:10.1016/j.autrev.2011.11.023.

Oksuzyan, Anna, Henrik Brønnum-Hansen, and Bernard Jeune. 2010. "Gender gap in health expectancy". *European Journal of Ageing* 7:213–218. doi:10.1007/s10433-010-0170-4.

Onodi, Fanny, et al. 2021. "SARS-CoV-2 induces human plasmacytoid predendritic cell diversification via UNC93B and IRAK4 SARS-CoV-2 and plasmacytoid predendritic cells". *Journal of Experimental Medicine* 218 (4). doi:10.1084/jem.20201387.

Owen, Jr, J A. 1975. "Physiology of the menstrual cycle". *The American Journal of Clinical Nutrition* 28 (4): 333–338. doi:10.1093/ajcn/28.4.333.

Pardi, Norbert, et al. 2018. "MRNA vaccines — a new era in Vaccinology". *Nature Reviews Drug Discovery* 17 (4): 261–279. doi:10.1038/nrd.2017.243.

Parmar, Kanak, Afzal Siddiqui, and Kenneth Nugent. 2021. "Bacillus Calmette-Guerin vaccine and nonspecific immunity". *The American journal of the medical sciences* 361 (6): 683–689. doi:10.1016/j.amjms.2021.03.003.

Parrish, Nicholas F., et al. 2013. "Phenotypic properties of transmitted founder HIV-1". *Proceedings of the National Academy of Sciences* 110 (17): 6626–6633. doi:10.1073/pnas.1304288110.

Parry, Chris M., et al. 2011. "Three Residues in HIV-1 Matrix Contribute to Protease Inhibitor Susceptibility and Replication Capacity". *Antimicrobial Agents and Chemotherapy* 55 (3): 1106–1113. doi:10.1128/AAC.01228-10.

Patel, Pragna, et al. 2014. "Estimating per-act HIV transmission risk: a systematic review". *AIDS* 28 (10): 1509. doi:10.1097/QAD.0000000000000298.

Payne, Rebecca, et al. 2014. "Impact of HLA-driven HIV adaptation on virulence in populations of high HIV seroprevalence". *Proceedings of the National Academy of Sciences* 111 (50): E5393–E5400. doi:10.1073/pnas.1413339111.

Payne, Rebecca P, et al. 2021. "Immunogenicity of standard and extended dosing intervals of BNT162b2 mRNA vaccine". *Cell* 184 (23): 5699–5714. doi:10.1016/j.cell.2021.10.011.

Peckham, Hannah, et al. 2020. "Male sex identified by global covid-19 meta-analysis as a risk factor for death and Itu Admission". *Nature Communications* 11. doi:10.1038/s41467-020-19741-6.

Pestka, Sidney, Christopher D. Krause, and Mark R. Walter. 2004. "Interferons, interferon-like cytokines, and their receptors". *Immunological Reviews* 202 (1): 8–32. doi:10.1111/j.0105-2896.2004.00204.x.

Peters, Solange, et al. 2001. "Resistance to Nucleoside Analog Reverse Transcriptase Inhibitors Mediated by Human Immunodeficiency Virus Type 1 p6 Protein". *Journal of Virology* 75 (20): 9644–9653. doi:10.1128/JVI.75.20.9644-9653.2001.

Pollard, Andrew J, and Else M Bijker. 2021. "A guide to vaccinology: from basic principles to new developments". *Nature Reviews Immunology* 21 (2): 83–100. doi:10.1038/s41577-020-00479-7.

Pons-Estel, Guillermo J., et al. 2010. "Understanding the Epidemiology and Progression of Systemic Lupus Erythematosus". *Seminars in Arthritis and Rheumatism* 39 (4): 257–268. doi:10.1016/j.semarthrit.2008.10.007.

Poss, M, et al. 1995. "Diversity in virus populations from genital secretions and peripheral blood from women recently infected with human immunodeficiency virus type 1". *Journal of Virology* 69 (12): 8118–8122. doi:10.1128/jvi.69.12.8118-8122.1995.

Prince, Jessica L., et al. 2012. "Role of Transmitted Gag CTL Polymorphisms in Defining Replicative Capacity and Early HIV-1 Pathogenesis". *PLOS Pathogens* 8 (11): 1–15. doi:10.1371/journal.ppat.1003041.

Psarras, Antonios, et al. 2021. "TNF-α Regulates Human Plasmacytoid Dendritic Cells by Suppressing IFN-α Production and Enhancing T Cell Activation". *The Journal of Immunology* 206 (4): 785–796. doi:10.4049/jimmunol.1901358.

Pulendran, B, S Arunachalam P, and O'Hagan DT. 2021. "Emerging concepts in the science of vaccine adjuvants". *Nat Rev Drug Discov* 20:454–75. doi:10.1038/s41573-021-00163-y.

Putri, Wayan C.W.S., et al. 2018. "Economic burden of seasonal influenza in the United States". *Vaccine* 36 (27): 3960–3966. doi:10.1016/j.vaccine.2018.05.057.

Rajendran, Madhusudan, Florian Krammer, and Meagan McMahon. 2021. "The Human Antibody Response to the Influenza Virus Neuraminidase Following Infection or Vaccination". *Vaccines* 9 (8): e846. doi:10.3390/vaccines9080846.

Redd, Andrew D., et al. 2012. "Previously Transmitted HIV-1 Strains Are Preferentially Selected During Subsequent Sexual Transmissions". *The Journal of Infectious Diseases* 206 (9): 1433–1442. doi:10.1093/infdis/jis503.

Rehwinkel, Jan, and Michaela U. Gack. 2020. "Rig-i-like receptors: Their regulation and roles in RNA sensing". *Nature Reviews Immunology* 20 (9): 537–551. doi:10.1038/s41577-020-0288-3.

Reizis, Boris. 2019. "Plasmacytoid Dendritic Cells: Development, Regulation, and Function". *Immunity* 50 (1): 37–50. doi:10.1016/j.immuni.2018.12.027.

Rettew, Jennifer A., Yvette M. Huet-Hudson, and Ian Marriott. 2008. "Testosterone Reduces Macrophage Expression in the Mouse of Toll-Like Receptor 4, a Trigger for Inflammation and Innate Immunity". *Biology of Reproduction* 78 (3): 432–437. doi:10.1095/biolreprod.107.063545.

Ritchie, Kenneth J, et al. 2004. "Role of ISG15 protease UBP43 (USP18) in innate immunity to viral infection". *Nature Medicine* 10 (12): 1374–1378. doi:10.1038/nm1133.

Roberts, Walden K., et al. 1976. "Interferon-mediated protein kinase and low-molecular-weight inhibitor of protein synthesis". *Nature* 264 (5585): 477–480. doi:10.1038/264477a0.

Robinson, Dionne P, and Sabra L Klein. 2012. "Pregnancy and pregnancy-associated hormones alter immune responses and disease pathogenesis". *Hormones and behavior* 62 (3): 263–271.

Robinson, Dionne P., et al. 2005. "The Effect of Combined Estrogen and Progesterone Hormone Replacement Therapy on Disease Activity in Systemic Lupus Erythematosus: A Randomized Trial". *Annals of Internal Medicine* 142 (12_Part_1): 953–962. doi:10.7326/0003-4819-142-12_Part_1-200506210-00004.

Rodrigues, Kameron B., et al. 2020. "Innate immune stimulation of whole blood reveals IFN-1 hyper-responsiveness in type 1 diabetes". *Diabetologia* 63 (8): 1576–1587. doi:10.1007/s00125-020-05179-4.

Rodrigues, Patrick Fernandes, et al. 2018. "Distinct progenitor lineages contribute to the heterogeneity of plasmacytoid dendritic cells". *Nature immunology* 19 (7): 711–722. doi:10.1038/s41590-018-0136-9.

Rotger, Margalida, et al. 2011. "Comparative transcriptomics of extreme phenotypes of human HIV-1 infection and SIV infection in sooty mangabey and rhesus macaque". *The Journal of Clinical Investigation* 121 (6): 2391–2400. doi:10.1172/JCI45235.

Sadler, Anthony J., and Bryan R. Williams. 2008. "Interferon-inducible antiviral effectors". *Nature Reviews Immunology* 8 (7): 559–568. doi:10.1038/nri2314.

Sagar, Manish, et al. 2009. "Selection of HIV variants with signature genotypic characteristics during heterosexual transmission". *The Journal of Infectious Diseases* 199 (4): 580–589. doi:10.1086/596557.

Sahakyan, Anna, Kathrin Plath, and Claire Rougeulle. 2017. "Regulation of X-chromosome dosage compensation in human: Mechanisms and model systems". *Philosophical Transactions of the Royal Society B: Biological Sciences* 372 (1733): 20160363. doi:10.1098/rstb.2016.0363.

Sampson, Oliver, et al. 2022. "A simple, robust flow cytometry-based whole blood assay for investigating sex differential interferon alpha production by plasmacytoid dendritic cells". *Journal of Immunological Methods* 504:e113263. doi:10.1016/j.jim.2022.113263.

Sandler, Netanya G., et al. 2014. "Type I interferon responses in rhesus macaques prevent SIV infection and slow disease progression". *Nature* 511 (7511): 601–605. doi:10.1038/nature13554.

Sasaki, Yuri, et al. 2012. "Adherence to antiretroviral therapy (ART) during the early months of treatment in rural Zambia: influence of demographic characteristics and social surroundings of patients". *Annals of clinical microbiology and antimicrobials* 11:1–11. doi:10.1186/1476-0711-11-34.

Savan, Ram. 2014. "Post-Transcriptional Regulation of Interferons and Their Signaling Pathways". *Journal of Interferon & Cytokine Research* 34 (5): 318–329. doi:10.1089/jir.2013.0117.

Schiffer, Lina, et al. 2023. "Classic and 11-oxygenated androgens in serum and saliva across adulthood: a cross-sectional study analyzing the impact of age, body mass index, and diurnal and menstrual cycle variation". *European Journal of Endocrinology* 188 (1): lvac017. doi:10.1093/ejendo/lvac017.

Schneider, William M., Meike Dittmann Chevillotte, and Charles M. Rice. 2014. "Interferon-stimulated genes: A complex web of host defenses". *Annual Review of Immunology* 32 (1): 513–545. doi:10.1146/annurev-immunol-032713-120231.

Schoggins, John W. 2019. "Interferon-Stimulated Genes: What Do They All Do?" *Annual Review of Virology* 6 (1): 567–584. doi:10.1146/annurev-virology-092818-015756.

Schurz, Haiko, et al. 2019. "The X chromosome and sex-specific effects in infectious disease susceptibility". *Human Genomics* 13 (2). doi:10.1186/s40246-018-0185-z.

Scott, Jennifer L., et al. 2015. "Estrogen Receptor α Deficiency Modulates TLR Ligand–Mediated PDC-TREM Expression in Plasmacytoid Dendritic Cells in Lupus-Prone Mice". *The Journal of Immunology* 195 (12): 5561–5571. doi:10.4049/jimmunol.1500315.

Scully, Eileen P., et al. 2020. "Considering how biological sex impacts immune responses and COVID-19 outcomes". *Nature Reviews Immunology* 20 (7): 442–447. doi:10.1038/s41577-020-0348-8.

See, Peter, et al. 2017. "Mapping the human DC lineage through the integration of high-dimensional techniques". *Science* 356 (6342): eaag3009. doi:10.1126/science.aag3009.

Seeds, Rosalind E., and Joanna L. Miller. 2011. "Measurement of Type I Interferon Production". *Current Protocols in Immunology* 92 (1): 14.21.1–14.21.11. doi:10.1002/0471142735.im1421s92.

Segal, Mark R, Jason D Barbour, and Robert M Grant. 2004. "Relating HIV-1 Sequence Variation to Replication Capacity via Trees and Forests". *Statistical Applications in Genetics and Molecular Biology* 3 (1). doi:doi:10.2202/1544-6115.1031.

Seillet, Cyril, et al. 2012. "The TLR-mediated response of plasmacytoid dendritic cells is positively regulated by estradiol in vivo through cell-intrinsic estrogen receptor α signaling". *Blood* 119 (2): 454–464. doi:10.1182/blood-2011-08-371831.

Shah, Nishel M., et al. 2019. "Progesterone-Related Immune Modulation of Pregnancy and Labor". *Frontiers in Endocrinology* 10. doi:10.3389/fendo.2019.00198.

Sharma, Salil, and Mansoureh Eghbali. 2014. "Influence of sex differences on microRNA gene regulation in disease". *Biology of sex differences* 5 (1): 1–8. doi:10.1186/2042-6410-5-3.

Sharma, Shilpee, et al. 2018. "PTAP motif duplication in the p6 Gag protein confers a replication advantage on HIV-1 subtype C". *Journal of Biological Chemistry* 293 (30): 11687–11708. doi:10.1074/jbc.M117.815829.

Shen, Ching-Fen, et al. 2022. "Innate Immune Responses of Vaccinees Determine Early Neutralizing Antibody Production After ChAdOx1nCoV-19 Vaccination". *Frontiers in Immunology* 13:83. doi:10.3389/fimmu.2022.807454.

Shepherd, Rebecca, et al. 2021. "Sexual dimorphism in innate immunity: the role of sex hormones and epigenetics". *Frontiers in immunology* 11:e604000. doi:10.3389/fimmu.2020.604000.

Shepherd, Rebecca, et al. 2022. "Gender-affirming hormone therapy induces specific DNA methylation changes in blood". *Clinical Epigenetics* 14:e24. doi:10.1186/s13148-022-01236-4.

Siegal, Frederick P., et al. 1999. "The Nature of the Principal Type 1 Interferon-Producing Cells in Human Blood". *Science* 284 (5421): 1835–1837. doi:10.1126/science.284.5421.1835.

Silvestri, Guido, et al. 2003. "Nonpathogenic SIV infection of sooty mangabeys is characterized by limited bystander immunopathology despite chronic high-level viremia". *Immunity* 18 (3): 441–452. doi:10.1016/s1074-7613(03)00060-8.

Sobolev, Olga, et al. 2016. "Adjuvanted influenza-H1N1 vaccination reveals lymphoid signatures of age-dependent early responses and of clinical adverse events". *Nature immunology* 17 (2): 204–213. doi:10.1038/ni0616-740b.

Souyris, Mélanie, et al. 2018a. "Female predisposition to TLR7-driven autoimmunity: Gene dosage and the escape from X chromosome inactivation". *Seminars in Immunopathology* 41 (2): 153–164. doi:10.1007/s00281-018-0712-y.

Souyris, Mélanie, et al. 2018b. "*TLR7* escapes X chromosome inactivation in immune cells". *Science Immunology* 3 (19): eaap8855. doi:10.1126/sciimmunol.aap8855.

Sparks, Rachel, et al. 2023. "Influenza vaccination reveals sex dimorphic imprints of prior mild COVID-19". *Nature*. doi:10.1038/s41586-022-05670-5.

Stacey, Andrea R., et al. 2009. "Induction of a Striking Systemic Cytokine Cascade prior to Peak Viremia in Acute Human Immunodeficiency Virus Type 1 Infection, in Contrast to More Modest and Delayed Responses in Acute Hepatitis B and C Virus Infections". *Journal of Virology* 83 (8): 3719–3733. doi:10.1128/JVI.01844-08.

Stelzer, Gil, et al. 2016. "The GeneCards Suite: From Gene Data Mining to Disease Genome Sequence Analyses". *Current Protocols in Bioinformatics* 54 (1): 1.30.1–1.30.33. doi:10.1002/cpbi.5.

Sterling, Timothy R., et al. 2001. "Initial Plasma HIV-1 RNA Levels and Progression to AIDS in Women and Men". *New England Journal of Medicine* 344 (10): 720–725. doi:10.1056/NEJM200103083441003.

Subramanian, Aravind, et al. 2005. "Gene set enrichment analysis: A knowledge-based approach for interpreting genome-wide expression profiles". *Proceedings of the National Academy of Sciences* 102 (43): 15545–15550. doi:10.1073/pnas.0506580102.

Sugrue, Elena, et al. 2022. "The apparent interferon resistance of transmitted HIV-1 is possibly a consequence of enhanced replicative fitness". *PLOS Pathogens* 18 (11): 1–29. doi:10.1371/journal.ppat.1010973.

Sutherland, Katherine A, et al. 2016. "Wide variation in susceptibility of transmitted/founder HIV-1 subtype C Isolates to protease inhibitors and association with in vitro replication efficiency". *Scientific reports* 6 (1): e38153.

Swiecki, Melissa, et al. 2011. "Type I interferon negatively controls plasmacytoid dendritic cell numbers in vivo". *Journal of Experimental Medicine* 208 (12): 2367–2374. doi:10.1084/jem.20110654.

Takahashi, Takehiro, and Akiko Iwasaki. 2021. "Sex differences in immune responses". *Science* 371 (6527): 347–348. doi:10.1126/science.abe7199.

Takahashi, Takehiro, et al. 2020. "Sex differences in immune responses that underlie COVID-19 disease outcomes". *Nature* 588:315–320. doi:10.1038/s41586-020-2700-3.

Talon, Julie, et al. 2000. "Activation of Interferon Regulatory Factor 3 Is Inhibited by the Influenza A Virus NS1 Protein". *Journal of Virology* 74 (17): 7989–7996. doi:10.1128/JVI.74.17.7989-7996.2000.

Tamiya, Sadahiro, et al. 2004. “Amino Acid Insertions near Gag Cleavage Sites Restore the Otherwise Compromised Replication of Human Immunodeficiency Virus Type 1 Variants Resistant to Protease Inhibitors”. *Journal of Virology* 78 (21): 12030–12040. doi:10.1128/JVI.78.21.12030-12040.2004.

Taubenberger, Jeffery K., and David M. Morens. 2008. “The Pathology of Influenza Virus Infections”. *Annual Review of Pathology: Mechanisms of Disease* 3 (1): 499–522. doi:10.1146/annurev.pathmechdis.3.121806.154316.

Teijaro, John R, and Donna L Farber. 2021. “COVID-19 vaccines: modes of immune activation and future challenges”. *Nature Reviews Immunology* 21 (4): 195–197. doi:10.1038/s41577-021-00526-x.

Teilmann, Stefan Cuoni, et al. 2006. “Expression and localization of the progesterone receptor in mouse and human reproductive organs", journal = "Journal of Endocrinology”. 191 (3): 525–535. doi:10.1677/joe.1.06565.

Thigpen, A E, et al. 1993. “Tissue distribution and ontogeny of steroid 5 alpha-reductase isozyme expression.” *The Journal of Clinical Investigation* 92 (2): 903–910. doi:10.1172/JCI116665.

Thompson, Ashley E, et al. 2016. “The influence of gender and other patient characteristics on health care-seeking behaviour: a QUALICOPC study”. *BMC family practice* 17 (1): 1–7. doi:10.1186/s12875-016-0440-0.

Thompson, Emma E, et al. 2018. “Global DNA methylation changes spanning puberty are near predicted estrogen-responsive genes and enriched for genes involved in endocrine and immune processes”. *Clinical epigenetics* 10:1–10. doi:10.1186/s13148-018-0491-2.

Tibshirani, Robert. 1996. “Regression shrinkage and selection via the lasso”. *Journal of the Royal Statistical Society: Series B (Methodological)* 58 (1): 267–288. doi:10.1111/j.2517-6161.1996.tb02080.x.

Tong, Orion, et al. 2021. “Plasmacytoid dendritic cells have divergent effects on HIV infection of initial target cells and induce a pro-retention phenotype”. *PLOS Pathogens* 17 (4): 1–29. doi:10.1371/journal.ppat.1009522.

Torcia, Maria Gabriella, et al. 2012. “Sex Differences in the Response to Viral Infections: TLR8 and TLR9 Ligand Stimulation Induce Higher IL10 Production in Males”. *PLOS ONE* 7 (6): 1–8. doi:10.1371/journal.pone.0039853.

Tough, David F., Persephone Borrow, and Jonathan Sprent. 1996. “Induction of Bystander T Cell Proliferation by Viruses and Type I Interferon in Vivo”. *Science* 272 (5270): 1947–1950. doi:10.1126/science.272.5270.1947.

Townsend, Jeffrey P., et al. 2022. “The durability of natural infection and vaccine-induced immunity against future infection by SARS-CoV-2”. *PNAS* 119 (31): e2204336119. doi:10.1073/pnas.2204336119.

Tran, Thi Anh Thu, et al. 2019. “Whole blood assay as a model for in vitro evaluation of inflammasome activation and subsequent caspase-mediated interleukin-1 beta release”. *PLoS ONE* 14 (4): 1–16. doi:10.1371/journal.pone.0214999.

Trask, Stanley A, et al. 2002. “Molecular epidemiology of human immunodeficiency virus type 1 transmission in a heterosexual cohort of discordant couples in Zambia”. *Journal of virology* 76 (1): 397–405. doi:10.1128/jvi.76.1.397-405.2002.

Trigunaite, Abhishek, Joana Dimo, and Trine N. Jørgensen. 2015. "Suppressive effects of androgens on the immune system". *Cellular Immunology* 294 (2): 87–94. doi:10.1016/j.cellimm.2015.02.004.

UNAIDS. 2022. "UNAIDS HIV Factsheet". *Accessed: May 2022*.

V'kovski, Philip, et al. 2021. "Coronavirus biology and replication: implications for SARS-CoV-2". *Nature Reviews Microbiology* 19:155–170. doi:10.1038/s41579-020-00468-6.

Van den Berge, Koen, et al. 2020. "Trajectory-based differential expression analysis for single-cell sequencing data". *Nature communications* 11:e1201. doi:10.1038/s41467-020-14766-3.

Van der Made, Caspar I., et al. 2020. "Presence of Genetic Variants Among Young Men With Severe COVID-19". *JAMA* 324 (7): 663–673. doi:10.1001/jama.2020.13719.

Van't Wout, AB, et al. 1994. "Macrophage-tropic variants initiate human immunodeficiency virus type 1 infection after sexual, parenteral, and vertical transmission." *The Journal of clinical investigation* 94 (5): 2060–2067. doi:10.1172/JCI117560.

Van Domselaar, Robert, et al. 2019. "HIV-1 Subtype C with PYxE Insertion Has Enhanced Binding of Gag-p6 to Host Cell Protein ALIX and Increased Replication Fitness". *Journal of Virology* 93 (9): e00077–19. doi:10.1128/JVI.00077-19.

Varga, Zsuzsanna T., et al. 2011. "The Influenza Virus Protein PB1-F2 Inhibits the Induction of Type I Interferon at the Level of the MAVS Adaptor Protein". *PLOS Pathogens* 7 (6): 1–16. doi:10.1371/journal.ppat.1002067.

Vazquez, Christine, et al. 2021. "SARS-CoV-2 viral proteins NSP1 and NSP13 inhibit interferon activation through distinct mechanisms". *PLOS ONE* 16 (6): 1–15. doi:10.1371/journal.pone.0253089.

Veazey, Ronald S, et al. 2016. "Prevention of SHIV transmission by topical IFN-$\beta$ treatment". *Mucosal immunology* 9 (6): 1528–1536. doi:10.1038/mi.2015.146.

Villadangos, José A., and Louise Young. 2008. "Antigen-Presentation Properties of Plasmacytoid Dendritic Cells". *Immunity* 29 (3): 352–361. doi:10.1016/j.immuni.2008.09.002.

Villani, Alexandra-Chloé, et al. 2017. "Single-cell RNA-seq reveals new types of human blood dendritic cells, monocytes, and progenitors". *Science* 356 (6335): eaah4573. doi:10.1126/science.aah4573.

Votteler, Jörg, et al. 2011. "Highly conserved serine residue 40 in HIV-1 P6 regulates capsid processing and virus core assembly". *Retrovirology* 8 (1). doi:10.1186/1742-4690-8-11.

Wang, Jennifer P, et al. 2012. "Plasmacytoid dendritic cell interferon-α production to R-848 stimulation is decreased in male infants". *BMC Immunology* 13 (1). doi:10.1186/1471-2172-13-35.

Wang, Weirong, et al. 1999. "RNA binding by the novel helical domain of the influenza virus NS1 protein requires its dimer structure and a small number of specific basic amino acids". *RNA* 5 (2): 195–205. doi:10.1017/S1355838299981621.

Wang, Yawen, et al. 2021. "TLR7 Signaling Drives the Development of Sjögren's Syndrome". *Frontiers in Immunology* 12:e676010. doi:10.3389/fimmu.2021.676010.

Wang, Zhongfang, et al. 2015. "Recovery from severe H7N9 disease is associated with diverse response mechanisms dominated by CD8+ T cells". *Nature Communications* 6. doi:10.1038/ncomms7833.

Warren, L, et al. 2010. "Daley GQ, Brack AS, Collins JJ, Cowan C, Schlaeger TM, Rossi DJ. 2010. Highly efficient reprogramming to pluripotency and directed differentiation of human cells with synthetic modified mRNA". *Cell Stem Cell* 7 (5): 618–630. doi:10.1016/j.stem.2010.08.012.

Waterhouse, Andrew M., et al. 2009. "Jalview Version 2—a multiple sequence alignment editor and analysis workbench". *Bioinformatics* 25 (9): 1189–1191. doi:10.1093/bioinformatics/btp033.

Webb, Kate, et al. 2019. "Sex and Pubertal Differences in the Type 1 Interferon Pathway Associate With Both X Chromosome Number and Serum Sex Hormone Concentration". *Frontiers in Immunology* 9. doi:10.3389/fimmu.2018.03167.

Weber-Gerlach, Michaela, and Friedemann Weber. 2016. "To Conquer the Host, Influenza Virus Is Packing It In: Interferon-Antagonistic Strategies beyond NS1". *Journal of Virology* 90 (19): 8389–8394. doi:10.1128/JVI.00041-16.

Weiss, Jonathan M., Carolyn A. Cuff, and Joan W. Berman. 1999. "TGF-Beta Downmodulates Cytokine-Induced Monocyte Chemoattractant Protein (MCP)-1 Expression in Human Endothelial Cells. A Putative Role for TGF-Beta in the Modulation of TNF Receptor Expression". *Endothelium* 6 (4): 291–302.

WHO. 2022a. "WHO Influenza (Seasonal) Factsheet". *Accessed: Sep 2022.*

— . 2022b. "WHO World Health Statistics". *Accessed: Sep 2022.*

Wilson, C.A., et al. 2003. "Estradiol Levels in Girls with Turner's Syndrome Compared to Normal Prepubertal Girls as Determined by an Ultrasensitive Assay". *Journal of Pediatric Endocrinology and Metabolism* 16 (1): 91–96. doi:doi:10.1515/JPEM.2003.16.1.91.

Wimmers, Florian, et al. 2018. "Single-cell analysis reveals that stochasticity and paracrine signaling control interferon-alpha production by plasmacytoid dendritic cells". *Nature communications* 9 (1): e3317. doi:10.1038/s41467-018-05784-3.

Wölfel, Roman, et al. 2020. "Virological assessment of hospitalized patients with Covid-2019". *Nature* 581 (7809): 465–469. doi:10.1038/s41586-020-2196-x.

Wright, Jaclyn K., et al. 2010. "Gag-Protease-Mediated Replication Capacity in HIV-1 Subtype C Chronic Infection: Associations with HLA Type and Clinical Parameters". *Journal of Virology* 84 (20): 10820–10831. doi:10.1128/JVI.01084-10.

Wright, Jaclyn K., et al. 2011. "Influence of Gag-Protease-Mediated Replication Capacity on Disease Progression in Individuals Recently Infected with HIV-1 Subtype C". *Journal of Virology* 85 (8): 3996–4006. doi:10.1128/JVI.02520-10.

Wright, Jaclyn K., et al. 2012a. "Impact of HLA-B*81-Associated Mutations in HIV-1 Gag on Viral Replication Capacity". *Journal of Virology* 86 (6): 3193–3199. doi:10.1128/JVI.06682-11.

Wright, Jaclyn K., et al. 2012b. "Lack of Association between HLA Class II Alleles and In Vitro Replication Capacities of Recombinant Viruses Encoding HIV-1 Subtype C Gag-Protease from Chronically Infected Individuals". *Journal of Virology* 86 (2): 1273–1276. doi:10.1128/JVI.06533-11.

Yang, Otto O., et al. 2017. "Demographics and natural history of HIV-1-infected spontaneous controllers of viremia". *AIDS* 31 (8): 1091–1098. doi:10.1097/qad.0000000000001443.

Yin, Zhiwei, et al. 2012. "Type III IFNs Are Produced by and Stimulate Human Plasmacytoid Dendritic Cells". *The Journal of Immunology* 189 (6): 2735–2745. doi:10.4049/jimmunol.1102038.

Yoshida, Masahiro, et al. 2022. "Local and systemic responses to SARS-CoV-2 infection in children and adults". *Nature* 602 (7896): 321–327. doi:10.1038/s41586-021-04345-x.

Young, Louise J, et al. 2008. "Differential MHC class II synthesis and ubiquitination confers distinct antigen-presenting properties on conventional and plasmacytoid dendritic cells". *Nature Immunology* 9 (11): 1244–1252. doi:10.1038/ni.1665.

Zeng, Fanfan, et al. 2020. "A comparison study of SARS-CoV-2 IgG antibody between male and female COVID-19 patients: A possible reason underlying different outcome between sex". *Journal of Medical Virology* 92 (10): 2050–2054. doi:10.1002/jmv.25989.

Zhan, Yifan, et al. 2016. "Plasmacytoid dendritic cells are short-lived: Reappraising the influence of migration, genetic factors and activation on estimation of lifespan". *Scientific Reports* 6 (1). doi:10.1038/srep25060.

Zhu, Tuofu, et al. 1993. "Genotypic and Phenotypic Characterization of HIV-1 Patients with Primary Infection". *Science* 261 (5125): 1179–1181. doi:10.1126/science.8356453.

Ziegler, Susanne M., et al. 2017. "Human pDCs display sex-specific differences in type I interferon subtypes and interferon α/β receptor expression". *European Journal of Immunology* 47 (2): 251–256. doi:10.1002/eji.201646725.

Zimmermann, Petra, and Nigel Curtis. 2019. "Factors That Influence the Immune Response to Vaccination". *Clinical Microbiology Reviews* 32 (2). doi:10.1128/cmr.00084-18.

Zuk, Marlene. 2009. "The Sicker Sex". *PLOS Pathogens* 5 (1): 1–3. doi:10.1371/journal.ppat.1000267.